J-PARC 11-03
KEK Progress Report 2011-4

Materials and Life Science Division
J-PARC Center
Tokai, Naka-gun, Ibaraki 319-1195, Japan

http://j-parc.jp/MatLife/en/index.html

MLF Annual Report 2010

MLF ANNUAL REPORT 2010

J-PARC/MLF

J-PARC

J-PARC 11-03

KEK Progress Report 2011-4

Materials and Life Science Division
J-PARC Center
Tokai, Naka-gun, Ibaraki 319-1195, Japan

Preface to the Annual Report of the Materials and Life Science Experimental Facility for Year 2010

We were running stably with a beam power at 220kW just before the earthquake occurred on March 11, 2011. Suddenly we were forced to stop the operation of the J-PARC facilities. It took over two months since that event to investigate and identify the damages, and we could finally determine the actions needed to restore the operations of the facility and the estimated restarting date, hopefully in December 2011. The most severe damages occurred in the Linac Tunnel and the peripheral utility facilities around the 3GeV ring. Those damages included subsidence of the tunnel floor, uncounted cracks in the wall associated with groundwater leakage, and breakdown of the power suppliers and the cooling systems. The most severe damages at the Materials and Life Science Experimental Facility (MLF) occurred at the boundaries between the main experimental hall and the annex buildings for long instruments extending to outside. The main front shields surrounding the target station also suffered severe displacement. However, we expect that the damaged areas in the MLF would be restored by December of this year. Currently all staffs are working hard with the spirit of resurrection.

The staffs show their spirit of resurrection in front of the MLF building on 24 June 2011.

In 2010, before the disaster struck, we made a few big steps in expanding the beam operation. The beam power increased stepwise from 100kW to 220kW with a very good availability of more than 90% by December 2010. The power reached is only 1/5 of the final goal, 1 MW, however it has already exceeded the power of ISIS, which had been the strongest pulsed neutron source for nearly 25 years since 1985. The performance of the state-of-the-art target-moderator system together with the instruments in MLF provided remarkably satisfactory output produced by those instruments.

We found out that the users successfully conducted most of their experiments even with this power level. We received over 350 proposals and the number of unique users exceeded 500. Those statistics show a strong demand from users to MLF, although the operated machine time was 2300 hours, which is half of the final goal.

In the beginning of 2010, the moderator cooling system experienced several faults, consisting of breaks in the accumulator of the cryogenic system and some problems in the filter system. Those were fixed during the summer shutdown in 2010 and after that the proton power was maintained stably at 100 kW.

Now, in July 2011, our staffs are making their best efforts to restore the work at the facility and we strongly hope to restart the MLF's operation soon.

Right after the disaster, we received many letters with condolences and support. Here I would like to express sincere gratitude to all our friends in the world. They encouraged us a lot. We were also offered time for conducting experiments for MLF users at facilities abroad, like SNS, LANCE, ANSTO, ILL and ISIS. Here, we genuinely thank them for their friendship.

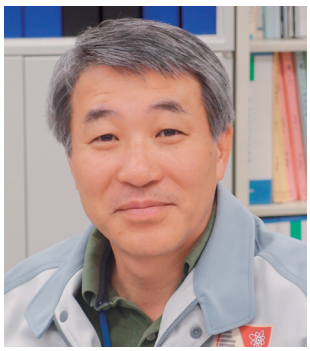

Masatoshi Arai
Division Director of the Materials and Life Science Experimental Facility,
J-PARC Center

Contents

Muon Science

Facility Report

Publicication List

MLF Division in J-PARC Center

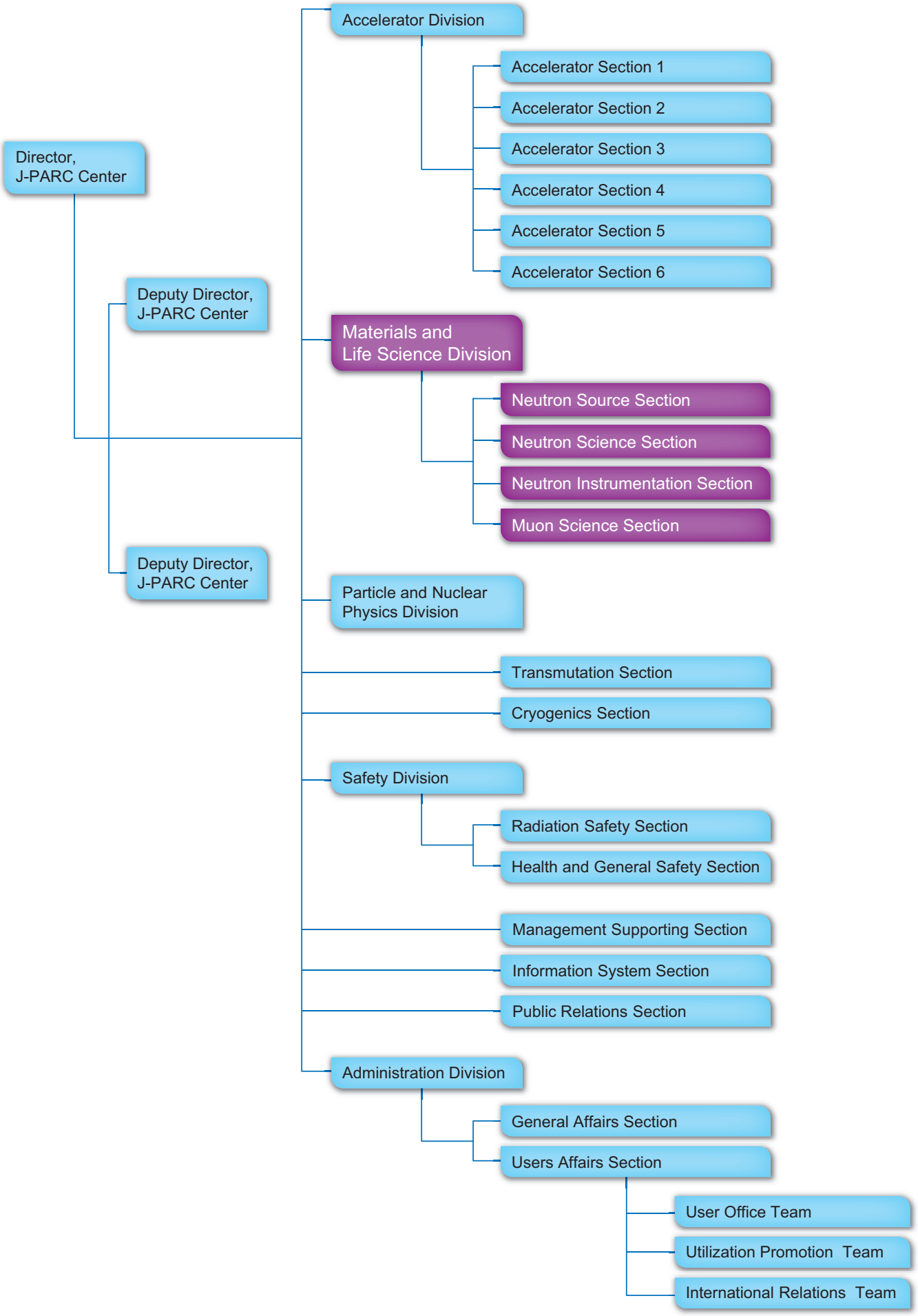

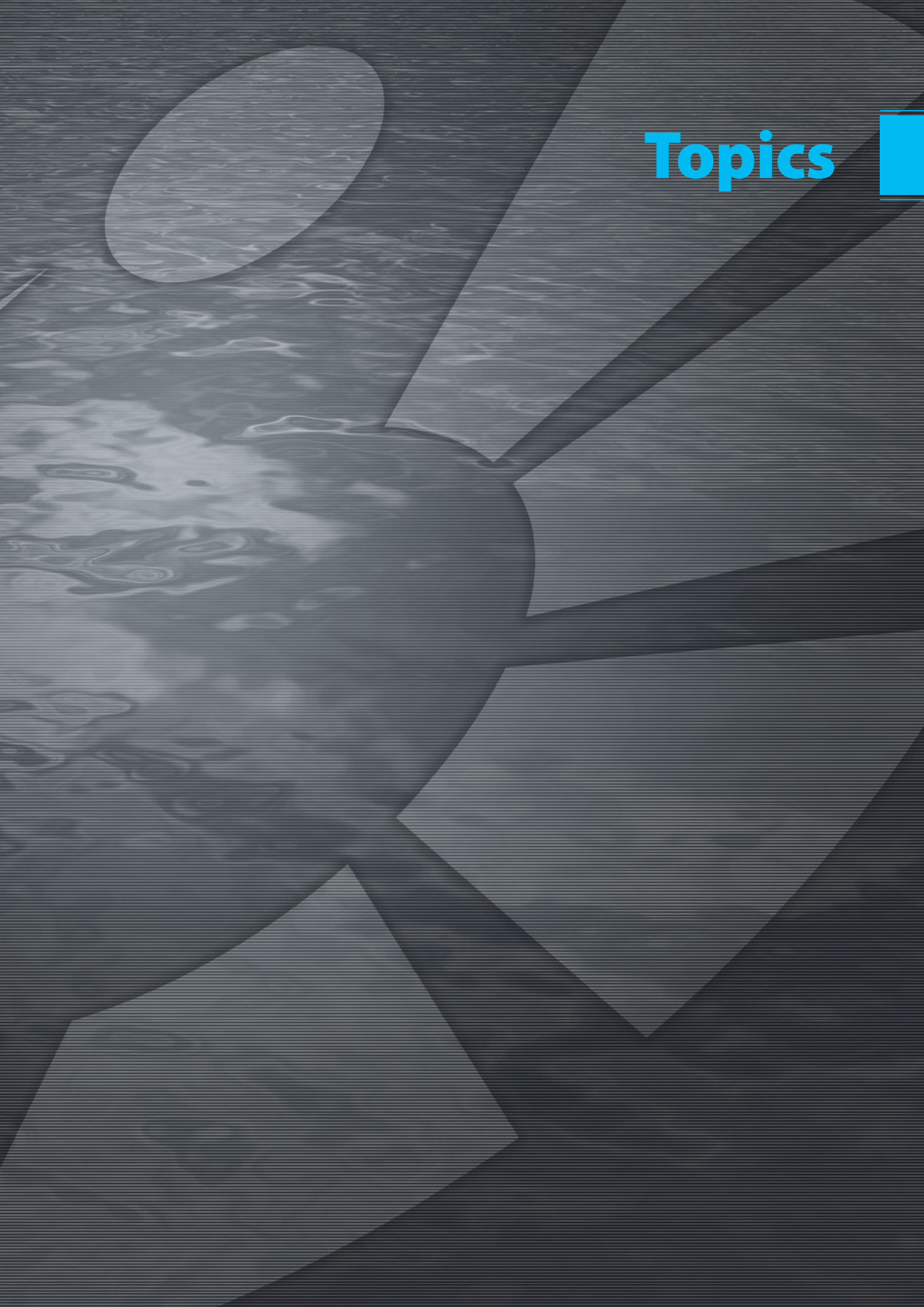

Topics

Status of Materials and Life Science Experimental Facility (MLF)

1. Introduction

In the fiscal year (FY) of 2010, 3 GeV, 120 kW proton beams were continuously supplied to the neutron and muon production target although a few troubles occurred at the cryogenic hydrogen loop in the neutron moderator system. After November, the beam power was increased up to 200 kW, operating continuously until the earthquake struck. We estimate that the number of days when the neutron-beam was available was around 120, with more than 10 days lost due to the earthquake. A beam operation history from the beginning of the operation is shown in Fig.1.

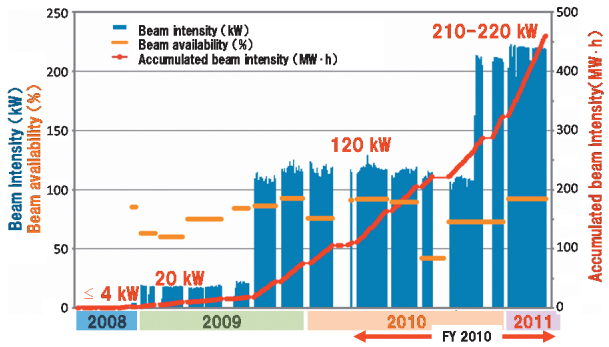

Figure 1. Chronograph of the beam operation.

2. The Earthquake on March 11

When the earthquake occurred, the leaders of MLF were in the JAEA Tokyo office, attending a meeting of the J-PARC/MLF Advisory Board. Right after the incident, the MLF staff in Tokyo and in Tokai could not contact each other by any means. All lines, telephone, mobile and internet, were cut for about two hours. Finally, the staff in Tokyo managed to establish a short communication with the staff in Tokai through a hard-wire telephone and they reported that all of the staff and users were safe, but there was some damage to the instruments and subsidence at the surrounding facility-buildings.

Since all traffic and lifelines were cut off and the Fukushima reactor emitted radioactivity in the atmosphere, some of the high officials were able to get together with only a few staffs and had to use a torch for a week to inspect the damage in the facility after the earthquake.

J-PARC is located near the shore of the Pacific Ocean, the ground is sandy and has a deep gravel layer. Hence, the main buildings have been underpinned by piling to the bed rock; however, the peripheral buildings have not been piled. Because of that, the damages to the main buildings were not as serious as those to the peripheral buildings. Subsidence areas were observed at the margins of the buildings. For instance, the subsidences, which occured at the Linac entrance, the 3-GeV synchrotron power supply yard, and the southeast part of the MLF building are shown in Fig.2 to 4, respectively.

Figure 2. Subsidence at the Linac entrance.

Figure 3. Subsidence at the 3-GeV power supply yard.

Figure 4. Subsidence at the southeast part of the MLF building.

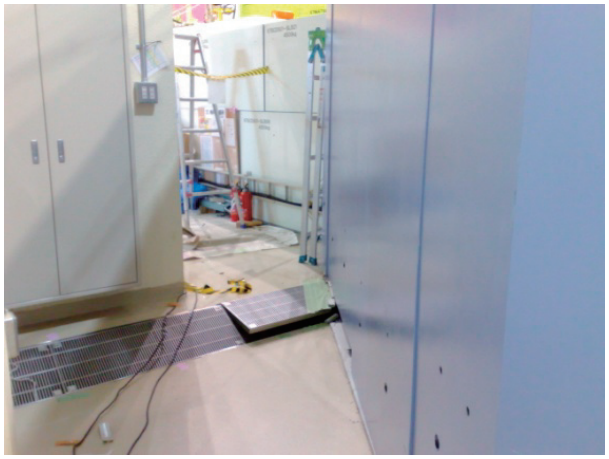

Figure 5. The peripheral building sank at more than 20 cm and the beam line was bent.

These subsidence areas cut off lifelines by damaging the electricity and water lines connecting to the buildings. The peripheral building of the MLF building sank at more than 20 cm, which bent the beam lines that go through the peripheral building as shown in Fig. 5.

However, most of the beam lines within the MLF building did not show serious damage except for the long instruments going through the annex buildings, although some shielding needs restoration and fixing.

We have initiated the restoration of the surrounding roads, accelerator tunnels, peripheral facilities shielding and instruments in the facility. We started to work on the re-construction, with the goal to restart the proton beam operation in December 2011 with a limited beam power.

3. Registered Institution for Facility Use Promotion

In 2009, the "Law for the Promotion of Public Utilization of the Specific Advanced Large Research Facilities" was amended and applied to the neutron experimental facility in J-PARC. Under this law, a budget for promoting neutron research including the portion of the proton beam operation cost has been supplied since 2009 and the Comprehensive Research Organization for Science and Society (CROSS) has been selected as a Registered Institution for Facility Use Promotion in March, 2011. The CROSS will start operation in JFY 2011 and the user program in MLF will be managed with the collaboration of the CROSS from the second proposal round in 2011.

H. Seto[1], and T. Kato[2]
[1]*Institute of Materials Structure Science, KEK;* [2]*Materials and Life Science Division, J-PARC Center*

Development for High Power Target System

Development of the Target System

High power proton beam bombard-ment into mercury target produces not only high intense neutron beam but also pressure waves in the mercury target. The pressure waves cause pitting-erosion damage to the mercury target vessel. This damage shortens significantly the lifetime of the target vessel.

To mitigate the pressure waves and the pitting-erosion damage, microbubbles will be injected into the mercury. The microbubbles play the role of cushion for the thermal expansion of mercury, which causes the pressure waves.

Microbubble Injection into Mercury Target

Pressure wave experiment

To inject the microbubbles into the mercury, a bubble generator (bubbler) will be installed in the mercury target vessel. Figure 1 shows a schematic of swirl bubbler which will be installed into the next mercury target vessel.

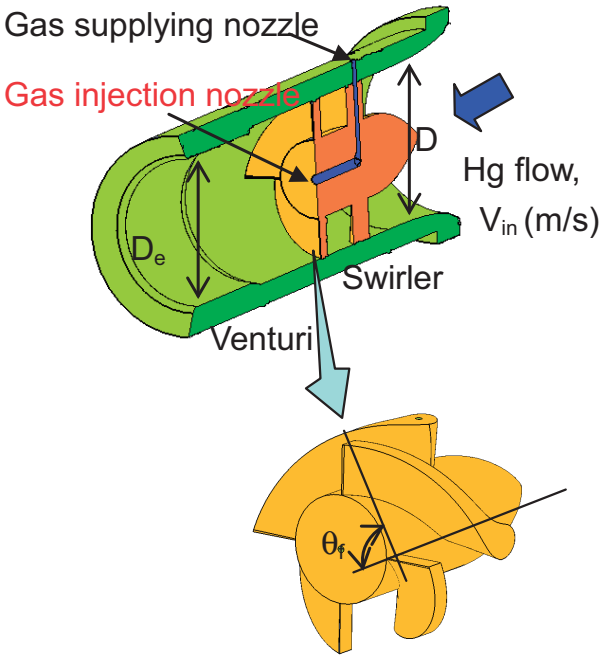

Figure 1. Schematic of swirl bubbler.

In order to investigate the effects of microbubbles on pressure wave mitigation by bubbles, water experiment was performed by using the swirl bubbler [1]. Intense pressure waves with a rise time of about 1.5 μs were produced by a spark discharge in water, and gas microbubbles were injected by using the swirl bubbler. A dependency of the radius and void fraction of the microbubbles on the mitigation of pressure waves was systematically examined by measuring the wall vibration by an accelerometer.

Figure 2 shows the time history of the acceleration on the channel wall. The peak radius of dispersed bubble is 50 μm. We found that the amplitude of wall vibration induced by the spark-induced pressure wave was dramatically decreased with increase in void fraction. This trend was identified with the evaluation, which we have done numerically so far.

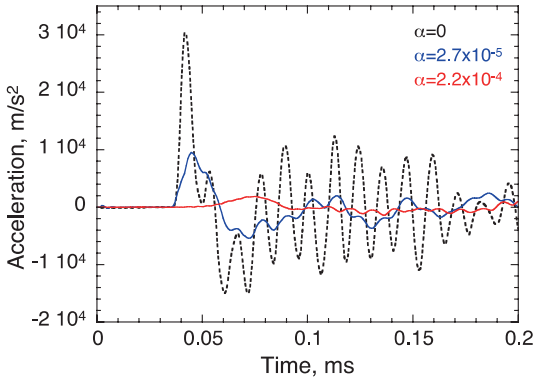

Figure 2. Time history of the acceleration on a channel wall.

Fabrication of a bubble generator for the next target vessel

The installation of bubbler in the mercury target will increase the flow resistance in mercury. The flow resistance should be less than 0.2 MPa because of the Hg pump ability. Flow resistance is affected by the shape of the bubbler.

Estimation methods determining the bubble size

and flow resistance were developed on the basis of experimental results such as taking into account the shape of the bubbler, the vane angle of the swirler, θ_f, ratio of the inlet area to the Venturi area, A/A_e, and inlet area, A. Figure 3 shows the estimated bubble size as a function of the vane angle. In Fig.3, the bubble size was estimated under the condition that the flow resistance became 0.2 MPa by varying A/A_e. The bubbler with small vane angle and large A/A_e (narrow Venturi) is effective when making small bubbles with low flow resistance. On the other hand, the bubbler with a large vane angle makes a strong swirl and reduces the pressure at the gas injection nozzle shown in Fig.1. That is, gas pressure to supply into the bubbler can be low, which results in stable operation.

Another problem was the swirl flow downstream of the bubbler, which gathers microbubbles in a center of the flow channel and induces bubble coalescence. This was solved by arranging a few bubblers in the cross section of the channel whose swirl direction became alternate. This arrangement weakens the swirl by interference in each swirl. The alternate-layout multi-bubbler was fabricated by taking into account the bubble size, flow resistance, required gas pressure supplied into the bubbler, setting position in the mercury target and fabricability as show in Fig.3 and it will be installed in the next target vessel.

In order to maximize the effect of pressure wave mitigation, bubbles of less than 100 μm in radius must be properly distributed in the peak heat load area, where is the source of strong pressure waves, with the volumetric fraction of more than 10^{-5}.

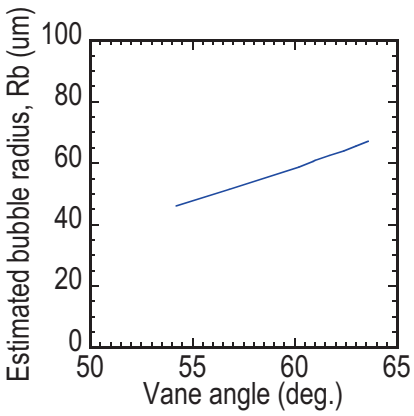

Figure 3. Estimated bubble radius under the condition that flow resistance become 0.2 MPa.

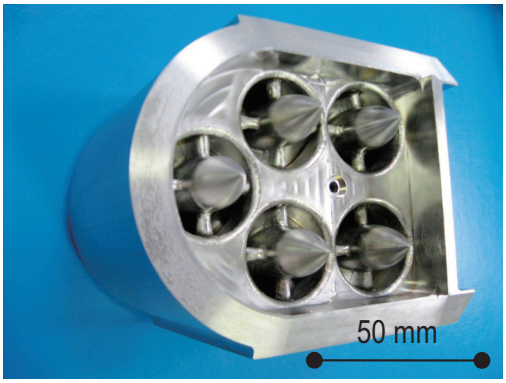

Figure 4. Fabricated alternate-layout multi-bubbler.

Development of a Beam Flattening System

It is well known that the damage at the mercury target vessel is proportional to the 4th power of the peak density of the beam (called P4 law). As the beam power increases, the damage on the target vessel becomes serious. In the MLF building, the temporary storage yard for the spent target and the proton beam windows with high radio-activities is not enough to store them throughout the MLF service-time. In order to extend the lifetime of the target, the beam peak intensity is required to be kept as lower as possible.

The beam expansion, by tuning of the quadrupole magnets at the beam transport, is very effective and simple way for reduction of the peak density. As beam size widens, on the contrary, the heat becomes higher at the target vicinities such as shield and refractors, where the allowable density of the heat deposition is less than 1 W/cc.

The peak density depends on the initial condition of the beam extracted at the 3-GeV Rapid Cycling Synchrotron (RCS). From the result of the simulation for the RCS, the distribution of the beam in the phase space becomes likely the Gaussian shape.

To reduce the peak intensity, we developed the beam flattering technique to reduce the damage in the target. By using the non-linear magnet, the distribution in the phase space is distorted. In Fig.5, one of the candidates of the octupole magnet is shown. Figure 6 shows a typical result of the beam simulation. It is shown that the peak tuned by the flattering system becomes 30% smaller than the Gaussian case. It is found the beam flattening system is feasible. In JFY 2011, the octupole magnet will be fabricated.

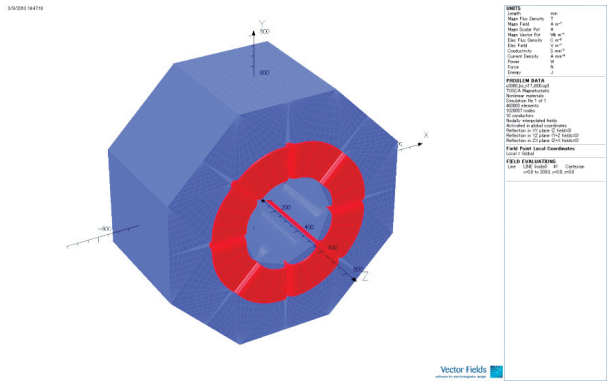

Figure 5. Schematic of octupole magnet for the beam flattening system.

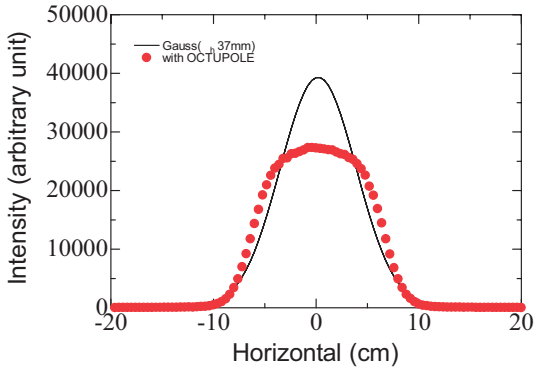

Figure 6. Comparison of the beam profile with and without flattening system.

Reference

[1] T. Naoe, H. Kogawa, M. Futakawa and M. Ida, J. Nucl Sci. Technol. **48**, 865 (2011).

H. Kogawa, T.Naoe, and S. Meigo
Materials and Life Science Division, J-PARC Center

Development of a Large Area Scintillator Detector for "SENJU"

A two-dimensional scintillator neutron detector module that has a large detective area was developed for "*SENJU*" instrument successfully [1,2]. 31 detector modules were delivered to the beam line by the end of Fiscal Year 2011 (JFY 2011).

SENJU is a time-of-flight Laue single crystal diffractometer designed for research of materials exposed to extreme external conditions such as low temperature, high magnetic field, and high pressure. The instrument requires a detector system that covers solid angle over 4sr around the sample while maintaining a high spatial resolution, high detector efficiency, and low gamma sensitivity. Since the requested detector specifications were quite unique, it was a challenge to deliver the components on time; all the detector modules had to be completed and delivered to the beam line within this fiscal year including the detector's R&D.

To fulfill the requirements, we developed the detector based on the scintillator/ wavelength shifting (WLS) fiber technology. Photo 1 shows the prototype detector system. The detector system accommodated the large detector head while the electronics hardware, encoder and DAQ, were similar to those used in the *iBIX* in order to maintain the system integrity.

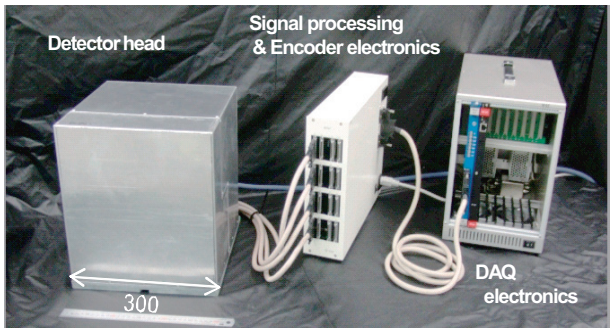

Photo 1. A detector module for *SENJU*.

In the detector head the WLS fibers were placed with a pitch of 4 mm to expand the neutron-sensitive area to 256 × 256 mm^2. The detector exhibited detecting efficiency of 40% for thermal neutrons. The gamma sensitivity was decreased to 3 × 10^{-6} by implementing the dedicated signal processing software into the encoder. Moreover, special care was taken of the magnetic shielding of the photomultipliers, ensuring the count rate stability under a stray field of 200 gauss. Figure 1 shows two-dimensional data of neutron diffraction from a single crystal tin sample measured in the BL10 (ToF = 10.0 ~ 10.1 ms). The detailed data analysis revealed the feasibility of the detector system.

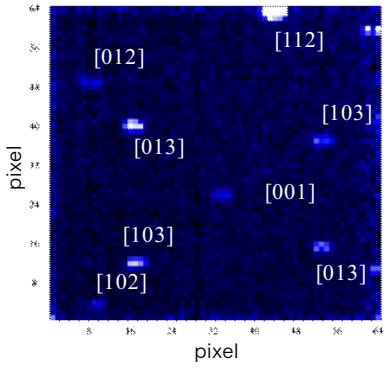

Figure 1. Two-dimensional data of the neutron diffraction from a single crystal tin sample measured with the *SENJU* detector module.

Photo 2. Detector modules installed in the north bank of SENJU (Before the earthquake).

The detector was also designed as compact as possible, with a size of 300 × 300 × 300 mm and weight of 15 kg. This added flexibility to the instrument design as well as a significant positive impact on reducing the instrument cost. It helped the concept of movable detector bank, which was one of the unique features of the *SENJU* (Photo 2).

References

[1] T. Nakamura *et al.*, to be submitted to Nucl. Instr. & Meth. A.

[2] T. Nakamura *et al.*, presented at 2011 IEEE Nuclear Science symposium and medical imaging conference, 23-29 October 2011, Valencia, Spain.

T. Nakamura[1], T. Kawasaki[1], K. Sakasai[1], K. Toh[1], H. Yamagishi[1], K. Soyama[1], T. Hosoya[2], and M. Katagiri[2]

[1]*Materials and Life Science Division, J-PARC Center,* [2]*Frontier Research Center for Applied Atomic Sciences, Ibaraki University*

Neutron Beam Focusing for Pulsed Neutrons with Supermirror Coated on Precisely Figured Surfaces

1. Introduction

Though the neutron source power is being drastically improved at MLF, J-PARC, high-performance focusing techniques are indispensable for small samples, micron-area measurements, grazing incidence small angle scattering, and so on. As for the focusing devices at spallation neutron sources, the achromatic optics is particularly important because most experiments are performed with wideband beams. Reflective focusing is therefore a prominent candidate for that purpose.

We have been developing focusing mirrors by combining a supermirror coating technique with ion-beam sputtering [1] and a precise aspheric surface figuring method with the numerically controlled local wet etching process [2]. In the past we fabricated a one-dimensional elliptic focusing supermirror of 90 mm (L) × 40 mm (H) and successfully focused wideband neutrons achieving beam width of 0.25 mm and peak intensity gain of 6 [3,4].

In this report, the performance tests of a larger-size one-dimensional (1-D) elliptic focusing mirror are described. The mirror is an m=4 NiC/Ti supermirror for 1:1 beam focusing. (i.e. initial beam width = focused width). It is of 1-D elliptic shape, 400 mm in length, with a focal length of 2100 mm. The detailed parameters and the photo of the fabricated mirror are shown in Table.1 and Fig.1, respectively.

Table 1. Design parameters of the focusing supermirror.

Ellipsoid	a=1050, b=25.65
1st focus-mirror center	1050 mm
Mirror center-2nd focus	1050 mm
Mirror length	400 mm
Mirror substrate	Quartz
Mirror coating	NiC/Ti (m=4)
Incident angle	1.40 deg
Wavelength	3.5 Å ~
Acceptable beam divergence	~ 0.53 deg

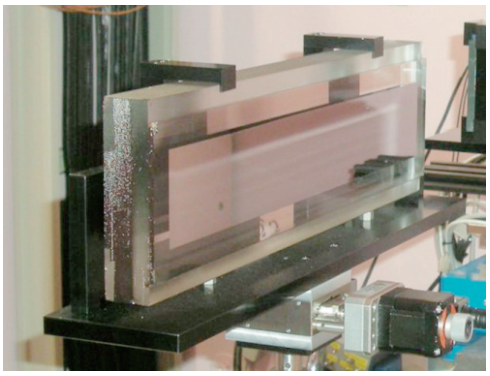

Figure 1. Focusing supermirror.

2. Figure Measurement

The figure errors and surface roughnesses of the mirror were measured before the beam experiment. The figure errors before and after the supermirror deposition were 1.33 μm (p-v) and 3 μm (p-v), respectively. The surface roughnesses were 0.15 nm (rms) and 0.20 nm (rms) before and after the deposition. The results show that the mirror has an excellent elliptic surface and that the supermirror deposition hardly degrades it.

3. Focusing Experiment

The focusing experiment was carried out at BL10 (NOBORU) of MLF. Figure 2 shows the beamline built on the experimental bench of BL10.

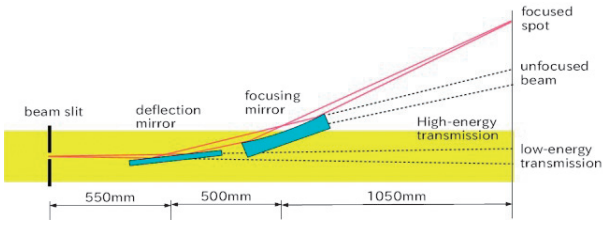

Figure 2. Beam line setup at BL10.

A manual beam slit narrows the incident neutron beam at the first focal point of the ellipsoid. The focusing mirror, installed at the 1050 mm point after the slit, reflects the diverging neutron beam and fo-

cuses it on the second focal point, 1050 mm after the mirror. The neutrons are detected at the second focal point. Additionally, we installed a flat supermirror just after the manual slit in order to kick the beam out of the high-energy direct beam area and reduce the background.

We took two-dimensional (2-D) images of the focused and unfocused beam with a same imaging plate placed at the second focal point. The slit's width (the initial spot size) was 0.10 mm. The 2-D images are shown in Fig.3 and horizontal cutouts of these images are shown in Fig.4. The intensities are expressed in units of PSL (photo-simulated luminescence). The focused peak was 0.20 mm in full width at half maximum (FWHM). The mismatch between the initial beam width of 0.10 mm and the focused width is attributed to the position alignment of the focusing mirror, particularly to the tilted setting. (Another experiment at the research reactor JRR-3 has demonstrated that the mirror can achieve 0.15 mm by adjusting the mirror settings.) The peak intensity gain was 52 compared with the unfocused beam. The signal to noise ratio of the focused peak was more than 2 orders of magnitude and no significant growths of backgrounds were observed by inserting the focusing mirror.

Figure 5 compares wavelength-distribution profiles of the focused and unfocused beams obtained by time-of-flight measurements. The rising edge of the focused beam profile at 3.5 Å corresponds to the critical reflection angle of the coated mirror Q_c=0.088 Å^{-1} (m=4) because the incident angle to the focusing mirror was 1.40 deg.

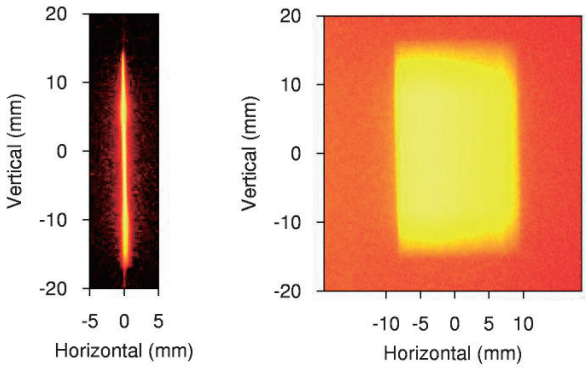

Figure 3. 2-D images of the focused beam (left) and unfocused beam (right). The intensities are shown on the log scale.

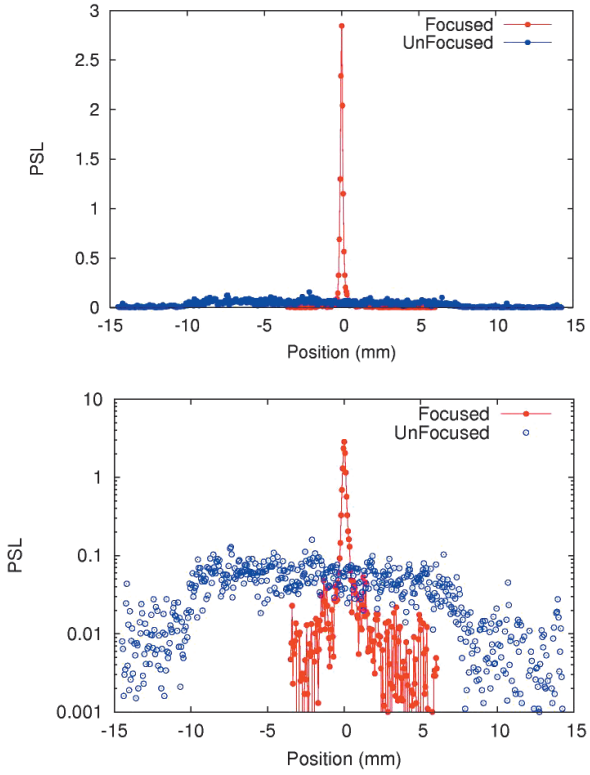

Figure 4. Horizontal cutout of the 2-D images of the focused and defocused beams at the vertical center: the upper panel is drawn on the linear scale while the lower panel is on the log scale.

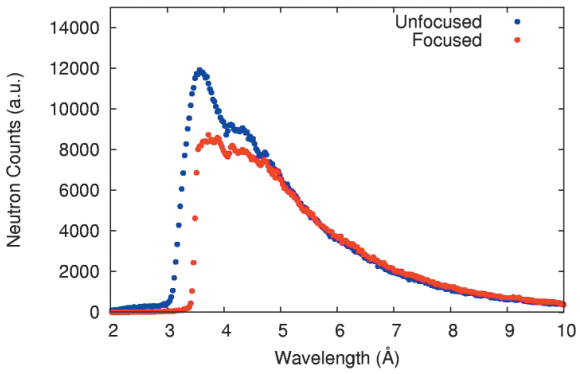

Figure 5. Wavelength distributions of the focused and unfocused beams. It should be noted that comparing the y-values of the two profiles in the figure is nonsense because the y-values of the unfocused beam are just the intensities of a portion of the unfocused beam multiplied by an arbitrary constant.

4. Summary

We have successfully fabricated a 400mm-length, one-dimensional elliptic focusing supermirror with exceptionally low figure errors and small

roughnesses. The focusing experiment showed a focused wideband neutron beam (λ > 3.5 Å) into 0.15~ 0.20 mm in width with large peak gain (52), with high S/N ratio and without significant growth of the back-ground. In the next phase we will try two-dimensional focusing by using two focusing mirrors in the Kirkpatric-Baez configuration. We are also developing stacked thin focusing mirrors for wider beam acceptance.

References

[1] R. Maruyama, D. Yamazaki, T. Ebisawa, K. Soyama, J. Appl. Phys. **105**, 083527 (2009), and references therein.

[2] K. Yamamura, Annals of the CIRP **56/1**, 541 (2007).

[3] K. Yamamura, M. Nagano, H. Takai, N. Zettsu, D. Yamazaki, R. Maruyama, K. Soyama, S. Shimada, Opt Express **17**, 6414-6420 (2009).

[4] D. Yamazaki, R. Maruyama, K. Soyama, M. Nagano, F. Yamaga, K. Yamamura., J. Phys: Conf. Series **251**, 012076 (2010).

D. Yamazaki[1], R. Maruyama[1], H. Hayashida[1], K. Soyama[1], M. Nagano[2], F. Yamaga[2], and K. Yamamura[2]

[1]Materials and Life Science Division, J-PARC Center; [2]Research Center for Ultra-precision Science and Technology, Osaka University

Strong $s_{\pm}$-like Spin Resonance in the Nodal Fe-Based Superconductor $BaFe_2(As_{0.65}P_{0.35})_2$

1. Introduction

The mechanism of high-transition temperature (high-T_c) superconductivity is one of the important problems in condensed-matter physics. The recent discovery of iron-based superconductors has renewed our interest in the relationship between unconventional superconductivity and magnetism. One of the consequences of the magnetism-mediated superconductivity is the momentum dependent superconducting (SC) order parameter, and its identification is of crucial importance to elucidate the pairing mechanism of high-T_c. As a typical example, cuprate high-T_c superconductors possess d-wave symmetry, and display line nodes due to the sign change of the order parameter which is characteristic to unconventional superconductors.

In the case of iron-based superconductors, whether line nodes exist or not depends on each material system. In the early stage of the researches, it was proposed theoretically that the superconducting gap changes its sign between disconnected pieces of the Fermi surface due to the repulsive nature of the pairing interaction mediated by spin fluctuations. This pairing state, now often called $s_{\pm}$ pairing, has been verified by several subsequent experimental studies. According to the systematic studies of the iron-based superconductors, in most of the superconductors with relatively high-T_c such as SmFeAs(O,F) (T_c=45 K), (Ba,K)Fe_2As_2 (T_c=38 K), $PrFeAsO_{1-y}$ (T_c= 35 K) and LiFeAs (T_c= 16 K), fully-gapped s-wave symmetry is confirmed. On the other hand, line node symmetry has been observed in lower-T_c counterparts, such as $LaFePO_{1-y}$ (T_c= 7 K) and KFe_2As_2 (T_c= 3 K). Therefore, iron-based superconductors are intriguing systems which allow us to investigate the relationship between nodal symmetry and T_c. However, this experimental tendency that the nodal symmetry is unfavorable for high-T_c turns out to be non-universal, since recent penetration depth, thermal conductivity and nuclear magnetic resonance (NMR) relaxation rate measurements on the $BaFe_2(As,P)_2$ superconductor have demonstrated that this material possesses line nodes in the order parameter, in spite of its relatively high-T_c of 30 K. Consequently, studying of this material will provide more important information to understand the effect of nodal symmetry on T_c. The urgent question to be answered here is whether the relevant SC order parameter of $BaFe_2(As,P)_2$ is essentially the same or distinct from other relatively high-T_c colleagues, and what causes the relatively high-T_c of this material.

A possible approach to answer the above question is to observe the magnetic resonance by neutron scattering, which has proved to be a powerful tool for detecting the sign reversal symmetry of the gap in unconventional superconductors. In this study, we have performed inelastic neutron scattering to characterize the magnetic excitation and the SC gap symmetry of $BaFe_2(As_{0.65}P_{0.35})_2$ on a ~ 36 g powder sample with T_c=30 K.

2. Experimental results

Figure 1(a) and (b) shows two-dimensional plots of dynamical structure factor $S(Q, E)$ of $BaFe_2(As_{0.65}P_{0.35})_2$ measured by The Fermi chopper spectrometer (4SEASONS) in J-PARC with incident energy of 45.5 meV at 5 and 32 K, respectively. The most apparent feature is a bright spot centering around Q ~1.2 Å^{-1} and E ~10-15 meV, which becomes more pronounced in the SC states. Scattering vector of Q ~1.2 Å^{-1} roughly corresponds to 1.13 Å^{-1} at Q = (1/2 1/2 0). It is therefore likely that the observed peak corresponds to the spin excitation at the antiferromagnetic wave vector Q_{AF} = (1/2 1/2). This feature shows similar characteristics to those of the spin resonance mode observed in other iron-based high-T_c superconductors [1,2].

Temperature dependence of the magnetic excitation at Q_{AF} has been precisely measured by using triple axis spectrometer (TAS-1) at JRR-3. On cooling, the peak intensity rises up at T=5 K, confirming

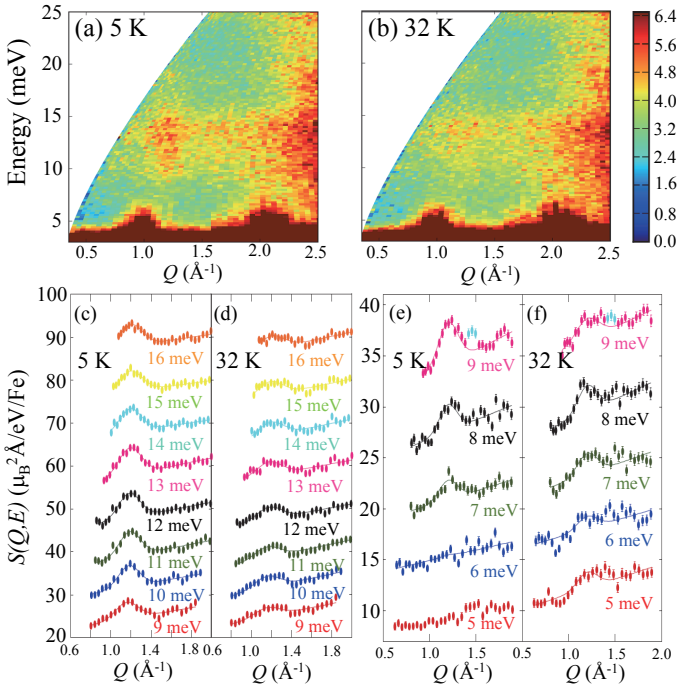

Figure 1. Dynamical structure factor $S(Q,E)$ of $BaFe_2(As_{0.65}P_{0.35})_2$ measured with E_i= 45.5 meV at (a) 5 K (below T_c) and (b) 32 K (above T_c). (c) and (d) show constant energy cuts of $S(Q, E)$ at 5 K and 32K, respectively, measured with E_i = 45.5 meV. (e) and (f) are those measured with E_i = 21.6 meV. Solid lines are the results of fits to a Gaussian function on a sloped background. The offset values of (c), (d) are 6, 12, 30, 40, 51, and 64 for 10-16meV, and 5, 10, 15, and 20 for 6-9meV of cuts (e), (f) for the clarity.

that the enhancement of the magnetic excitation at Q_{AF} and E=12 meV is indeed the resonance which is a signature of the sign inversion in the SC order parameter. The resonance peak energy corresponds to $E_{res} \sim 4.6 k_B T_c$, which agrees well with that of other relatively high-T_c iron-based superconductors [1, 2].

Figure 2 shows the E-dependences of the dynamical spin susceptibility $\chi''(E)$, which is calculated by integrating the fitted results of Figs. 1 (c)-(f) over Q. At 32 K (> T_c), $\chi''(E)$ is finite for the entire E-range and exhibits gradual increase with E up to E=14 meV. The absolute value of $\chi''(E)$ is comparable with that of normal state of superconducting sample of LaFeAs(O,F) [2]. On the other hand, $\chi''(E)$ spectrum at 5 K (< T_c) shows a gap below 6 meV and a peak centered at E_{res} = 12 meV. The resonance enhancement is of factor 1.7 at E_{res} = 12 meV. which is similar to those seen in $Ba(Fe,Co)_2As_2$ and LaFeAs(O,F) [1, 2].

All these experimental results indicate that $BaFe_2(As,P)_2$ has similar characteristics to iron-based superconductors with fully-gapped $s_{\pm}$- wave. The spin resonance in the neutron spectrum is caused via BCS coherence factor:

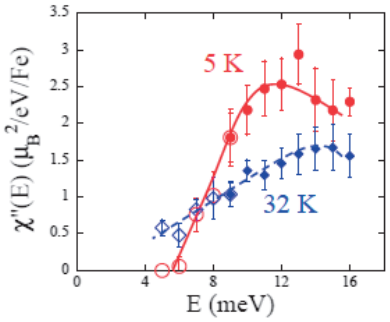

Figure 2. Temperature dependence of magnetic excitation peak height observed at Q = 1.2 Å^{-1} and E = 12 meV. Circles and diamonds represent data measured by TAS-1 and 4SEASONS, respectively. The solid line is a guide to the eye.

$$\frac{1}{2}\left(1-\frac{\varepsilon_k \varepsilon_{k+q}+\Delta_k \Delta_{k+q}}{E_k+E_{k+q}}\right) \approx \frac{1}{2}\left(1-\frac{\Delta_k \Delta_{k+q}}{|\Delta_k||\Delta_{k+q}|}\right)$$

where $E_k = \sqrt{\varepsilon_k^2 + \Delta_k^2}$ is quasi-particle dispersion relation and Δ_k is band energy measured relative to Fermi energy. The $\chi''(Q_{AF}, E)$ in SC state is modified by this coherence factor. In $s_{\pm}$-wave case, signs of the order parameter are reversed ($\Delta k = -\Delta_{k+QAF}$) on different FSs, and the coherence factor becomes almost 1, resulting in spin resonance. Conversely,

when the signs of order parameter are the same, the coherence factor becomes zero, then $\chi''(Q_{AF}, E)$ is suppressed. On the other hand, the nodal order parameter revealed in $BaFe_2(As,P)_2$ by other techniques results in the existence of region where the sign of order parameter is reversed on a single FS. Such a region should decrease the resonance enhancement. The observed enhancement ratio of 1.7 is comparable to that in other iron-based systems without nodes (~2). This suggests that similar amounts of sign reversed process to the case of $s_{\pm}$-wave occurs between Γ and M FSs in the present compound. This situation may be the possible reason why $BaFe_2(As,P)_2$ can hold the comparable T_c (= 30 K) to those of the iron-based high-T_c superconductors without nodes despite the existence of nodal symmetry [3].

References

[1] M. D. Lumsden *et al.*, Phys. Rev. Lett. **102**, 107005 (2009).

[2] S. Wakimoto *et al.*, J. Phys. Soc. Jpn. **79**, 074715 (2010).

[3] M. Ishikado, Y. Nagai, K. Kodama *et al.*, Phys. Rev. B **84**, 144517 (2011).

M. Ishikado[1, 2, 3], K. Kodama[1, 3], R. Kajimoto[4, 3], M. Nakamura[4], Y. Inamura[4], S. Wakimoto[1, 3], A. Iyo[2, 3], H. Eisaki[2, 3], M. Arai[4, 3], and S. Shamoto[1, 3]

[1]Quantum Beam Science Directorate, Japan Atomic Energy Agency (JAEA); [2]Photonics and Electronics Research Institute, National Institute of Advanced Industrial Science and Technology; [3]JST, TRIP; [4]J-PARC Center, JAEA

High Pressure Neutron Diffraction Measurements of LaD_2 Using NOVA

1. Introduction

Properties of metal hydrides have been investigated focusing on the hydrogen-metal and hydrogen-hydrogen interactions under high pressure. Hydrogen atoms which are located in the interstitial sites play an essential role in structural and electronic properties of metal hydrides. We have investigated rare-earth metal hydrides as typical examples. Rare-earth metals form various hydrogen-concentration states, RH_x, starting from a solid state solution and ending with trihydride RH_3 through dihydride RH_2. Many RH_2 commonly has an fcc metal lattice, in which the two tetrahedral sites are almost fully occupied by hydrogen atoms while one octahedral site remains empty. In this study, we investigated high-pressure transformation of LaD_2.

Recently, we found the cubic to tetragonal structural transition and a successive phase separation into two different molar volumes phases at high pressure using synchrotron radiation x-ray diffraction experiments [1]. Observed phase separation of LaH_2 suggests that the interstitial hydrogen atoms are transferred from T-sites and the dihydride forms domains of the hydrogen-poor hydrogen-rich phases spontaneously by pressurization. To understand the origin of the above structural transformations, the information on the interstitial hydrogen atoms is indispensable. Hence, we attempt to determine the hydrogen concentration and occupation sites of phase separation products at high pressures. The pressure for the phase separation is ~11 GPa, which is too high to be easily examined. So, first we developed the high-pressure device for neutron diffraction [2] and then applied it to the high-intensity total diffractometer, NOVA.

2. Development of High Pressure Device

Neutron diffraction experiments at high pressure have already been performed in foreign neutron facilities but those have not been so popular in Japan. This is because the neutron flux of Japanese neutron facilities was not enough for high pressure experiments. J-PARC enables us to perform the high pressure experiments. Among several spectrometers in MLF/J-PARC, NOVA is one of the beamlines suitable for the high pressure neutron experiments for its high detection efficiency.

We selected a Paris-Edinburgh (PE) press (VX4, max. load 200 ton) with toroidal anvils as the high-pressure device among several kinds of large volume presses. It is because the PE press can generate pressures of more than 10 GPa with maintaining relatively large sample volume (88 mm^3 for the 10 GPa-range use and 40 mm^3 for the 20 GPa-range use) and it is compact enough to be installed in the vacuum chamber of NOVA. The PE presses have been already used in many neutron facilities and many productive results have been obtained.

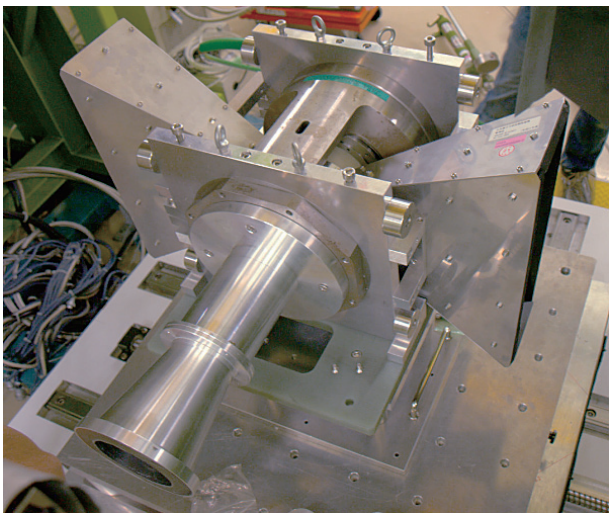

Figure 1. PE press with the incident and receiving collimators.

In order to install the PE press in the vacuum chamber of NOVA, the press and the adjustment stages are hung from the flange. The neutron beam impinges into the sample from the breech of PE press and the scattered neutrons are detected with the 90 degree bank detectors. The incident beam is truncated into an appropriate size using the in-

cident collimator made of hexagonal BN to reduce the background. The guide tube made of B_4C resin is also attached over the incident collimator to avoid the contamination of the air scattering. The receiving collimators made of B_4C rubber is attached to the both sides of the press to reduce the background from the sample surrounding materials (see Fig. 1). Using these assemblies, we succeeded in getting the neutron diffraction patterns with a relatively low background (see Fig. 2). The typical measuring time was 12 hours for measurements below 10 GPa at 100 kW accelerator power, and 12+α hours for measurements above 10 GPa at 200 kW accelerator power Furthermore, we succeeded in measuring the diffraction patterns up to 17 GPa, which is highest pressure in domestic neutron diffraction experiments.

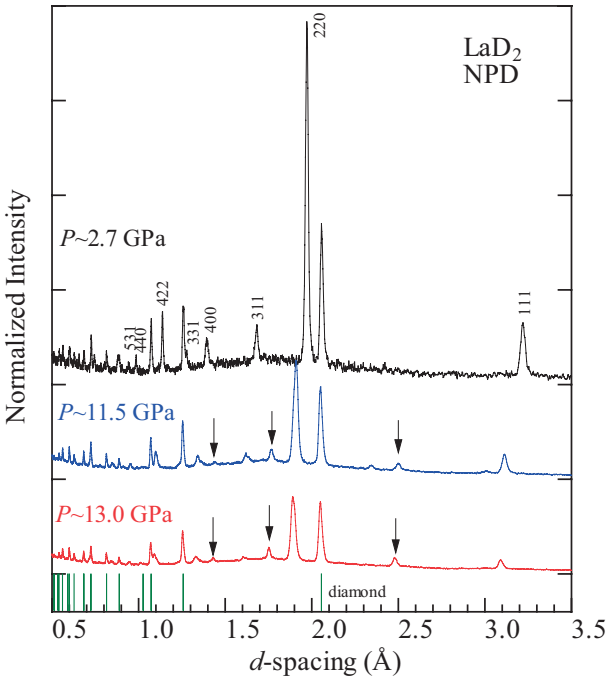

Figure 2. Selected neutron diffraction patterns of LaD_2 at high pressures. Each profile is shifted for better visualization, and the base line for each pattern is shown by the stick marks on vertical axes. Background is not subtracted, showing the background is low even for high pressure diffraction.

3. High Pressure Neutron Diffraction

Powder sample of LaD_2 was encapsulated together with a pressure transmitting medium (deuterated methanol-ethanol 4:1 mixture) in a metal gasket made of a TiZr null alloy, and was pressurized between the opposing double-toroidal anvils made of WC or sintered diamonds. The sample pressures were estimated from the pressure-volume relation obtained by the x-ray diffraction measurement beforehand.

Figure 2 shows the selected neutron diffraction patterns of LaD_2 under high pressure. At low pressure (2.7 GPa), Bragg reflections except those from diamond (vertical bars at the bottom) were well indexed with the cubic structure (*Fm*-3*m*, *Z*=4). With increase of pressure, each reflection peak of LaD_2 was shifted to a small *d*-value. Above 11 GPa, several new reflection peaks (indicated by arrows) appeared. This pressure value agrees with the phase separation pressure determined by the x-ray diffraction experiments. The intensity of the newly appeared peak increased when the pressure was increased from 11.5 GPa to 13.0 GPa while that of the original reflections was weakened. These features confirmed the occurrence of the phase separation.

4. High Pressure Formation of New Hydrogen Concentration State

When we compare the patterns of the hydrogen-poor phase between neutron and x-ray diffraction, marked difference was observed in their intensity. The intensity of the Bragg peaks with the odd-number indices in neutron diffraction pattern is much weaker than those in x-ray diffraction. The simulation of the diffraction profile indicates the formation of a NaCl-type phase, namely the O-sites in La fcc lattice are fully occupied by the deuterium atoms while the T-sites are empty. For the first time, the formation of the NaCl-type monohydride in the rare-earth metal hydrides is confirmed by this study[3]. The present result indicates that rare-earth metals can exhibit series of stoichiometric hydrides, such as mono-, di-, and tri-hydride. Our discovery of rare-earth metal monohydride will open the way to clarify the site-dependent nature of hydrogen-metal interactions through comparison studies among mono-, di-, and tri-hydride.

This work has been partially supported by the New Energy and Industrial Technology Development Organization (NEDO) under Advanced Fundamental Research on Hydrogen Storage Materials (Hydro-Star).

References

[1] A. Machida, T. Watanuki, D. Kawana, and K. Aoki, Phys. Rev. B **83**, (2011) 054103.

[2] T Hattori, Y Katayama, A Machida, T Otomo and K Suzuya, J. Phys.: Conference Series **215**, 012024 (2010).

[3] A. Machida *et al.*, submitted.

A. Machida[1], M. Honda[1], T. Hattori[1,2], A. Sano-Furukawa[1,2], Y. Katayama[1], K. Aoki[1], K. Komatsu[3], H. Arima[3], H. Ohshita[4], and T. Otomo[4]

[1]*Quantum Beam Science Directorate, JAEA;* [2]*J-PARC Center, JAEA;* [3]*Graduate School of Science, University of Tokyo;* [4]*Institute of Materials Structure Science, KEK*

Crystal Structure Change of Cathode for Li Ion Battery During Charge of Coin Type Cell Observed by Ex-Situ Time-of-Flight Neutron Diffraction

1. Introduction

Many lithium-intercalated transition metal oxides have been studied as cathode materials in high energy density rechargeable Li ion batteries. In our research, we have focused on the $Li(Ni,Co)O_2$ system in which Co is substituted for Ni in $LiNiO_2$. We synthesized a material in which a portion of the (Ni, Co) is replaced by low-valence Cu with the aim of reducing the Ni^{2+} content to reduce cation mixing and thereby enhance the battery characteristics.

Crystal structure analysis has mainly been performed on the powder form that has not been subjected to charge - discharge cycling, but to determine the battery characteristics it is essential to determine the changes in the crystal structure during the cycle. However, as the electrodes in coin type cells contain relatively small amounts of active material, it has not been possible to perform structure analysis by neutron diffraction of samples subjected to charge - discharge.

In the present study, we performed new ex-situ measurements of the change in the crystal structure of a cathode containing the composite material in a coin type cell subjected to a charge - discharge cycle fabricated for this purpose.

2. Experimental

$Li(Ni,Co,Cu)O_2$ was synthesized through the solid-state method. In the synthetic process, the final sintering was carried out at 800°C in air for 15 h. The obtained samples were identified by powder XRD. Compositional analysis of the metal content of the sample was performed using an ICP. The cell used for the charge - discharge experiments was a coin type cell(Figure 1). The cathode was prepared by mixing $Li(Ni,Co,Cu)O_2$ powder, acetylene black and PVdF at a weight ratio of 85:10:5. This mixture was then dispersed in N-methylpyrrolidone to form a slurry and applied to an Al foil (circular diameter: 1 cm). The electrolyte was 1mol L^{-1} $LiPF_6$ in EC:DMC (vol. 1:2) solution. The cathode after charging was obtained in the second cycle at 30% Li separation (SOC 30%) after one charge - discharge cycle. The crystal structure was determined by time-of-flight neutron diffraction using iMATERIA(BL20, J-PARC) (Figure 2). The active material content of the cathode prior to charging and after charging was only ca. 8.5 mg and the measurement time was 188 min and 383 min, respectively. Rietveld refinements were performed with these data using Z-Rietveld (ver.0.9.34).

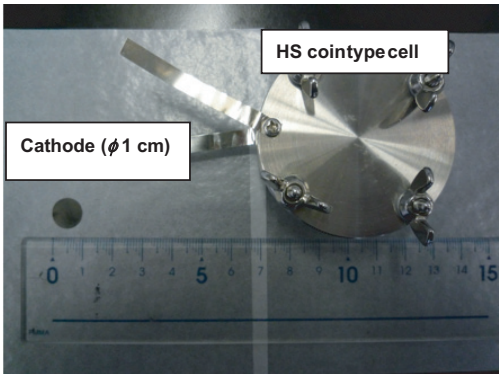

Figure 1. Coin type cell and cathode (ϕ 1cm).

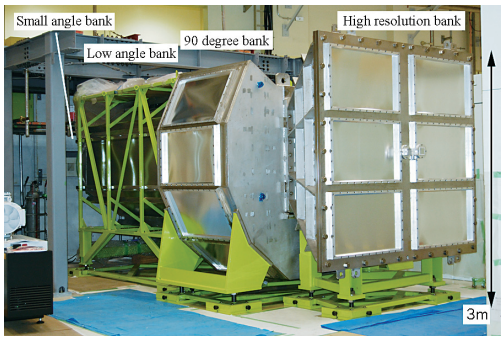

Figure 2. IBARAKI Materials Design Diffractometer, iMATERIA without detector for each bank and instrument shielding.

3. Results and Discussion

The XRD patterns of obtained samples showed that all peaks were assignable to an octahedral crystal (space group *R-3m*), indicating that the powder consists of a single phase. The analytical metal

composition was analyzed by ICP and it was close to the nominal composition. The large irreversible capacity evident is attributable to the formation of a solid electrolyte interface layer in the first cycle. The sample after charging was the second-cycle (SOC 30%) sample.

When investigating the crystal structure of the powder sample and the electrode before and after charging, analysis was performed for a hexagonal crystal (space group: *R-3m*). The metal component occupancies were analyzed by employing the Li and Ni occupancy ratio as the variable for determining the cation mixing amount and by using the composition determined by ICP as a reference. The second phase could not be observed by X-ray diffraction; however, because the Li_2CO_3 peak was observable in neutron diffraction, it was taken to be the second phase. For all the samples, there was close agreement between the measured and calculated values.

Figure 3 shows the profile fitting results for the cathode of the coin type cell after charging. These results show close agreement between the cathode prior to charging and the powder, despite the cathode active material content being approximately 1/100 from that of the powder. This demonstrates that it is possible to evaluate the 8.5 mg of active material in the cathode (containing the binder) by neutron diffraction. The calculated Li content of the active material is in fair agreement with the analytical Li content by ICP. The results demonstrate that it is possible to use neutron diffraction to quantitatively determine the lithium content of the active material and the amount of Li/Ni cation mixing in a coin type cell cathode containing a binder and conductive materials after charging. The cathode charging reduced lattice parameter *a* and increased lattice parameter *c*. The contraction in the *a*-axis direction is attributable to Li separation and the elongation in the *c*-axis direction to increased repulsion between oxygen ions. The results also indicate that the second phase Li_2CO_3 is eliminated by charging and that the difference in cation mixing amount in the cathode before and after charging is not large, indicating that little or none of the mixed Li separates during charge and discharge. In the electrode after charging, the bond valence sum of the MO_6 octahedron was higher, which is presumably attributable to an increase in the valence of the Ni accompanying Li separation. The increases in the distortion, λ and σ^2 [1] of the MO_6 octahedron after charging clearly show that MO_6 octahedral distortion in the cathode is increased by charging [2].

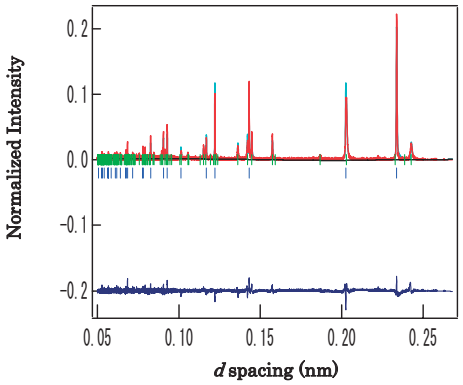

Figure 3. Rietveld refinement patterns using iMATERIA for cathode of $Li_{0.613}Ni_{0.8}Co_{0.19}Cu_{0.01}O_2$ (after charging, Raw-BKG). The vertical marks indicate positions of allowed Bragg reflections. The curve at the bottom is the difference between the observed and calculated intensities on the same scale.

In summary, the results of this study demonstrate that it is possible to perform ex-situ structural analysis by time-of-flight neutron diffraction of only 8.5 mg of an active material in a cathode together with the cathode fabrication materials. It will also be possible to perform crystal structure analysis of such cathodes during charge – discharge cycle by in situ neutron diffraction.

References

[1] R. Keith, V. G. Gibbs and H. P. Ribbe, Science, **172**, 567 (1970).

[2] Y. Idemoto, Y. Tsukada, N. Kitamura, A. Hoshikawa and T. Ishigaki, Chemistry Letters, **40**, 168 (2011).

Y. Idemoto[1], N. Kitamura[1], and T. Ishigaki[2]

[1]Department of Pure and Applied Chemistry, Tokyo University of Science; [2]Frontier Research Center for Applied Atomic Science, Ibaraki University

Developments of an In-Situ SEOP Polarized ^{3}He Neutron Spin Filter System at J-PARC

1. Introduction

Polarized ^{3}He gas functions as a neutron spin filter (NSF) based on the following ^{3}He characteristics: a ^{3}He atom only absorbs neutrons in the opposite spin state to that of the ^{3}He nucleus while the scattering cross section is small. We developed a compact in-situ spin exchange optical pumping (SEOP) [1] NSF system to use as a polarizer for incident beams and performed a neutron beam test. We also demonstrated a polarized neutron scattering experiment using the NSF system.

2. Design of Optics

Figure 1 shows a schematic drawing of the optics design. The optics are put in a laser shield box with a size of 55 × 40 × 60 cm^3, which is made of black anodized aluminium boards for laser safety. The linear polarized laser beam emitted from the laser diode passes through the half-wave (λ/2) plate to rotate the direction of polarization. The polarizing beam splitter (PBS) separates the laser beam into the p-phase and the s-phase components. Then the p-phase and s-_phase components are sent to an external cavity and beam transform optics, respectively. The external cavity controls the wavelength to the Rb D_1 resonance line (794.7 nm) and reduces the bandwidth of the laser to 0.17 nm [2]. The beam transform optics enlarges the laser beam spot size enough to illuminate the entire cell and converts the linearly polarized laser into circularly polarized laser light using quarter-wave (λ/4) plate.

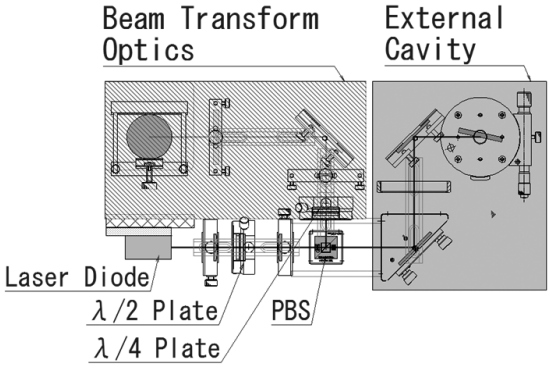

Figure 1. Design of the laser optics.

3. Neutron Beam Test

We performed a neutron beam test at the NOP beamline of JRR-3. The NOP beamline can provide a highly polarized neutron beam (P>99%) with a wavelength of 0.8nm. Figure 2 shows the time development of the ^{3}He polarization of in-situ SEOP NSF system. The beam test continued for 27 hours. The ^{3}He polarization was considered to be saturate at 65.3%. We continue to develop the in-situ SEOP NSF system to obtain higher ^{3}He polarization.

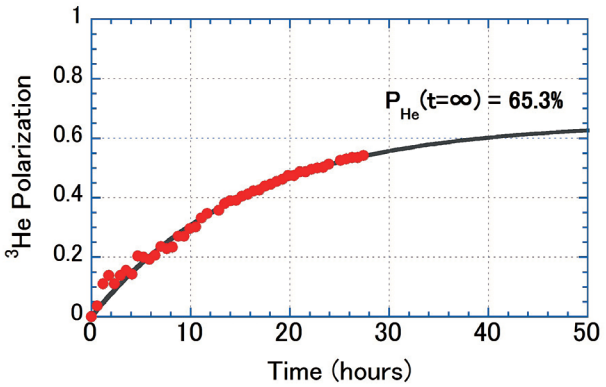

Figure 2. Time dependence of ^{3}He polarization on optical pumping.

4. Demonstration

We demonstrated a polarized neutron scattering experiment at the BL10 beamline of J-PARC. Figure 3(a) shows the experimental setup of the experiment. We chose Ni as the sample because of its ferromagnetism. The sample has the cylindrical shape with 8mm in diameter and 40mm in length and we applied to it a magnetic field of 3500 G. A neutron beam monitor, the NSF system and Ni rod sample were located at 12.6, 13.0 and 14.0 m distance from the moderator, respectively. The NSF was used as a polarizer for incident beam polarization. The beam size was set to 12 × 12 mm^2. A neutron spin flipper,

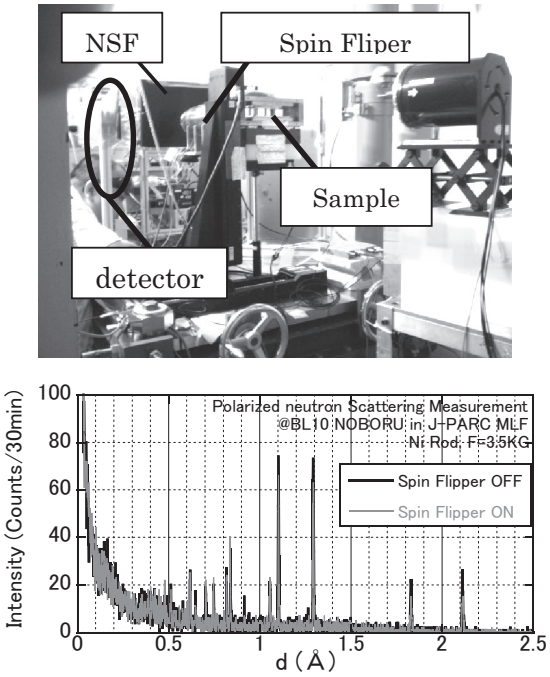

Figure 3. (a) Experimental setup of the polarized neutron scattering experiment and (b) diffraction patterns of ferromagnetic Ni measured with polarized neutron beam.

which could reverse the neutron spin state, was located at the downstream of the NSF. A ^{3}He detector was located 0.8 m far from the sample and at a scattering angle of 170°. Figure 3(b) shows the diffraction patterns of the Ni. All the observed peaks can be indexed to the bulk Ni. A significant difference was observed between two diffraction patterns measured with spin flipper on and off. The difference between the two diffraction patterns seems to be due to magnetic reflections of the ferromagnetic Ni. We are analyzing the data in detail.

References

[1] T. G. Walker and W. Happer, Rev. Mod. Phys. **69,** 629 (1997).

[2] Y. Arimoto, T. Ino, H. M. Shimizu *et al.*, PhysicaB, in press.

H. Kira[1], Y. Sakaguchi[2], T. Oku[3], J. Suzuki[3], M. Nakamura[3], M. Arai[3], K. Kakurai[1], Y. Endoh[1], Y. Arimoto[4], T. Ino[4], L. J. Chang[5,6], and T. Kamiyama[3,4]

[1]Quantum Beam Science Directorate, JAEA; [2]Comprehensive Research Organization for Science and Society; [3]Materials and Life Science Division, J-PARC Center; [4]High Energy Accelerator Research Organization; [5]Nuclear Science and Technology Development Center, National Tsing Hua University, Taiwan; [6]Department of Physics, National Cheng Kung University, Taiwan

ANNRI Project Team Wins the 2011 AESJ Award

The 2011 Technical Development Award of the Atomic Energy Society of Japan (AESJ) was presented to the ANNRI project team, which is composed of the researchers of Hokkaido University, Tokyo Institute of Technology, and Japan Atomic Energy Agency [1]; the title of the award is "Development of Accurate Neutron- Nucleus Reaction Measurement Instrument". This award evaluates how superior accomplishments have been achieved in large scale technological developments for the peaceful use of atomic energy. This is the first time that the researchers have received this honor for research performed at J-PARC.

Figure 1. The 2011 Technical Development Award of the Atomic Energy Society of Japan.

ANNRI is the abbreviation of Accurate Neutron-Nucleus Reaction measurement Instrument. It was constructed to supply accurate neutron capture cross sections of minor actinides and fission products required for developing innovative nuclear systems.

The ANNRI project team has developed a neutron beam line optimized for neutron time-of-flight experiments, advanced Ge and NaI spectrometers for detecting prompt γ rays, and a measurement method for neutron capture cross sections. The team has started the measurements of neutron capture cross sections since 2009, and successfully obtained the neutron capture cross section of ^{244}Cm at the resonance energy region in 2010 [2]. This is the first experiment of its kind in the world, except the nuclear bomb experiment. It was achieved by using the world's strongest pulsed-neutron beam.

Figure 2. Inside of the J-PARC/MLF/ANNRI, where the Ge spectrometer is shown at the center.

Those achievements were recognized in the world. They were presented at the nuclear data conference, ND2010, as a keynote talk and also as an invited talk.

To commemorate the accomplishment of the ANNRI, a memorial symposium was held in February 2011 in Tokai. About 60 scientists in the field of nuclear data, nuclear astrophysics, and trace element analysis got together at the symposium, and discussed the possible future use of the ANNRI. The ANNRI will be open for researchers in these fields under the MLF user program from February 2012 [3].

References

[1] http://www.aesj.or.jp/awards/H22gakkaisyo.pdf.

[2] S. Goko, A. Kimura, H. Harada, *et al.*, J. Nucl. Sci. Technol. **47**, 1097 (2010).

[3] http://j-parc.jp/MatLife/en/applying/koubo.html.

Figure 3. A photograph of scientists, who attended the memorial symposium, on the ANNRI.

H. Harada[1], A. Kimura[1], K. Furutaka[1], S. Goko[1¥], M. Igashira[2], T. Kamiyama[3], T. Katabuchi[2], T. Kin[1], K. Kino[3], F. Kitatani[1], Y. Kiyanagi[3], M. Koizumi[1], M. Mizumoto[2], S. Nakamura[1], M. Ohta[1$], M. Oshima[1], and Y. Toh[1]

[1]Nuclear Science and Engineering Directorate, JAEA; [2]Research Laboratory for Nuclear Reactors, Tokyo Institute of Technology; [3]Graduate School of Engineering, Hokkaido University; Present address [¥]Hokkaido University, [$]Osaka University.

Improvement of Muon Beam Transport at D-Line

1. Introduction

The first beamline in MUSE was designed to transport the muons from decay-in-flight pions. The front-end part of this decay-muon beamline (D-line) is in an M2-tunnel, and is connected to the downstream part in experimental hall #2 through the 6-m super conducting solenoid magnet as the pion-to-muon decay section. The front-end magnets are operated under high radiation field due to the muon production target, that's why they were newly designed and installed, while the other magnets, located downstream from the solenoid including the solenoid itself, were relocated from the Tsukuba campus, KEK in order to reduce the construction cost. 15 quadrupoles, 2 dipole magnets and a wien filter (DCsep) were assembled in the downstream, as shown in Fig. 1. These magnets had been used in a few different beamlines, and thus their bore radii and field lengths are different from one another. This caused a constraint of the beam transmission in the D-line. Namely, muon beam loss occured at small bore magnets.

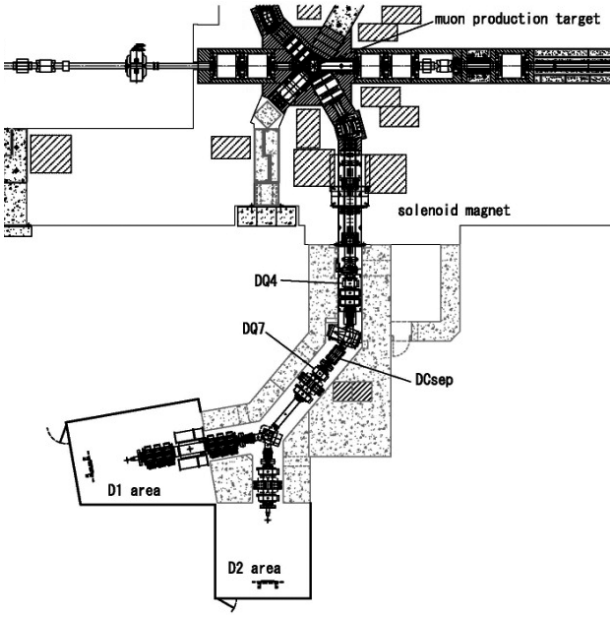

Figure 1. A cross-sectional view of D-line.

To increase the beam transmission efficiency, a wien filter (DCsep) was replaced with a wide-gap, 200 mm, one in the last fiscal year [1]. In this fiscal year, the electric-field power supplier of DCsep was replaced with a higher-voltage one, and two limiting quadrupole magnets, DQ4 and DQ7, were replaced with large-bore, ϕ300 mm, ones. The replacement work was done during the summer shutdown, and the commissioning works, aging of the wien filter and beam tuning were performed in the autumn-cycle of 2010. We will report the progress in this article.

2. Installation of New Magnets

The replacement work was done in August, and it took about three weeks. DQ4 is a part of the DQ456 triplet, so this triplet was removed from the beamline, and then overhauled to install a new DQ4 and a new vacuum duct, as well as DQ7. A part of the old DQ4 was slightly activated below 1 μSv/h.

Figure 1. DQ456 triplet installation.

3. Beam Tuning Results

The map of the magnetic field was measured before installing. The effect of the fringing field was not negligible for a thin magnet like DQ4 and DQ7. Thus, taking the measured fringing field into account, the beam envelope was evaluated through optics calculations. Figure 2 shows a typical result

of the surface muon transmission to the D2 area. The improvement due to the new DCsep and DQ7 is clearly seen. DQ4 plays an important role to capture the decay muons at the exit of the solenoid.

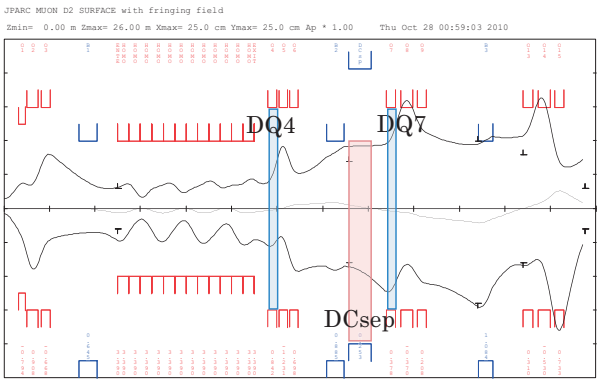

Figure 2. The evaluated beam envelop for surface muons to the D2 area by TRANSPORT.

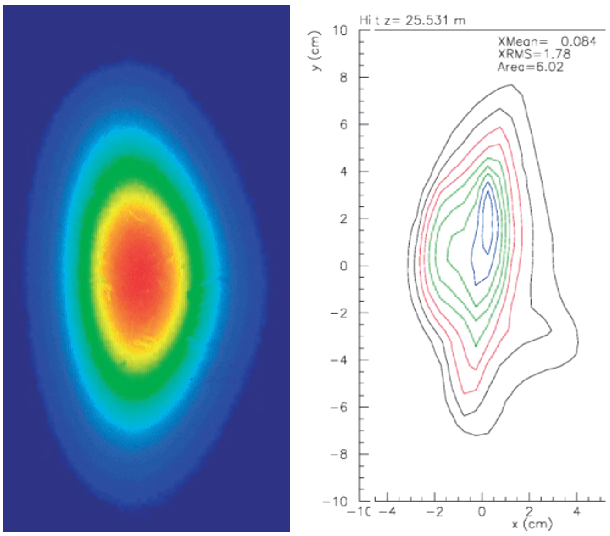

Figure 3. A typical beam profile obtained by imaging plate. σ_x=14mm and σ_y =28mm (left) and the result of TURTLE (right)

According to the beam envelope calculation, beam tuning was performed, and the beam profile became much sharper than before, as shown in Fig. 3. This was consistent with the Monte-Carlo calculation. The beam intensity was also measured to be 3.1×10^6 surface muons per second under 220 kW proton beam. The 50-MeV/c decay muon beam intensity was around one third of the surface one, and the positive and negative muon beam intensity was almost the same. This result is unexpected from the point of view of a previous estimation based on a pion production model, but it is certainly good news for researches who use negative muons.

3. Summary

The new magnets installed in the D-line dramatically improved the muon beam intensity and its profile. However, the tendency of the beam intensity was found to be inconsistent with the calculations. Especially, the negative muon intensity is much higher than expected. Further investigation will be performed to clarify the origin of this mystery.

References

[1] K. Nishiyama *et al.*, MLF Annual Report 2009, 105.

N. Kawamura, K. Ninomiya, H. Fujimori, Y. Kobayashi, K. Nishiyama, and Muon Sci. Sec.
Materials and Life Science Division, J-PARC Center

Development of New Positron/Electron Detector System for Pulsed μSR

At pulsed muon facilities, muons come in a pulse of a time width of several ten nano-seconds. The time differential muon spin relaxation (μSR) measures the relative time from the muon coming and the decay positron/electron events in the muon decay $\mu^{\pm} \rightarrow e^{\pm} + \nu$. The requirement for the positron/electron detectors for pulsed μSR is a minimum countloss, despite the huge event rate right after the arrival of the muons. The Decay muon channel (D-line) of MUon Science Establishment (MUSE) delivers 180,000 positive muons per pulse at D1 experimental area for 300 kW operation [1]. These muons decay into positrons with an average life time of 2.2 micro-seconds, resulting in an average count-rate of 180,000/2.2 μs ≈ 100 giga counts/second (Gcps) for the entire solid angle.

The general purpose μSR spectrometer (DΩ-1) installed at the D1 experimental area currently has 128 segmented counter pairs (256 single counters), covering approximately 8% of the solid angle around the sample. With the full beam, the average count-rate for each counter yields $100 \times 10^9 \times 0.08/128$ = 60 Mcps. This is still a high-rate because each counter experiences approximately 60Mcp × 2.2 μs ≈ 120 counts/pulse, which corresponds to 2.2 μs /120 ≈ 20 ns for the average event separation. This event separation is comparable with or shorter than the typical recovery time of photo-multiplier-tubes (PMTs: ~20 ns) or avalanched photo diodes (APDs: ~ 40 ns), and we reduce the muon beam intensity to ~ 1/10 by collimators and slits, so that the event-rate may be handled by the existing detectors. In order to enjoy the high beam intensity of pulsed muons at MUSE, the DΩ-1 spectrometer has to realize much higher counting rate by tiling smaller counters and much larger solid angle coverage with affordable cost.

In JFY 2010, we developed a prototypical detector system, which can sit on a palm-top and were able to observe μ-e decay time spectrum (Fig.1). It is composed of three blocks: a detector block, analogue board and digital board.

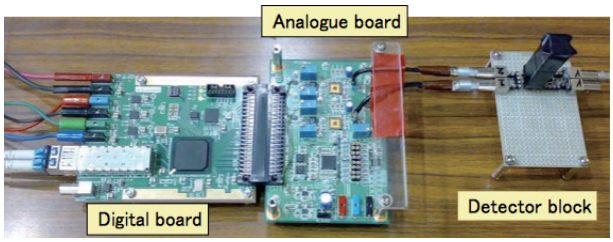

Figure 1. Prototypical new positron/electron detector system and the schematic strucuture of the counter pair.

The detector block is composed of plastic scintillator, wave-length shifting fiber and a multi-pixel avalanched photo diode (APD), specifically, Multi-Pixel Photon Counter (MPPC) made by Hamamatsu Co. Ltd. The m-APD has some major advantages, such as lower cost (~40 dollars/channel) and higher tolerance to magnetic fields (~Tesla) over usual PMTs.

The largest advantage of our new detector system is that the electronics (the discriminator, TDC and memory) are built in as the front-end circuit. The analogue board of the prototype will be integrated into the next generation ASIC chip which is currently being fabricated [2].

The main component of the digital board is the Field Programable Gate Array (FPGA) which is the largest black chip in Fig.1. The time-to-digital converter (TDC) counts up clocks starting at the LEMO input signal and the event timing is recorded into the memory configured in FPGA. The stored event timing is read from the memory, formed into ethernet packet and sent to data acquisition DAQ-PC as a series of SiTCP packet [3]. The packet structure of the new detector is set in exactly the same way as that of the existing DAQ at DΩ-1 spectrometer, and hence, the new detector will seamlessly merge with and be able to replace the existing PMT based detectors.

In Fig.2, the first time spectrum taken in this prototypical detector system is shown. Beam intensity was reduced to that for typical measurements with the existing detectors. The μ-e decay lifetime

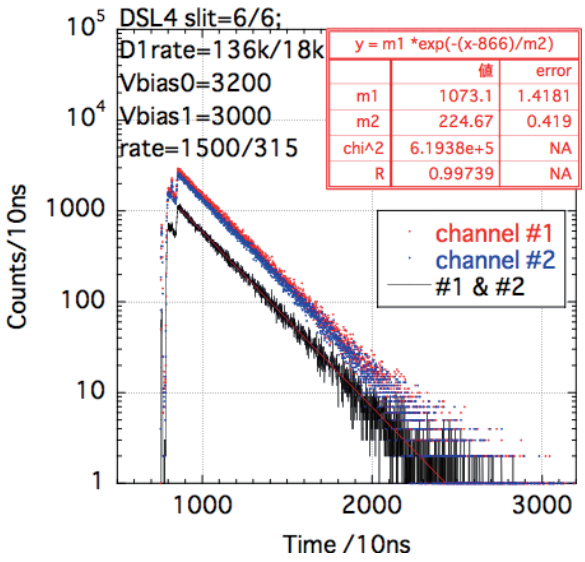

Figure 2. The first μ-e decay time spectra taken by the prototypical detector system.

of coincidenced spectrum (#1 & #2) is estimated to be 2.24 μs, which is a reasonable value without a count-loss correction. One lucky finding is that a single counter without coincidence (channel #1 or #2) already gives a background and distortion-free μ-e decay signal, thanks to the small scintillator size. This may open a path to an easier design of a spectrometer without counter coincidence.

References

[1] Yomiuri News Paper Ibaraki-ed., March 16 (2010).

[2] M. Tanaka, specification memo of ASIC x10Amp2011 (2011).

[3] T. Uchida, IEEE Trans. Nucl. Sci. **55**, 1631 (2008).

K.M. Kojima[1,2], A. Koda[1,2] S.Y. Suzuki[3], R. Kadono[1,2], M. Miyazaki[2], M. Hiraishi[2], T. Murakami[4], M. Ikeno[4], M. Saito[4], T. Uchida[4], and M. Tanaka[4]

[1]Institute of Materials Structure Science, High Energy Accelerator Research Organization (KEK-IMSS) and J-PARC; [2]Department of Materials Structure Science, The Graduate University for Advanced Studies (SOK- ENDAI); [3]Computer Research Center (KEK-CRC); [4]Institute of Particle and Nuclear Study (KEK-IPNS); All are members of Open Source Consortium of Instrumentation: http://openit.kek.jp

μSR Study on Materials Potentially Applicable for Future Automobiles

1. Introduction

Secondary batteries and fuel cells are thought to be key components for future automobiles. Therefore, the materials concerning these components are naturally good targets for μSR measurements, particularly because μSR provides microscopic magnetic information on such materials. We have thus initiated μSR studies of battery materials since 2005 and of fuel cell materials since 2003. Here, we wish to summarize the current situation of our research of these materials.

2. Battery Materials

Since lithium-ion batteries (LIB) posess the highest energy density, a "secondary battery for future automobiles" is most likely an equivalent to "LIB" at present. The basic principle behind the operation of LIB is a reversible intercalation/deintercalation of Li^+ ions in solids. A self-diffusion coefficient of Li+ (D_{Li}) is, thus, one of the crucial physical parameters to determine the charge/discharge rate of LIB. Although Li-NMR is a powerful tool to detect D_{Li} in solids, a reliable D_{Li} has been never obtained for positive electrode materials, because of the effect of magnetic ions on the spin-lattice relaxation rate.

On the contrary, we found that μSR clearly detects the change in the internal magnetic field due to Li diffusion through a dynamic Kubo-Toyabe behavior. Furthermore, the magnitude of D_{Li} estimated by the field fluctuation rate (ν) for Li_xCoO_2 [1] was comparable to the predicted value from the first principles calculations. Since then, we have made systematic experiments for clarifying D_{Li} for several positive electrode materials (Fig. 1).

3. Fuel Cell Materials

Complex borohydrides and related materials are possible candidates for future onboard hydrogen storage materials; [2] however, their slow dehydrogenation kinetics and high hydrogen desorption temperature (T_d) need to be drastically improved, if they are to enable a practical hydrogen storage system. We have, thus, investigated the nature of borohydrides and related compounds by μSR [3].

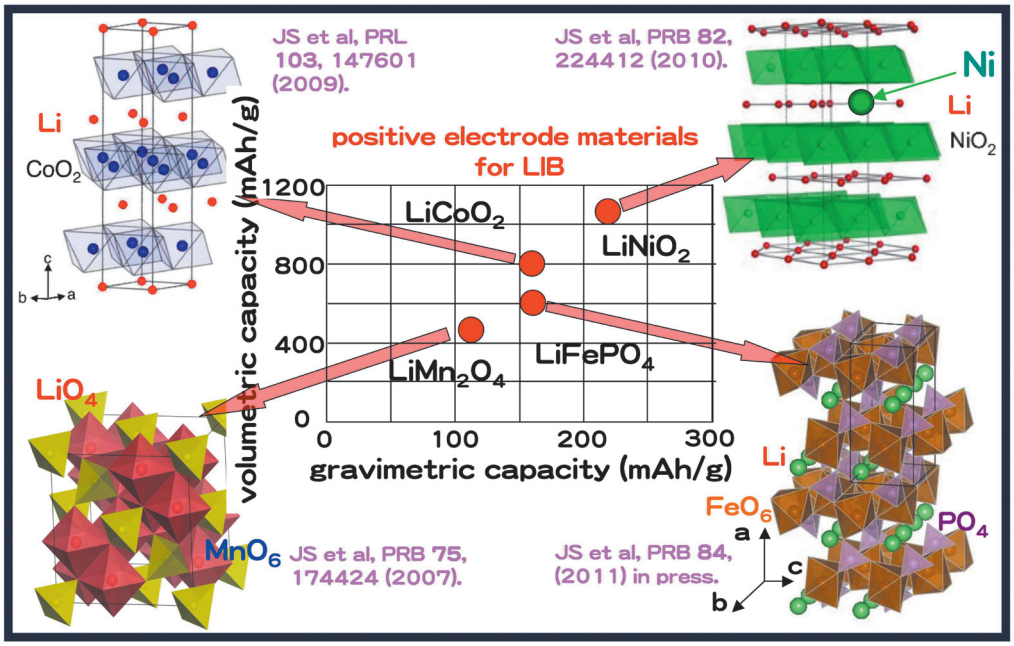

Figure 1. Several positive electrode materials for LIB and our μSR work on them.

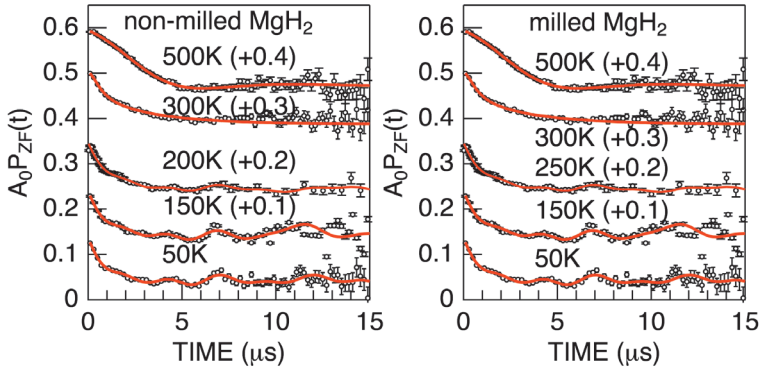

Figure 2. *T* variation of the ZF-spectrum for (left) non-milled MgH_2 and (right) milled MgH_2.

Particularly, for a very simple system, MgH_2, we have found a drastic change in the ZF-spectrum by milling, probably due to the formation of H-μ/H-μ-H bonds on the new surface (Fig. 2). In order to clarify the interrelationship between the H-μ/H-μ-H bonds and T_d, we need additional experiments at temperatures below the vicinity of T_d (= 550-650 K).

References

[1] J. Sugiyama *et al.*, Phys. Rev. Lett. **103**, 147601 (2009).

[2] L. Schlapbach and A. Zuttel, Nature **414**, 353 (2001).

[3] J. Sugiyama *et al.*, Phys. Rev. B **81**, 092103 (2010).

J. Sugiyama
Toyota Central R&D Laboratories, Inc.

Neutron Source

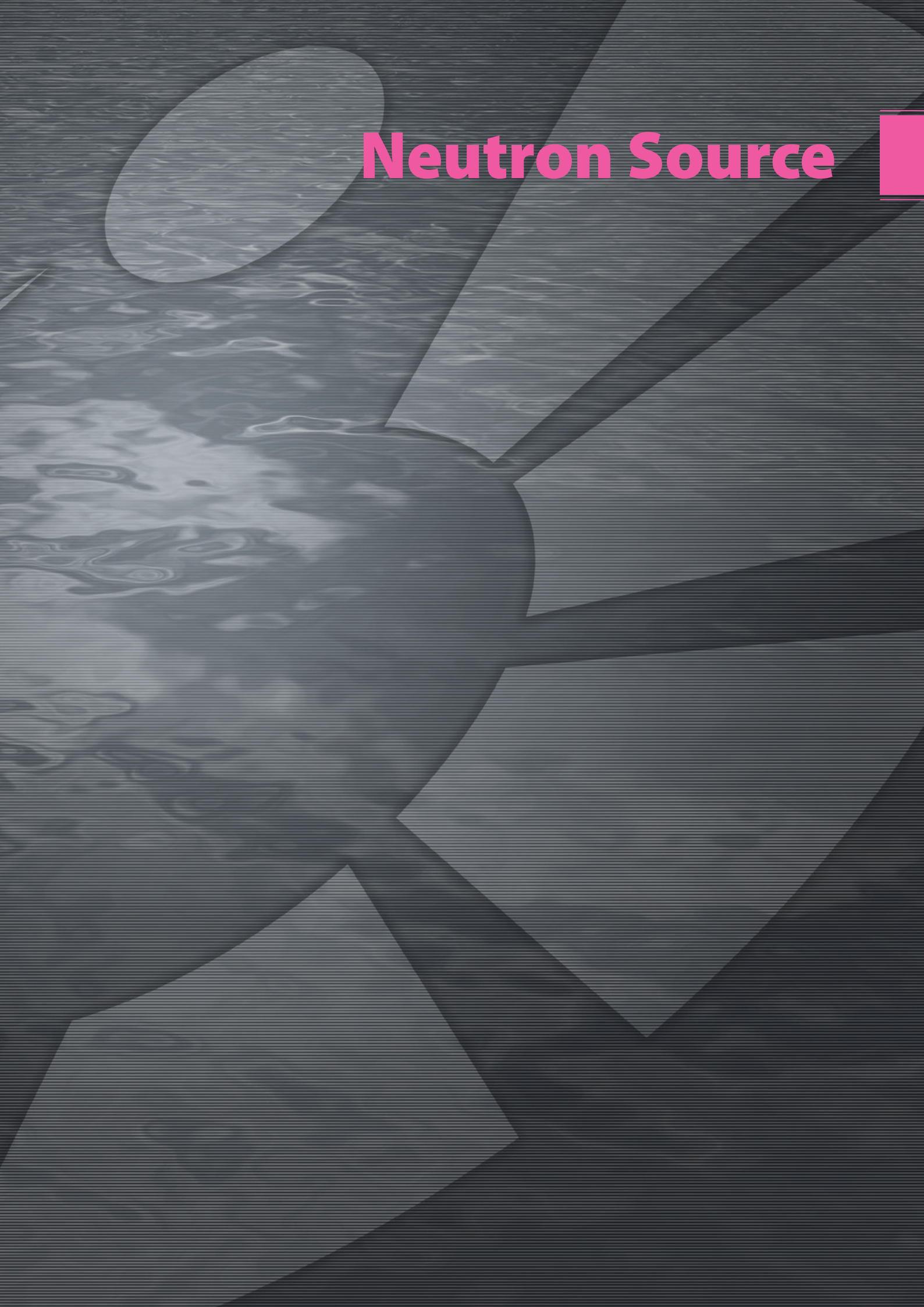

Very High Intense Proton Beam Commissioning

In November 2009, we started to deliver 120-kW proton beam to the target with the remarkably high availability of about 90%. In a short test about 1 hour, we demonstrated the capability of 300-kW beam operation to the spallation neutron source. We confirmed that the beam loss was very small and the operational beam status was very stable. Even after a beam operation at 300 kW, the residual dose in the beam transport system was as small as the background level. Since November 2010, we had carried out the beam operation with the power of 200 kW. As a trial case, the beam acceleration and extraction capability was demonstrated at the 3-GeV Rapid Cycling Synchrotron (RCS) with beam power of 450 kW for several shots on the beam dump located at the extraction of the RCS.

As the beam power increases, precision beam tuning is required in order to avoid the high residual radiation caused by beam loss around the beam duct and the magnets. On the other hand, it is better to minimize the duration for beam tuning in order to increase the beam time required by the users. In order to perform the beam tuning efficiently, we developed an expert beam operation system, which simulated the beam status from the result of the beam position obtained by the beam monitors. Through the result of the simulation code of the MAD, the correction angle for the beam can be obtained at the steering magnets so that the correction currents at the steering magnets could be supplied automatically. By using the present system, the beam tuning period was decreased drastically.

At the SNS in ORNL, a pitting damage was found at the mercury target vessel after the completion of a beam operation. Until the summer of 2010, we did not have any spare mercury target vessels. Without a spare target, if the vessel was broken, the beam had to stop operating for a long period of time to fabricate a new vessel. We maintained the beam power at 120 kW before the preparation of the spare target.

With the increase of the beam power, the beam profile becomes more important. We continued the development of the proton beam profile on the target by the activation technique using an imaging plate (IP). Through remote handing, the IP is directly attached to the target vessel. The IP was delivered to the target by a crane and attached to it with the help of manipulators. The typical duration of the exposure time was 5 min. After the exposure, the image of the radiation was read out by the reader of the IP.

In Fig. 1, we show the beam profile result obtained by the IP after 200 kW beam irradiation in December 2010. In the distribution, it was observed that a clear Gaussian peak exists without tilting. We should note that the result was obtained after 6 days of cooling time for residual radiations. It was demonstrated that the present technique can give reliable profile without saturation of the radiation for 1 MW operation with certain cooling period. Simultaneously, a thermo luminescence dosimeter (TLD) was placed on the IP holder. Unfortunately, the dose observed by the TLD was saturated, which implied that the radiation was higher than 16 Sv/h at the target center.

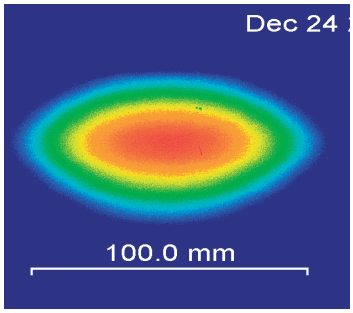

Figure 1. Beam profile after 200 kW operation.

During beam operation, the beam profile was continuously measured by the multi wire profile monitor (MWPM) located on the proton beam window. To obtain a long life time of the target, we expanded gradually the beam size through an in-

crease of the beam power. The measurement of the beam width obtained by the IP and the MWPM showed good agreement, which implies that a reliable beam profile can be obtained on time by the MWPM.

It was a well-known fact that the damage to the target vessel caused by the beam was proportional to 4th power of the peak intensity. Therefore, careful beam tuning was required to avoid the damage to the target. As the profile expands, the heat deposition around the target increases mainly due to the beam halo, which is difficult to observe. We have developed a new technique to observe the heat deposition at the target vicinities by using the beam halo monitor made of thermocouples. Before prolonged beam operation, the heat deposition was obtained by measuring the temperature rising speed at the vicinities. It was confirmed that the heat deposition at the vicinities was 0.3 W/cc which was smaller than the allowable level of 1 W/cc. By confirming the heat deposition, we can confidently perform 0.2 MW beam delivery with the low peak heat deposition of 1.7 J/cc/pulse.

We are proud and honored that thanks to the proper operation of the beam transport system, the beam was not stopped for long periods of time in JFY 2010. During the beam study period, we observed some minor problems with the power supplies of the magnet, however, these troubles did not interrupt users' beam time period. In JFY 2011, we will increase the beam power for users to about 300 kW.

The earthquake on March 11th caused profound damage to the beam transport system. For example, the beam tunnel wall significantly collapsed and the magnets were displaced. After repairing the wall and restoring the alignment of the magnets, we will begin beam operation at a power level of about 100 kW.

S. Meigo, M. Ohi, K. Ikezaki, A. Akutsu, H. Fujimori, and S. Sakamoto
Materials and Life Science Division, J-PARC Center

Mercury Target System

1. Overview of the Target Operation in JFY 2010

Until November, the target system consisting of a mercury target vessel, mercury circulation system and target trolley operated with 120 kW proton beam power, then the power was increased to 210 kW. The system could be operated without any unusual phenomena such as an unexpected temperature rise of the mercury, pressure increase in the system and a drop of the mercury flow rate until March 11 2011 when the big earthquake occurred.

We proceeded developing a pressure wave mitigation technique. The pressure waves are generated in mercury by rapid thermal expansion caused by proton beam bombardment. They induce the cavitation pitting/erosion damage to the mercury target vessel which shortens substantially the lifetime of the target vessel. A microbubble injection into mercury mitigates the pressure waves and the damage because microbubbles act as an absorber against thermal expansion. A new target vessel with microbubble injector is being fabricated, which will be installed into the system in October 2011.

2. Earthquake Report

Mercury Circulation System

The mercury circulation system (MCS), which provides flowing mercury for the target vessel and removes heat generated in the mercury target, mainly consists of the surge tank, a permanent magnet rotating type induction pump (PM pump) [1] and a heat exchanger. When the big earthquake occurred, mercury flowed with proper flow rate, 41 m^3/h but the proton beam was not injected to the mercury target system.

Figure 1 shows the time histories of the mercury flow rate, the motor torque of the pump, the pressure in the system and the mercury level in the surge tank. The big earthquake occurred at 14:46. The electric power stopped 2 min after the earthquake and then the motor and mercury flow stopped. The pressures at inlet, P_{in}, and outlet, P_{out}

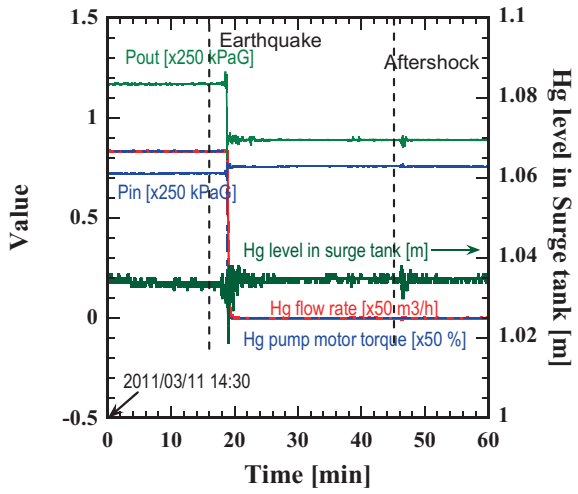

Figure 1. Time histories of process values in mercury circulation system.

were changed by the pump stopping. P_{out} dropped down due to lack of pump discharge force and P_{in} rose up due to lack of pump suction force. The mercury level did not change between before and after the earthquake which indicates no leak of mercury from the system. A big aftershock occurred at 15:15. In the histories of the level and pressures, intense vibration was observed which was caused by big seismic motions.

Target Vessel and Target Trolley

When the big earthquake occurred, the target system was at beam operation position. In normal operation, the position of the target trolley is locked by the rod fixed to the floor, which engages with the detent fixed on the target trolley. The rod is raised up by the air cylinder, and stops the target trolley from moving by the pushing force of the pillow seal mounted on the target vessel as shown in fig. 2. Under the strong seismic motion, the pressurized air supply line to the air cylinder was broken and the rod went down by its own weight releasing the target trolley. Since the helium gas supply to the pillow seal still continued, the bellows of the pillow seal inflated pushing the target trolley backward, and fi-

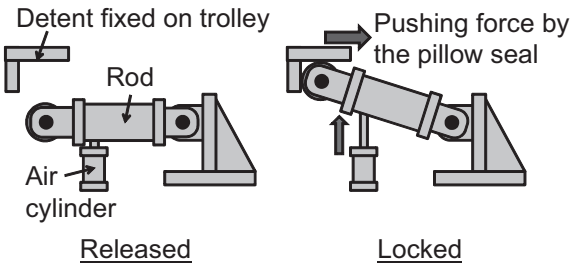

Figure 2. Movement of the target trolley lock system.

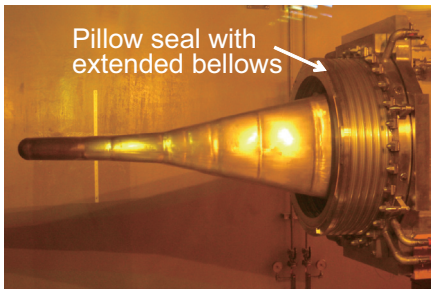

Figure 3. Pillow seal mounted on the target vessel with extended bellows.

nally the bellows were broken. Figure 3 shows the target vessel with the damaged pillow seal on it. The length of the bellows extended 200 mm longer than the normal length of 100 mm.

The target vessel will be replaced by a new one in 2011, in which we will install a pressure wave mitigation system, such as microbubble injection system into mercury.

Reference

[1] H. Kogawa, *et al.*, Nucl. Inst. and Meth. in Phys. Res. A **600** 97-99 (2009).

H. Kogawa, K. Haga, and T. Wakui
Materials and Life Science Division, J-PARC Center

The Cryogenic Hydrogen System

1. Introduction

The cryogenic hydrogen system provides supercritical hydrogen at 18 K and 1.5 MPa to three moderators of JSNS, and absorbs nuclear heating of about 3.8 kW generated in these moderators. The system consists of a helium refrigerator system and a hydrogen circulation system as shown in Fig. 1 [1]. One of the unique features of the cryogenic hydrogen system is that the pressure fluctuation in the closed hydrogen loop caused by switching the proton beam on and off, is mitigated by a hybrid pressure control system consisting of an accumulator and a heater. The accumulator uses variable volume to passively absorb the volume fluctuation while the heater compensates the heating power during the beam off mode. Another unique feature is the adoption of a pair of centrifugal type pumps for hydrogen circulation.

When we operated the system in 2008-2009 operations, we struggled with some troubles in the hydrogen pumps: excessive vibration of the rotor shafts and extreme cooling of the pump flanges, which should be kept at room temperature. As a result of the appropriate steps we took to resolve the problems, the operation of the hydrogen pumps was quite stable throughout the Japan Fiscal Year (JFY) 2010. However, we encountered two other challenges we need to overcome in JFY 2010: an accumulator failure and some impurities in the helium refrigerator system. Figure 2 shows the operation history of the cryogenic hydrogen system in JFY 2010.

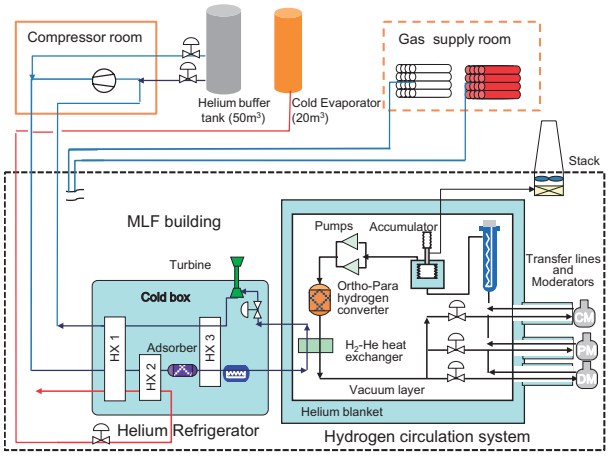

Figure 1. The cryogenic hydrogen system.

2. Recovery from the Accumulator Failure

In the beginning of February 2010, we discovered leakage in the accumulator bellows. It was a serious leakage because the boundary function between the hydrogen and the helium regions was lost. The user service operations in February and March (Runs #30 & #31) were cancelled to take emergency measures against the trouble. Although the accumulator is indispensable for operations under 1-MW beam power, our analysis showed that

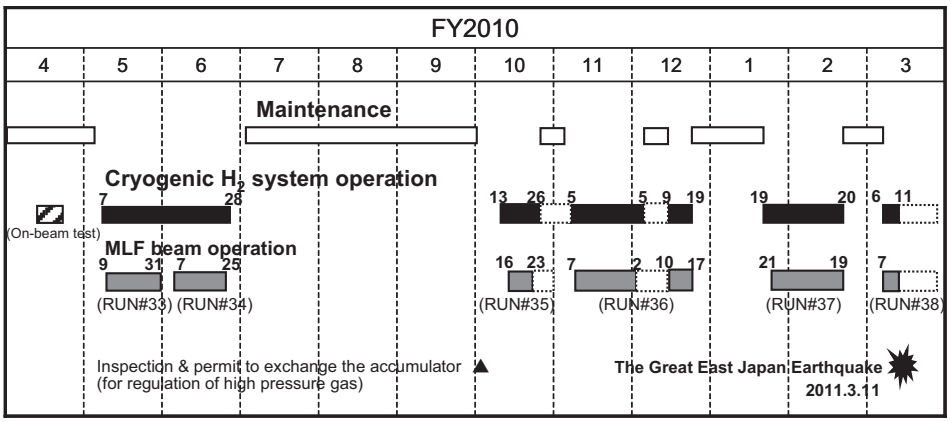

Figure 2. Operation history in JFY 2010.

we could operate the system without the accumulator function but only with the heater control under the beam power at that time, 120-kW. The idea was confirmed to be valid through an on-beam commissioning operation in April. The pressure rise for the 120-kW operation was 40 kPa, which was 10 times higher than that under normal conditions, but still below the design limit value of 50 kPa as expected (see Fig. 3) [2]. Accordingly, a two-cycle, 37-day operation at 120-kW was executed successfully in May and June (Runs #33 & #34).

The failed accumulator was replaced with a new one during the summer shutdown period. To decrease the mechanical load to the bellows and to improve its maintainability, the variable volume of the accumulator bellows was reduced from 16 L to 6 L. Figure 4 shows photographs of the new and old accumulators and the inside of the hydrogen cold box. After the replacement, we carried out an on-beam commissioning operation to confirm that

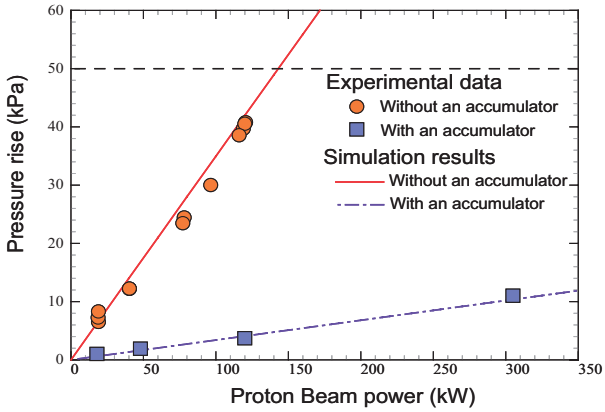

Figure 3. The hydrogen pressure rise for the proton beam power.

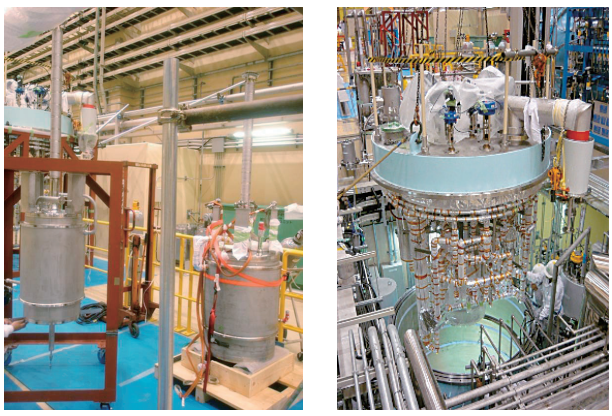

Figure 4. The new and old accumulators and the opened hydrogen cold box.

the new accumulator was functioning properly. The pressure rises were 4 kPa and 8 kPa for the 120-kW and 220-kW proton beam operations, respectively, as expected. Then, on October 15, the MLF user operations for Run #35 were finally resumed.

3. Impurity Issue in the Helium Refrigerator

From October through December (Runs #35 & #36) we had to halt the operation twice due to heat exchange degradation in the helium refrigerator system. Contamination caused by impurities (most likely water vapor) in the helium gas was the possible reason. A new charcoal filter in the helium refrigerator, which was exposed to ambient air during exchanging work during the summer shutdown period, could be the source of the impurities.

During the October operations, a pressure drop in the heat exchanger increased gradually as shown in Fig. 5 probably due to water adhesion to heat exchange surfaces. This caused decrease in the thermal conduction through the heat exchange surfaces and then increase in the outlet temperature of the heat exchanger. We tried to stabilize the outlet temperature by introducing liquid nitrogen pre-cooling. However, the pressure drop and the outlet temperature kept on increasing until they forced a system halt. The cryogenic hydrogen system was once warmed up for recovery. The heat exchanger was purged using dry nitrogen gas. The charcoal filter was regenerated using hot dry nitrogen gas. After a dew point at the outlet of the charcoal filter was reduced to -57 degrees C, the cryogenic operation resumed for Run #36. Despite the fact that the conditions improved, the cryogenic hydrogen system needed another halt in December during Run #36 for recovery.

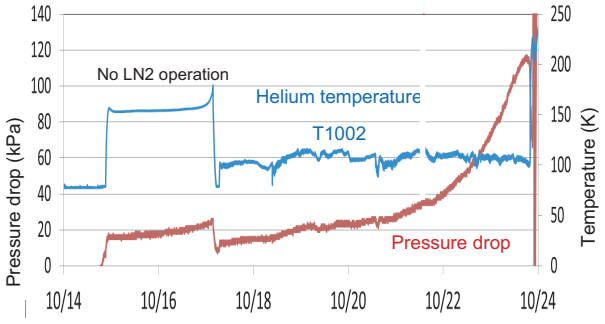

Figure 5. Pressure drop and helium temperature of the outlet of the heat exchanger at Run #35.

After Run #36, we worked even during the New Year's holidays to regenerate thoroughly the charcoal filter and some other components and remove the impurities from the system. Because of those efforts, we were able to operate the cryogenic hydrogen system almost stably from late January to March 11 (Runs #37 & #38). The pressure drop and the outlet temperature of the heat exchanger could be kept constant during the operations as shown in Fig. 6. As a result of the lessons we learned from the impurity issue, we will introduce a regeneration system, consistng of a cryogenic purification unit, a drier unit and a heater unit, into the helium refrigerator system during the coming summer shutdown period.

4. The Great East Japan Earthquake

At the time of the earthquake, the cryogenic hydrogen system was in operation under the rated condition of 20 K and 1.5 MPa. Several minutes after the beginning of the earthquake, the system was stopped by an interlock signal due to the power failure. The hydrogen gas was discharged safely through a release line as usual. Since the MLF building itself withstood the enormous quake and didn't suffer substantial damage, the damages of the cryogenic hydrogen system in the MLF building were not very serious. However, the ground surrounding the main building subsided severely, which broke the outside facilities. A liquid nitrogen storage tank and a helium buffer tank for the cryogenic hydrogen system, both of which are 2.5 m in diameter and 10 m in height, leaned to a degree and the associated pipes were bent due to the subsidence. We will investigate thoroughly the damages caused by the earthquake, and try to resume the cryogenic operation in 2011.

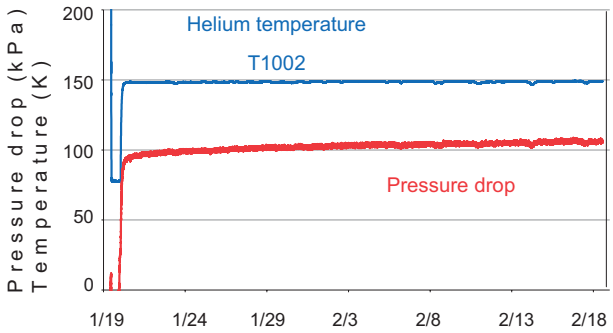

Figure 6. Pressure drop and helium temperature of the outlet of the heat exchanger at Run #37.

Figure 7. Condition of the tanks and the pipes of the cryogenic system outside of the MLF building.

References

[1] T. Kato, *et al.*, Journal of the Cryogenic Society of Japan, Vol.42 No.8 277-264 (2007).

[2] H. Tatsumoto, *et al.*, Advances in Cryogenic Engineering, "Dynamic behavior of the cryogenic hydrogen system using only a heater control", accepted and printing now.

T. Aso, H. Tatsumoto, S. Hasegawa, K. Ohtsu, T. Uehara, Y. Kawakami, and H. Sakurayama
Materials and Life Science Division, J-PARC Center

Neutron Target Station

1. Overview

All the neutron target station components, such as the hydrogen moderators, reflectors, helium-vessel and neutron beam shutters, were operated mostly without serious troubles throughout JFY 2010 but only until the earthquake on March 11, 2011.

The most significant trouble was a control error of the shutter system. On November 8, an encoder attached to a servo-motor to drive one of the 23 shutter blocks failed. The error caused a total of 11 shutters in the 2nd experimental hall to become uncontrollable for 4 hours. The shutter system was restored by resetting the control system with forcing a proton beam outage for half an hour.

Vacuums for many of the neutron beam ducts in the shutter blocks were broken by the earthquake because the bolts fastening a metal O-ring on a duct flange were loosened by the impulsive force. All the ducts are to be recovered by the autumn of 2011 by taking some countermeasures. Despite the tremendous earthquake, this was all of the significant damage we found in the target station.

2. Outstanding Neutronic Performance

The proton beam power was raised to 220 kW in December 2010. The number of neutrons emitted from the coupled hydrogen moderator per unit solid angle per pulse was found to be 3.8×10^{12} [1]. As of 2010, the corresponding neutron intensities in the world's major spallation neutron sources were 4.2×10^{12} at the Spallation Neutron Source (SNS) facility in U.S.A., and 4.0×10^{12} at the ISIS facility in UK (Fig.1). Thus it was confirmed that the neutron intensity achieved at J-PARC was almost comparable with that at the world's major pulsed spallation neutron sources. J-PARC's neutron intensity will eventually be three times that of SNS when the beam power is raised to the rated 1 MW.

The number of pulses per second is suppressed to 25, compared to 60 at SNS, to increase the number of neutrons in each pulse. The unique moderator design represented in its cylindrical shape, which was found through an extensive optimization study on the materials, dimensions, and configurations of the neutron source components, is another reason to push up the neutron intensity.

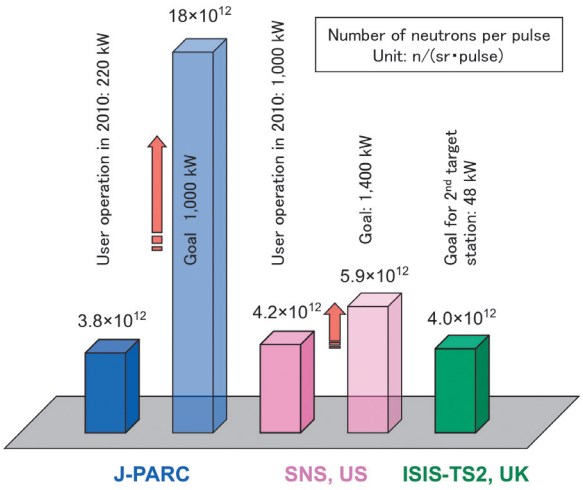

Figure 1. Comparison of neutron intensities of the world's major pulsed spallation neutron sources.

3. R&D on Hydrogen Moderators

Some R&D activities are ongoing to procure spare hydrogen moderators. One of the activities is a development of low activation neutron absorbing material "decoupler", and this topic is described elsewhere in this report (the section for resonance absorption imaging).

Another activity is devoted to facilitating the manufacturability of the moderators because it is not easy to manufacture moderators with thin five-fold coaxial tube structure made of aluminum alloy and stainless steel.

A low thermal expansion material "Invar" is to be introduced to minimize thermal shrinkage of the 4-m long moderator tubes when they are cooled down to 20 K. Weldability and bendability of Invar tubes have been confirmed to be workable. We greatly appreciate the SNS/ORNL team for their useful suggestions on treating Invar.

- A combined component of multiple tubes including a dissimilar joint of aluminum alloy and stainless steel by the hot isostatic pressing method was fabricated successfully as depicted in Fig. 2. This will contribute to the easier concentric alignment and certain airtightness at the joints.
- Dissimilar joints of aluminum alloy and Invar were produced successfully by the friction welding method. According to a series of tensile tests of the joints at 77 K and 300 K (Fig. 3), it was found that the joints are strong enough as the moderator parts are, even at the low temperature.

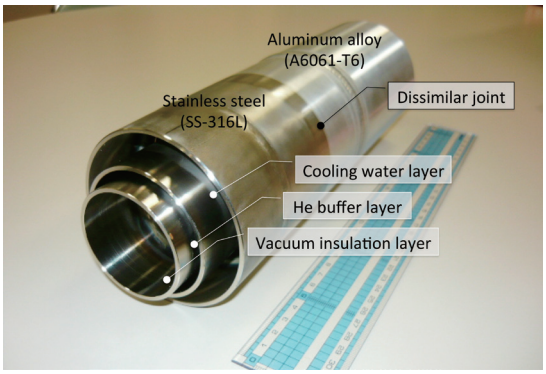

Figure 2. A combined component of triple tubes used for the room temperature region.

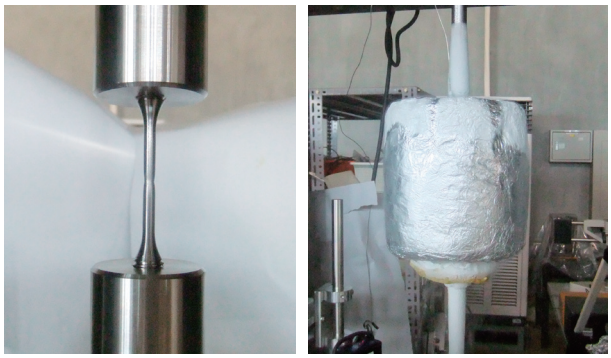

Figure 3. Tensile test at the room temperature (left) and at 77 K in an LN_2 bath (right).

References

[1] F. Maekawa, M. Harada, M. Teshigawara, *et al.*, Nucl. Instr. Meth. A **620** 159 (2010).

[2] M. Harada, M. Teshigawara, F. Maekawa and M. Futakawa, J. Nucl. Mater. **398** 93 (2010).

[3] M. Ooi, M. Teshigawara, T. Wakui, T. Nishi, *et al.*, J. Nucl. Mater., to be published.

[4] M. Teshigawara, M. Harada, M. Ooi, T. Kai, *et al.*, J. Nucl. Mater., to be published.

F. Maekawa, M. Teshigawara, M. Harada, K. Oikawa, M. Ooi, and Y. Kasugai
Materials and Life Science Division, J-PARC Center

Radiation Safety

Applications for the radiological license updates were submitted twice in the 2010 fiscal year. The first application, submitted in June 2010, included the following items: (i) Power-up of the proton beam intensity from 250 kW to 320 kW, (ii) Installation of the neutron beam lines of BL11 and 15 and (iii) Changing some shield configurations for preparation of the installations of BL02, 17 and 18. The application was approved in November 2010, and we started the test operations with 300 kW in December 2010 and the test use of BL11 and 15 in February 2011. The final government inspection was scheduled for March 15, 2011. However, due to the March 11 disaster, the final inspection was postponed. The residual inspection will be carried out after the proton beam operation is resumed in December 2011.

The second application, which included the items on the new neutron-beam lines (BL02, 17 and 18) and the setting of the controlled area in the additional building for BL09, was submitted in December 2010 and approved in February 2011. The government inspection for both applications will be conducted simultaneously after the recovery of J-PARC.

In the second application process, MEXT (Ministry of Education, Culture, Sports, Science and Technology) changed the way of the application process of the secondary-beam lines. The new beam lines had to be reviewed before the construction. In addition, previously, minor changes of the configurations, such as modification of shielding components, installation of collimators etc., also had to be reviewed in terms of the radiation safety. However, MEXT allowed us to do such minor changes under the responsibility of J-PARC. The new process at J-PARC will be standardized and become effective in 2011 fiscal year.

In January 2011, the mandatory periodical government inspection, carried out every five years according to the radiation hazard laws, took place at all J-PARC facilities. The inspection covered the followings: (i) Radiological records and documents, (ii) Radiological placards posted at the exits of controlled areas, (iii) Interlock system and (iv) Radiation dose during the beam operation. We passed the inspection without any problem.

Fortunately, there were no severe radiological problems associated with the March 11 disaster, though we will need to restore a significant number of shielding blocks in order to resume the beam operation scheduled for December 2011.

Y. Kasugai, M. Ooi, and T. Kai
Materials and Life Science Division, J-PARC Center

Neutron Science

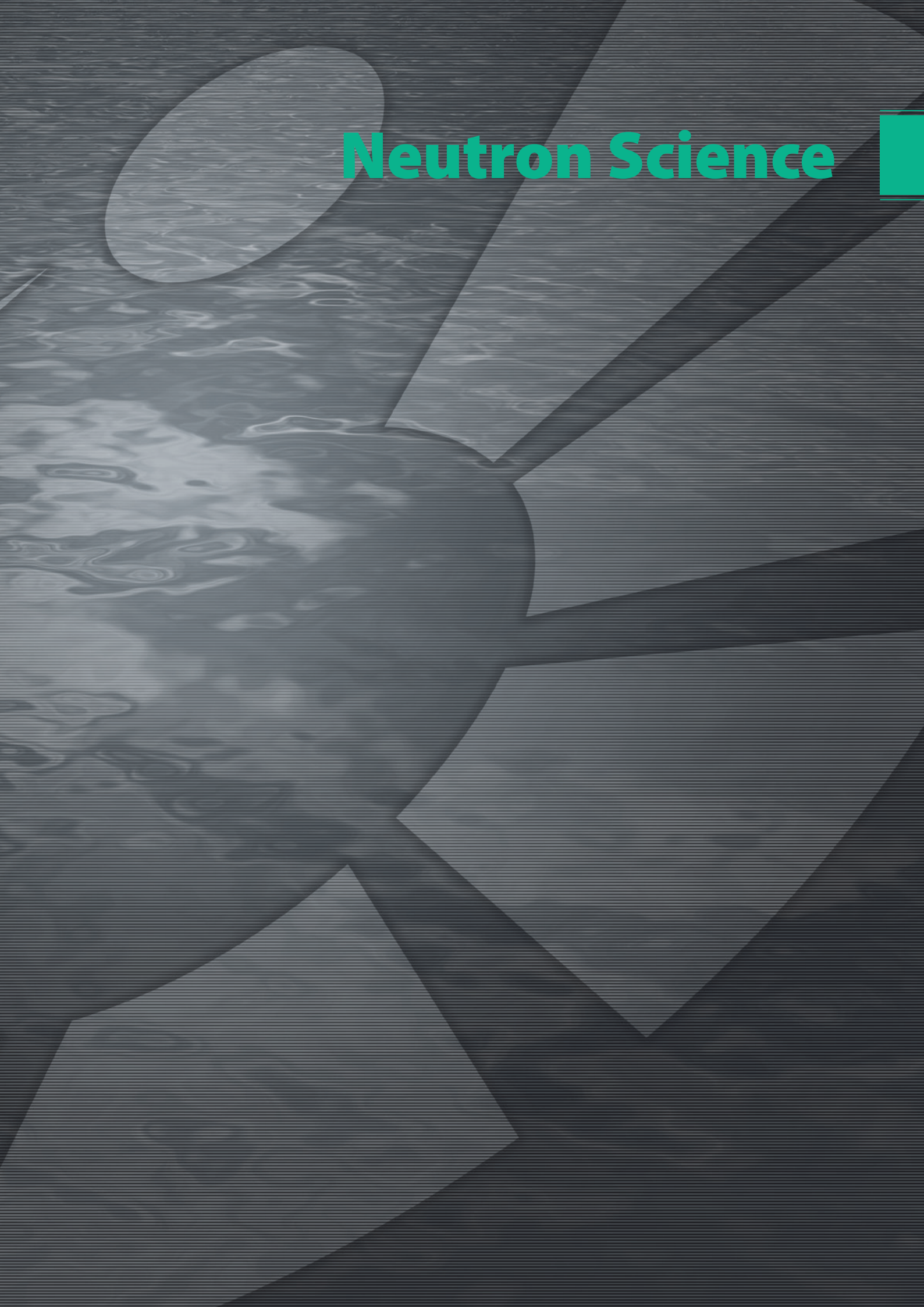

Since the first beam with a power of 20 kW was successfully supplied on May 30th, 2008, followed by the user operation, which started on December 23rd, 2008, the number of users has been increasing and users' demands for beam time have been stronger than ever. In order to meet the users' demands as well as to continue the instrumental developments, we have several proposal categories for JAEA/KEK instruments and Ibaraki prefecture neutron instruments. For the JAEA/KEK instruments, these are 'General Use' for the standard route to apply for beam time, 'Project Use' for KEK/JAEA projects, and 'Instrument Development Group Use' for maintenance, improvement and other R&D activities. For the Ibaraki prefecture neutron instruments, they are 'General Use' for which J-PARC calls for proposals, and 'General Industrial Use' and 'Ibaraki Prefecture Project Use' for which Ibaraki prefecture calls for proposals.

'General Use' proposals are recruited and peer reviewed twice a year by the Neutron Science Proposal Review Committee (NSPRC). In order to promote internationalization, all academic proposals are requested to be written in English. This implies that the MLF proposal-reviewing process is in English. Each 'General Use' proposal will be peer reviewed by referees in advance followed by a discussion in NSPRC to allocate beamtime for each proposal topics. Once it is adopted, the validity period will be half a year.

Since the user operation has started, the total number of submitted proposals for both 'General Use' and 'General Industrial Use', including proprietary use, has been increasing as follows: 54 (in 2008B term, including 7 for muon), 173 (2009A & B, 25 for muon) and 227 (2010A and B, 25 for muon). The total number of approved proposals for corresponding ones was 31(2008B, 6 for muon), 150(2009A & B, 24 for muon) and 176 (2010A and B, 24 for muon).

An outstanding characteristic of the MLF uses shown in Fig. 2 is that the ratio of proposals from industrial users has reached nearly 1/3 of the total proposals. This was achieved through the frequent outreach activities led by the Ibaraki prefecture people, *etc*. as well as the trial use system introduced in JRR-3.

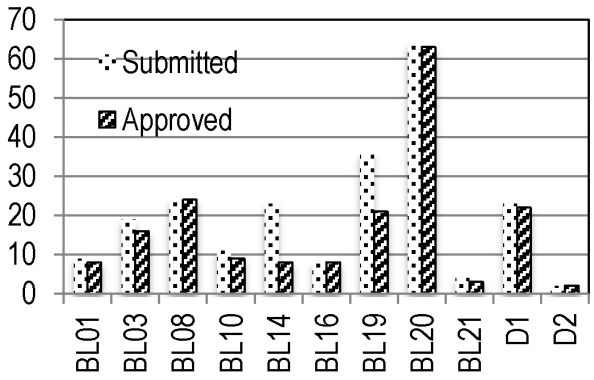

Figure 1. Number of general proposals for each instrument in 2010. Both 'General Use' and 'General Industrial Use' are included. In total, 227 proposals were submitted and 176 of them were approved.

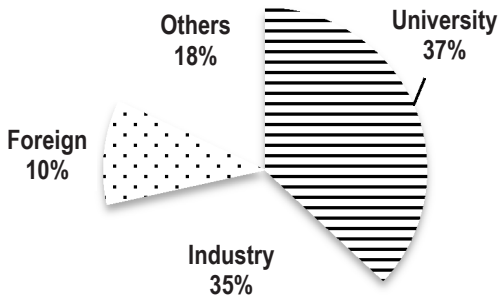

Figure 2. Affiliations of applicants in 2010.

In 2010, we have been operating 12 instruments, and were constructing the following six instruments: DNA (BL02), SPICA (BL09), PLANET (BL11), TAIKAN (BL15), SHARAKU (BL17), and SENJU (BL18). All instruments under operation and construction are shown in Table 1 and Figure 3.

Table 1. Instrument specifications of instruments currently scheduled and under construction*.

Instrument	Beamline / moderator**	Target	Specifications
4D Space Access Neutron Spectrometer (4SEASONS)	BL01 / C	Spin and lattice dynamics in condensed matter.	$5 < E_i < 300$ meV, $\Delta E/E_i > 5$ %
Biomolecular Dynamics Spectrometer (DNA)	BL02 / C	Dynamics of biomolecules and soft materials.	Scan energy: $-25 < E < 45$ meV, (Si analyzer (111): resolution ~1.2 meV)
IBARAKI Biological Crystal Diffractometer (iBIX)	BL03 / C	Biological neutron crystallography.	Maximum lattice constant ~150 Å
Accurate Neutron-Nucleus Reaction Measurement Instrument (ANNRI)	BL04 / C	Nuclear data, nuclear astrophysics, and trace element analysis.	Two spectrometers. Ge detectors array (L1=21.5 m), NaI(Tl) detectors (L2=27.9 m)
Neutron Optics and Fundamental Physics Beam Line (NOP)	BL05 / C	Fundamental physics. Neutron b decay measurement etc.	Three (small divergence, high intensity, high polarization) beamlines
Super High Resolution Powder Diffractometer (SuperHRPD)	BL08 / DCP	Analysis of complicated and hierarchical structures.	d = 0.3~45 Å, $\Delta d/d$=0.1~3.0 % (best 0.035 % at 2θ=175°)
Special Environment Neutron Powder Diffractometer (SPICA)	BL09 / DCP	Materials science for batteries.	d=0.1~125 Å, $\Delta d/d$>0.08 %
NeutrOn Beam-line for Observation & Research Use (NOBORU)	BL10 / DC	Test beam port for R&Ds, imaging, and neutronics research.	L1=14 m, $\Delta d/d$=0.33 %, band width ~9 Å, L/D=140~1875, max. beam size 100×100 mm
High Pressure Neutron Diffractometer (PLANET)	BL11 / DC	Neutron diffraction under high pressure.	d=0.21~4.1 Å, $\Delta d/d$~0.5 % Pressure and temperature: 0~20 GPa, 10 K-2000 K
High Resolution Chopper Spectrometer (HRC)	BL12 / DC	Phonon vibration and dispersion, elemental spin and orbital excitation in magnetic systems.	$1 < E_i < 2000$ meV, $\Delta E/E_i \geq 2.5$ % (1 % in the future)
Cold-neutron Disk-chopper Spectrometer (AMATERAS)	BL14 / C	Quasielastic & inelastic scattering for dynamical properties in atomic, molecular and magnetic systems.	$1 < E_i < 80$ meV, $\Delta E/E_i > 1$ % (at E_i=20 meV)
Smaller-Angle Neutron Scattering Instrument (TAIKAN)	BL15 / C	Analysis of nanostructures and microstructures in hard and soft, and biological materials.	Q=0.003~13 Å^{-1}, Q_{min}=0.0005 Å^{-1} (in focusing mode)
Soft Interface Analyzer (SOFIA)	BL16 / C	Surface and interface structure in softmatter materials.	Q=0.005~0.4 Å^{-1}, $\Delta Q/Q$ >1 %,
Polarized Neutron Reflectometer with a Vertical Sample Geometry (SHARAKU)	BL17 / C	Magnetic structures in thin films and multilayers.	Q=0.005~1.2 Å^{-1}, $\Delta Q/Q$ >1 %, λ = 2.1~7.5 Å (in polarized mode), λ =2.4~6.4 Å (in poralization-analysis mode), λ = 1.0~8.8 Å (in unpolarized mode)
Single Crystal Neutron Diffractometer under Extreme Condition (SENJU)	BL18 / DCP	Structure of functional materials under controlled environmental conditions.	Maximum lattice constant ~50 Å
Engineering Materials Diffractometer (TAKUMI)	BL19 / DCP	Stress/strain measurements in materials science and mechanical engineering.	d=0.5~2.7 Å, $\Delta d/d$=0.4 % (best $\Delta d/d$=0.2 %)
IBARAKI Materials Design Diffractometer (iMATERIA)	BL20 / DCP	Structural and chemical analysis for materials developments.	d=0.09~58 Å, $\Delta d/d$=0.16 % (at d=0.18~2.5 Å)
High Intensity Total Diffractometer (NOVA)	BL21 / DC	Structures of hydrogen-storage materials and disordered materials.	Q=0.01~100 Å^{-1}, $\Delta Q/Q$=7~0.35 %

* See J-PARC/MLF website http://j-parc.jp/MatLife/en/instrumentation/ns_spec.html for further details.

** C: coupled H_2 moderator; DC: decoupled H_2 moderator; DCP: decoupled-poisoned H_2 moderator

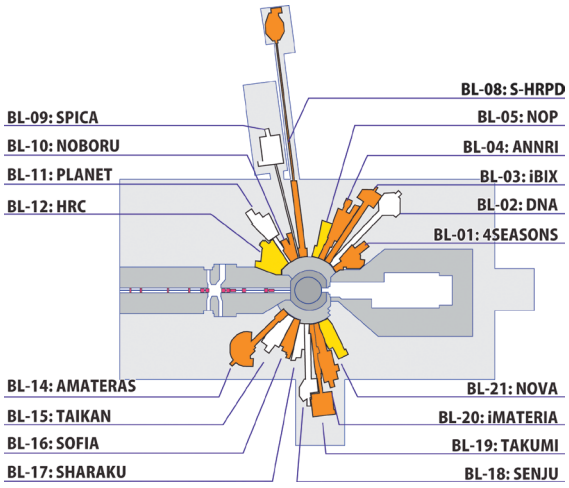

Figure 3. Layout of the neutron instruments at MLF as of 2010.

Diffractometers

iBIX (BL03), SuperHRPD (BL08), TAKUMI (BL19), iMATERIA (BL20) and NOVA (BL21) have been operated. In 2010, the construction of three diffractometers was started: a high pressure diffractometer, PLANET (BL11), a single crystal diffractometer for solid state science, SENJU (BL18), and a special environment powder diffractometer, SPICA (BL09).

In iBIX, the first TOF neutron diffraction data of a protein crystal of RNase A (ribonuclease A), soaked in heavy water, was obtained for about 10 days under 120kW. The crystal volume was 4.7 mm^3. The cell parameters were a = 30.4 Å, b = 38.6 Å, c = 53.4 Å, β = 105.8° in a monoclinic form, respectively. The example of TOF diffraction pattern is shown in Figure 4. The data reduction was carried out by using the data processing software "STARGazer".

In SuperHRPD, high resolution powder diffraction has been pursued to understand the structure physics by revealing tiny structure distortion, such as the case of the long period spin structure seen in $BiFeO_3$. As shown in Figure 5, we can see only one peak with a conventional neutron powder diffractometer, while with SuperHRPD we clearly notice the split peaks.

iMATERIA was used in 2010 by 96 user groups including the 'Project Use' group (67% were industrial users with (non) proprietary and urgent use). Once the beam power reached 100kW, many users strived to achieve successful structure analyses with minimum amount of samples. Recently, Rietveld analyses of a cathode active material in the

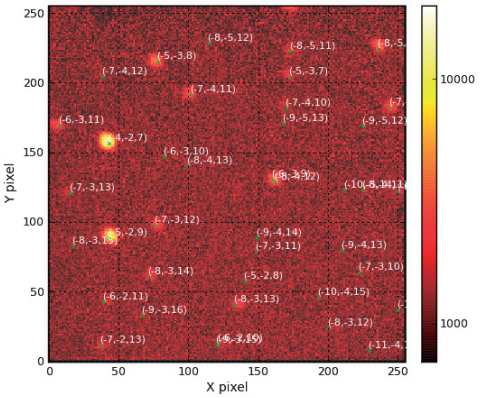

Figure 4. The first diffraction pattern of a protein crystal of RNase A.

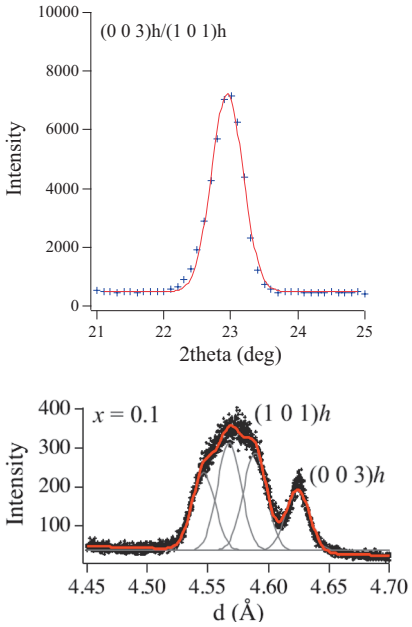

Figure 5. Magnetic peaks of (1-x)BFO-xBTO (x = 0.1) at room temperature using HERMES(top) and SuperHRPD(down).

amount as small as 8.5 mg extracted from a Li-ion battery coin-type cells (*ex situ* measurement) were successful.

In Takumi, one of the most important projects is the residual strain studies on ITER superconducting wires. In JFY 2009, residual strains for Nb_3Sn phases in ITER-TF conductors were measured. In JFY 2010, strains in ITER-CS conductor with the outer dimension of 49 mm were being carried out until the earthquake (Figure 6). The heat-treated specimen was measured and thermal phase strains in Nb_3Sn phases during the heat treatment were obtained; the thermal residual strain in axial direction for Nb_3Sn was –0.2 %.

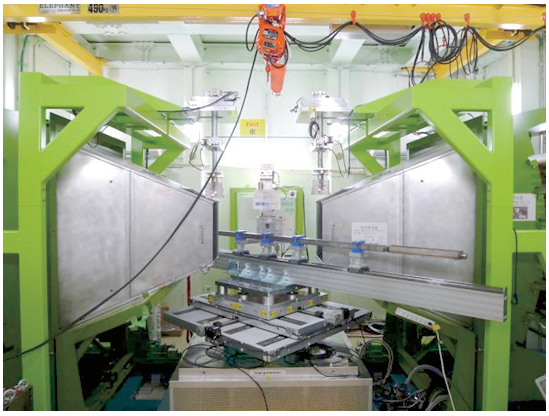

Figure 6. Off-line test at Takumi: 3.6 m long ITER- CS conductor.

NOVA is funded by the NEDO project "Advanced Fundamental Research Project on Hydrogen Storage Materials (Hydro-Star)". In JFY 2010, the performance of NOVA was evaluated using various samples of crystaline, amorphous and liquid materials, and the reliability of the hardware and software was confirmed. NOVA started a general user operation from 2010B with 10 % beamtime. The structural change during hydrogen desorption of AlD_3 was studied with NOVA and the study revealed that χ-Al_2O_3 forms on the surface of AlH_3 (AlD_3) by the desorption of solvated ether.

Chopper Spectrometers

At present, 4SEASONS (BL01), HRC (BL12) and AMATERAS (BL14) have been operated. In 2010, the construction of a backscattering spectrometer, DNA (BL02), was started.

4SEASONS operated quite stably in 2010. Inelastic scattering data of superconductors, multiferroic materials, relaxers, charge-ordered magnets, frustrated magnets, *etc*. were measured [1]. In Fe-based superconductor $BaFe_2(As_{0.65}P_{0.35})_2$, a magnetic excitation signal is observed as a bright spot at $|\boldsymbol{Q}| \sim 1.2$ Å^{-1} and $E \sim 10$–15 meV, which likely corresponds to the spin excitation at the antiferromagnetic wave vector Q_{AF} = (1/2 1/2) (Figure 7(a) and (b)). The excitation spectra of the spin-Peierls compound $CuGeO_3$ are good examples of the multi-E_i measurement, from which we could see the whole picture of the magnetic excitations and the detailed structure of the low-energy part simultaneously (Figure 7(c) and (d)). The two-dimensionality of the magnetic excitations in

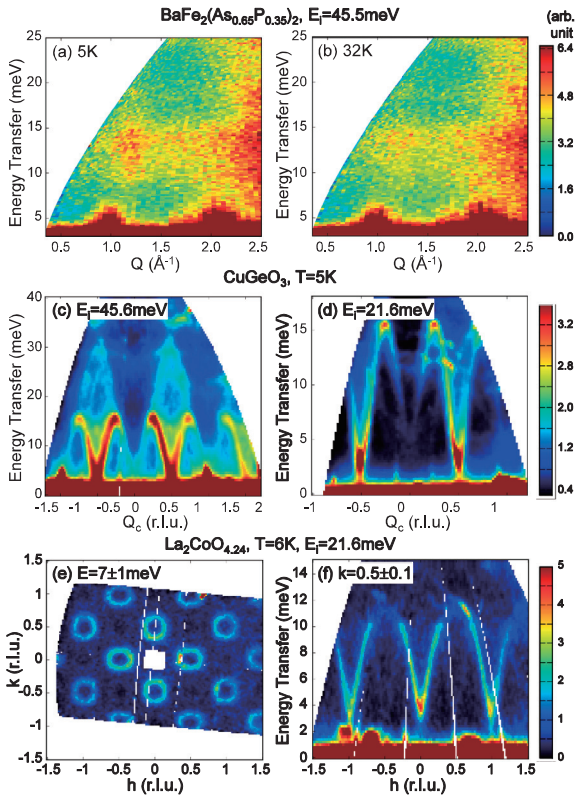

Figure 7. *Q*–*E* maps of excitation spectra of (a) a powder sample of $BaFe_2(As_{0.65}P_{0.35})_2$ at 5 K and (b) 32 K with E_i = 45.5 meV, (c) single crystals of $CuGeO_3$ at 5 K by multi-E_i measurement with E_i = 45.6 meV and (d) 21.6 meV. Two-dimensional cut of the excitation spectra of a single crystal of $La_2CoO_{4.24}$ at 6 K with E_i = 21.6 meV on the (e) *h*–*k* plane at *E* = 7±1 meV and (f) that on the *h*–*E* plane at *k* = 0.5±0.1 r.l.u.

a single crystal of $La_2CoO_{4.24}$ allows us to project the data on the plane perpendicular to the *c* axis (Figure 7(e) and (f)). We can see that the cones of spin wave dispersions develop around (*h*, *k*) = (half integer, integer) or (integer, half integer).

In HRC, a new scattering chamber, detectors and new choppers were installed and a ceremony for cerebrating the completion of HRC was held in March, 2010. The 'Nishikawa Award' was awarded by the Foundation for High Energy Accelerator Science for the 100Hz T0 & Fermi choppers development.

AMATERAS has moved into a full-scale user program operation in 2010. 80% of the beamtime was provided to the user program, while 20% was spent for commissioning and covering of users' beam-time lost by accidental problems. Eight accepted general user proposals have large variety in their research fields, such as strongly correlated electron systems, biomaterials, ionic conductors and liquid.

Reflectometers and Smaller-angle Scattering Instrument

Presently, SOFIA (BL16, upgraded from ARISA-II) has been operated. TAIKAN (BL15) has been constructed and started on-beam commissioning in 2010. The construction of SHARAKU (BL17) has started.

By upgrading to SOFIA, a wider scattering vector region can be accessible with the 5.71° beam line in addition to the present 2.22° beam line. More precise slit system than that of ARISA-II was incorporated. Many new components replaced the old ones while the T0 chopper, disk chopper, NiC mirror, and 2-dimensional scintillation detector (^{6}LiF/ZnS) have been recycled. The performance of SOFIA was evaluated using a deuterated polystyrene (d-PS) thin film spun-cast on a silicon substrate. Figure 8 shows that the reflectivity reaches 1×10^{-7} at q~4 nm^{-1}.

Most of the TAIKAN components, including the vacuum chambers, were already installed at BL15 in 2010. 608 ^{3}He PSD tubes with 8 mm in diameter and 500 - 1,000 mm in effective length were mounted on the detector bank. On March 8, 2011, the first neutron image was successfully taken as shown in Figure 9.

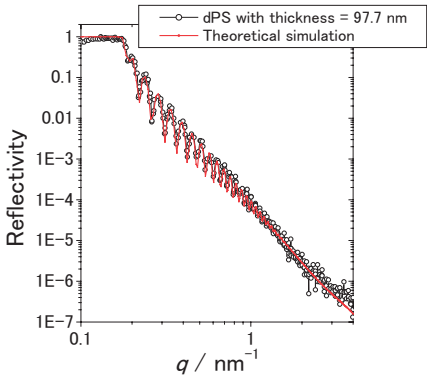

Figure 8. NR profile of deuterated polystyrene (d-PS) thin film on a Si substrate with a theoretical profile (red line).

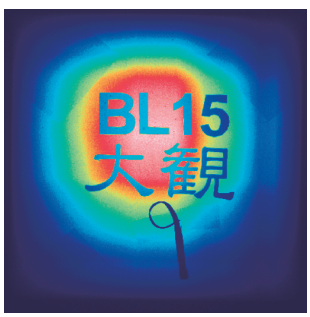

Figure 9. The first neutron image taken at the BL15 with a mask of “BL15” and “TAIKAN” in Japanese writing.

Other Beamlines in Operation

Currently, ANNRI (BL04), NOP (BL05) and NOBORU (BL10) have been operated.

ANNRI has been developed to obtain accurate data of neutron-capture cross sections of minor actinides (MAs) and long-lived fission products (LLFPs) in a collaborative project of Hokkaido University, Tokyo Institute of Technology and the Japan Atomic Energy Agency. The neutron capture cross sections of ^{93}Zr, ^{99}Tc, *etc*. were measured using the Ge and NaI(Tl) spectrometers installed in the ANNRI. The primary transitions from the p-wave 225-eV resonance state to the low-lying states of 1-, 2+ and 4+ were clearly observed. The decay pattern was quite different between 110- and 225-eV resonances of ^{93}Zr.

In the NOP beamline, the 100m-curvature benders split cold neutrons into three beam branches: a low-divergence beam branch for neutron interferometry, an unpolarized one for the search of unknown medium range interactions between neutrons and neutral atoms and a polarized one for the study of the neutron decay. In the polarized beam branch, a time projection chamber (TPC) and a spin flip chopper (SFC) have been developed and are currently under commissioning. In the unpolarized beam branch, a moving multilayer mirror of m=10 is installed to convert very cold neutrons (v~ 140 m s^{-1}) to ultracold neutrons by the Doppler shift.

Beam times of NOBORU were devoted to neutron source characterization and commissioning of newly installed devices; R&D on energy-selective imaging, neutron detectors and optical devices, and TOF-type prompt gamma-ray analysis were conducted. For pulsed neutron imaging, NOBORU is now the best in the world with energy resolution (Δt/t: 0.3%), wide band width up to 9Å, variable and high collimator ratio (L/D = 140, 190, 600, 1,875), large field of view (100×100 mm^2) and intensity, *etc*. The experimental results in imaging techniques at NOBORU are now utilized for the design of a new dedicated imaging instrument at MLF.

Reference

[1] R. Kajimoto *et al*., J. Phys. Soc. Jpn. Suppl., to be published

BL 01: Fermi-Chopper Spectrometer 4SEASONS

1. Introduction

4SEASONS (*4*-Dimensional *S*pace *A*ccess Neutr*on* *S*pectrometer; *SIKI* in Japanese) is a Fermi-chopper spectrometer to provide high counting rate with a middle energy resolution [1]. In JFY 2010, 4SEASONS operated quite stably, though some kinds of upgrades are still in progress. The instrument conducted three general proposals, in addition to one project proposal and one instrument group proposal. Inelastic scattering data of more than 10 samples of superconductors, charge-ordered magnets, frustrated magnets, ferroelectric materials, etc. were measured, some of which will be published soon [2–4]. Most of the measurements utilized multiple incident energies (E_i's) (multi-E_i measurement), which is enabled by the repetition rate multiplication technique and is one of the advantageous features of 4SEASONS [5].

2. Examples of Inelastic Scattering Data

Here we show some examples of inelastic scattering data obtained on 4SEASONS [1]. Figures 1(a) and 1(b) show the excitation spectra of a powder sample of an Fe-based superconductor $BaFe_2(As_{0.65}P_{0.35})_2$ measured at 5 K (a) and 32 K (b) with E_i = 45.5 meV [2]. A magnetic excitation signal is observed as a bright spot at $|\boldsymbol{Q}| \sim 1.2$ Å^{-1} and $E \sim 10$–15 meV, where $\boldsymbol{Q}$ and E are the momentum transfer and energy transfer. The intensity of the magnetic excitation increases the superconducting transition temperature T_c = 30 K, suggesting a close relationship between the magnetic excitation and the superconductivity.

Figures 1(c) and 1(d) show examples of data from a single crystal sample of a one-dimensional (1D) system. They are the excitation spectra of the spin-Peierls compound $CuGeO_3$ measured at 5 K with E_i = 45.6 meV (c) and 21.6 meV (d). This compound has 1D spin chains with S = 1/2 along the c axis. Since the magnetic excitation is 1D along the c direction, we presented the data as a function of the c component of $\boldsymbol{Q}$ (Q_c). These two data sets are good examples of the multi-E_i measurement, from which we could see the whole picture of the magnetic excitations [Fig. 1(c)] and the detailed structure of the low-energy part [Fig. 1(d)] simultaneously.

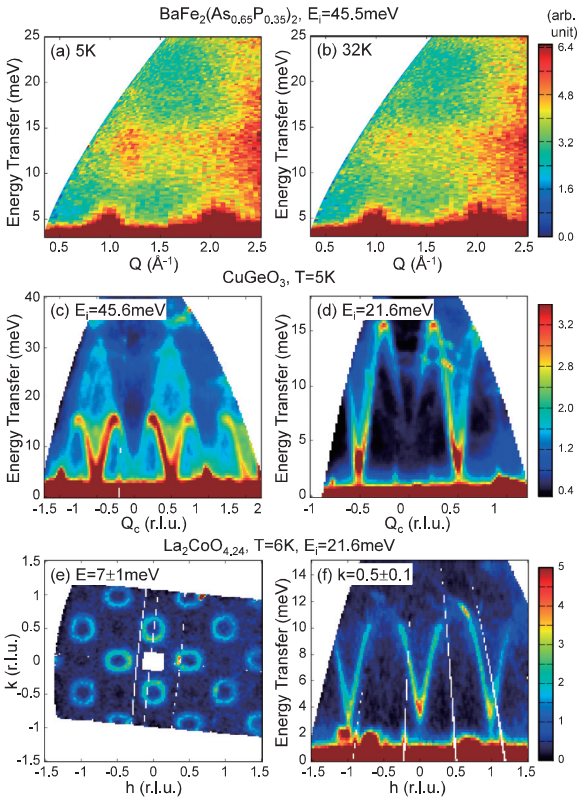

Figure 1. Examples of inelastic scattering data on 4SEASONS [1]. (a),(b) Q–E maps of excitation spectra of a powder sample of $BaFe_2(As_{0.65}P_{0.35})_2$ at 5 K (a) and 32 K (b) with E_i = 45.5 meV. (c),(d) Q_c–E maps of excitation spectra of single crystals of $CuGeO_3$ at 5 K by multi-E_i measurement with E_i = 45.6 meV (c) and 21.6 meV (d). (e),(f) Two-dimensional cut of the excitation spectra of a single crystal of $La_2CoO_{4.24}$ at 6 K with E_i = 21.6 meV on the h–k plane at E = 7±1 meV (e) and that on the h–E plane at k = 0.5±0.1 r.l.u. (f).

Figures 1(e) and 1(f) show examples of measurements of a single crystal of a two-dimensional (2D) system, $La_2CoO_{4.24}$, measured with E_i = 21.6 meV at 6 K. The compound has a layered perovskite structure, where spins of Co ions form 2D layers perpen-

dicular to the *c* axis. Excess oxygen atoms introduce holes on the Co layers by an amount of ~50% per Co site; this modifies the magnetic structure as well as the magnetic excitations. In this experiment, the crystal was aligned so that the incident beam was parallel to the *c* axis. The two-dimensionality of the magnetic excitations allows us to project the data on the plane perpendicular to the *c* axis. Accordingly, we can observe a wide region in the *h*–*k* plane on the 2D detector. Figure 1(e) shows a 2D map of the magnetic excitations on the *h*–*k* plane at $E \sim 7$ meV, and Fig. 1(f) shows the 2D map on the *h*–*E* plane at $k \sim 0$. We can see that the cones of the spin wave dispersions develop around (*h*, *k*) = (half integer, integer) or (integer, half integer).

In the case of a three-dimensional (3D) system, the projection of the data as described above is not allowed. In order to obtain data at arbitrary ***Q*** and *E* positions, one must rotate the crystal or change E_i during the measurements so that the curved scan trajectory covers the entire four-dimensional space of ***Q*** and *E*. We are developing data acquisition and analysis software for such measurements, and some measurements on 3D systems have already been performed.

3. Recent Upgrades

In parallel with the execution of the user program, we carried out several upgrades of the instrument. They are suppression of the background scattering, progress in the automatic control of the sample environment, and further development of the data analysis software.

Here we briefly describe the progress in the suppression of the background scattering. One of the most effective measures to suppress the background, especially in high-energy regions with $E_i >$ ~100 meV, is to reduce the very high energy neutrons as much as possible using the T0 chopper. Though the T0 chopper was once installed in fiscal 2009, it did not work well. However, the T0 chopper was finally reinstalled and we could start the steady operation since late 2010. Figure 2 shows a comparison of data with and without the T0 chopper. These data are measurements of magnetic excitations in a single crystal of a mother compound of the Fe-based superconductor $BaFe_2As_2$. In this compound, magnetic excitations from the antiferromagnetic ordering of Fe spins exist up to $E > 100$ meV. In the data obtained without the T0 chopper [Fig. 2(a)], the signal is severely contaminated by background scattering, and we can barely distinguish the magnetic excitations. On the other hand, the data obtained with the T0 chopper is clean, and we can easily distinguish the signals [Fig. 2(b)].

Figure 3 shows another measure to reduce the background scattering. We installed a baffle made of B_4C resin between two detector banks [Fig. 3(a)]. It could significantly reduce the noises originating from scattering inside the vacuum scattering chamber [Fig. 3(b)]. We are going to install similar baffles between all the detector banks.

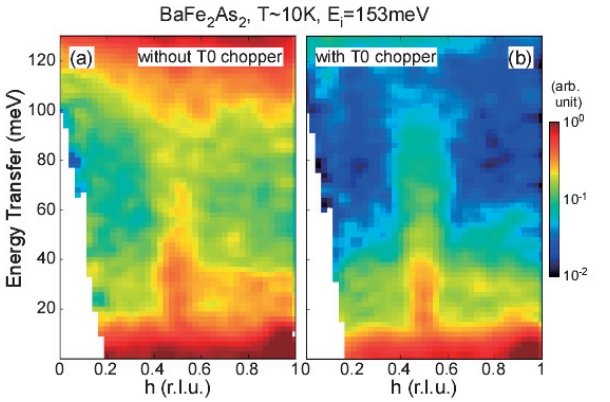

Figure 2. Excitation spectra of a single crystal of $BaFe_2As_2$ at ~10 K on the *h*–*E* plane at $k = 0 \pm 0.2$ r.l.u. The utilized E_i is 153 meV. (a) Without the T0 chopper. (b) With the T0 chopper (b) [1].

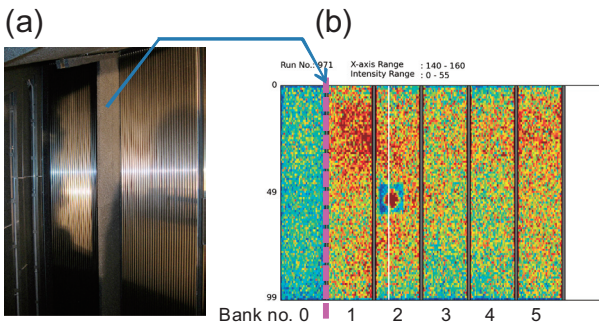

Figure 3. (a) Baffle installed between the detector bank 0 and 1 inside the vacuum scattering chamber. (b) Detector map of a measurement with a single crystal. The direct beam goes through bank 2. The background level of bank 0 becomes much lower than those of the other banks, because the baffle blocks scattered neutrons from the right part.

References

[1] R. Kajimoto *et al*., J. Phys. Soc. Jpn. Suppl., to be published

[2] M. Ishikado *et al.*, Phys. Rev. d **84** 144517 (2011).

[3] K. Iida *et al*., Phys. Rev. d **84** 060402(R) (2011).

[4] M. Sato *et al.*, J. Phys. Soc. Jpnd **80** 093709 (2011).

[5] M. Nakamura *et al.*, J. Phys. Soc. Jpn. **78** 093002 (2009).

R. Kajimoto*, and M. Nakamura

Materials and Life Science Division, J-PARC Center

**Present address: Research Center for Neutron Science and Technology, CROSS*

BL 02: The Si Crystal Analyzer Backscattering Spectrometer DNA

1. Introduction

The Si crystal analyzer backscattering spectrometer DNA was under construction at the port BL02 in JFY 2010. Those type spectrometers cover the area of the micro-eV energy range in the Q-E space, where it is expected to explore sciences on atomic, molecular and spin dynamics in the nano-second time range.

Then scientific research fields planned to be performed with the DNA spectrometer are very wide including soft matter dynamics, bio-molecular dynamics, chemical molecular dynamics, characterization of functional materials and spin dynamics in magnetism.

The instrumental specifications for DNA are shown in Table 1.

This report describes mainly construction works for the BL02 beam line in JFY 2010.

Table 1. Instrumental specifications of DNA.

Items	Specification
Neutron source (NS)	Coupled Liquid H_2 Moderator
L_1 (source-sample)	42 [m]
L_2 (sample-analyzer)	~ 2.3 [m]
L_3 (analyzer-detector)	~2.0 [m]
Pulse sharping chopper	300Hz at ~7.5m from NS
Crystal Analyzer	
Crystal and reflection index	Si(111)
	Si(311)
Bragg angle of analyzers	~87.5 [deg.]
Energy resolution	~1.5 [μeV]: Si(111)
	~5 [μeV]: Si(311)
Momentum range	0.07 < Q < 1.98 [$Å^{-1}$]: Si(111)
	0.60 < Q < 3.80 [$Å^{-1}$]: Si(311)
Scan energy range	-25 < E < 45 [μeV]:
	Single pulse scan around E_f
	-300 < E < 5100 [μeV]:
	RRM scan in second frame

(the plan as of the end of march 2011)

2. Construction Works in JFY 2010

In JFY 2010, there were following construction works in the BL02 beam line.

The insertion of a super mirror guide into the biological radiation shield on BL02 was done in mid-July 2010. Figure 1 shows a scene of the insertion (fig.1).

Along the guide line of BL02, many struts for mounting super-mirror guide tubes and disk choppers were installed on the basis of a detailed survey on beam line alignment from the mid-July to the end of August 2010 (figs.2 & 3).

From mid-August to mid-October 2010, the installation of radiation
shields for the beam line of BL02 was accomplished. (fig.4)

Figure 1. The insertion of a super mirror guide into the biological radiation shield on BL02.(July 16, 2010).

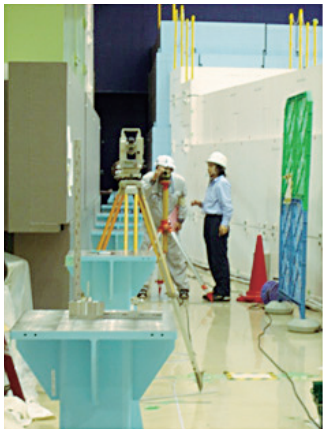

Figure 2. A survey of the neutron beam line on BL02. (July 28, 2010).

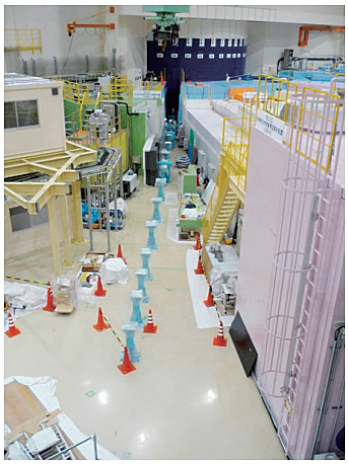

Figure 3. The installation of the struts for mounting super-mirror guide tubes and disk chopper. (August 31, 2010).

Figure 5. The installation of radiation shields for the DNA vacuum chamber. (February 19, 2011).

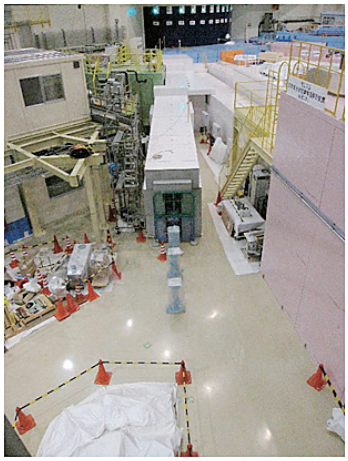

Figure 4. The installation work of radiation shield for beam line BL02. (October 12, 2010).

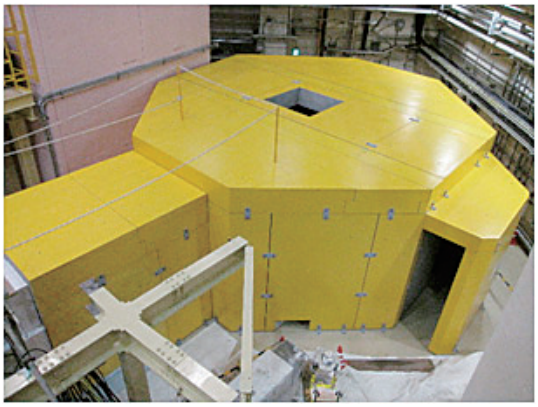

Figure 6. The radiation shields for the DNA vacuum chamber. (February 10, 2011).

From the end of November 2010 to the mid-February, the installation work of radiation shields for a DNA vacuum chamber was done. (figs.5 & 6)

After the installation of the radiation shield for the DNA vacuum chamber, some additional works around the radiation shields were continued until March 11, 2011. Then all construction works were stopped for about 4 months by the earthquake.

3. Schedule in JFY 2011

The main construction of DNA will be completed at the end of November 2011, and then the commissioning will start either off beam and on beam for about 4 months. Some preliminary user program will start from the mid-March 2012.

References

[1] N. Takahashi, *et al.*, Journal of Physics and Chemistry of Solids 68, 2199-2203(2007).

K. Shibata[1], N. Takahashi[2], Y. Kawakita[2], K. Kamazawa[1], T. Yamada[1], K. Nakajima[2], Y. Inamura[2], T. Nakatani[2], K. Oikawa[2], W. Kambara[2], T. Iwahashi[2], Y. Ito[2], H. Tanaka[2] , K. Aizawa[2], M. Arai[2] , H. Nakagawa[3], and S. Fujiwara[3].

[1]Research Center for Neutron Science and Technology, Comprehensive Research Organization for Science and Society (CROSS); [2]Materials and Life Science Division, J-PARC Center; [3]Quantum Beam Science Directorate, JAEA

BL 03: IBARAKI Biological Crystal Diffractometer –iBIX

1. Introduction

IBARAKI biological crystal diffractometer called iBIX is a high performance time of flight neutron single crystal diffractometer applied to biological macromolecules and organic compounds. It is designed to measure samples with cell edges up to around 150 Å with a resolution up to 1.2 Å in case of biological macromolecules, and a resolution up to 0.7 Å in case of organic compounds. It should be possible to collect a full dataset in three to four days for a crystal of 2 mm^3 in volume, and/or in about one month for a crystal of 0.1 mm^3 in volume of biological macromolecules under 1MW operation of accelerator power in J-PARC [1].

2. Status of iBIX

To realize the performance as mentioned above, iBIX has been installed on a coupled moderator which provides more intense peak and integrated intensity but wider pulse shape than a decoupled one because biological neutron crystallography is an intensity limited technique and the pulse repetition rate of J-PARC provides an advantage of a high resolution measurement in time. To be taken prior to the time resolution, the distance between the moderator and the sample (L_1) is 40 m. The beam divergence is optimized to ±0.2° at the sample position by the combination of specially designed guide tubes composed of super-mirrors with different reflectivity. The guide tubes have a total length of 25 m in order to achieve the requirements of crystal cell dimension and the observable minimum d-spacing [2].

iBIX requires a completely new detector system to achieve high efficiency. We developed a two-dimensional position sensitive detector using ZnS:Ag/$^{10}B_2O_3$ scintillator with wavelength shift fiber system which has high spatial resolution, less dead area, low ϒ–ray sensitivity, high counting rate and high efficiency [3]. Currently, 14 detector units have been installed on the position to bring more efficiency at a distance of 0.49 m from sample positions (Fig. 1). The current parameters of the detectors are as follows, sensitive area: 133 mm × 133 mm, efficiency: 20 - 50 %, spatial resolution: about 1 mm, counting rate: about 500 kcps and □/neutron ratio 10^5. The total solid angle of detectors is 9.1 % of 4π. The specifications of iBIX are shown in Table 1.

Data reduction (to extract an structure factor list from raw data) software named “STARGazer” has been developed based on ISAW (Argonne National Laboratory, USA) and available[4]. STARGazer is composed of a data processing part and a data visualization part. In 2010, new refinement component for UB matrix has been developed in order to obtain more accurate integration data. In recent experiments, the data processing for both organic compounds and biological macromolecules has been successfully accomplished by STARGazer.

Since the end of 2008, iBIX has been available to users supported by Ibaraki University. In 2009, the full data sets of several organic compounds were obtained and the structure analyses were successfully completed. In 2010, 5 organic compounds and 4 biological macromolecules were provided to the diffraction experiments by using iBIX.

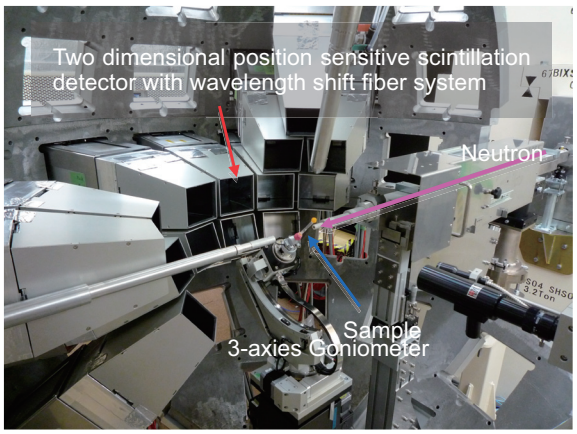

Figure 1. Diffractometer of iBIX.

Table 1. Specifications of BL03 iBIX.

Moderator	Coupled H_2 para 100 × 100 mm^2
Range of d-spacing	0.35 Å<*d*<50 Å
Max. unit cell length	~150 Å
Range of wavelength	0.5 Å <λ<8 Å
Neutron flux	7 × 10^7 n/sec/cm^2*1
Standard size of sample	1 mm^3
Standard measurement time	0.5 days organic compounds 3 days biological macromolecules*2
Sample environment	Gas flow type cooling system He: ~20 K, N_2: ~90 K

*1 Estimation between 0.5 Å <λ<3.9 Å when 1 MW

*2 When sample volume 2 mm^3, 30 detctors and 1 MW

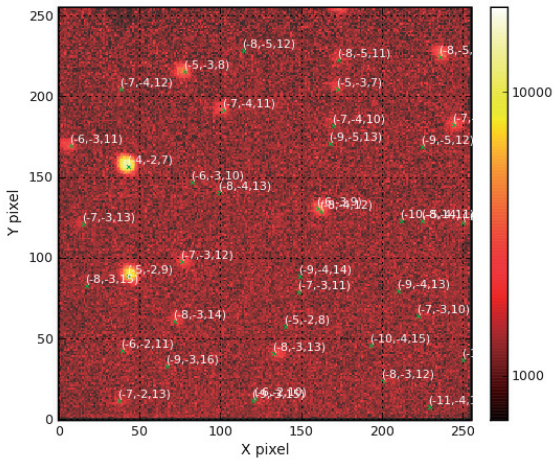

Figure 3. TOF diffraction pattern of RNase A after indexing.

3. Example of Experiments

We tried to collect the first TOF neutron diffraction dataset of a protein crystal by using iBIX in order to estimate the performance and characteristics of iBIX. The selected crystal for the purpose was ribonuclease A soaked in heavy water for about 10 days (Fig.2). The crystal volume was 4.7 mm^3. The cell parameters were *a*=30.4 Å, *b*=38.6 Å, *c*=53.4 Å, b=105.8° in a monoclinic form, respectively.

The measurement conditions were as follows: the accelerator beam power: 120 kW, the pulse repetition: 25 Hz, the range of wavelengths: 1.5~4.5 Å (the 1st frame), 4.2~7.5 Å (the 2nd frame), the number of measurement settings: 100 settings (1st frame: 67 settings, 2nd frame: 43 settings), the exposure time: 5 hours/setting (the 1st frame), 1 hour/setting (the 2nd frame), the total amount of measurement time for full dataset: 17 days. The example of TOF diffraction pattern is shown in Fig. 3.

The data reduction was carried out by using the data processing software “STARGazer”. The data reduction for almost all of the both frame data was finished and consequently HKLF list was obtained. The completeness of Bragg reflections was 88.8 % of 1.7 Å resolution. The structure refinement was carried out with this intensity dataset. We succeeded in obtaining the reasonable structure (Fig. 4) after structure refinement by comparing with the already-reported structure [5].

After the accelerator power in J-PARC reaches 1MW and the total number of detectors for iBIX becomes 30, the full dataset of standard sample RNaseA which is 1 mm^3 in volume can be collected in about 3 days. We have already decided to install additionally the new 16 detectors and to improve the 14 existing detectors in 2012.

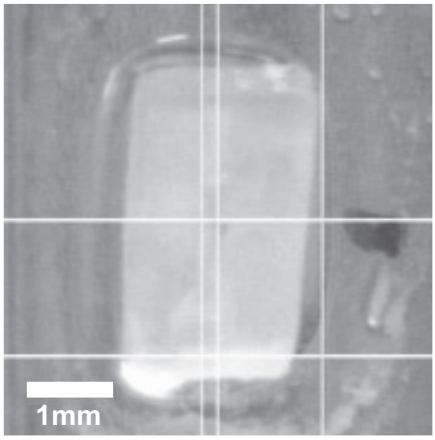

Figure 2. Single crystal of RNase A.

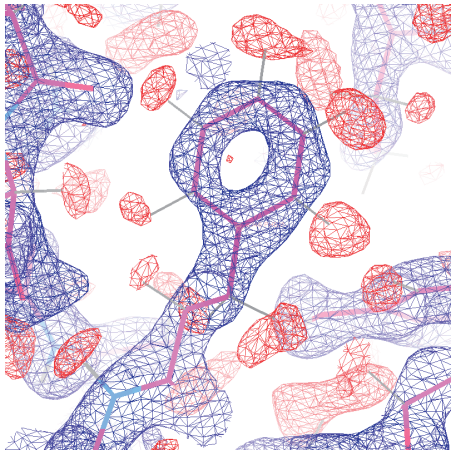

Figure 4. A part of neutron scattering density map of RNase A.

References

[1] I. Tanaka, K. Kusaka, T. Hosoya, N. Niimura, T. Ohhara, K. Kurihara, T. Yamada, Y. Ohnishi, K. Tomoyoria and T. Yokoyama Acta Cryst. D**66** 1194 (2009).

[2] T. Hosoya, T. Nakamura, M. Katagiri, A. Tirumachi,M. Ebine, K. Soyama NIMA A **600** 217 (2009).

[3] K. Kusaka,T. Ohhara, I. Tanaka, N. Niimura, T. Ozeki, K. Kurihara, K. Aizawa, Y. Morii, M. Arai, K. Ebagta, Y. Takano Physiva B **385-286** 1062 (2006).

[4] T. Ohhara, K. Kusaka, T. Hosoya, K. Kurihara, K. Tomoyori, N. Niimura, I. Tanaka, J. Suzuki, T. Nakatani, T. Otomo, S. Matsuoka, K. Tomita, Y. Nishimaki, T. Ajima, S. Ryuuhuku NIMA **600** 195 (2009).

[5] D. Yagi, T. Yamada, K. Kurihara, Y. Ohnishi, M. Yamashita, R. Kuroki, I. Tanaka, N. Niimura, Acta Cryst. D **65**, **892** (2009).

K. Kusaka[1], I. Tanaka[1], T. Hosoya[1], N. Niimura[1], T. Ohhara[2], K. Kurihara[3], T. Yamada[1], K. Tomoyori[1], and T. Yokoyama[1]

[1]*Frontier Research Center for Applied Atomic Sciences, Ibaraki University;* [2]*Center for Neutron Science & Technology,CROSS;* [3]*Quantum Beam Science Directorate, JAEA*

Recent Progress in BL04, ANNRI

1. Introduction

Accurate data of neutron-capture cross sections of minor actinides (MAs) and long-lived fission products (LLFPs) are required for developing innovative nuclear systems. However, accurate measurements of these cross sections are very difficult due to the high radioactivity of these samples. To overcome the difficulty, the Accurate Neutron-Nucleus Reaction measurement Instrument (ANNRI) was developed in a collaborative project of Hokkaido University, Tokyo Institute of Technology and Japan Atomic Energy Agency. The ANNRI is located on beam line no. 04 of MLF at J-PARC. We have started measurements of MAs and LLFPs with high intensity pulsed neutrons since 2009. The Ge spectrometer and the NaI(Tl) spectrometer installed in the ANNRI have been used for measuring neutron capture cross sections. The progress is presented in this report.

2. Measurements and Results

2.1 Beam Characteristics

The energy spectra and spatial distributions of neutron beams were measured with the position-sensitive Li-glass scintillation detector at the 21.5-m sample position[1]. The measurements were performed in the neutron energy range of 1.5 meV to 10 keV. The energy spectra show a typical feature of para-hydrogen moderator, and the absolute intensities almost agree with the prediction based on the simulation calculation. The measured spatial distributions of the beams are consistent with those expected from the collimator-system design of the beam line. The edges of the spatial distributions are sharp. This feature is important for measuring cross sections accurately.

2.2 Prompt Gamma Rays from ^{93}Zr

We measured the neutron capture gamma rays from the 110- and 225-eV resonances of ^{93}Zr with the large Ge-spectrometer at the ANNRI as shown in Fig. 1 [2]. The relative intensities of the primary transitions were derived as shown in Fig. 2 [2]. We found out that the decay pattern is quite different between the two resonances. It is worth noting that the primary transitions from the p-wave 225-eV resonance state to the low-lying states of 1-, 2+ and 4+ were clearly observed. The spin and parity (J^{π}) of the 225-eV resonance was reported as 4- by the previous work [3]. Assuming the E1 or E2 transition for the observed gamma rays, however, the J^{π} of the resonance was assigned to 3-.

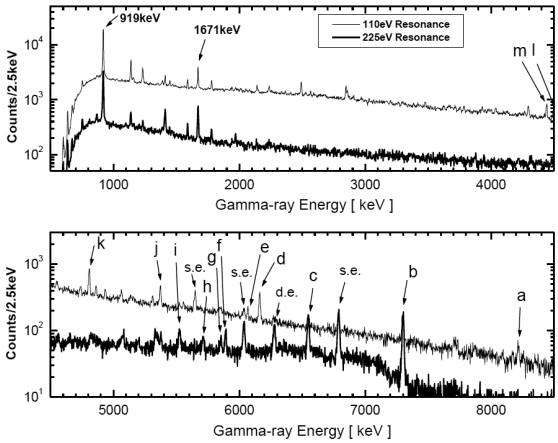

Figure 1. Gamma-ray pulse-height spectra for the 110- and 225-eV resonances of ^{93}Zr. The observed primary transitions are indicated by the arrows with symbols from a to m, respectively.

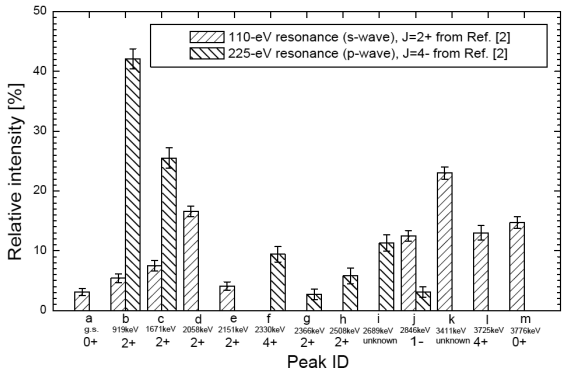

Figure 2. The relative intensities of primary transitions for the 110- and 225-eV resonances of ^{93}Zr. The energy, spin and parity of each final state are also indicated.

2.3 An Example of the Measurements with the NaI(Tl) Spectrometer

The neutron capture cross section of ^{99}Tc was measured with the NaI(Tl) spectrometer. The ^{99}Tc sample was metal ^{99}Tc cased in an aluminum disk container with inner diameter of 6.3 mm and inner thickness of 0.28 mm. The amount of ^{99}Tc was 78 mg. The sample was placed in continuous helium gas flow through a beam duct made of carbon fiber. The gamma-rays emitted from the sample were measured with the NaI(Tl) spectrometer. Measurements were made for the ^{99}Tc sample and an aluminum dummy container. The pulse height and TOF of each event was measured with a multi-stop time-to-digital converter and recorded in list format data files for offline data analysis. The obtained capture cross section of ^{99}Tc is shown in Fig. 3.

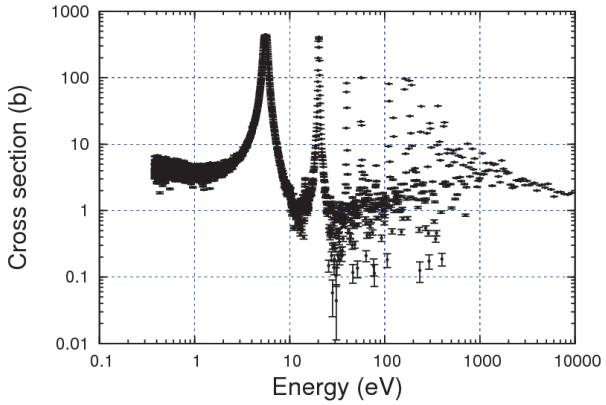

Figure 3. Neutron capture cross section of ^{99}Tc.

3. Summary

The neutron capture cross sections have been measured using the Ge and NaI spectrometers installed in the ANNRI. The neutron beam characteristics have also been measured in detail. From Feb. 2012, the ANNRI will be open for researchers under the MLF user program in the fields of nuclear data, nuclear astrophysics and quantitative analysis.

References

[1] K. Kino, M. Furusaka, *et al.*, Nucl. Instrum. Methods. Phys. Res. A, **626**, 58-66, (2011).

[2] J. Hori, *et al.*, Proc. of the Korean Nuclear Society, Spring Meeting, Taebaek, Korea, May 25-27 p.127-128 (2011). [CD-ROM]

[3] R. L. Macklin, J. A. Harvey, N. W. Hill, Nucl. Sci. Eng., **92** 525 (1986).

A. Kimura[1], M. Furusaka[2], K. Furutaka[1], H. Harada[1], J. Hori[3], M. Igashira[4], T. Kamiyama[2], T. Katabuchi[4], T. Kin[1], K. Kino[2], F. Kitatani[1], Y. Kiyanagi[2], M. Koizumi[1], M. Mizumoto[4], S. Nakamura[1], M. Oshima[1], and Y. Toh[1]

[1]*Nuclear Science and Engineering Directorate, JAEA;* [2]*Hokkaido University;* [3]*Research Reactor Institute, Kyoto University;*
[4]*Research Laboratory for Nuclear Reactors, Tokyo Institute of Technology;*

Studies of Neutron Optics for Physics Researches

1. Introduction

Neutron optics is a powerful tool to increase the utilization efficacy of neutrons to enhance the sensitivity in fundamental physics and material researches. A neutron beamline "Neutron Optics and Physics (NOP)" has been constructed at the port BL05 of the Materials and Life-science research Facility (MLF) of the J-PARC[1]. It is under commissioning for the study of neutron optics and fundamental physics.

Applications of developed optical devices to material researches are also in progress.

The BL05 beamline views the coupled moderator. A shutter and a biological shield are located in the regions of L=2.3-4.3 m and L=4.3-7.2 m, respectively, where L is the distance from the moderator. Supermirrors of m=2 with a cross section of 100 mm × 110 mm are installed in the shutter and biological shields are transporting neutrons into the inlet of the beam benders. A pre-position shield covers a region of L=7.2-12 m. The beam benders are installed in the void space inside the pre-position shield with height and width of 2 m and 1 m, respectively. The benders with curvature radii of approximately 100 m distribute cold neutrons into three beam branches: the low-divergence beam branch, unpolarized beam branch and polarized beam branch. The interiors of beam benders are filled with helium gas. Fast neutrons are absorbed in the beam dump placed in the region of L=12-16 m. The bent neutrons are transported into beam holes penetrating the beam dump and measuring approximately 15 cm × 15 cm. The configuration of the NOP beamline is shown in Fig.1.

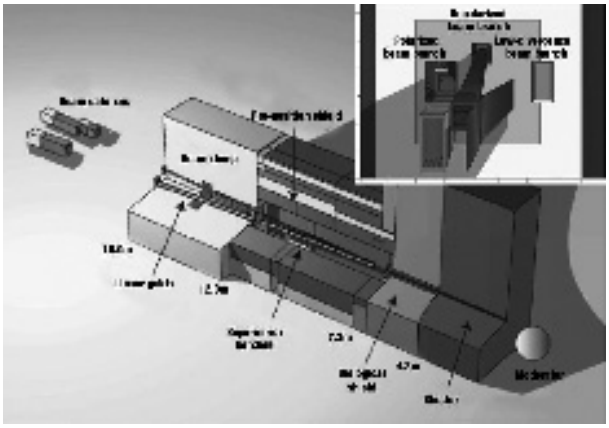

Figure 1. Schematic view of the configuration of the NOP beamline for study of neutron optics and fundamental physics at the beam port BL05.

2. Low-Divergence Beam Branch

The low-divergence beam branch is designed for the multilayer neutron interferometry. Two supermirrors of m=3 are installed to transport neutrons slower than 1.2×10^3 m s^{-1} with the density of 1.8×10^6 cm^{-2} μsr^{-1} s^{-1} MW^{-1}. A multilayer interferometer with spatially separated paths was successfully demonstrated for the steady beam from the reactor neutron source[2].

Further development to accept the pulsed beam is in progress. Additionally, an extension to the energy region of the very-cold neutrons (VCN) is also in progress. A possibility of unknown medium-range force searches is under discussion[3,4] in the VCN interferometry.

This beam branch was applied as the test port for the MIEZE (modulated intensity by zero effort) -type spin echo and also for the study of specularity of the neutron reflection on the surface of neutron mirrors[5]. The installation of the MIEZE-type spin echo at the J-PARC is in progress at port BL06.

3. Polarized Beam Branch

The polarized beam branch is designed for the study of neutron decay. A multichannel magnetic supermirror bender with m=2.8 is installed to provide polarized neutrons. The length of the bender is 4.5 m and the cross section is 10 cm × 4 cm. The bent neutrons are designed to be transported by an m=2 straight guide in the region of L=12-16 m, which has not been installed yet. After the completion of the additional guide installation and alignment, the flux

of 4.0×10^8 cm^{-2} s^{-1} MW^{-1} and polarization of 99.8% can be obtained for the neutron energy of larger than 1.5 meV[6,7]. Currently a measurement of the neutron lifetime is under development.

We measure the decay rate by counting decayed electrons using a time projection chamber (TPC). The detection gas contains the diluted ^{3}He and the incident neutron number is measured by counting the protons produced through the ^{3}He(n,p)^{3}H reaction. To reduce the background events efficiently, we developed a spin flip chopper (SFC)[8]. Fig.2 shows the experimental setup at the beginning of the R&D phase of the SFC and TPC. The developed SFC and a TPC are currently at the commissioning phase.

Figure 2. Installation of a spin flip chopper for the measurement of neutron lifetime at the polarized beam branch of the NOP beamline.

4. Unpolarized Beam Branch

The unpolarized beam branch is designed to be versatile. A measurement of angular distribution of scattering cross section is planned to search unknown medium range interactions between neutrons and neutral atoms. A five-channel supermirror bender is installed to bend neutrons upward with a curvature radius of 100 m. The length of the bender is 4 m and the cross section is 5 cm × 4 cm. The bent neutrons are designed to be transported by an m=2 straight guide in the region of L=12-16 m, which has not been installed yet. A neutron flux of 1.2×10^9 cm^{-2} s^{-1} MW^{-1} is expected after the completion of the additional guide installation and alignment.

Currently, a principle-proof experiment of the time-focusing of ultracold neutrons (UCNs) is in preparation at the unpolarized beam branch[9]. The time-focusing can be applied as an efficient transport of pulsed UCNs, which is proposed for the measurement of neutron electric dipole moment at J-PARC. We have successfully produced ultra cold neutrons (UCN) for the principle-proof experiment[10]. The very cold neutrons contained in the cold neutron beam are converted to UCN by the Doppler shift on the reflection by a moving mirror. The Doppler shifter is shown in Fig.3. It is designed to decelerate the v~140 m s^{-1} neutrons to UCNs with the multilayer mirror, which has the m-value of m=10.

A moving multilayer mirror of m=10 is installed to convert very cold neutrons (v~ 140 m s^{-1}) to ultracold neutrons by the Doppler shift.

Acknowledgement

This work was partially supported by the Creative Scientific Research Grant (no.19GS0210) of the Japan Society for Promotion of Science and the S-type Research Program (no.2009S03) of the Institute of Material Structure Science of KEK.

Figure 3. Doppler shifter installed at the unpolarized beam branch of the NOP beamline for the study of neutron optics and fundamental physics at the beam port BL05.

References

[1] K. Mishima *et al.*, Nucl. Instrum. Methods Phys. Res. **A600** 342 (2009).

[2] Y. Seki *et al.*, J. Phys. Soc. Jpn. **79** 124201 (2010).

[3] V.Gudkov, G.L.Greene, H.M.Shimizu, Nucl. Instrum. Methods Phys. Res. **A611** 153 (2009).

[4] V.Gudkov, H.M.Shimizu, G.L.Greene, Phys. Rev. C **83** 025501 (2011).

[5] M.Kitaguchi *et al.*, Physica B **406** 2470 (2011).

[6] T.Ino *et al.*, Physica B **406** 2424 (2011).

[7] Y.Arimoto *et al.*, Physica B **406** 2439 (2011).

[8] K.Taketani *et al.*, Nucl. Instrum. Methods Phys. Res. **A634** 134 (2011).

[9] H. M. Shimizu *et al.*, Nucl. Instrum. Methods Phys. Res. **A634** 25 (2011).

[10] S.Imajo, Master thesis, Faculty of Science, Kyoto University, Mar. 2011.

Y.Arimoto[1], N.Higashi[1], T.Ino[1], K.Mishima[1], T.Morishima[1], S.Muto[1], H.M.Shimizu[1,6,8], K.Taketani[1], N.L.Yamada[1], T.Yoshioka[1,A], T.Shima[2], H.Funahashi[3], M.Hino[4], M.Kitaguchi[4], Y.Iwashita[5], M.Yamada[5], S.Imajo[6], K.Asahi[7], K.Hirota[8], Y.Otake[8], Y.Seki[8], A.Yoshimi[8], H.Oide[9], H.Otono[9], S.Yamashita[9], and K.Sakai[10]

[1]*High Energy Accelerator Research Organization (KEK);* [2]*Research Center for Nuclear Physics, Osaka University;* [3]*Institute for the Promotion of Excellence in Higher Education, Kyoto University;* [4]*Research Reactor Institute, Kyoto University;* [5]*Institute for Chemical Research, Kyoto University;* [6]*Faculty of Science, Kyoto University;* [7]*Department of Physics, Tokyo Institute of Technology;* [8]*RIKEN;* [9]*International Center for Elementary Particle Physics, University of Tokyo;* [10]*Japan Atomic Energy Agency;* [A]*Faculty of Science, Kyushu University*

BL 08: Super High Resolution Neutron Powder Diffractometer SuperHRPD

1. Introduction

The goals of the NPD (Neutron Powder Diffraction) project at J-PARC/MLF are to 1) explore the science regions not accessible with existing NPD, plunge into 2) real time studies and *in situ* studies, 3) high throughput measurements and analytical use of NPD, and develop 4) dedicated NPD's [1,2]. While 2) – 4) will be the goals of the MLF powder diffractometers, NOVA, iMATERIA, PLANET and SPICA, 1) is the goal of SuperHRPD. Our work was interrupted by the earthquake, but here we report on our activity before the earthquake.

1) is only possible with the highest resolution without sacrificing intensity. Although the ultimate instrumental resolution at the highest scattering angle is evaluated with a Si single crystal to be Δd/d = 0.035%, the use of recycled one-dimensional He-3 detectors limits the best resolution as 0.06% even with a limited detector area and a slender type of sample holder (3 mm in diameter). In low beam power, large amount of powder sample and large solid angle are practically necessary which resulted in ordinary resolution of 0.1% in 2010. In November 2010, the neutron beam power reached 200 kW, implying that our goal should be pursued with continuously improving resolution. With the use of the best resolution, we have been planning to a) conduct a study on the structural physics in strongly correlated electron systems especially in the system where lattice – charge or lattice - spin interactions are dominant and small distortion within 0.001 – 0.01 Å is expected, and b) conduct a study on the structural physics with multiple competitive interactions where various phases are expected under changing sample environments, c) do structural studies on newly synthesized materials such as superionic conductors, superconductors, organic-inorganic hybrid structures, supramolecule, pharmaceutical, and other inorganic/organic compounds with large unit cells. We are doing a) and c) now and have reported the results elsewhere.

2. Present Status

The new SuperHRPD can be installed with at most 1500 one-dimensional ^{3}He position-sensitive detectors (PSDs) of 1/2 inch in diameter, but presently 384 PSD's (80 % of total), 288 (50 %) and 144 (30 %) in the backward bank, 90 degrees bank, and low-angle bank, respectively. In near future, high resolution detectors will be installed at the high angle side in the backward detectors bank. We have repeated commissioning carefully until we achieved reliable structural analyses [2 - 4].

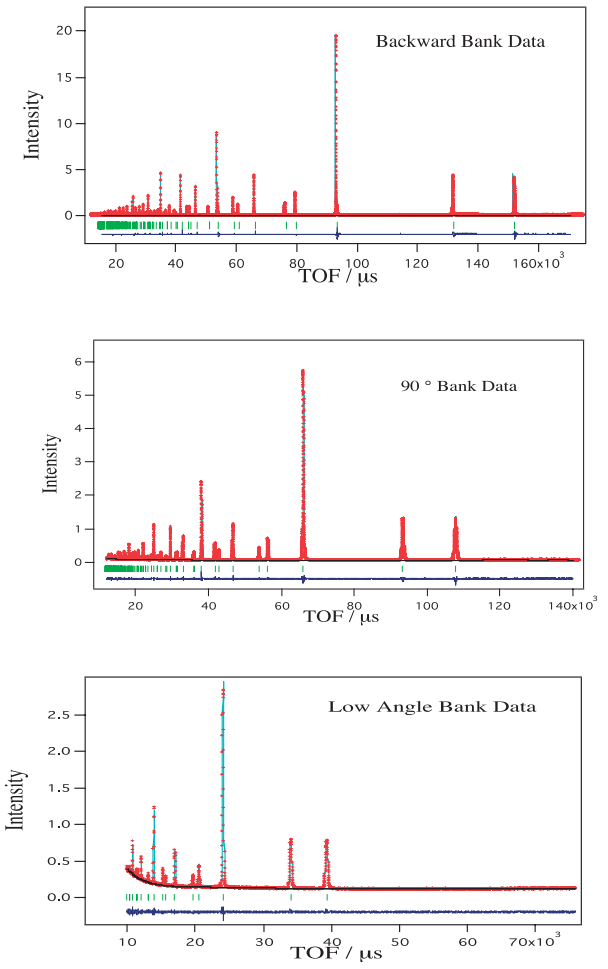

Figure 1. The Rietveld analysis patterns of CeO_2 for three banks: backward, 90°, low angle banks.

For all data from the three banks, Rietveld analyses were successfully carried out using a newly developed code, Z-Rietveld. For the standard Silicon of NIST (National Institute of Standards and Technology), the values of chi**2 and atomic displacement parameters obtained from Z-Rietveld are satisfactory: 2.03 and 0.46, 1.14 and 0.47, 1.12 and 0.76 for backward, 90° and low angle bank, respectively. Similar quality of analysis was obtained for other samples and the results were reasonable. Fig. 1 is the Rietveld fitting patterns of CeO_2 for three banks data [2 - 4].

3. User Programs

In the fiscal year of 2010, 24 general user proposals were submitted (18 in JFY 2009), and all proposals were approved (15 in JFY 2009). More than 40 % of the available beamtime was supplied to the general user program and the rest mainly to instrumental group use, and partially to the project use. Three general proposals could not be carried out due to the earthquake.

Beam times for instrumentation were primarily used for instrument maintenance including updating calibration data, establishment of the reliable structural analysis using three banks, and developments of sample environments. It was also used for the resolution studies and moderator performance studies described below.

4. Moderator and Pulse Shape Study

SuperHRPD is looking at a high-resolution poisoned decoupled hydrogen moderator (thin side), developed by the MLF moderator group. In order to attain narrow and symmetrical pulse shape in the wide energy range, several moderator parameters were chosen in 2002: the poisoning material (Cd), the poisoning position (20 mm), poisoning thickness (1.25 mm considering decrease in thickness on operation), AIC decoupler (decoupling energy of 1 eV) to reduce pulse tail in short wavelength region compared with Cd (0.4 eV). After continuous R & D by the MLF moderator group, they developed a high resolution moderator [2, 5, 6]. Detailed comparison between designed performance and experimental results were carried out for the first time.

Bragg spots of a silicon single crystal were measured with beam size of 10 mm × 10 mm. Bragg spot size was 38 mm (corresponding to three PSD's) × 30 mm (height) at the backward bank. Incident horizontal beam divergence was 0.3 mrad. AIC data used for the present McStas calculation was the same as before [5, 6] and Cd data was supplied by M. Harada. The detector pixel size for calculation was 12.7 mm × 10 mm. The results are shown in Figure 2 and 3. As shown in Figure 2, the Bragg peak profile shapes of the 400, 800 and 1600 reflections calculated from AIC data agree with experimental data in two order of magnitude.

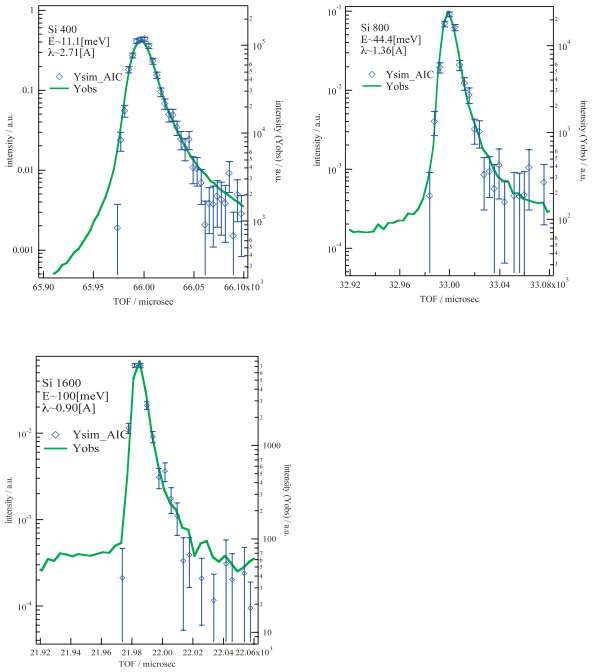

Figure 2. The comparison of Bragg peak profiles between experiments and McStas simulation calculated from Silver-Indium-Cadmium (AIC) alloy data. The solid line is observed data and marks are simulation from AIC data.

Figure 3 shows the comparison of Bragg peak shapes between observed and calculated from both AIC and Cd data. Using Cd data, the resolution worsens to 0.043 %. It was confirmed by the present study that the world highest resolution was accomplished by the use of the AIC decoupler.

5. Application

Towards the goal of SuperHRPD, several experiments have been proposed and some of them were already done.

One of the topics a) described in the introduction section is the long period spin structure seen in

$BiFeO_3$. Figure 4 shows the reported magnetic satellite peaks using a single crystal by Julia Herrero-Albillos *et al*. When we use a single crystal sample, all peaks are separated and it is easy to get high-resolution. The period of the spin cycloid structure is about 625 Å on this compound. When the same peak is measured using a conventional neutron powder diffractometer, it is almost impossible to see the split peaks.

The left hand panel in Fig. 5 is taken at HERMES diffractometer at JRR-3. This difractometer is a high-intensity and medium-resolution machine. We can see only one peak at (1/2 1/2 1/2)c position, which corresponds to the G-type magnetic structure. On the other hand, the data taken with SuperHRPD clearly shows the split peaks as shown at the right panel of Fig. 5. Then, we can measure the peak positions as a function of the composition x of mixed sample between $BiFeO_3$ and $BaTiO_3$ [8].

In the 4*d* metal system, distortion has rarely been detected so far. We planned to detect tiny distortion in 4*d* metal system such as $SrRuO_3$ at the phase transition observed by the resistivity mea-

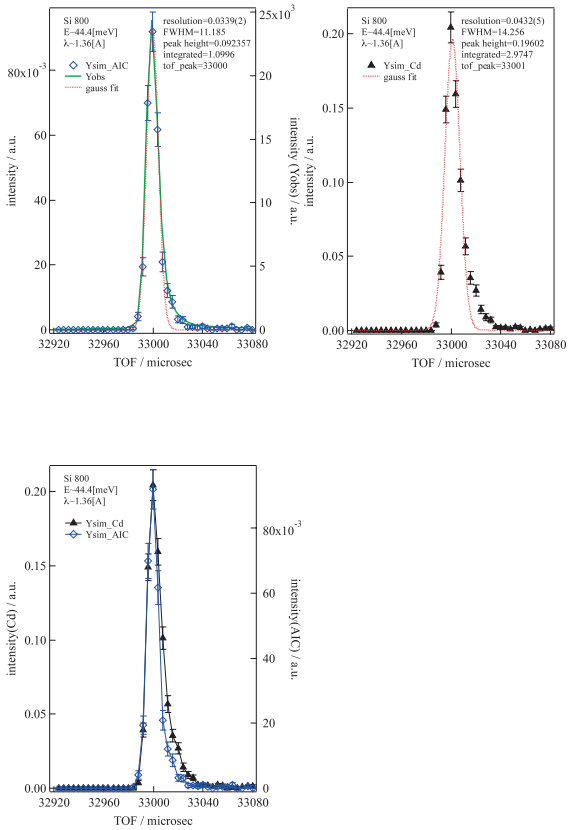

Figure 3. The comparison of Bragg peak shapes between observed and AIC simulation (top left, calculated resolution of 0.034 %), Cd simulation (top right, 0.043 %), and the comparison between AIC and Cd (rest) simulation. It is confirmed that the highest resolution was accomplished by the use of the AIC decoupler.

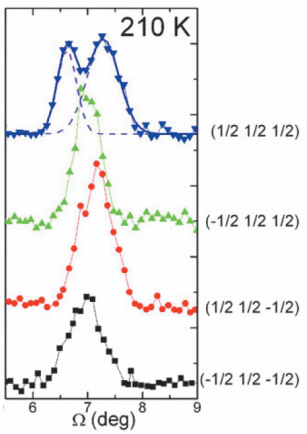

Figure 4. Magnetic satellite peaks of $BiFeO_3$ using single crystal after Julia Herrero-Albillos [7]. Indices of the top profile are $(1/2\ 1/2\ 1/2)_c \pm (\delta, -\delta, 0)$.

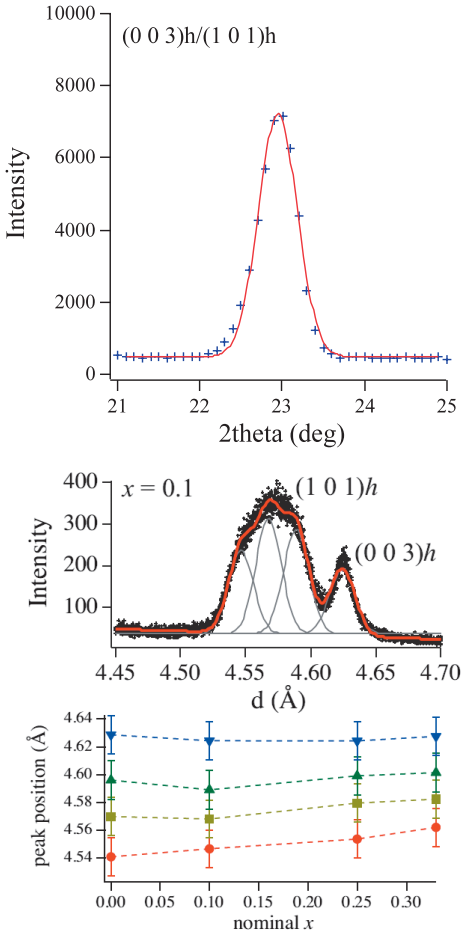

Figure 5. Magnetic peaks of (1-*x*)BFO-*x*BTO (*x* = 0.1) at room temperature using HERMES(top) and SuperHRPD(medium).

surements. The $SrRuO_3$ is the only ferromagnet in 4*d* perovskites. Our high resolution experiments revealed unusual temperature dependence of Ru-O bonds which may be a key to explain the unique ferromagnetism in the system [9].

Table I. Instrumental parameters of SuperHRPD.

Moderator	Poisoned decoupled hydrogen moderator
Primary flight path L_1	94.2 m
Curved guide	31.245 m (m = 3, r = 5 km)
Straight guide	51.4 m (m = 3)
Position for disk choppers	7.1 m (single), 12.75 m (double)
backward bank	
2θ	$150^\circ \leq 2\theta \leq 175^\circ$
L_2	2.0 - 2.3 m
d-range	0.3 - 4.0 Å
Resolution $\Delta d/d$	0.03 - 0.15 %
90 degree bank	
2θ	$60^\circ \leq 2\theta \leq 120^\circ$
L_2	2.0 - 2.3 m
d-range	0.4 - 7.5 Å
Resolution $\Delta d/d$	0.4 - 0.7 %
low-angle bank	
2θ	$10^\circ \leq 2\theta \leq 40^\circ$
L_2	2.0 - 4.5 m
d-range	0.6 - 45 Å
Resolution $\Delta d/d$	0.7 - 3.0 %

L_2 is the scattered flight path.

The structure and its relation to the piezoelectric properties of the lead-free ferroelectric material $(Bi_{0.5}K_{0.5})TiO_3$ - $BiFeO_3$ were studies by SuperHRPD and showed that the structural phase boundary from rhombohedral to pseudocubic structures exists in a ferroelectric phase at $0.4 < x < 0.43$. It is this point (x = 0.4) that the piezoelectric properties are superior [10].

Reference

[1] T. Kamiyama and K. Oikawa, ICANS-XVI, 309-314 (2003).
[2] S. Torii *et al.*, MLF Report (2009)
[3] S. Torii *et al.*, J. Phys. Soc. Jpn. **80** (2011) accepted.
[4] Panca *et al.*, Journal of Material Science, Proc. of ICMST(Jakarta, 2010)
[5] M. Harada, *et al.*, Proc. ICANS-XVI, 697-706 (2003).
[6] M. Harada, *et al.*, Proc. ICANS-XVI, 677-687 (2003).
[7] Julia Herrero-Albillos, *et al.*, J. Phys: Condens. Matter **22**, 256001 (2010).
[8] R. Kiyanagi *et al.*, submitted.
[9] J-G Park, *et al.*, submitted.
[10] H. Matsuo, Y. Noguchi *et al.*, J. Appl. Phys. **108**, 104103 (2010).

T. Kamiyama[1], S. Torii[1], J. Zhang[1], M. Yonemura[1], T. Panca[1], M. Ping[1], T. Muroya[1], R. Tomiyasu[1], Y. Noda[2], R. Kiyanagi[2], K. Mori[3], J-G Park[4], R. Kanno[5], Y. Idemoto[6], T. Kiyotani[7], and C-H. Lee[8]

[1]*Institute of Materials Structure Science & J-PARC center, KEK;* [2]*Institute of Multidisciplinary Research for Advanced Materials, Tohoku University;* [3]*Research Reactor Institute, Kyoto University;* [4]*Department of Physics & Astronomy, Seoul National University;* [5]*Interdisciplinary Graduate School of Science and Engineering, Tokyo Institute of Technology;* [6]*Faculty of Science and Technology, Tokyo University of Science;* [7]*The Instrument Analysis Equipment Research Center, Showa Pharmaceutical University;* [8]*Energy Technology Research Institute, National Institute of Advanced Industrial Science and Technology*

BL 09: Special Environment Neutron Powder Diffractometer SPICA

1. Introduction

A new neutron powder diffractometer, SPICA, at the ninth beamline (BL09) has been designed for the study of materials under special environments, such as battery research. Lithium ion batteries (LIB) are promising power sources for devices such as cell phones and laptop computers because of the high energy density. If the power capability could be improved, new applications such as a battery for electrical vehicles (EV) will spread out. In order to improve or innovate the battery characteristics, it would be very important to clarify the structure in materials of the electrodes (i.e., cathode and anode) and their solid electrolyte interface at an atomic level and this information will become a technological lodestar.

2. Design Concept of SPICA

The design concept of SPICA is to investigate the atom configuration of materials under special environments. In order to measure precisely the atom location or the change in the atomic configuration under special environments, SPICA was designed to have high resolution and high intensity. Therefore, the BL09 beamline for SPICA views the decoupled-poisoned moderator. Moreover, SPICA will be set with the flight path of L_1 = 52 m, which is the distance from the moderator to the sample position. The neutron guide was designed to keep the high intensity at the sample position. A high-performance focusing system with an elliptic supermirror was adopted to suppress the diffuse intensity. According to the preliminary simulation of the neutron guide, the elliptic guide shows an excellent performance over a wide range of wavelengths, in particular at short wavelength. Since in the beam line we have three disk choppers and one T_0 chopper, the neutron guide is divided into nine sections.

The flight path of 52 m from the moderator to the sample position means that SPICA is located outside of the main hall of the Materials and Life Science Facility (MLF). Then we constructed an annex experiment building for SPICA, as shown in Figs.1 and 2. The experiment building with about the size of 12(w) × 32(l) × 10(h) meters was designed to consist of two areas, that is, an experiment room and experimental preparation room.

SPICA consists of three detector banks that are the backward detector bank (150-175º), the multipurpose detector bank (13-140º) and the forward (small angle) detector bank (1-25º), as shown in Fig. 3. The distance L_2 from the sample to the detectors is about 2 m for all banks. The backward detector bank is used specifically to perform the high-resolution measurement of lattice parameters caused by reducing the $\cot\theta\Delta\theta$ contribution to the overall resolution. To cover this large detector area, about 1500 one-dimensional ^{3}He position-sensitive detectors (PSD's: 64 cm in length x half inch in diameter) will be used.

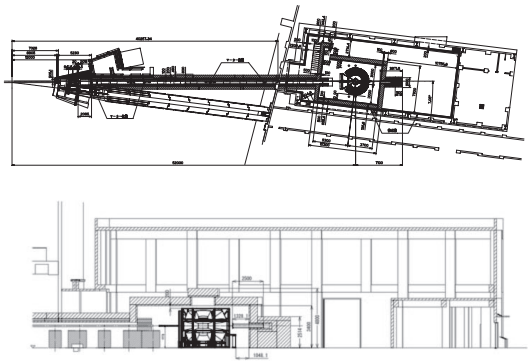

Figure 1. The ground plan of BL09 and the cross-section drawing of the experiment building for SPICA.

Figure 2. The view of the experiment building of BL09 (SPICA).

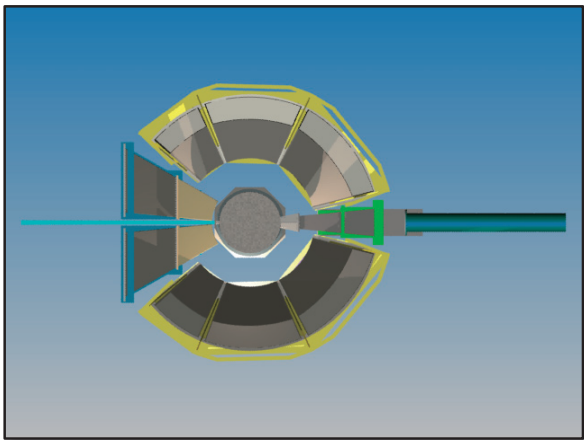

Figure 3. Three detector banks (blue: backward detector bank of 150-175º, yellow: multipurpose detector bank of 13-140º, green: forward detector bank of 1-25º) of SPICA.

The wide angle detector system with the backward detector bank, the multipurpose detector bank and the forward detector bank allows us to measure the diffraction data in the wide scattering vector *Q* range or the wide lattice space *d* range. More importantly, an in-situ observation of the atomic structure can be carried out under various special conditions. Therefore, all detectors of the three banks play an important role to detect tiny change and time-dependent change in the structure of the charging/discharging process of the battery.

In order to fulfill the role and aim of the detector banks, the chamber of the backward detector bank is evacuated for the high-resolution measurement on lattice space and the chamber of the forward detector bank is also evacuated to reduce the background caused by the downstream neutron beam. In contrast, the multipurpose detector bank has air scattering chambers in order to make it a snap to handle the various specialized equipment around the sample.

Kino et al. have reported loss of neutrons and contamination of scattered neutrons obtained by numerical calculation and simulation to materialize the air scattering chamber [1]. The loss of neutrons is 6 to 11 % although it is almost double compared to that of the vacuum scattering chamber. The contamination of the scattered neutrons by air is less than 1% when placing blades made of B_4C resin in the chamber as dense as possible. The contamination is seen on the TOF spectrum as continuous backgrounds between diffraction peaks. The air scattering chamber with the blades is acceptable for the multipurpose detector bank of SPICA diffractometer. A partially schematic perspective view of SPICA is shown in Fig. 4. In Fig. 5, an example of radiation calculation of SPICA is shown.

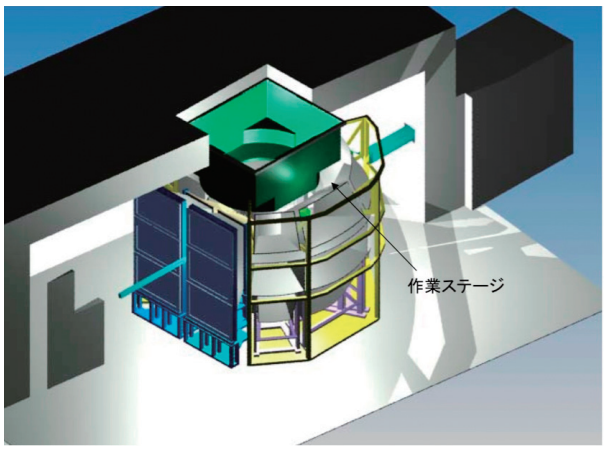

Figure 4. Partially schematic perspective view of SPICA.

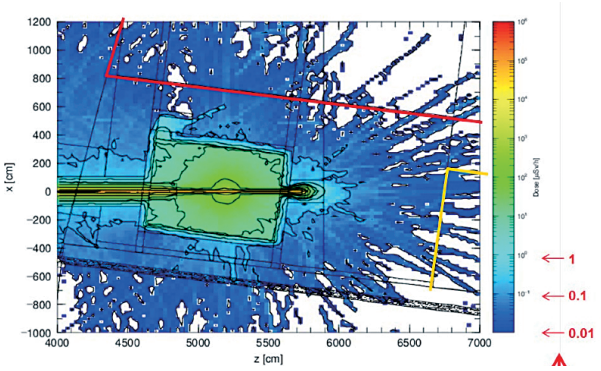

Figure 5. An example of radiation calculation of SPICA.

Reference

[1] K. Kino, K. Mori, M. Yonemura, S. Torii, M. Kawai, T. Fukunaga, T. Kamiyama, J. Phys. Soc. Jpn. **80** (2011) accepted.

K. Mori[1], M. Yonemura[2], T. Kamiyama[2], S. Torii[2], K. Kino[2], M. Kawai[2], and T. Fukunaga[1]
[1]Research Reactor Institute, Kyoto University; [2]Institute of Materials Structure Science & J-PARC center, KEK;

BL 10: NOBORU

1. Overview

NOBORU [1,2], "Neutron Beam- line for Observation and Research Use", is a versatile neutron instrument, which can serve as a test beam port. Beam times for the instrument group use were devoted for neutron source characterization and commissioning of newly installed devices. Three project use experiments, i.e., R&D on energy-selective imaging led by Dr. Matsubayashi of JAEA, R&D on neutron detectors and optical devices by Dr. J. Suzuki of JAEA, and Time-Of-Flight (TOF) -type prompt gamma-ray analysis by Dr. Y. Kasugai of JAEA were conducted. In addition, *NOBORU* welcomed four and five general use experiments in the first and second halves of JFY 2010, respectively. Industry people proposed three of nine general use experiments.

Energy-selective imaging with a pulsed neutron beam is one of the important experiments at *NOBORU*. As described later, we upgraded a rotary collimator, and newly installed a neutron filter device for this purpose. Bragg edge imaging, resonance absorption imaging and magnetic field imaging are promising techniques in the energy-selective imaging, and the test results are described in other sections in this report.

Many types of 2-D neutron detectors and cameras were tested to demonstrate their performance in terms of spatial resolution, temporal resolution, uniformity and high-counting rate capability. For example, a micro pixel chamber detector (μ-PIC), developed by Prof. T. Tanimori of Kyoto University, achieved spatial resolution of 400 μm and temporal resolution of several μs with a 10 cm square detector. Dr. T. Nakamura of JAEA confirmed a proper operation of a large area (256 × 256 mm) scintillation detector with a pixel size of 4 mm to be used for the *SENJU* instrument (BL18) as described elsewhere in this report.

As for optical devices, for example, R&Ds on high performance aspheric supermirrors for neutron focusing, a new slit package for Fermi choppers in which neutron supermirrors are coated, and a He-3 spin filter

Figure 1. Dr. A. Tremsin of UC Berkeley is assembling his multi-channel-plate type 2-D detector for imaging experiment.

based on the spin exchange optical pumping (SEOP) method to polarize neutrons were conducted by Drs. D. Yamazaki, M. Nakamura and H. Kira of all JAEA, respectively. In December 2010, Dr. H. Kira was awarded an encouraging prize by the Japanese Society for Neutron Science as a representative of the He-3 spin filter development team. The details of the three topics are described elsewhere in this report.

A workshop on "JAEA Project Researches at J-PARC/MLF" to discuss the research activities at BL04 and BL10 was held on October 28, 2010. The status of the instruments and the recent results were reported, and presentation materials were compiled during the proceedings [3].

2. Upgrade & Installation of Devices

NOBORU is equipped with a rotary collimator at about the middle of the beamline (L= 8 m) to make various pinhole geometries. Four collimation sizes, *Open*, *Large*, *Middle* and *Small* as explained in Table 1, are selectable to change the so-called collimator ratio (L/D) for imaging experiments. We found in 2009 that the neutron beam could be collimated with maintaining good signal to noise ratio even if the *Small* size was selected. To further collimate the neutron beam for higher L/D ratio, in JFY 2010, the *Middle* size col-

limator was replaced with the *Tiny* one (see Table 1).

Figure 2 compares neutron transmission images of a watch measured by neutron image plates with two collimator conditions, *Small* (L/D = 600) and *Tiny* (L/D = 1,875). The watch was set at 100 mm upstream to the image plate. It is obvious from Fig. 2 that very fine structures of the watch such as a thread and cog for the *Tiny* case are depicted much clearer than that for the *Small* case.

When a detector is exposed by the direct beam, such situation often occurs in imaging experiment, the neutron beam and gamma-flash are sometimes too intense to the detector. To mitigate the situation, a remote-controlled filter device was introduced in the beamline (see Fig. 3). A 6-mm-thick acrylic resin plate and a 1-mm-thick borosilicate glass are used to attenuate epi-thermal neutrons and cold neutrons, respectively. The lead metal and bismuth single crystal plates attenuate the gamma-flash. Figure 4 indicates reduction of neutron flux intensity behind the filters deduced by calculations.

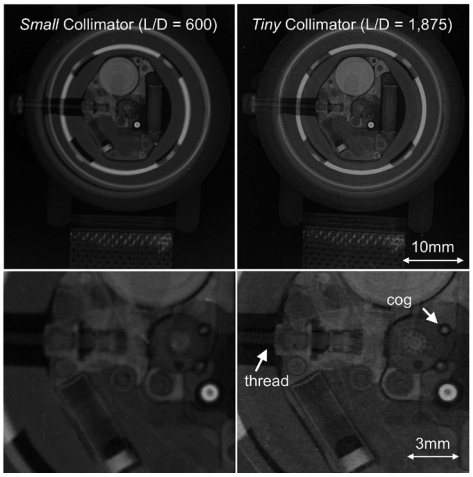

Figure 2. Comparison of neutron trans-mission images of a watch measured with the collimator conditions Small & Tiny (top: whole view, bottom: expanded view).

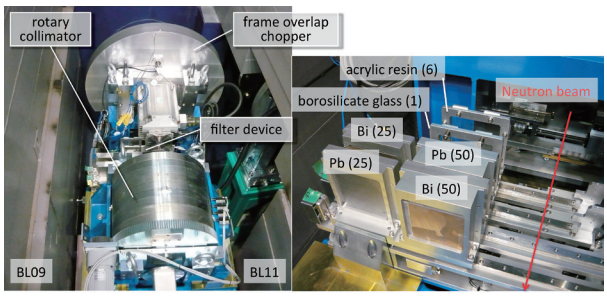

Figure 3. Beam controlling devices in the beamline (left) and a close view of the filter device (right).

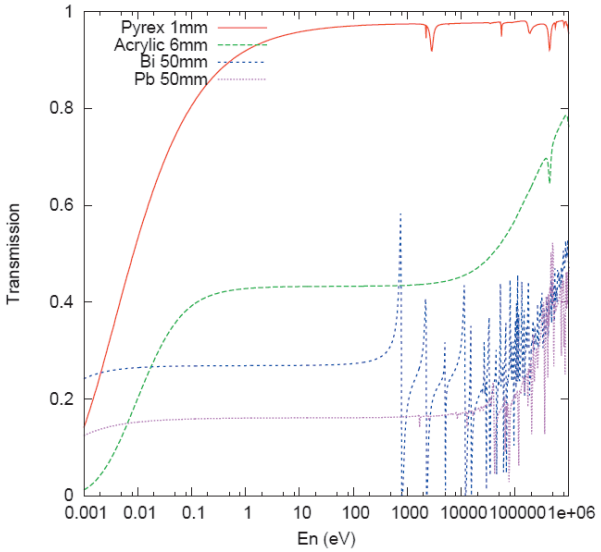

Figure 4. Reduction of neutron flux intensity behind the various filters.

3. The Best Pulsed Neutron Imaging Instrument in the World

Due to the upgrading efforts, *NOBORU* is now the best pulsed neutron imaging instrument in the world as as shown below:

- Good energy resolution ($\Delta t/t$: 0.3%) due to the short pulsed source and the decoupled moderator
- Wide band width up to 9 Å due to the short L1 (14 m) and long pulse interval (40 ms/25 Hz)
- Intense cold neutron flux (4.8×10^7 n/s·cm^2 at 1 MW)
- Variable and high collimator ratio (L/D = 140, 190, 600, 1,875)
- Small beam divergence due to neutron guide-less beam-line design
- Epi-thermal and fast neutrons, and even gamma-rays available
- Large field of view (100×100 mm^2), the largest in MLF
- High n/γ ratio by the TOF separation
- Versatile experimental space of 2.5 (W) $\times$ 3.5 (L) $\times$ 3.0 (H) m^3 to introduce various experimental setups
- Strong radiation shield to accept large samples

The experiences with imaging techniques accumulated so far at *NOBORU* are now utilized for design of a forthcoming new instrument dedicated for imaging at J-PARC/MLF.

Table 1. Selectable collimation sizes, L/D ratios and collimation areas of the rotary collimator.

Diminutive	Size [mm]	L/D Ratio	Collimation Area [mm^2]	Remarks
Open	100.0 × 100.0	140	10,000	
Large	31.6 × 31.6	190	1,000	
Middle	17.8 × 17.8	337	300	dismantled
Small	10.0 × 10.0	600	100	
Tiny	3.2 × 3.2	1,875	10	newly introduced

References

[1] K. Oikawa, F. Maekawa, M. Harada, T. Kai, *et al.*, Nucl. Instr. Meth., A **589** 310 (2008).

[2] F. Maekawa, K. Oikawa, M. Harada, T. Kai, *et al.*, Nucl. Instr. Meth., A **600** 335 (2009).

[3] R. Kajimoto, F. Maekawa, H. Arima, *et al.* (Ed.), JAEA-Review 2011-014 (2011, in Japanese).

F. Maekawa, M. Harada, K. Oikawa, M. Ooi, and T. Kai

Materials and Life Science Division, J-PARC Center

BL 11: High Pressure Neutron Diffractometer PLANET

PLANET is a powder diffractometer specifically designed for high-pressure use, which is now being constructed at BL11 in MLF/J-PARC. The purpose of the beamline is to study the effects of the water on the static and dynamic structures of the Earth. By employing diffraction and radiography techniques, we can reveal the microscopic and macroscopic structures of the hydrogen-bearing materials, such as hydrous minerals and magma, at the condition relevant to the Earth's upper mantle (~20GPa, ~3000K). In 2008, we finished the grand design, and started construction in 2009.

This year, we installed all the optical devices scheduled for the upper stream part, such as collimators, supermirror guides, two disc choppers, and two 4D-slits, and constructed the control cabin with a sample preparation area (Fig. 1).

We also installed the interlock system for the radiological safety and received the first beam on March 8, 2011. The obtained 2D image is shown in Fig. 2. The beam distribution agrees well with the one predicted by the ray-tracing simulation.

Together with the installation, we manufactured the large press, detector banks and hardware for data acquisition. Among them, the high-pressure press is a key device to determine the success of this beamline. This year, we made a big change in its design. So far, we plan to install the combinational DIA-type multi-anvil apparatus which is widely used in synchrotron facilities in Japan. In this system, six anvils are synchronously proceeded by guide blocks, but these blocks severely restrict the opening angles. In synchrotron x-ray diffraction, this does not matter due to the sufficiently large beam flux. However, it becomes a big disadvantage in neutron diffraction because the detection efficiency is usually gained by increasing the detector covering solid angle against the insufficient flux of neutron source. So, we decided to employ the recently invented 6-ram, 6-axis multi-anvil press.

Figure 3 shows the new press to be installed in

Figure 1. PLANET and the control cabin.

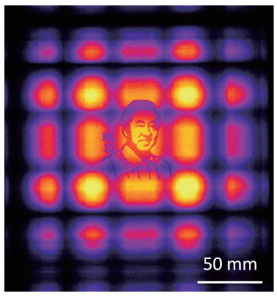

Figure 2. Beam distribution at the down stream of the sample position (To check the resolution, the beam is partially masked by a figure).

BL11. It's called "ATSU-HIME(圧姫)" meaning "high pressure princess" in Japanese. The press has six independently controlled hydraulic rams (max. load is 500 ton per axis), and each ram is regulated so that the difference between their strokes is kept within 10μm. The independent nature of each ram also enables the deformation experiments at high-*PT* conditions. The non-use of the guide blocks offers wide scattering angles of 2θ = 90±14° as well as a closer approach of the radial collimator to the sample, which eliminates the background from sample surrounding materials.

As already described, we received the first beam and held the celebration ceremony on March 11, 2011(Fig. 4). While waiting for the neutron beams offered that evening, the Great East Japan Earthquake hit the J-PARC. Fortunately, everyone evacuated safely and the damage to PLANET is insignificant. We will finish the recovery and the construction in 2011, and start the commissioning in 2012.

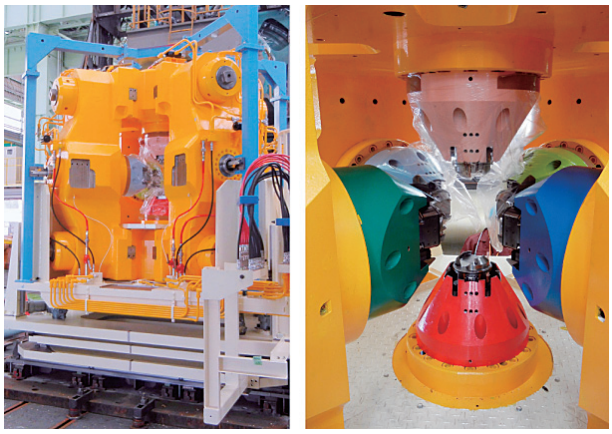

Figure 3. Overview (left) and the center part(right) of the 6-axis multianvil press “ATSU-HIME”

Figure 4. Photo at the first beam ceremony, taken just before the big earthquake.

This project is supported by Grant-in-Aid for Creative Scientific Research (19GS0205) from the Japan Society for Promotion of Science and Grant-in-Aid for Scientific Research on Innovative Areas (No. 20103001) from the Ministry of Education, Culture, Sports, Science and Technology (MEXT) of Japan.

T. Hattori[1, 2], H. Arima[2], A. Sano[1, 2], W. Utsumi[1, 2], H. Kagi[3], and T. Yagi[4]

[1]Quantum Beam Science Directorate, JAEA; [2]Materials and Life Science Division, J-PARC Center; [3]Graduate School of Science, The University of Tokyo; [4]The Institute of Solid State Physics, The University of Tokyo

Performance of High Resolution Chopper Spectrometer (HRC)

1. Introduction

The High Resolution Chopper Spectrometer (HRC) was installed at the BL12 beamline at MLF to study dynamics in materials in a wide energy momentum space with high resolutions and relatively high-energy neutrons. HRC has been almost completed and we evaluated its performance [1,2].

2. Performance of HRC

To evaluate the HRC performance, a monochromatic neutron beam with the Fermi chopper or a white neutron beam without the Fermi chopper was incident on the vanadium standard sample, and the scattered neutrons were observed at the array of 128 position sensitive detectors (PSDs) located at scattering angles between 3° and 40°. The neutron intensities at the PSD array for the white beam are plotted in Fig. 1(a). The observed intensities were in good agreement with the calculations in the absolute values within a factor. Figure 1(b) shows the elastic scattering energy spectrum for the incident neutron energy of E_i = 203 meV with the optimum chopper at 600 Hz, which provides roughly the optimum condition $\Delta t_{ch} = \Delta t_m$, where Δt_{ch} is the chopper open time and Δt_m is the pulse width, as a function of the energy transfer. The solid line is a calculated curve without any adjustable parameters. The energy resolution obtained from the observed energy width was ΔE = 5.2 meV, i.e., $\Delta E/E_i$ = 2.5%. The observed neutron intensities for monochromatic and white beams agreed with the calculations in absolute values, it was also confirmed that $\Delta E/E_i$ = 2.5% in the energy resolution, as designed for the optimum condition.

The T0 chopper is a key device to reduce background noise originating from high energy neutrons emitted during neutron production at time zero. Figure 2(a) shows the TOF spectrum at the PSD array from the standard vanadium sample with the T0 chopper running at 100 Hz, and with the T0 chopper off. The Fermi chopper was operated at 600 Hz.

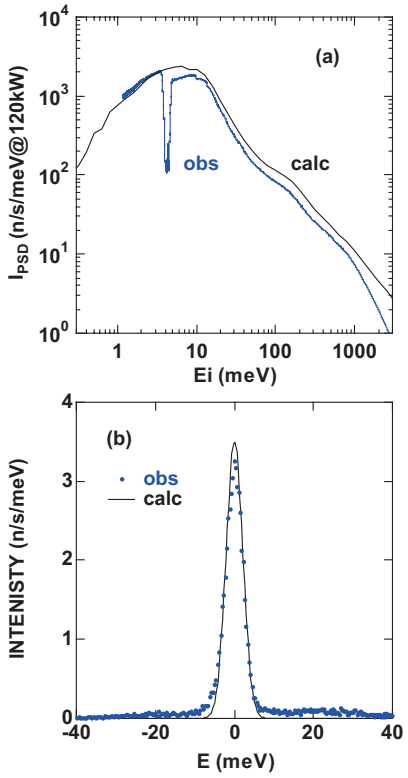

Figure 1. Neutron intensities at the PSD array for white neutron beam (a) and for E_i = 203 meV (b). The dip in (a) is caused by the operation of the T0 chopper.

Since the slit width of the Fermi chopper is coarse, the neutron beam passes through the Fermi chopper every half turn, causing the appearance of many peaks. The neutron energy of the peak at TOF = 2000 μs corresponds to 0.5 eV. We successfully reduced the background noise at neutron energies near 0.5 eV by two orders of magnitude. Figure 2(b) shows the T0 chopper transmission observed with the white beam for the standard sample. We confirmed that the transmission recovers below 2.5 eV at 100 Hz, as designed. The energy for 50% transmission at 100 Hz is 10 eV, then, eV neutrons can be utilized with a slight reduction in intensities.

3. Observation of Excitations

After confirming the performance of HRC, we measured the magnetic excitations in the one-

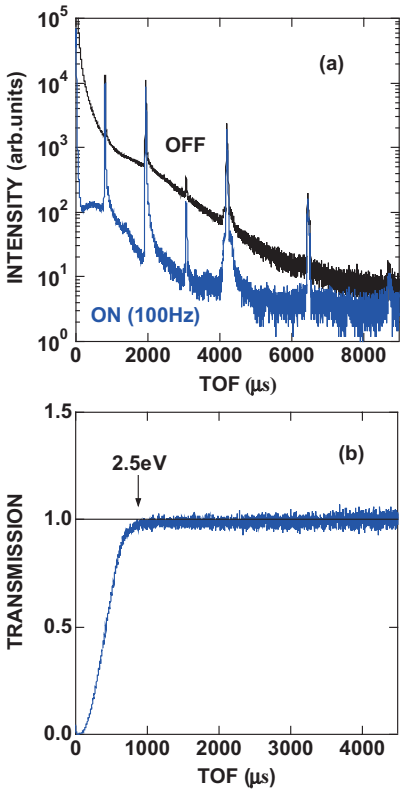

Figure 2. Background noise reduction for a monochromatic beam (a): TOF spectra with operating the T0 chopper at 100 Hz (ON) and without operation (OFF). Transmission at 100 Hz measured with a white beam (b).

dimensional (1D) antiferromagnet $CsVCl_3$ at 20 K above T_N = 13 K, where the 1D nature is dominant. It took 56 hours for the sample and 24 hours for the empty scan at 120 kW of proton beam power. Figure 3 shows the background subtracted intensity. The dispersion curve of magnetic excitations starting at the magnetic zone center at q = 1 $Å^{-1}$, and the excitations near the magnetic zone boundary at q = 1.5 $Å^{-1}$ and E = 75 meV were clearly observed. This experiment indicates that the overall excitations can be clearly observed in 56 hours, which is expected to be reduced to only 7 hours for the full power operation of J-PARC (1MW). The counting rate is improved by using long PSDs, and the energy and the momentum resolutions are also improved by integrating intensities within a PSD after correcting the energy transfers at the positions of detected neutrons with high positional resolutions. As a result, the dispersion curve including the weak intensity parts was clearly observed.

Also, excitations were observed in the three-dimensional (3D) system MnP, which is ferromagnetic below T_C = 291 K. The dispersion of ferromagnetic magnons in the energy momentum space exhibits a parabolic surface whose apex is on the reciprocal lattice point. Scattering intensities were observed on the ring crossing between the scanning surface of the detectors and the parabolic dispersion surface. The ring shown in Fig. 4 includes magnons. Phonons also exist in the same position, so magnons could be separated by comparing the data at 300 K.

4. Summary

The construction of HRC has been almost completed. We confirmed that, under limited conditions, the neutron intensity and the energy resolution were in good agreement with the design values. Also, we verified the data analysis process by visualizing excitations in 1D and 3D single-crystal magnetic systems.

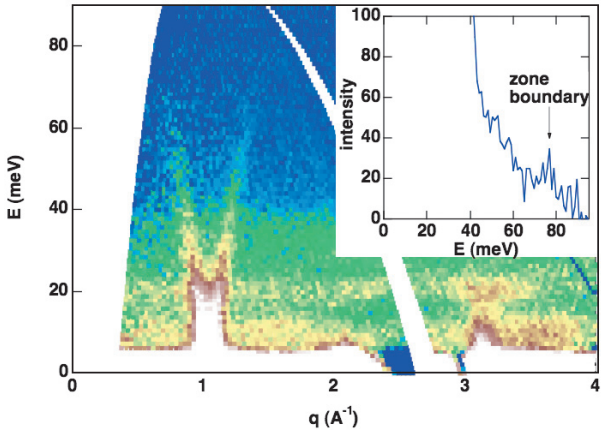

Figure 3. Excitation spectrum in $CsVCl_3$ observed at 20 K with E_i = 100 meV. The inset shows the zone boundary spectrum.

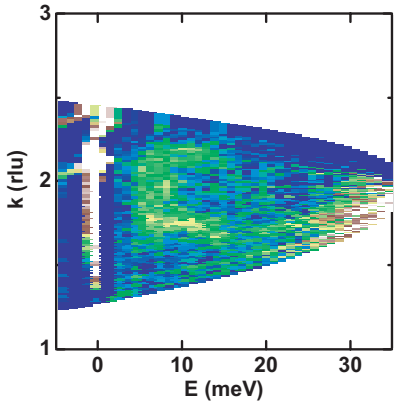

Figure 4. Excitation spectrum in MnP observed at 60 K with E_i = 35.8 meV.

References

[1] S. Itoh, T. Yokoo, S. Satoh, S. Yano, D. Kawana, J. Suzuki and T. J. Sato, Nucl. Instr. Meth. Phys. Res. A **631** 90 (2011).

[2] S. Yano, S. Itoh, S. Satoh, T. Yokoo, D. Kawana and T. J. Sato, Nucl. Instr. Meth. Phys. Res. A **654** 421 (2011).

S.Itoh[1], T.Yokoo[1], D.Kawana[1], S.Yano[2], S.Satoh[1], T.J.Sato[3], T.Masuda[3], and H.Yoshizawa[3]

[1]*Institute of Materials Structure Science, KEK;* [2]*Graduate School of Science and Engineering, Aoyama Gakuin University;* [3]*The Institute for Solid State Physics, The University of Tokyo*

BL 14: AMATERAS

1. Introduction

In JFY 2010, AMATERAS (Fig. 1) moved into full-scale user program operation. We provided 80% of the beam-time to the user program, while 20% was spent for commissioning works and covering users' beam-time lost by accidental problems. Although we had four days of down time due to a problem with the main chopper, we had no other serious instrumental problems. One of the significant events at AMATERAS this year was that a post-doctoral fellow, Dr. T. Kikuchi, joined our group. From JFY 2010, three members of AMATERAS including two instrumental scientists, K. N. and S. O-K. are mainly taking care of users.

2. User Program

AMATERAS accepted three project-use proposals and eight general-user proposals in JFY 2010. The accepted project-use proposals are 'magnetic excitations in quantum spin systems and frustrated magnets (PI (principal investigator): K. Kakurai),' 'neutron scattering study of high-T_c superconductors (PI: M. Arai),' and 'dynamical studies of functional materials from the perspective of glassy science (PI: M. Nakamura).' Eight accepted general-user proposals deal with a large variety of research fields, such as strongly correlated electron systems, biomaterials, ion conductors and liquid. We spent 92 days on these proposals. It should be noted that two of general-user proposals were cancelled due to the earthquake on March 11, 2011.

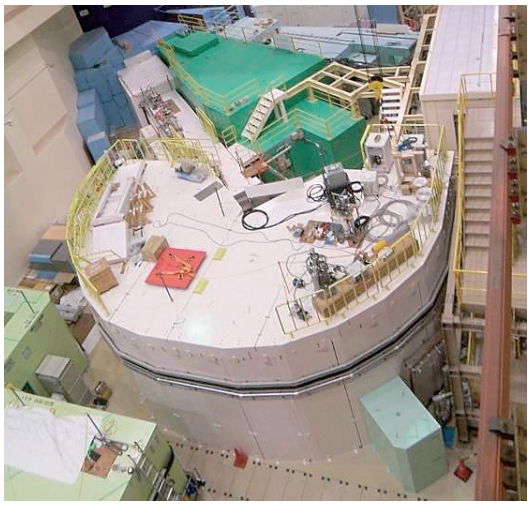

Figure 1. Recent photo of AMATERAS.

Figure 2. Prof. Yamamuro (Univ. of Tokyo) (upper right) and his colleagues preparing their experiment with Dr. Kikuchi (upper left), a new post-doctoral fellow at AMATERAS.

Figure 3. Prof. Iwasa (Tohoku Univ.) (upper left) watching setting-up of his carry-in cryostat. It was March 11 and just after taking this photo, the earthquake hit MLF, J-PARC.

The scientific output from AMATERAS is already being made public. By the end of JFY 2010, two scientific papers were published and one was submitted. More than 30 presentations were contributed to scientific meetings (annual meetings of academic societies, international symposiums, domestic meetings etc.) in JFY 2010.

3. Instrumentation

In JFY 2010, 25 days of beamtime were spent to provide spare beam-time to users, whose experiments were disturbed by unexpected problems, and for commissioning works.

One of the issues of instrumental studies is enhancing the performance of multi-E_i (Repetition Rate Multiplications) measurements on AMATERAS. Part of users' interest regarding multi-E_i measurements on AMATERAS is obtaining data at different resolutions to view the dynamics of different time scales through a single measurement. An energy resolution variation of more than three orders of magnitude is possible on AMATERAS. However, the E_is' range which we could use in a single experiment so far was rather limited, because we were working at one frame time-length to avoid frame overlapping. We studied the possible operation modes of 5 sets of choppers on AMATERAS and found a solution at which we can obtain almost two order of magnitude in the range of the energy resolution difference. At one of the conditions, for example, we can get access to four different E_is, i.e., 42.4 meV, 7.8 meV, 3.1 meV and 1.7 meV without overlapping up to the energy transfer of 0.53E_i. This combination corresponds to the variation of the energy resolution from 10 μeV to 0.9 meV. Another effort has been done in preparing data analysis software, which can simultaneously handle the data obtained by several different E_is. A preliminary version of the fitting software is now available, however we need further development to prepare a software package that can be used by the general users.

Also, some of the commissioning beam-time was consumed for measurements of standard samples for instrumental performance tests, commissioning of sample environments including users' carry-in devices, background measurements and test experiments. A part of the results of the recent commissioning works can be found in the latest AMATERAS paper [1].

We have also found several problems in the spectrometer during this year's operation. A distribution in neutrons' arrival time at the elastic channel was found during high resolution experiments. This was caused by tiny tilting and shifting of detector banks, which resulted in a few mm deviations from the assumed flight path lengths. These path lengths were calibrated by using obtained data on the analysis software. One of the user groups found serous background, which can be seen as a dispersive excitation on a Q-ω map of powder average data. It is caused by an aluminum radiation shield of a cryostat (t = 10 μm). The most effective counter- measure is introducing a radial collimator, which is still missing on AMATERAS. We have started to prepare the collimator and it will be installed in JFY 2011.

As of the instrumental upgrading, we have introduced several auxiliary facilities. We installed a jib crane (Fig. 4), which is used for sample environments exchange. Also, a He recovery line has been prepared for future experiments using liquid He. From the end of JFY 2009 to the beginning of JFY 2010, we installed additional shielding materials in the beam line (Fig. 5) and in front of the scattering chamber to reduce the background. During the same period, a Cd beam duct and a new beam narrower were installed inside the scattering chamber (Fig. 6), which also contributed to reduction in the unexpected scattered neutrons observed by the detectors. Additional upgrading of the utilities (installing new cooling water connections, adding new electric power lines etc.) was also done to improve users' convenience.

Figure 4. A jib crane newly installed at AMATERAS

Figure 5. Installation of polyethylene blocks at the beam line.

40% of the detector banks are still empty. Also, the realignment of the miss-aligned super-mirror beam transport remains to be done. These items

Figure 6. Installation of a Cd beam duct and a beam narrower in the scattering chamber.

are homework left from JFY 2009 and are still listed in our future tasks. Installing monitor counters and a radial collimator are also left in the to-do-list for JFY 2011 with other small items.

Reference

[1] K. Nakajima, S. Ohira-Kawamura, T. Kikuchi *et al.*, Submitted to J. Phys. Soc. Jpn.

K. Nakajima[1], S. Ohira-Kawamura[1], and T. Kikuchi[1]
[1]*Materials and Life Science Division, J-PARC Center*

Development of the Smaller-Angle Neutron Scattering Instrument TAIKAN

The small-angle neutron scattering technique is indispensable in research of microstructures, higher-order structures, and hierarchical structures in materials science and life science. However, the recent progress in nanotechnology and research of complex multi-component or multi-phase systems and non-equilibrium systems created the need to enable the SANS instrument to measure structural information more efficiently with higher structural and time resolution. In order to meet those requirements, the smaller-angle neutron scattering instrument TAIKAN has been constructed at BL15 in MLF of J-PARC since JFY 2009.

TAIKAN is composed of a set of independent components: a shield, optical devices, 4 choppers, a sample stage, a scattering chamber, 5 detector banks, and a DAQ system. Most of them were installed at BL15 in JFY 2010.

The external appearance of TAIKAN is shown in Fig. 1. The sample stage, scattering chamber, and the 5 detector banks are installed in a green shield. On the shield there are a door to go in the shield and a hatch to bring in accessories for sample environment. Figure 2 shows a picture of members of a TAIKAN development group or contractors with the scattering chamber in the background, which was taken in the early morning of December 23, 2010. Figure 3 shows the vacuum chambers for the optical devices and disk choppers set in the upper stream of the sample stage. In the vacuum chambers, xy-slits and collimators have been already installed, supermirror and quadrupole polarizers guide coils, spin flippers, and sextupole magnetic lenses will be installed in JFY 2011~2012. Figure 4 shows a small-angle detector bank, which is installed in the scattering chamber. 608 ^{3}He PSD tubes with 8 mm in diameter and 500, 800, or 1,000 in effective length were mounted on the detector bank. The pressure of the ^{3}He gas is about 0.6 MPa. Figure 5 shows a picture of a TAIKAN development group with the research fellow Dr. V.K. Aswal and the student Y. Su, which was taken on

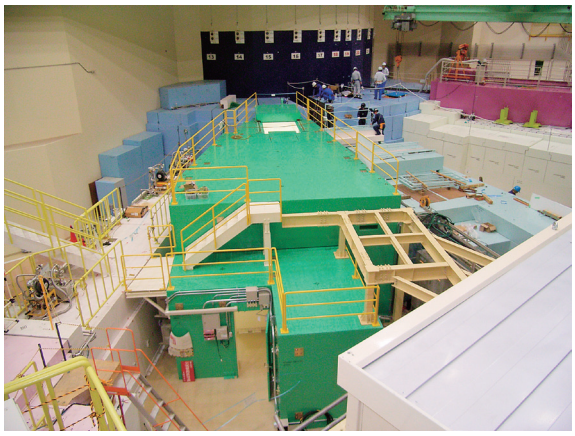

Figure 1. The external appearance of TAIKAN with a green shield.

Figure 2. A souvenir picture taken on the day of installing the scattering chamber at BL15.

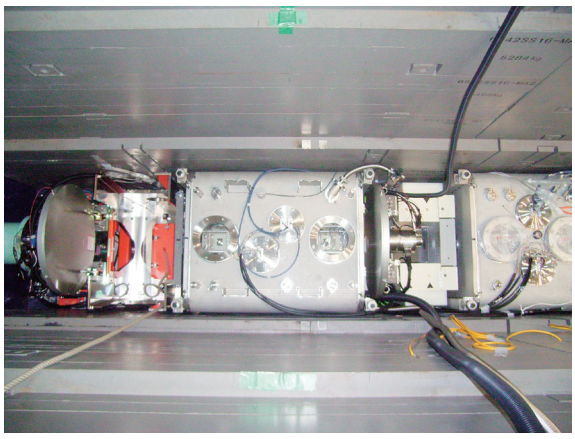

Figure 3. Optical devices and disk choppers installed in the beam line shield.

Figure 4. A small-angle detector bank with ^{3}He PSD tubes.

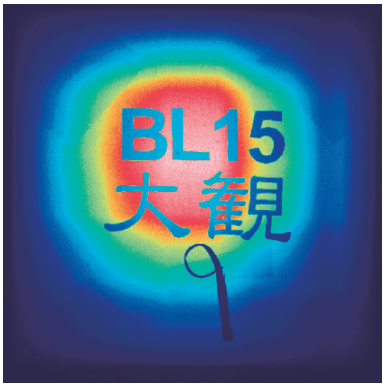

Figure 6. The first neutron image taken at the BL15 with a mask of "BL15" and "TAIKAN" in Japanese writing.

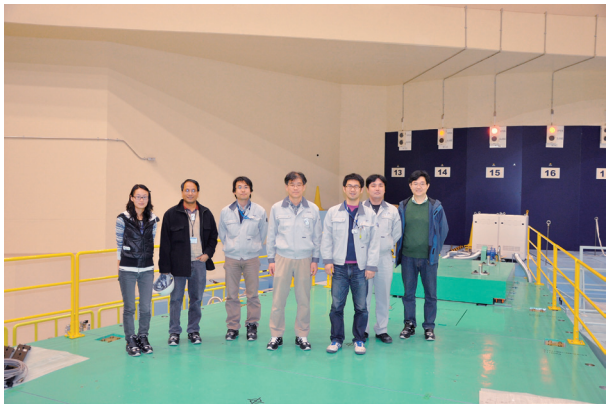

Figure 5. A souvenir picture taken on the day of receiving the first neutron pulse at BL15 with Dr. V.K. Aswal and Y. Su.

March 8, 2011. On that day the first neutron image was successfully taken at BL15 as shown in Fig. 6.

The beam commissioning began smoothly but was unfortunately interrupted by the big earthquake. It will be resumed at the end of the JFY 2011 and after that we will start the user program.

J. Suzuki[1], S. Takata[1], T. Shinohara[1], T. Oku[1], H. Kira[1], T. Nakatani[1], Y. Inamura[1], T. Ito[1], K. Suzuya[1], K. Aizawa[1], M. Arai[1], T. Otomo[1,2], and M. Sugiyama[3]

[1]Materials and Life Science Division, J-PARC Center; [2]Institute of Materials Structure Science, KEK; [3]Research Reactor Institute, Kyoto University

Horizontal-type Neutron Reflectometer SOFIA

1. Introduction

Neutron reflectometry is a powerful method for investigating the surface and interfacial structures of materials in the spatial range from nanometers to sub-micrometers. BL16 at MLF in J-PARC is dedicated for a horizontal type reflectometer. In this beam line, neutrons are transported downward at two different angles, 2.2° and 5.7°, relative to the horizontal. In December 2008, we started to accept the neutron beam at BL16 with the old ARISA reflectometer [1] relocated from KENS facility, KEK, Japan. This reflectometer, ARISA-II, was open for users from 2009, and made a scientific publication [2-6].

This year, we installed a T0 chopper to cut fast neutrons, a NiC mirror to cut very slow neutrons, and a brand-new reflectometer to replace old ARISA components. The novel reflectometer "SOFIA (SOFt-Interface Analyzer)" started running at the end of January 2011 [4,7]. In this report, we will present the design and performance of the SOFIA reflectometer. All measurements were performed at proton power level of 220 kW before the earthquake of March 11, 2011.

2. Performance of SOFIA reflectometer

Figure 1 shows a drawing of SOFIA in the experimental hutch. SOFIA reutilizes the same T0 chopper, disk chopper, NiC mirror, and 2-dimensional scintillation detector (^{6}LiF/ZnS) as ARISA-II. With the new slits, sample, and detector stages, we can accept both the 2.22° and 5.71° beam lines. This enables us to measure NR over wide scattering vector (q) region on free liquid surfaces. Also, the slit system of SOFIA is very precise compared with that of ARISA-II. The specification of the minimum aperture of SOFIA is 0.01 mm in the vertical direction and 2 mm in the horizontal direction, which is dozens of times less than that of ARISA-II. This enables us to irradiate a square area of 10 mm, which is the typical sample size of advanced materials in the research phase, with an angular resolution of 3%.

To check the performance of SOFIA, we performed a NR measurement using a deuterated polystyrene (d-PS) thin film spun-cast on a silicon substrate. Figure 2 shows the obtained NR profile. The reflectivity reaches 1×10^{-7} at q~4 nm^{-1}, and is well reproduced by a theoretical curve considering a plausible scattering length density of d-PS (6.46×10^{-4} nm^{-2}) and thickness evaluated by ellipsometery (98 nm). The typical duration times for the specular reflectivity measurement are shown in Table 1. In the case of deuterated polymers with a scattering length

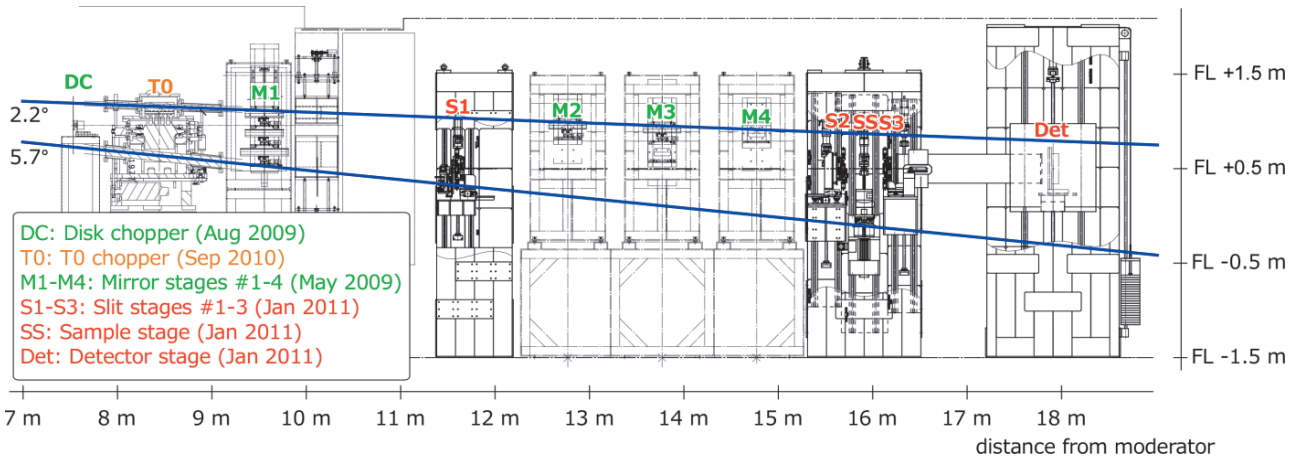

Figure 1. Side view of SOFIA reflectometer placed at BL16 in J-PARC/MLF.

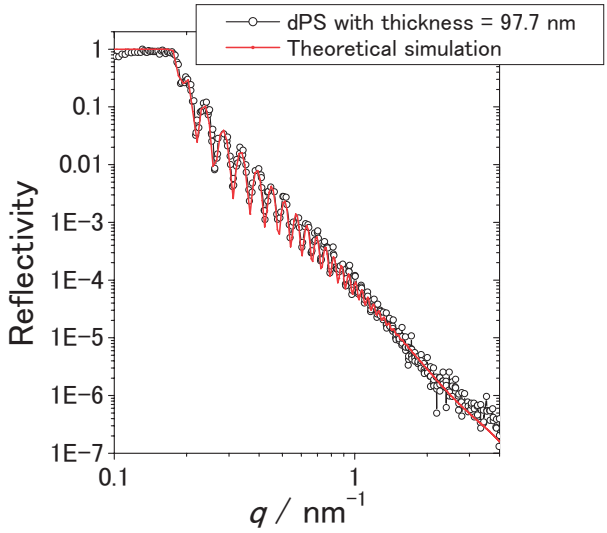

Figure 2. NR profile of deuterated polystyrene (d-PS) thin film on a Si substrate with a theoretical profile (red line).

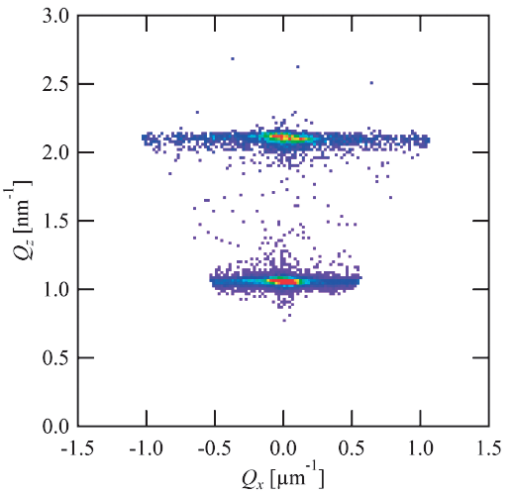

Figure 3. Reflectivity map of d-DPPC depending on the momentum transfer in the direction of parallel (Q_x) and normal (Q_z) to the substrate.

Table 1. Typical duration time for specular reflectivity measurement depending on the experimental conditions.

ρ [nm^{-2}]	size	q [nm^{-1}]	duration
6.5×10^{-4}	3"ϕ	<1	5 min
6.5×10^{-4}	3"ϕ	<2	20 min
6.5×10^{-4}	3"ϕ	<4	1 h
0.9×10^{-4}	3"ϕ	<2	2 h
2.5×10^{-4}	15 mm □	<2	5 h

density ρ of 6.5×10^{-4} nm^{-2}, the measurement was finished within 1 h for full-q region and time resolved measurement over the duration of a few minutes is possible in low-q region. We also measured the reflectivity with weak-reflection samples. The duration times of a hydrogenated polymer film (ρ~0.9×10^{-4} nm^{-2}) with a diameter of 3" and a polymer mixture film (ρ~2.5×10^{-4} nm^{-2}) with a square area of 15 mm were 2 h and 5 h, respectively.

Since SOFIA is equipped with a 2-dimensional detector, we can simultaneously measure both the specular and off-specular reflections at the same time. For the test measurement, we used a stacking of deuterated dipalmitoylphosphatidylcholine (d-DPPC) bilayers on a Si wafer. According to the literatures, this sample shows the off-specular reflection caused by the thermal undulation of bilayers [8] as well as the surface roughness [9]. Figure 3 shows the reflectivity map depending on Q_x and Q_z, the momentum transfer in the direction of parallel and normal to the substrate, respectively. The conversion was successfully performed and the streaks caused by the off-specular reflection extend in the direction of Q_x from the Bragg peaks of the bilayer stacking.

3. Conclusion

At BL16 in J-PARC/MLF, we have constructed a horizontal type neutron reflectometer SOFIA after ARISA-II. Thanks to the high flux beam and instrumental upgrades, the specular reflectivity can be measured up to 10^{-7} within a few hours for a 3 inch substrate at 220 kW. We also made possible a time resolved measurement with the slice of a few minutes and an off-specular reflectivity measurement with a position sensitive detector.

As a further upgrade, we developed a focusing mirror system [10]. The sample focusing mirror reduces further the measurement time and sample area, and the detector focusing mirror with a 2-dimensional detector provides high intensity with keeping an angular resolution in the grazing incidence small-angle neutron scattering measurement.

References

[1] N. Torikai *et al.*, Appl. Phys. A **74** (2002) S264.
[2] A. Horinouchi *et al.*, Chem. Lett. **39** (2010) 810.
[3] M. Kobayashi *et al.*, J. Phys.: Conf. Ser. **272** (2011) 012019.

[4] K. Mitamura *et al.*, J. Phys.: Conf. Ser. **272** 012017 (2011).
[5] Y. Terayama *et al.*, J. Phys.: Conf. Ser. **272** 012010 (2011).
[6] N. Torikai *et al.*, J. Phys.: Conf. Ser. **272** 012027 (2011).
[7] N. L. Yamada *et al.*, Euro. Phys. J. Plus, submitted.
[8] M. C. Rheinstödter *et al.*, Phys. Rev. Lett. **97** 048103 (2006).
[9] M. Hishida *et al.*, Phys. Rev. E **80** 051407 (2009).
[10] N. Torikai *et al.*, J. Phys.: Conf. Ser., in press.

N. L. Yamada[1], N. Torikai[2], K. Mitamura[3,4], H. Sagehashi[1], S. Sato[1], H. Seto[1], T. Sugita[5], S. Goko[5], M. Furusaka[5], T. Oda[6], M. Hino[6], and A. Takahara[3,4]

[1]Neutron Science Laboratory, KEK; [2]Graduate School of Engineering, Mie University; [3]JST,ERATO, Takahara Soft Interfaces Project; [4]Institute for Materials Chemistry and Engneering, Kyushu University; [5]Research Reactor Institute, Kyoto University; [6]Department of Quantum Science and Engineering, Hokkaido University

Construction of a Polarized Neutron Reflectometer with Vertical Sample-Plane Geometry, BL17（写楽）

It is not exaggerative to say that every neutron experimental facility has more than one neutron reflectometer at the present time. This is because the neutron reflectometry has been widely recognized as an indispensable tool of investigations on the surface and interface sciences which are closely related to nanomaterial science and its industrial applications.

In the end of 2009, the Japanese government decided to construct the 2nd neutron reflectometer at MLF by allocating a supplementary budget in the stimulus package of 2009. The budget was funded under the condition that the installation of the reflectometer had to be completed by the end of March 2011 which is the end of JFY 2010. It means that the time of construction was very short and only 15 months.

In Japan, we already have two neutron reflectometers, SUIREN (apparatus for SUrface and Interface investigations with Reflection of Neutrons), and MINE-II (Multilayer Interferometer and reflectometer for NEutron-II), at a research reactor JRR-3 (20 MW) in JAEA, and the 1st neutron reflectometer, SOPHIA, at MLF. SOPHIA is the neutron reflectometer dedicated to investigation of the free surface and interface, and its main target is soft matter science. After an intense and concentrated discussion, we finally decided to design the 2nd neutron reflectometer at MLF as a polarized neutron reflectometer with vertical sample-plane geometry (Fig. 1), and focus on solid sate physics, especially on magnetism in magnetic thin films. The reflectometer was installed at BL17 next to SOPHIA at BL16.

Figure 2 shows the expected reflectivity curves with error bars, and measuring times for unpolarized neutron reflectivity measurements of Ni thin films with thickness of 300 nm on Si substrates estimated using a neutron ray-trace simulation package McStas [1, 2] when the proton beam power is assumed to be 1 MW. The reflecting area of each sample is (a) 30 × 30 mm^2, and (b) 10 × 10 mm^2, respectively. These graphs suggest that a typical unpolarized neutron reflectivity measurement will be completed within a few minutes for a sample with the assuming typical sample size at BL17 in Fig. 2 (a) or several hours even for the tiny sample in Fig. 2 (b).

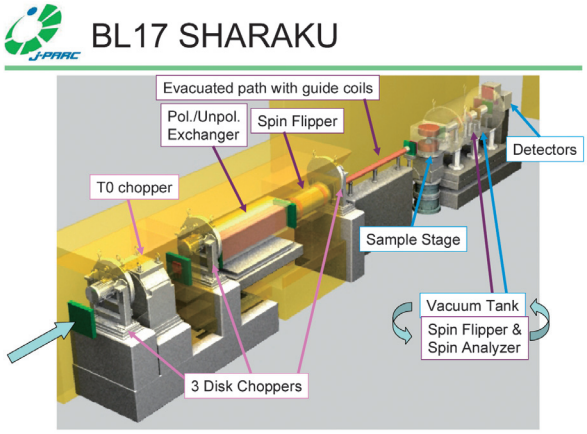

Figure 1. The image of the polarized neutron reflectometer with vertical sample-plane geometry SHARAKU at BL17, and its main beam line components.

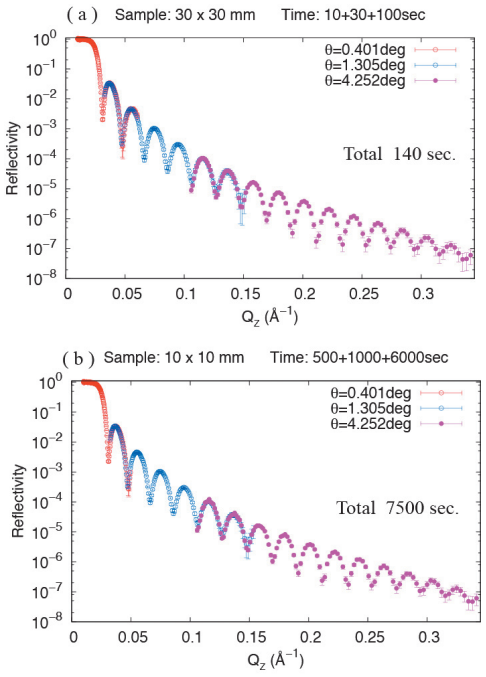

Figure 2. Expected durations for unpolarized neutron reflectivity measurements from Ni thin films simulated by McStas.

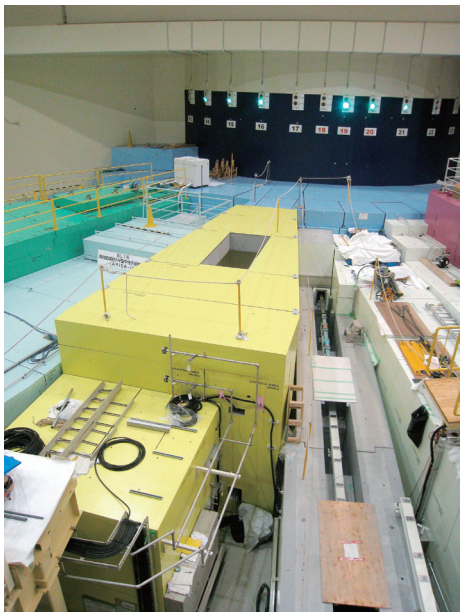

Figure 3. A picture of the shielding wall of the polarized neutron reflectometer (写楽: SHARAKU) installed at BL17. This picture was taken on the 7th March 2011 just before the massive earthquake.

In the beginning of March 2011, the installation was expected to be completed at the end of the month as scheduled (Fig. 3). The construction, however, was interrupted by the massive earthquake which hit North-East Japan. Now all of the researchers and technicians working in J-PARC make efforts to recover as soon as possible from the damages on the accelerators and facilities caused by the earthquake. We expect to start the commissioning and the user program on this polarized neutron reflectometer in the beginning of the next year (2012).

References

[1] K. Lefmann and K. Nielsen, Neutron News **10**, 20 (1999).

[2] P. Willendrup, E. Farhi and K. Lefmann, Physica B, **350** 735 (2004).

M. Takeda[1, 2, 3], D. Yamazaki[1, 2], K. Soyama[1, 2, 3], R. Maruyama[2], H. Hayashida[2], H. Asaoka[1, 2], T. Yamazaki[1], K. Aizawa[2], M. Arai[2], Y. Inamura[2], T. Itoh[2], W. Kambara[2], K. Kaneko[1, 2], T. Nakamura[2], T. Nakatani[2], K. Oikawa[2], T. Ohhara[1, 2], K. Sakasai[2], T. Shinohara[2], J. Suzuki[2], K. Suzuya[2], N. Takahashi[2], S. Takata[2], I. Tamura[2, 3], K. Toh[2], H. Yamagishi[2], and T. Hirano[4]

[1]Quantum Beam Science Directorate, JAEA; [2]Materials and Life Science Division, J-PARC Center; [3]Department of Research Reactor and Tandem Accelerator, JAEA; [4]Hitachi Research Laboratory, Hitachi Ltd., Hitachi

BL 18: Single Crystal Neutron Diffractometer under Extreme Condition (SENJU)

SENJU, named after the thousand-armed Goddess of Mercy, is a single crystal time-of-flight Laue diffractometer proposed to the MLF at J-PARC. The diffractometer is dedicated for precise crystal and magnetic structure analyses under combined extreme conditions using a small sample less than 1 mm^3 [1]. SENJU has been funded by a supplementary budget from the stimulus package in the winter of 2009. We have reorganized a design team to devise the specifications of the instrument within a month before the bidding because of the quick budget. All contracts of the instrument components had to be installed by the end of March 2011.

In order to confirm and improve the instrumental specifications of SENJU, the international advisory committee on SENJU was held in Aug. 30 - 31, 2010. The IAC members are Prof. Laurent Chapon, Chairman (ISIS, UK), Dr. Matthias Gutmann (ISIS, UK), Dr. Eddy Lelièvre-Berna (ILL, France), and Dr. Leighton Coates (SNS, US). The instrumental specifications proposed by SENJU project team were discussed, and they were finally approved with some productive suggestions. The general specifications of SENJU are shown in Table 1, and the top and side views of SENJU are shown in Fig. 2.

Table 1. General specifications of SENJU.

Moderator	Decoupled poisoned H_2 (20K)
L_1 and L_2	34.8 m and 0.8 m
Guide geometry	Straight, square elliptic tube
Neutron wavelength	0.4 ~ 4.4 Å (1^{st} frame) 4.6 ~ 8.8 Å (2^{nd} frame)
Neutron flux and divergence	0.6×10^6 n/s/mm^2 (± 0.3˚) 1.3×10^6 n/s/mm^2 (± 0.45˚)
Sample vol.	0.1 ~ 10 mm^3
Lattice const.	Max. 50 Å
Detector	WLSF-type scintillator
	4×4 mm^2 / pixel
	256×256 mm^2 / scintillator
	Number of det.: 31 (max. 37)
	Horizontal coverage: −13° ~ −167°, +58° ~ +167° Vertical coverage: −29° ~ +29° Solid angle: 4 sr. (max. 4.8 sr.)
Beam monitor	N_2 ($\varepsilon = 3 \times 10^{-5}$) @ 33.66 m
Throughput	24 MWh for org. compounds

Figure 1. The IAC members and SENJU project team at the MLF-BL18 area.

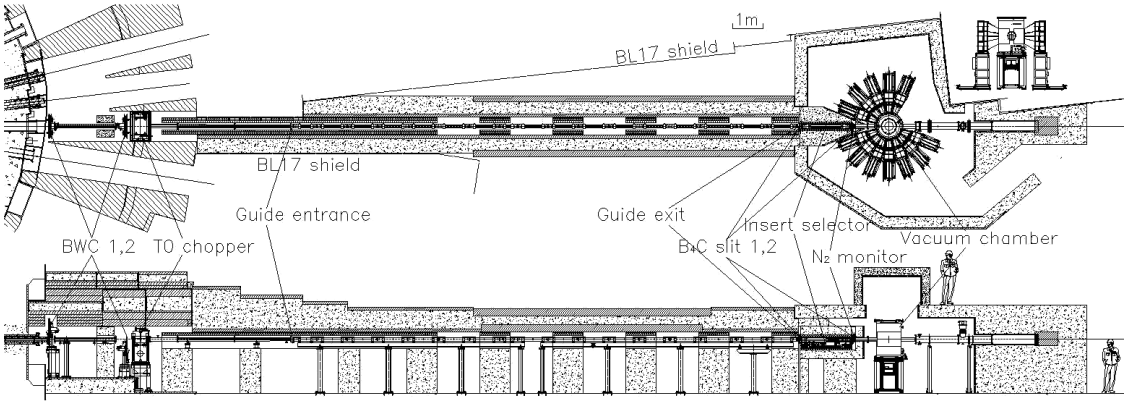

Figure 2. Top and side views of SENJU at BL18.

The success of SENJU depends on the reliability and stability of the detector system. A wavelength-shifting fiber type scintillator detector developed for iBIX [2] was modified at the request of SENJU. The details in this report have been provided by T. Nakamura (p.7).

It is also particularly important to have software able to utilize the capabilities of SENJU. We developed software to operate the devices from GUI and to perform the data reduction and visualization. The later components are based on STARGazer [3].

The installation of the SENJU equipment started in September 2010. The beamline components such as a shutter and a bulkshield inserts at target station, steel collimators and neutron guide tube, choppers, as well as shielding blocks, were almost installed within half a year. Figure 3 shows the photo of BL18 in early March. Most of the shielding enclosure of SENJU was constructed and the detectors with electronics were already arranged in the proper configuration. The last main component, a vacuum chamber, was ready to be installed, but the earthquake on March 11 struck us. Although the construction schedule has been delayed, SENJU will be reinstalled starting from the fall, and the on-beam commissioning will begin in 2012.

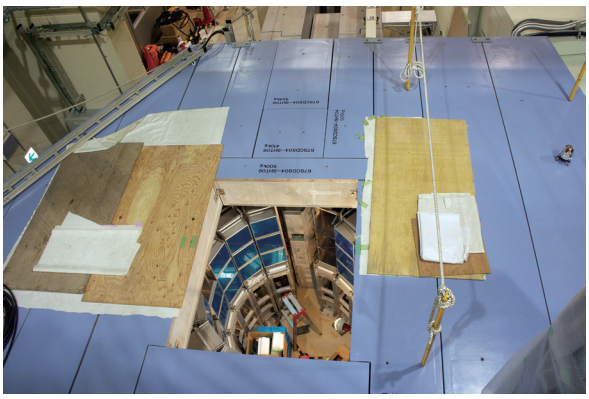

Figure 3. A photo of BL18 taken in early March, 2011.

References

[1] I. Tamura *et al.*, to be published in J. Phys.: Conf. Ser. (ECNS 2011).

[2] T. Hosoya *et al.*, Nucl. Instr. Methods Phys. Res. A **600** 217 (2009).

[3] T. Ohhara *et al.*, Nucl. Instr. Methods Phys. Res. A **600** 195 (2009).

K. Oikawa[1], and T. Ohhara[2]

[1]Materials and Life Science Division, J-PARC Center; [2] Comprehensive Research Organization for Science and Society

TAKUMI at BL19

1. Instrumentation

The Engineering Materials Diffractometer TAKUMI is a dedicated neutron diffractometer to promote scientific and industrial studies in areas of materials science and engineering and mechanical engineering. Since the commissioning phase has been finished, the development of sample environment devices and upgrading experimental methods, including software, are the next tasks starting from JFY 2010.

The newly developed sample environment (SE) devices are 5 mm width radial collimators and a driving part for the cryogenic loading machine. The commissioning for the upgrade includes optimization of new devices and Z-Rietveld application to bulk materials. We also conducted development of software for measurement and analysis of texture. Figure 1 shows lattice strains during tensile deformation of A2024 alloy evaluated from lattice parameters analyzed through both single peak analysis and Z-Rietveld refinement. Lattice strains evaluated from *d*-spacing values show different scales relating to different diffraction elastic moduli of *hkl* orientations, while those evaluated from lattice constants show a good agreement with bulk strain obtained by strain gauges pasted on the specimen. The texture analysis software was developed using Z-Rietveld as the core, and the data obtained was in a good agreement with that obtained by conventional angular dispersive method at the research reactor, JRR-3.

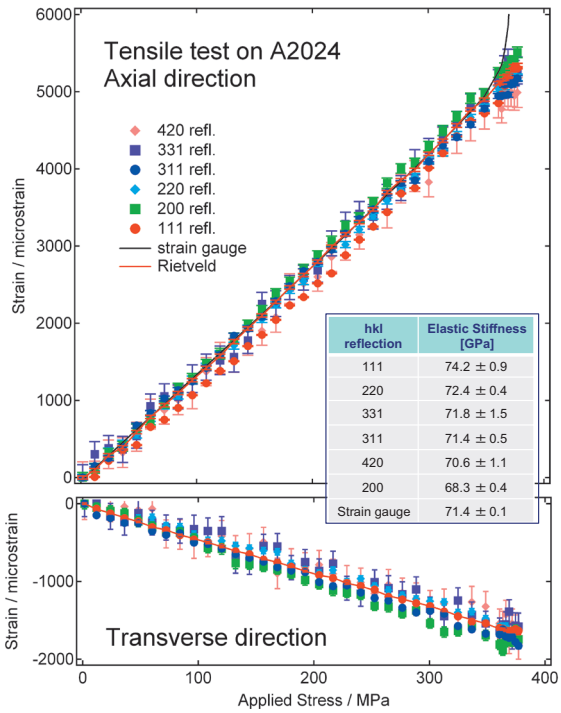

Figure 1. Lattice strain evolution during tensile deformation of A2024 alloy

2. User Programs

During JFY 2010, TAKUMI was also one of instruments at MLF which was utilized by many users. The proposals approved to be conducted during JFY 2010 included 23 general uses, 2 project uses and an instrumental use. There were 6 approved proposals coming from industrial companies, and propriety uses were conducted as well. The allocated beam times are shown in Figure 2, showing that the general use exceeded 50%. The beam times allocated for project uses were almost unchanged compared to those for JFY 2009, but the beam times for instrumentation decreased significantly, since the commis-

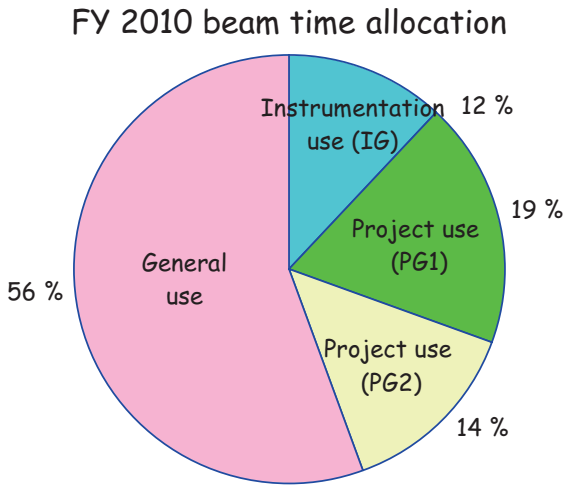

Figure 2. Beam time allocation at JFY 2010.

sioning finished. The beam times for instrumentation were mainly used for development of sample environmental devices and measurement techniques such as texture measurement, and instrument maintenance, including upgrading calibration data.

The number of repeate users increased and this helped additionally the instrument scientists, because they could operate TAKUMI with less support. Figure 3 shows users in the process of preparation for their experiments.

Figure 3. Users are setting the samples for their experiments by loading the machine.

3. Highlights

As a continuation of the success in measurement of residual strains for Nb_3Sn phases in ITER-TF conductors with an outer diameter of 42.6 mm during JFY 2009 (120 kW), strains measurements in ITER-CS conductor with an outer dimension of 49 mm were extended when the neutron beam power increased to 200 kW (ITER: International Themonuclear Experimental Reactor). A schematic view of ITER-CS conductor is shown in Figure 4, in which the steel jacket thickness is thicker and the Nb_3Sn amount is less than that of ITER-TF conductor. The first trial was done by preparing a 100 mm long cut specimen. The specimen was heat-treated to formed Nb_3Sn phases and the thermal phase strains generated during the heat treatment were measured. Nb_3Sn diffraction peaks were weaker than those of ITER-TF even though the same gauge volume was used. These may have been caused by the thick steel jacket and also by the smaller Nb_3Sn amount. However, by applying multi peak analysis using Z-Rietveld, the residual strains with good reliablity were succesfully evaluated. Thermal residual strain in axial direction for Nb_3Sn was -0.2 %.

Now we are interested in measuring strain levels in ITER-CS conductor in practical use. We have prepared to measure residual strains generated after a performance test at SULTAN facility, i.e. cryogenic temperature, high magnetic field, cyclic high electric current. Figure 5 shows the off-line preparation done in the beginning of March, but the Great East Japan Earthquake came earlier before the measurements were conducted.

Figure 6 shows our preliminary test to do thermo-mechanical treatment of steel (2Mn-0.2C). It is known that the equilibrium phase transformation in steel can be accelerated by applying strain or stress, i.e. dynamic transformation. This experiment shows that neutron diffraction can be used to observe such phenomena by performing in situ measurement during high temperature deformation.

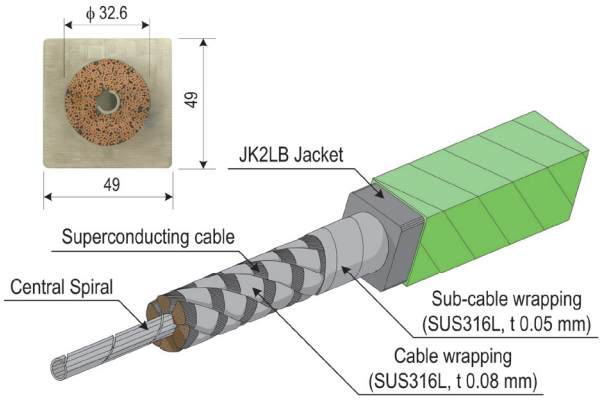

Figure 4. Schematic view of ITER-CS conductor

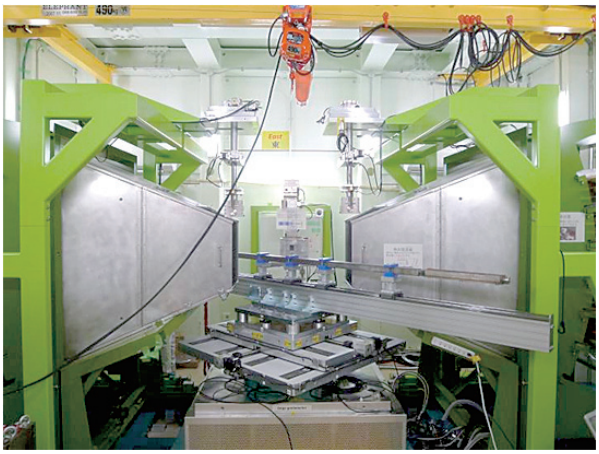

Figure 5. Off-line test using 3.6m long ITER- CS conductor.

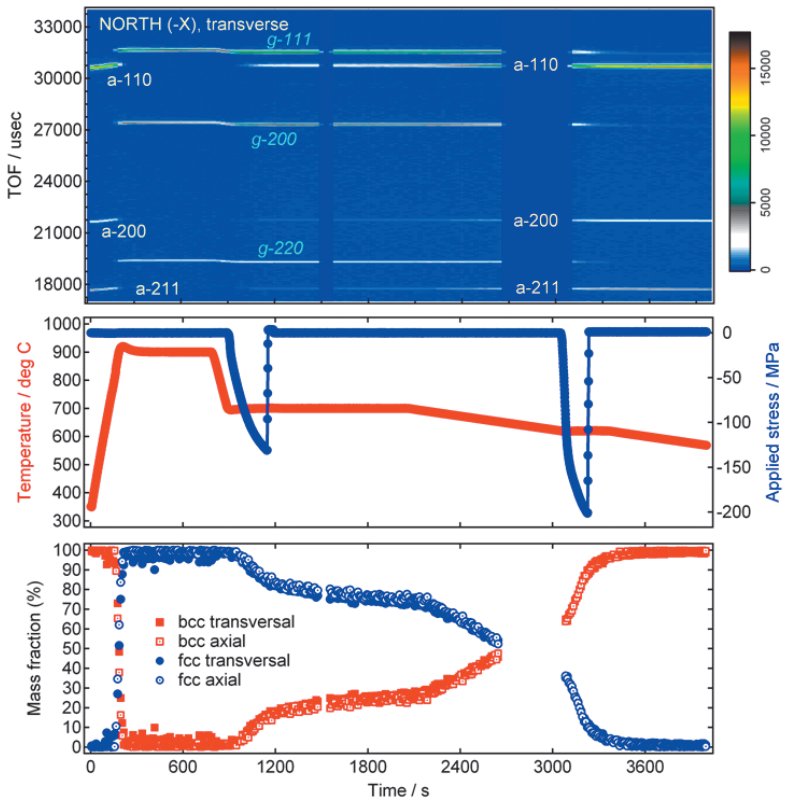

Figure 6 Results from Thermo-Mechanical-Process simulation using a 2Mn-0.2C steel

S. Harjo[1], K. Aizawa[1], T. Ito[1], J. Abe[2], H. Arima[1], and T. Iwahashi[1]

[1]*Materials and Life Science Division, J-PARC Center;* [2]*Quantum Beam Science Directorate, JAEA*

The Current Status of Versatile Neutron Diffractometer, iMATERIA

1. Introduction

Ibaraki prefecture, the local government of the area where J-PARC sites in Japan, has decided to build a versatile neutron diffractometer (IBARAKI Materials Design Diffractometer, iMATERIA [1]) to promote industrial applications for the neutron beam in J-PARC. iMATERIA is planned to be a high throughput diffractometer so that materials engineers and scientists can use it as a chemical analytical instruments in their materials development process.

The roles for neutron diffraction in materials science are (1) to do structural analyses of newly developed materials, (2) to clarify the correlation between structures and properties (functions), and (3) to clarify the relation between structural changes and improvements of functions especially for practical materials. To carry out such purposes, a diffractometer with super high resolution is not required. The matching among intermediate resolution around $\Delta d/d = 0.15\%$, high intensity and wide d coverage is more necessary.

This diffractometer is designed to face a decoupled-poisoned liquid hydrogen moderator (36 mm, off-centered) (BL20), and to have the incident flight path (L1) of 26.5 m with three wavelength selection disk-choppers and straight neutron guides with the total length of 14.0 m. The instrumental parameters are listed in Table 1. There are four detector banks including a low angle and a small angle scattering detector bank. The angular coverage of each detector bank is also shown in Table 1. The rotation speeds for the disk-choppers are the same with the pulse repetition rate 25 Hz for the most applications (normal mode). In this case, the diffractometer covers $0.18 < d\ (Å) < 2.5$ with $\Delta d/d = 0.16\ \%$ and covers $2.5 < d\ (Å) < 800$ at three detector banks of 90 degree, low angle and small angle with gradually changing resolution. When the speed for wavelength selection disk-choppers is reduced to 12.5 Hz(wide-d mode), we can access a wider d-range, $0.18 < d\ (Å) < 5$ with $\Delta d/d = 0.16\ \%$, and $5 < d\ (Å) < 800$ with gradually changing resolution.

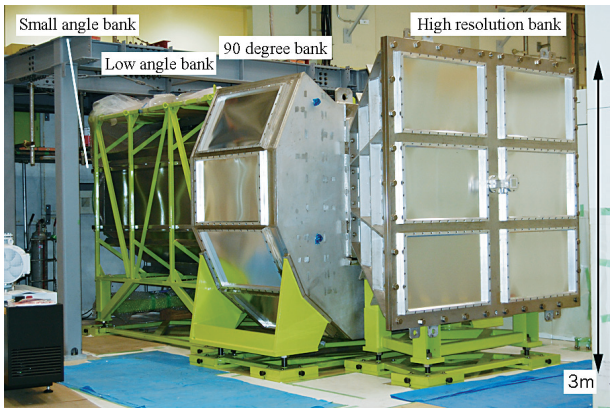

Figure 1. IBARAKI Materials Design Diffractometer, iMATERIA without detector for each bank and instrument shielding. High-resolution bank, special environment bank (90 degree bank), low angle bank, can be seen from right to left. Small angle detector bank, which are not shown in picture, are situated in the low angle vacuum chamber (left hand of the picture).

Table 1. Instrumental parameters of iMATERIA. L2 is the scattered flight path. The d-range for each bank is the maximum value for 2 measurement mode.

L1		26.5m
Guide length		Total 14m (3section)
Position of Disk choppers		7.5m(double)
		11.25m(single)
		18.75m(single)
High	2θ	$150^\circ \le 2\theta \le 175$
Resolution	L2	2.0 - 2.3m
Bank	d-range	$0.09 \le d(Å) \le 5.0^\circ$
Special	2θ	$80^\circ \le 2\theta \le 100^\circ$
Environment	L2	1.5m
Bank	d-range	$0.127 \le d(Å) \le 7.2$
Low	2θ	$10^\circ \le 2\theta \le 40^\circ$
Angle	L2	1.2 - 4.5 m
Bank	d-range	$0.37 \le d(Å) \le 58$
Small	2θ	$0.7^\circ \le 2\theta \le 5^\circ$
Angle	L2	4.5 m
Bank	d-range	$1.69 \le d(Å) \le 800$

2. Current Status

The three banks (high resolution bank (BS bank), special environment bank (90 degree bank) and low angle bank) are operational. It takes about 15 minutes (25 Hz, normal mode) to obtain a 'Rietveld-quality' data in high resolution bank at 200kW beam power for few grams of standard oxide samples. Figure 2 is Rietveld refinement pattern for $YBa_2Cu_3O_{7-d}$ at the high resolution (BS) bank, special environment bank (SE) and low angle bank (25 degree) by multi bank analysis function of Z-Rietveld[2]. In this data, it takes 35min at 12.5Hz wide-d mode to collect Rietveld available data. The χ^2 vale for this refinement was 3.08 (over all).

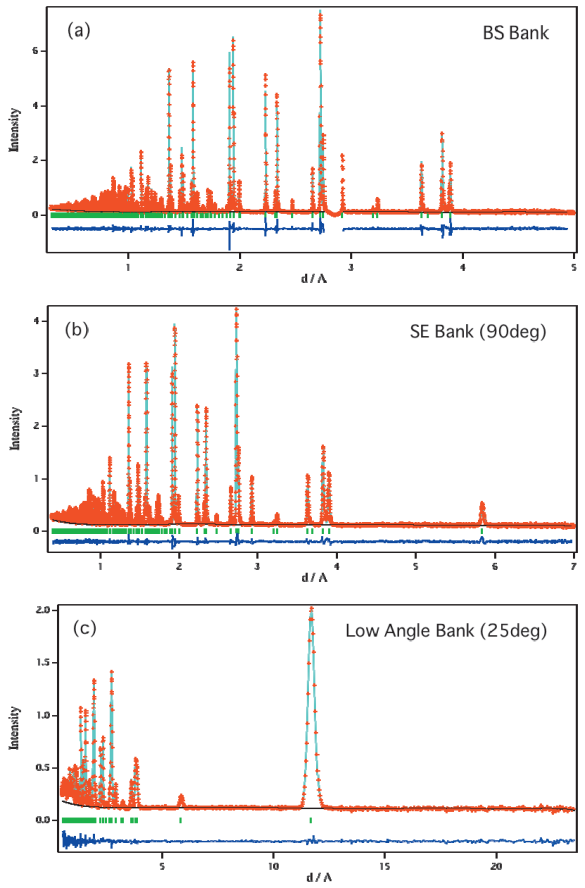

Figure 2. Rietveld refinement pattern for YBa2Cu3O7-d at (a) high resolution bank, (b) special environment bank and (c) low angle bank (25deg) of iMATERIA.

The automatic measurement with auto sample exchange system [3] has been already working for user experiments from October, 2010 (see another article in this report). The V-furnace (~900C) has been already completed for conducting experiments. The Gas furnace (~900C) and the crio-furnace with sample change mechanics will be ready in 2011.

3. Recent Results

In 2010, 96 user groups used iMATERIA (67% are industrial users, which includes proprietary and urgent use). Half of the industrial users performed research of battery materials.

There are some progressive works done using iMATERIA. Prof. Idemoto's group successfully collected the diffraction data from 8.5 mg of active material for Li-ion battery[4] (see the related topics of this report). Dr. Suzuya's and Prof. Kameda's groups tried to analyze the structure of disordered materials using low angle data. Figure 4 shows a result of structure analysis of D_2O from low angle data[5]. The instrument group also tried to measure non-deuteried organic compound. Figure 5 shows a temporal result of structure analysis of guanosin ($C_{10}H_{13}N_5O_5$) for SE bank data. It takes 14 hours to measure one set of data at 100 kW beam power.

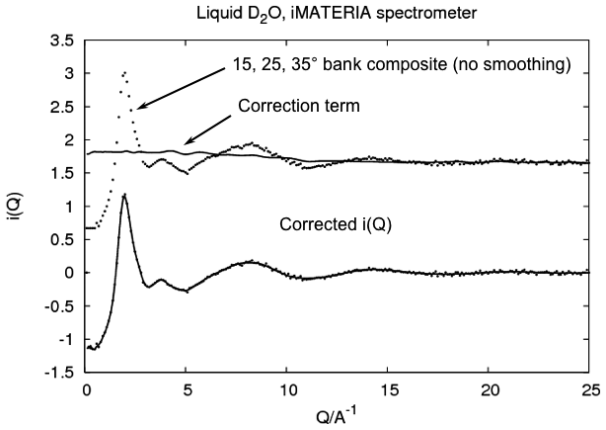

Figure 4. i(Q) pattern of liquid-D_2O from low angle data of iMATERIA.

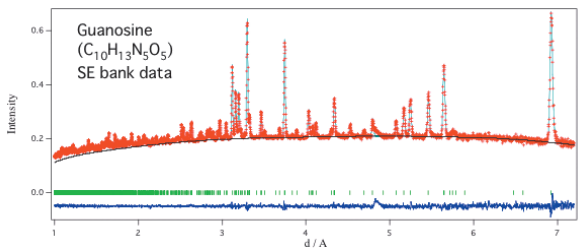

Figure 5. Rietveld analysis pattern of guanosin ($C_{10}H_{13}N_5O_5$) from SE bank data of iMATERIA.

4. Conclusion

At the Great East Japan Earthquake, iMATERIA was also damaged at pre-shields and beam stop. It will be restored at the beginning of October.

iMATERIA, with four detector banks, is designed for wide d range coverage. The wide d coverage and the short measuring time for this diffractometer will lead to a holistic understanding of materials structure and their function for materials development.

References

[1] T. Ishigaki *et. al.*, Nucl. Instr. Meth. Phys. Res. A, **600**, 189-191 (2009).

[2] R. Oishi, *et. al.*, Nucl. Instr. Meth. Phys. Res. A**600**, 94–96 (2009).

[3] A. Hoshikawa *et. al.*, Nucl. Instr. Meth. Phys. Res. A, **600**, 203-20

[4] Y. Idemoto, Y. Tsukada, N. Kitamura, A. Hoshikawa and T. Ishigaki, Chemistry Letters, **40** 168 (2011).

[5] Y. Kameda, private communication.

T. Ishigaki[1], A. Hoshikwa[1], M. Yonemura[2], K. Iwase[1], D. S. Adipranoto[1], and T. Kamiyama[2]

[1]Frontier Research Center for Applied Nuclear Sciences, Ibaraki University; [2]Materials and Life Science Division, J-PARC Center and Institute of Materials Structure Science, KEK;

Structural Studies Began on the High Intensity Total Scattering Diffractometer (NOVA)

1. Introduction

Total scattering is a technique that had been developed for studies of liquid and amorphous materials and is now widely used to observe non-crystalline features in a variety of materials, including crystalline. Many of the materials are of non-crystalline nature which seriously affects materials' properties and functionalities. By adapting neutron total scattering to hydrogen storage materials, it is expected to extract a variety of structural information such as hydrogen-hydrogen correlation even in disordered phase.

In JFY 2010, an evaluation of the instrument performance of the High Intensity Total Diffractometer (NOVA) at BL21 was conducted. By performing neutron diffraction on various samples, including samples of liquids and amorphous materials, the reliability of the hardware and software was confirmed.

2. High-Q Measurements on NOVA

As a total diffractometer, a high-Q value measurement of the static structure factor, $S(Q)$, is quite essential to obtain a reliable pair correlation function, $g(r)$. It has been confirmed that the statistical accuracy of the $S(Q)$ of NOVA is high and Q_{max} can be 60 Å^{-1} so far in case of silica glass (Fig. 1). This is achieved by the high neutron flux and low intrinsic noise of NOVA. It is essential for a high-intensity diffractometer to achieve high S/N ratio for small-amount samples and/or short time measurements. Utilizing the high neutron flux and S/N ratio, a one-second measurement is feasible on NOVA at 1 MW operation. This implies that NOVA is a powerful tool for observing time-transient phenomena.

3. Structural and Hydrogen Desorption Properties of Aluminum Hydride [1]

Aluminum trihydride (AlH_3, alane) is of interest as a possible hydrogen storage material because of its high gravimetric and volumetric hydrogen densities

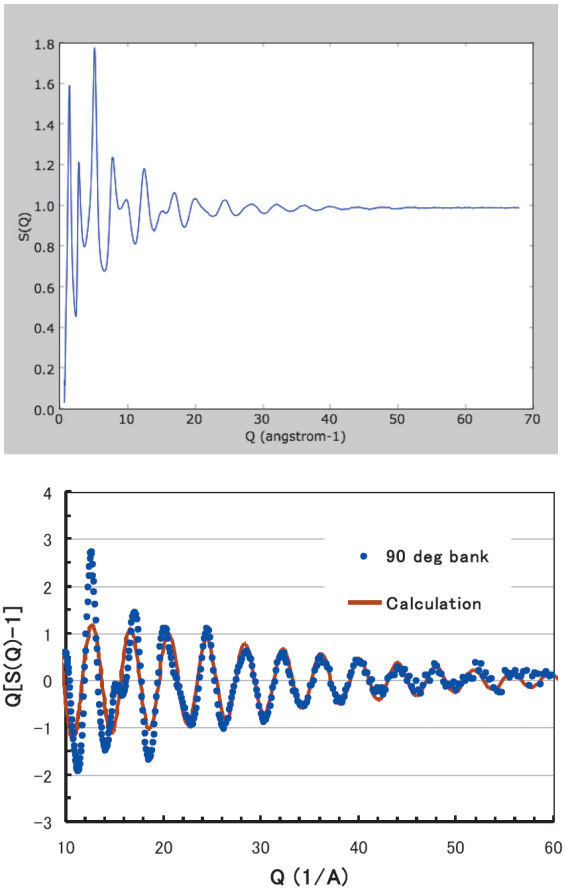

Figure 1. High-Q measurement of silica glass on NOVA. Above: Measured $S(Q)$ of silica glass. Below: Plot of $Q[S(Q)-1]$ which directory affects the reliability $g(r)$. Solid line shows the calculated Si-O correlation.

(10.1 mass% and 149 kgH^2/m^3, respectively) and its simple hydrogen desorption reaction, in which AlH_3 decomposes to Al ($AlH_3 \rightarrow Al + 3/2H_2$) at 370–470 K. Recently, *in situ* microscopic observations and *in situ* X-ray photoelectron spectroscopy revealed that AlH_3 particles (size 100 nm–1 μm) are covered by an Al_2O_3 layer (thickness 3–5 nm), and at room temperature, the hydrogen desorption reaction is prevented by the oxide layer on the surface of AlH_3. The reaction begins only when the layer breaks up because of the thermal volume expansion of the underlying bulk AlH_3. The layer apparently forms after the thermal desorption of the solvated ether from

AlH_3–etherate, which is prepared by the following reaction between $LiAlH_4$ and $AlCl_3$ in an ether solution:

$$3LiAlH_4 + AlCl_3 + n[(C_2H_5)_2O] \rightarrow 4AlH_3–n[(C_2H_5)_2O] + 3LiCl \rightarrow 4AlH_3 + 3LiCl + n[(C_2H_5)_2O]$$

To obtain precise structural information regarding the surface layer, we performed high-intensity neutron diffraction measurements on NOVA and a Rietveld refinement of α-AlD_3. The Rietveld refinement was performed with Z-Code. The diffraction profiles show small diffraction peaks in addition to the peaks of α-AlD_3, as seen in Fig. 2. These lattice spacing values for the neutron and X-ray diffraction profiles are close to those of χ-Al_2O_3 (corresponding to 101–107% of the values in the literature). Therefore, the present result suggests that χ-Al_2O_3 forms on the surface of AlH_3 (AlD_3) by the desorption of solvated ether. Furthermore, the short-range order (0.18 ± 0.021 nm for Al–O; 0.28 ± 0.058 nm for O–O; 0.32 ± 0.055 nm for Al–Al) of amorphous Al_2O_3 suggested by electron-energy-loss spectroscopy (EELS) may be observed under the diffraction peaks of the crystal structures in Fig. 2.

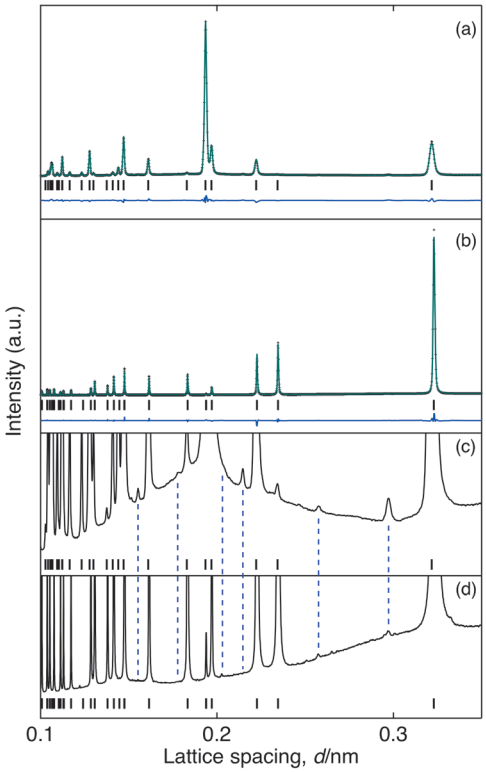

Figure. 2. High-intensity (a) neutron diffraction profile of α-AlD_3 and (b) X-ray diffraction profile of α-AlH_3 on a linear scale. Rietveld refinement results: observed (cross), calculated (line), and residual (line below vertical bars) diffraction profiles. Tick marks show Bragg-reflection positions of α-AlD_3 and α-AlH_3. Vertical enlargements (70×) of the diffraction profiles are shown in (c) for (a) α-AlD_3, and in (d) for (b) α-AlH_3. Positions, except for those of α-AlD_3 and α-AlH_3, are shown by dashed lines.

4. In-Situ Measurements on NOVA

Figure 3 shows an example of a time-transient measurement on NOVA. By increasing the temperature over time, the structure of a hydrogen storage material ($Li^{11}BD_4$) was changed from the low temperature phase to the high temperature one. In this case the time-interval was fixed at 1 min. The time interval can be optimized after the experiment by the benefits of event-recording type DAQ system of MLF.

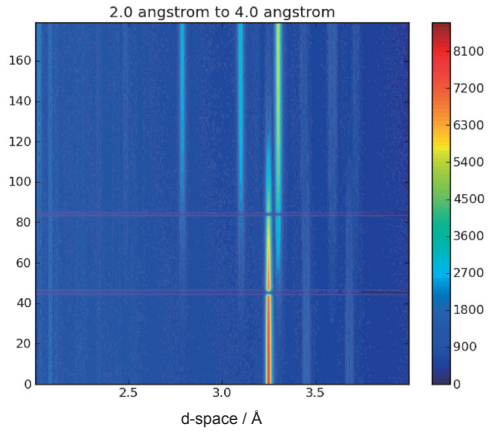

Figure 3. Test measurement of time-transient phenomena on NOVA.

In addition to NOVA, which delivered excellent performance as a high-intensity neutron diffractometer, equipments for hydrogen study have been fabricated and installed: 1) a sample exchanger that can load 10 samples, 2) equipment for an *in-situ* experiment for an H_2/D_2 gas atmosphere (max. pressure is 10 MPa and temperature range is 50 K~473 K), and 3) a vanadium foil heater furnace (room temperature to 1373 K). The performance of the in-situ gas equipment for a pressure-composition-temperature (PCT) measurement was confirmed, and the neutron diffraction of $LaNi_5$-D_x was successfully measured at the end of JFY 2010. Using a Fermi

chopper, inelastic scattering experiments were performed on NOVA. With this device, the R&D studies of incoherent-inelastic corrections of hydrogen atoms will be advanced to improve the accuracy of the hydrogen position information. It is expected that full-scale research on hydrogen storage materials will be starting soon.

NOVA is supported by the NEDO project "Advanced Fundamental Research Project on Hydrogen Storage Materials (Hydro-Star)".

Reference

[1] K. Ikeda, H. Ohshita, N. Kaneko, J. Zhang, M. Yonemura, T. Otomo, K. Suzuya, H. Yukawa, M. Morinaga, H.-W. Li, S. Semboshi, S. Orimo, Materials Transactions, **52** 598-601 (2011).

T. Otomo[1,2], K. Suzuya[1], M. Misawa[2], H. Ohshita[2], N. Kaneko[1,2], K. Ikeda[2], M. Tsubota[2] on behalf of NOVA group

[1]*Materials and Life Science Division, J-PARC Center;* [2]*Institute of Materials Structure Science, KEK*

Si Crystal Analyzer Manufacturing for DNA

1. Introduction

A Si-crystal analyzer backscattering spectrometer DNA (figures 1 & 2) is characterized as high energy resolution δE, that is about 1 micro-eV for E = 2 meV elastic neutron energy ($\delta E/E \sim 0.05$ %). A time-of-flight method in long flight length to analyze the incident neutron energy and an extreme backscattering condition in Bragg's reflection on Si perfect single crystal to analyze scattered neutron energy precisely promise this high performance of energy resolution to be achievable.

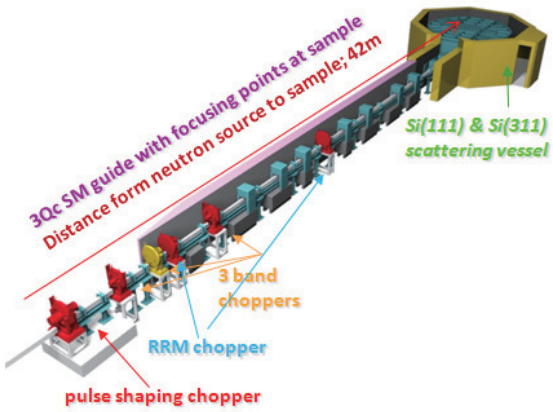

Figure 1. Overview of the DNA spectrometer.

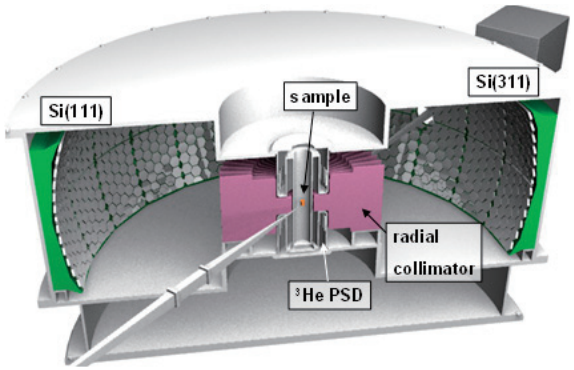

Figure 2. Inner view of the scattering vessel

Si-crystal analyzer is fabricated by gluing numbers of single-crystal silicon wafers on aluminum plates with high-precision spherical surface. Some of fabrication technologies have been newly developed for DNA, the first backscattering spectrometer with Si-crystal analyzer in Japan.

2. Fabrication of the Si Crystal Analyzer

An assembly lab in HENDEL building is equipped with two placing machines, one 3D-Digitizer (position measurement system) and one Si wafer dicer (up to 6 inch Dia.). Three dedicated stuffs in house are assembling the analyzer units.

The coincidence of the crystal axis Si<111> with the perpendicular direction to Si wafer surface is one of the important factors to determine the accuracy of the analyzer crystal (see figure 3). Thus, the crystal axis for all Si crystal wafers was checked by precision X-ray diffraction measurements with accuracy of $d\omega \sim 0.002$ deg. by RENESAS CO.,LTD and the wafers with the condition $\alpha < 0.05$ deg. are selected to be fabricated.

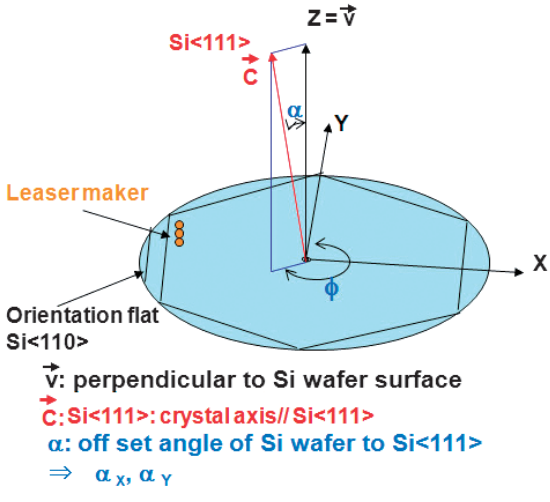

Figure 3. Orientation for Si wafer.

The results of X-ray measurements of the crystal axis are shown in figure 4.

Figure 5 shows the process on gluing the Si wafer on the Al plate and a section structure.

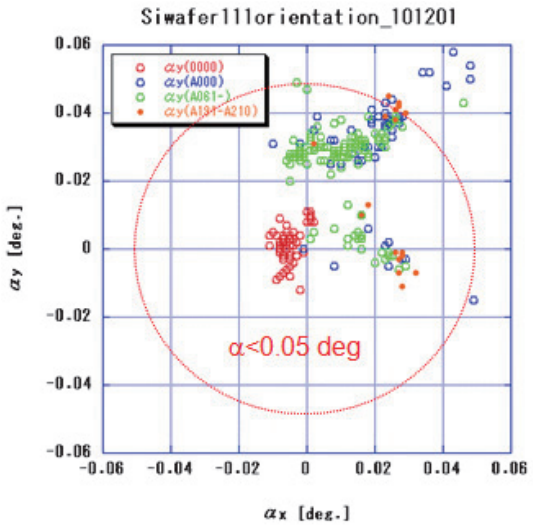

Figure 4. The results of X-ray measurements for Si<111> direction for some wafers.

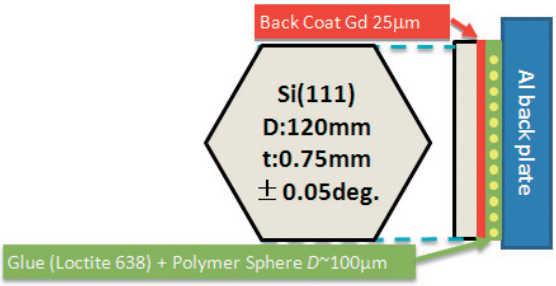

Figure 5. Gruing Si wafers on Al plates.

Figures 6 & 7 show the procedure of gluing a Si wafer on the spherical surface of a Al unit by a placing machine.

The accuracy of spherical surface on Si-wafer gluing on Al plate was checked by a 3D-digitaizer. Figure 8 shows the difference between the real surface and the ideal spherical surface (R = 2300 mm + 875 micro m). Acceptable tolerance is about in +- 50 micro m in total on one Al plate.

Figure 9 shows a Si pasted Al unit and a strut for installation into the DNA scattering vessel. One Al unit needs about 50 Si wafers to cover the analyzer surface. As shown in figure 9, two Al units are installed to the upper and lower parts of one strut. Then, 27 struts will be installed into the DNA scattering vessel at maximum.

First phase of experimental use for DNA will start with about 20 plates of Si<111> crystal analyzer units at the end of JFY 2011,

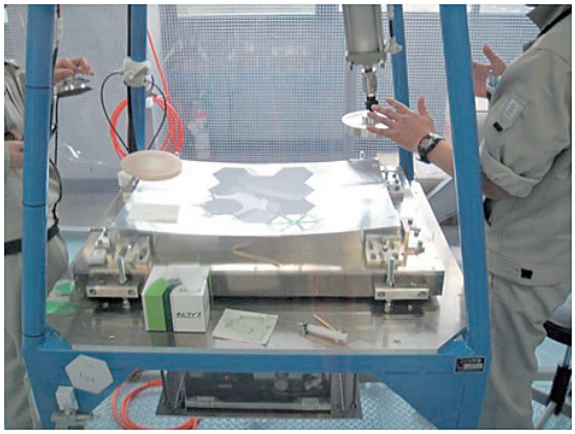

Figure 6. Procedure of gluing a Si wafer to the Al plate No.1.

Figure 7. Procedure of gluing a Si wafer to the Al plate No.2.

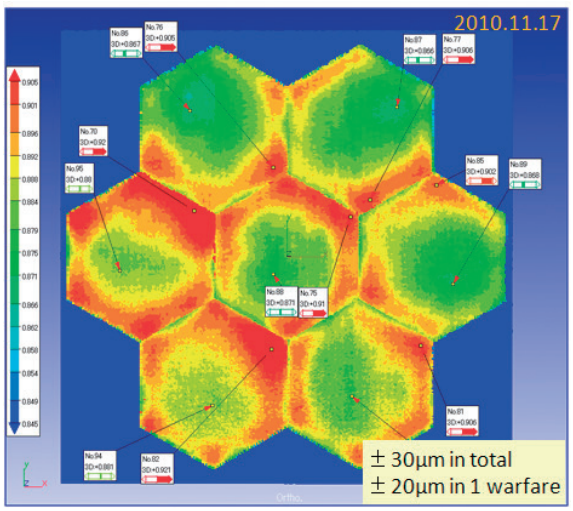

Figure 8. An example of measurement result of 3D-digitaizer on Si-wafer pasting on Al plate.

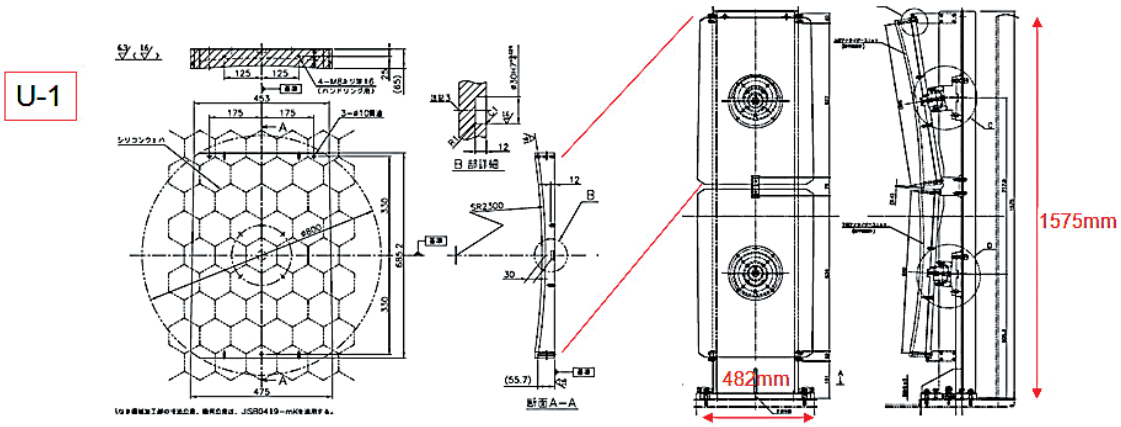

Figure 9. A Si-glued Al unit U1 and a strut for installation into the DNA scattering vessel.

To meet the final specification on DNA, 30 plates of Si<111> crystal analyzer units and 24 plates of Si<311> crystal analyzer units are required.

Reference

[1]. N. Takahashi, *et al.*, Journal of Physics and Chemistry of Solids **68**, 2199-2203 (2007).

K. Shibata[1], W. Kambara[2], K. Aoyama[3], K. Inoue[3], H. Asai[3], N. Takahashi[2], Y. Kawakita[2], K. Kamazawa[1], T. Yamada[1], K. Nakajima[2], T. Hosoya[2], T. Iwahashi[2], Y. Ito[2], H. Tanaka[2] , K. Aizawa[2], and M. Arai[2]

[1]Research Center for Neutron Science and Technology, Comprehensive Research Organization for Science and Society (CROSS), [2]Materials and Life Science Division, J-PARC Center; [3]NucleusAdvanced Technology Co.LTD.

1. Introduction

The neutron experimental instruments in J-PARC/MLF are equipped with large area detector system which has thousands of pixels and many sample environment devices. High intensity pulsed neutron source in J-PARC/MLF sufficiently provides us with an opportunity of acquiring data with changing the sample conditions in a short time. Then, these data are analyzed in multidimensional condition. However, it is impracticable to perform this measurement and analysis manually. Therefore, we need an automatic experimental environment and a flexible data management system.

This year, preparing for the automatic experimental environment, we developed an automatic measurement software to execute series of measurement commands sequentially, in collaboration with a researcher in ISIS. This software called "Experiment Scheduler" controls the data acquisition system and the sample environment devices through the MLF software framework [1] called "IROHA". By using this software, we can get many raw data under various measurement conditions. These raw data are also analyzed in multidimensional conditions. The conditions and results, except raw data, of the analysis as well as those of the measurement are called experimental meta-data. We have planned to introduce a flexible database to manage both raw data and the meta-data. This year, we developed the experimental meta-data database combined with the IROHA. This database becomes a part of the MLF experiment database. The meta-data of the measurement with the Experiment Scheduler is managed by the IROHA, stored in the database, indexed and re-usable.

2. Automatic Measurement Software

The Experiment Scheduler consists of two software components, "Script generator" and "Script status". The Script generator is a sequence editor of the measurement scenario. For example, if you want to run the data acquisition system under several sample conditions, you can sequentially select measurement commands from a pull down menu in the Script generator and input the parameters of the sample conditions. Because a loop function is implemented in the Script generator, you can easily create a series of automated measurements. All parameters, which are out of range, are checked. After creating the scenario, you can run it on the Script status. The Script status sequentially executes the commands in the scenario. If you want to change the parameters in the running scenario, you can change them by pausing the Script status. In addition, because the Script generator and the Script status have a function to graph the parameters, you can check the parameters visually and prevent an unintentional run under those parameters.

The final goal of this software is the integration of measurement and analysis on the IROHA. Because this software is written in Python, we can easily combine the IROHA written in Python and ManyoLib which has the Python interface. Eventually we will introduce this software to the real instruments and begin to use it.

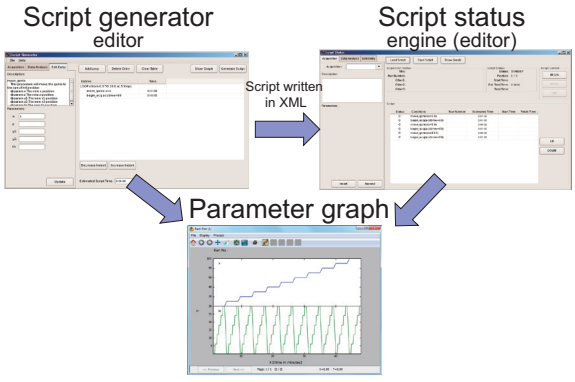

Figure 1. The graphical user interfaces of the Experiment Scheduler.

3. Development of the Experimental Meta-Data Database

Figure 2 shows the schematic view of the data flow of the MLF experiment. The IROHA, which is running on CPU UI, manages the experimental meta-data, which consist of the conditions and results of measurement and analysis, in XML (eXtended Mark-up Language) format. The IROHA collects the conditions and results of the measurement and the analysis from the data acquisition system (CPU DAQ) and analysis server (CPU Ana) and saves them as the experimental meta-data files. We have utilized the RCM System Software (RCM) [2] in development of the experimental meta-data database. The reason that the RCM is introduced to our MLF experiment database is that the RCM is a flexible XML database software which has a Web interface, a user customized workflow and flexible management of authentication / authorization. The experimental meta-data database stores and indexes the experimental meta-data which are collected by the IROHA. We can search the meta-data by some conditions with a web browser and reuse the search result.

4. Conclusion

This year, we developed the automatic measurement software and the experimental meta-data database to prepare for the automatic experiment environment and the MLF experiment database. We will introduce these softwares to the real instruments.

Reference

[1] T. Nakatani, Y. Inamura, T. Ito, S. Harjo, R. Kajimoto, M. Arai, T. Ohhara, H. Nakagawa, T. Aoyagi, T. Otomo, J. Suzuki, T. Morishima, S. Muto, R. Kadono, S. Torii, Y. Yasu, T. Hosoya, M. Yonemura, The proceedings of ICALEPCS 673-675 (2009).
http://www.i4s.co.jp/rcm/rcmabs.html (in Japanese)

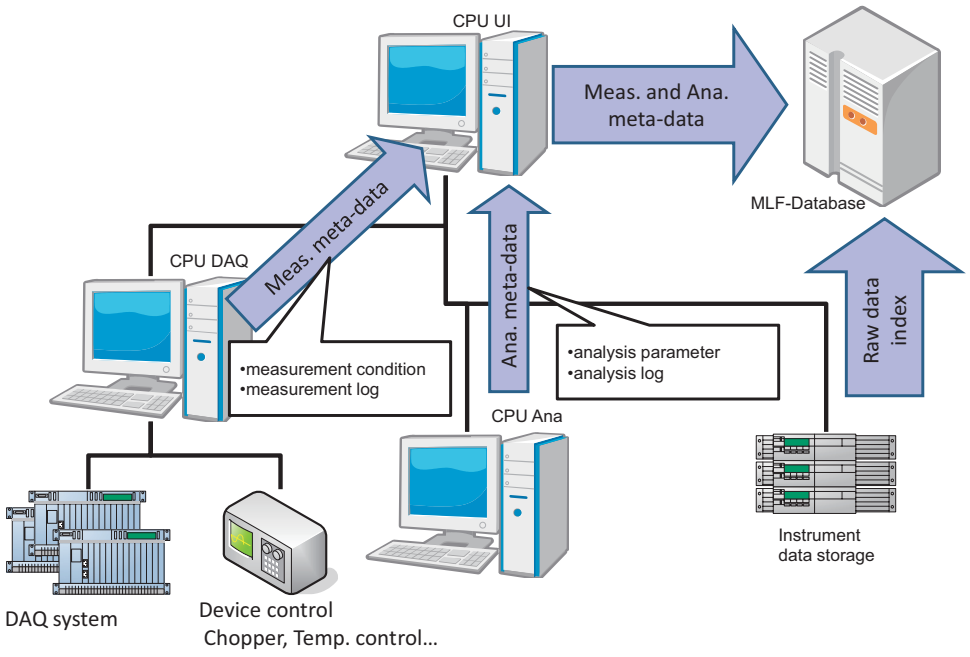

Figure 2. The schematic view of the data flow of the MLF experiment.

T. Nakatani[1], Y. Inamura[1], T. Ito[1], and T. Otomo[2]
[1]*Materials and Life Science Division, J-PARC Center,* [2]*Institute of Materials Structure Science, KEK*

Development of General Purpose Event Module (TrigNET) for J-PARC/MLF

A general purpose event module (TrigNET) is a data logger for neutron scattering experiments. TrigNET has been developed based on a NeuNET [1] which is an encoder module for neutron detectors. In the same manner as NeuNET, TrigNET can be embedded into DAQ system. NeuNET has been widely used in neutron scattering instruments at Materials and Life Science Experimental Facility (MLF) in Japan Proton Accelerator Research Complex (J-PARC).

The characteristics of TrigNET as an analog interface are shown in Table 1. Input A is a 24-bit analog input with maximum sampling rate of 1 kHz. This is called “Slow readout.” By using this input, temperature measurement of a high-temperature oven, pressure measurement of a PCT (Pressure Capacity Temperature) instrument and phase shifting measurement of an optical chopper are possible.

Table 1. TrigNET Analog Interface.

Analog Input	Sampling Rate (max)	Resolution
A	1 kHz	24 bit
B	100 MHz	12 bit

T0 input is for T0 signals sent from a GateNET [1]. The T0 signals are generated in the timing of the collision between the proton beam and neutron target. GateNET receives the T0 signal and outputs an epoch time, which corresponds to the received timing. By identifying the T0 signal, the measurement data of TrigNET are related to neutron detector data measured by NeuNET.

A Field-Programmable Gate Array (FPGA) for data encoding is mounted in TrigNET. As an event data, analog data are generated in the FPGA. Since an 8 kbyte FIFO memory is also equipped in the FPGA, counting loss is not observed in neutron scattering experiments.

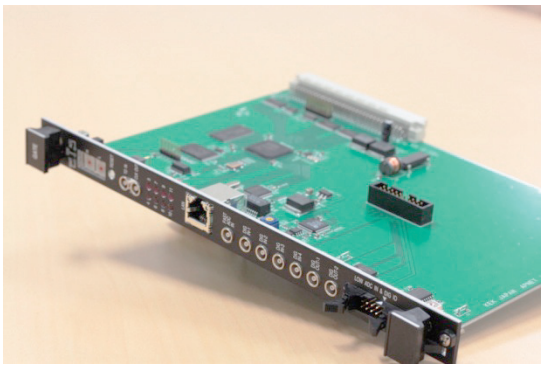

Figure 1. The prototype of the TrigNET.

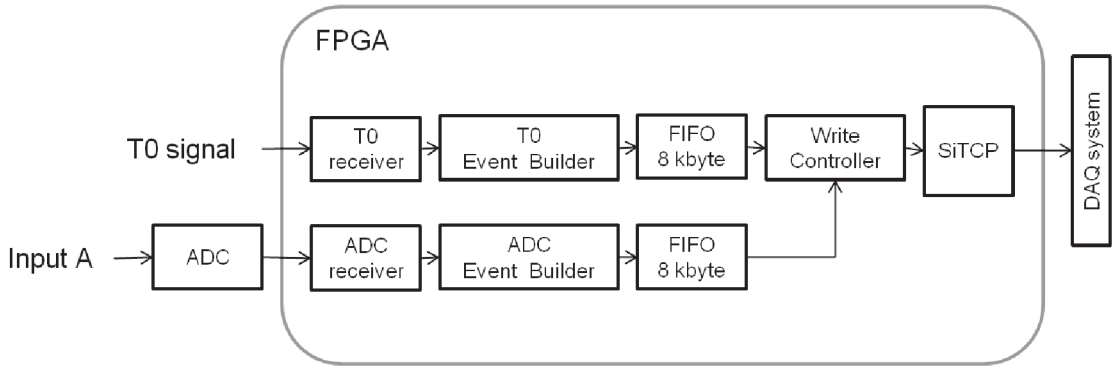

Figure 2. Block diagram of TrigNET.

SiTCP [2] is utilized for data transfer from TrigNET to disk storage. SiTCP is a hardware-based TCP Processor which is loaded onto the FPGA. The maximum data transfer rate is 100 Mbps. Its maximum value is limited by Ethernet specifications. Binary data are saved in a disk storage. We can identify data from TrigNET by checking the data tag.

Input B is still in a state of development. This is a 12-bit analog input with maximum sampling rate of 100 MHz, which aims at measuring signals of ^{3}He gas neutron detectors.

T. Seya, S. Muto, and S. Satoh
Institute of Materials Structure Science, KEK

References

[1] S. Satoh, S.Muto, N.Kaneko, T.Uchida, M.Tanaka, Y.Yasu, K.Nakayoshi, E.Inoue, H.Sendai, T.Nakatani and T.Otomo: Nucl. Instr. and Meth. A **600** 103-106 (2009).

[2] T. Uchida: IEEE Trans. Nucl. Sci. NS-**55** 1631 (2008).

Feasibility Demonstration of a New Fermi Chopper with Supermirror-Coated Slitpackage

1. Introduction

In June 2009 we succeeded to experimentally demonstrate that the measurement efficiency of the inelastic neutron scattering experiment can be markedly improved by using the multiple incident energies simultaneously [1]. We refer to this experimental technique as Multi-E_i method which has been already widely used at J-PARC.

It must be noted that the Multi-E_i method in a conventional chopper spectrometer involves a crucial problem. Usually, the chopper opening time Δt_{ch} is tuned to the pulse width emitted from moderator Δt_m, because the relation of $\Delta t_m \sim \Delta t_{ch}$ is an optimized condition for inelastic neutron scattering measurement by a chopper spectrometer. However, the Δt_m depends on energy and the Δt_{ch} of a conventional chopper keeps constant at all times, and so the Multi-E_i method using a conventional chopper cannot realize the optimized experimental condition for each of the incident energies.

In order to overcome this difficulty, we proposed a new Fermi chopper with supermirror-coated straight slits (MAGIC chopper). MAGIC chopper increases the effective chopper opening time at lower incident energies by virtue of characteristic properties of neutron supermirror, and consequently the optimized experimental condition is expected to be satisfied over the wide range of incident energies. The basic concept and expected performance of MAGIC chopper is described in detail in Ref. 2. We have developed a prototype of MAGIC chopper, and carried out the transmittance experiment on pulsed neutron beam at J-PARC.

2. Experimental Details

Two types of slitpackages with and without neutron supermirrors were prepared in order to elucidate the characteristic properties of MAGIC chopper. The slitpackages are composed of Si wafer and ^{10}B sandwich structure. The Si wafer whose thickness is 150 μm is used as neutron transmitting material. The ^{10}B as neutron absorbing material has thickness of around 15 μm. In the case of a supermirror-coated slitpackage, a coating of Ni/Ti supermirrors with m = 3 is made on both sides of the Si wafer. Here m is the critical angle of the supermirror divided by that of the Ni mirror. After the coating of supermirrors on Si wafers, ^{10}B coating was made on the wafers. The size of both slitpackages is 30 mm x 30 mm x 17 mm (D).

Furthermore, we developed a rotation testing machine (RTM) in-house to investigate the performance of slitpackages in rotating state. The rotation of RTM is driven by a servomotor with mechanical bearings, and synchronized with a trigger signal of the repetition rate of pulsed neutron source.

Neutron transmittance experiments using the RTM have been carried out on the BL10. The RTM incorporating the slitpackage was located at 13400 mm from the neutron moderator. The rotation frequency was 100 Hz for two different slitpackages with and without neutron supermirrors, where the phase delay was identical for each measurement. Transmitted neutrons were detected by a two-dimensional neutron detector whose surface was located at 13880 mm from the neutron moderator.

3. Results and Discussions

The TOF spectra of transmitted neutrons with and without supermirrors are shown in Fig.1, where the rotation frequency was 100 Hz, and the phase delay was identical for both slitpackages. Intensities given in Fig. 1 are normalized by the intensity of direct beam measurement which is the transmittance experiment removing the slitpackage from the neutron beam path. In case of 100 Hz rotation without neutron supermirrors, we can observe several peaks at every ~5179 μs, which corresponds to one-half of the RTM rotation period at the detector position, i.e., 1/100 x 1/2 x 13880 / 13400 x 10^6 μs. There is little difference between the two slitpackages in shorter TOF region (higher energy region), however, the differences become clear in the lower energy region, where the intensity distribution be-

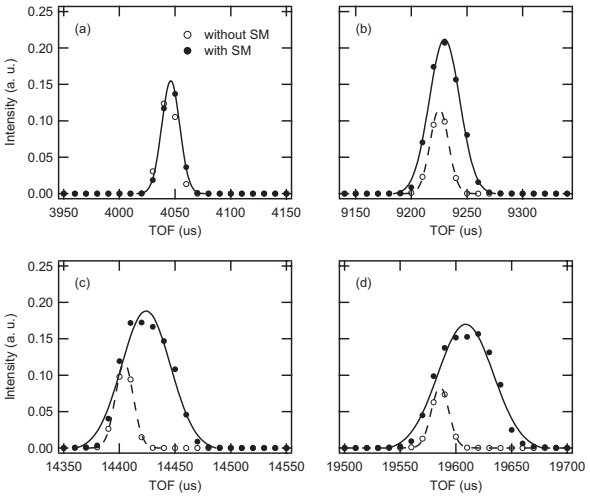

Figure 1. The TOF spectra of transmitted neutrons from rotating slitpackages with and without neutron supermirrors (m = 3). Rotation frequency is 100 Hz for both cases.

comes wider and shifts toward longer TOF side compared with a slitpackage without neutron supermirror. Moreover, an increase of peak height in supermirror-coated slitpackage is also observed.

The pulse width transmitted by a rotating slitpackage, Δt_{ch}, can be estimated from the observed pulse width at a detector, Δt_d, shown in Fig. 1,

$$\Delta t_{ch} = \Delta t_d \times (13400/13800), \qquad (1)$$

where the distance from the moderator to the slitpackage is 13400 mm, and the distance from the moderator to the detector is 13880 mm. Two pulse widths transmitted slitpackages with and without neutron supermirrors are plotted in Fig. 2. The pulse width of the supermirror-coated slitpackage increases in the lower energy region. This feature is exactly the essential characteristic of MAGIC chopper. These experimental results have validated the conceptual design of MAGIC chopper; that is, MAGIC chopper can realize the optimal condition for each of the incident energies for inelastic neutron scattering measurement with Multi-E_i method.

In Ref. 2, the effective chopper opening time is expected to obey the following relation,

$$\Delta t_{ch} = 2 \times \frac{17.3 m \lambda_i}{2\pi f} \times 10^3 (\mu s), \qquad (2)$$

where m is the m-value of the supermirror, f (Hz) the chopper frequency, and the term $17.3m\lambda_i$ (mrad) corresponds to the critical angle for incident neutron λ_i (nm). The calculated result with m =3 and f =100 Hz in Eq. (2) is also plotted in Fig. 2. The calculated result provides good agreement with the experimental results.

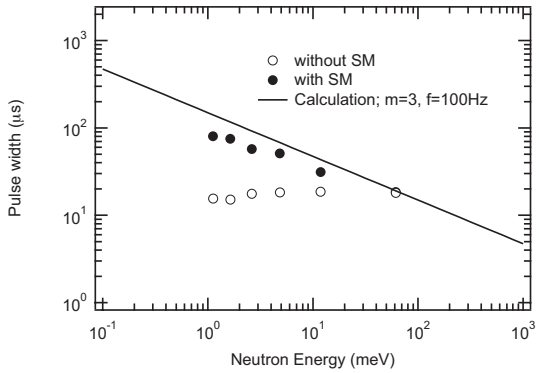

Figure 2. The energy dependence of pulse widths by rotating slitpackages with and without neutron supermirrors (m = 3). Rotation frequency is 100 Hz for both cases. Calculated result from Eq. (2) is also plotted.

4. Summary

It is found that a rotating supermirror-coated slitpackage increases the effective chopper opening time in the lower energy region, which confirms that the MAGIC chopper can overcome the difficulties in optimizing the inelastic neutron scattering experiment with Multi-E_i method. This study experimentally proved that the MAGIC chopper can significantly improve the measurement efficiency of the inelastic neutron scattering experiment by a chopper spectrometer, and thus contribute to opening up a new field of materials science.

References

[1] M. Nakamura, R. Kajimoto, Y. Inamura, F. Mizuno, M. Fujita, T. Yokoo, M. Arai, J. Phys. Soc. Jpn. **78** 093002 (2009).

[2] M. Nakamura, M. Arai, R. Kajimoto, T. Yokoo, K. Nakajima, Th. Krist, J. Neutron Res. **16** 87 (2008).

M. Nakamura[1], W. Kambara[1], T. Shinohara[1], K. Ikeuchi[2], R. Kajimoto[2], Th. Krist[3], H. Tanaka[1], J. Suzuki[2], M. Harada[1], K. Oikawa[1], F. Maekawa[1], M. Arai[1]

[1]Materials and Life Science Division, J-PARC Center; [2]Research Center for Neutron Science and Technology, CROSS; [3]Helmholtz Zentrum Berlin for Materials and Energy, Germany

Sample Environment at MLF

1. Introduction

By the year 2010, the construction of many of the MLF neutron beam lines have been completed and started neutron experiments of user program. The demand for sample environment (SE), thus, abruptly increased. One of the key issues in carrying out the required neutron experiments is to have well established SE devices and supports as required by a world leading neutron facility. The MLF neutron SE team organized just a couple of years ago is still in its infancy and having some difficulties to overcome. The biggest problem for the SE team is that there is no specialist who is responsible for focusing on SE in the terms of technical guidance and also administration. Under these circumstances, we are gradually advancing as mentioned in the following sections.

2. SE Standardization

In the recent years, we spent some time to establish the standard of MLF-neutron devices and interfaces of SE. In particular, flange specifications are very important for standardizing conventional (common) devices. The advantage of SE standardization is to save resources, costs, time and manpower. Also, we have a profitable of easy to use, maintenance, handle addition to that we can share the devices. The MLF-neutron "SE Protocol" has been set up in 2005, where the standard of beam-flange distance, vacuum couplings, cryostat specifications involving temperature sensors, sample cans, motor controllers, and so forth are described in addition to vacuum flange specifications [1]. The protocol is revised for the appropriate period.

3. SE Devices in MLF-Neutron

The SE Devices currently installed in MLF-neutron are listed in Table 1. Since the funding of each beam line is different, it is quite difficult to prepare those equipments along the unified strategy of MLF.

Table 1. SE devices installed at the MLF-neutron facility.
(TL: top-loading, ASC: auto sample changer)

Beam Line	SE Devices	Options
BL01 (4SEASONS)	4 K-TL Cryostat	w-gonio 600 K heater
BL03 (iBIX)	Gas-flow Cryostat	
BL04 (ANNRI)	ASC	
BL05 (NOP)		
BL08 (S-HRPD)	4 K Cryostat 10K-TL Cryostat ASC	
BL10 (NOBORU)	Gonio (5-ax)	
BL12 (HRC)	4 K Cryostat 1 K Cryostat	w-gonio
BL14 (Amateras)	4 K Cryostat	
BL16 (SOFIA)	ASC	w-gonio
BL19 (TAKUMI)	Loading machine 1000˚C furnace	in-situ dilatometer
BL20 (iMATERIA)	ASC	
BL21 (NOVA)	ASC Vanadium oven (RT~1370 K)	in-situ gas flow measurement

It is necessary to obtain a large budget for SE, in which we should consider the ground design of the sample environment and the related including infrastructure. Also, we plan to install 7 and 14 Tesla vertical magnets in the next year. Within a couple of years, the basic part of SE devices should be set for full operation of the user programs.

4. SE Handling Area

One of the "gradual progresses" is that we set the SE handling area in MLF experimental hall 1 as shown in Fig. 1. The area of less than 10 m × 10 m is not enough space to handle all the SE devices installed in MLF. However, we can start some small maintenance, repair, preparation and tests. Also in this area, appropriate electrical power supplies are prepared (100 V and 200 V 3p) as in Fig. 2. This could be the first step of considering the next comprehensive SE support. In the next year, we plan to set up the same type of SE handling area in experimental hall 2. As a perspective, a larger functional area (building) should be prepared for providing sophisticated user support.

5. KENS SE Devices

The neutron facility (KENS) in KEK used to use lots of neutron SE devices when proton synchrotron was operated until 2006. From the piles of these previously valuable devices, we selected a few to bring to J-PARC. We are going to re-use them with minimum repairs (modifications). This is quite useful particularly for the beam line which does not have its own equipment. Since it takes, however, time and costs, the maintenance will be done within several years.

6. Workshop

The 6th International Workshop on SE at Neutron Scattering Facilities was held in Munich, Germany, from September 29th to October 1st, 2010. Some members of the SE team (T. Yokoo, S. Kawamura, W. Kambara, K. Kaneko and A. Hoshikawa) attended this workshop. About 60 people from neutron facilities in various countries attended the workshop, where new techniques of SE devices and special environments were reported. It was the first time for a Japanese group to participate in the workshop. One of the most impressive things was that the participants really welcomed the Japanese group to join their community and are interested in J-PARC/MLF. We were able to get lots of valuable advices and participate in fruitful discussions with SE people from other countries. The next one will be held in Australia in 2012.

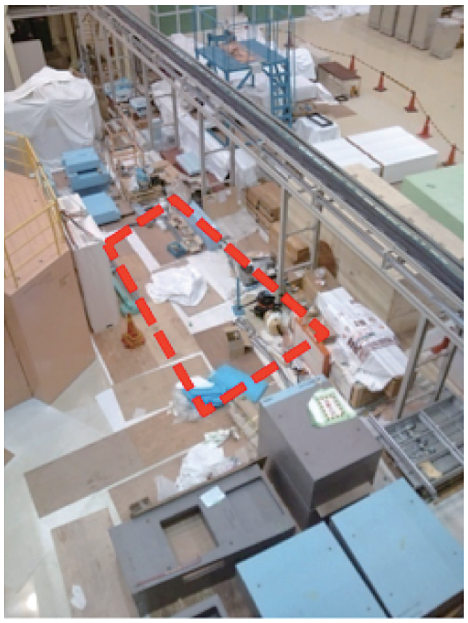

Figure 1. The reserved SE handling area (indicated by red line) in MLF experimental hall 1. It is right next door to BL11.

Figure 2. Electric power supply newly set at the SE handling area.

7. Stepping Forward

Realistic user program just began in MLF neutron. Now it is a time to give considerations to users and experiments apart from constructions. We definitely need to secure funds for SE and have devices along facility ground design. Also, the human resources, which are the most universally crucial, should be seriously considered for the next step of SE team.

Reference

[1] "SE-Protocol on Neutron Science Section" 5th edition.

T. Yokoo[1,2], S. Kawamura[1], and W. Kambara[1]

[1]Materials and Life Science Division, J-PARC Center; [2]Institute of Materials Structure Science, KEK

Magnetic Field Imaging Using Polarized Pulsed Neutrons

1. Introduction

Magnetic field imaging using a polarized neutron beam is one of the new techniques to visualize the spatial distribution of the magnetic field in a space or inside materials [1]. This technique is based on the motion of a neutron spin passing through a magnetic field, and the rotation of a neutron spin due to the Larmor precession is measured as the change in the neutron polarization with spatial resolution using a 2D neutron detector.

As the polarization measurements with one certain wavelength condition possess an uncertainty of the rotation angle due to the periodicity of 2π, study of wavelength dependence is befitting to determine the absolute rotation angle. Then, the accumulated magnetic field along the flight path of the neutron beam can be quantified. Thus, usage of a pulsed neutron beam is suitable for the quantitative analysis of the magnetic field [2]. In addition, three-dimensional analysis of the polarization change due to the spin rotation in a magnetic field gives the vector information of the magnetic field, as the change in the polarization can be described by a (3 × 3) matrix $\boldsymbol{D}$, whose elements D_{ij} (i, j = x, y, z) are expressed by direction cosines of the magnetic field vector [3]. Therefore, measuring and analyzing the wavelength dependence of each element of matrix $\boldsymbol{D}$ at each position allow determination of the spatial distribution of the magnetic field vector.

2. Experiments

Magnetic field imaging experiments with 3D polarization analysis were performed at the beam line of BL10 “NOBORU” installed in MLF at J-PARC. The photograph and the schematic illustration of the experimental setup are shown in Fig.1 and Fig.2. Transmission type polarizer and analyzer, which consist of magnetic super-mirrors, were used for the measurements. Two spin rotators were placed before and after the sample for the neutron spin controlling. The 2D detector, which was composed of a position-sensitive photomultiplier and a ZnS scintillator, was used to record the information about the time-of-flight and the position for each event. Its channel width was 0.25 mm and the spatial resolution was 0.8 mm.

Figure 1. Photograph of the experimental setup at BL10.

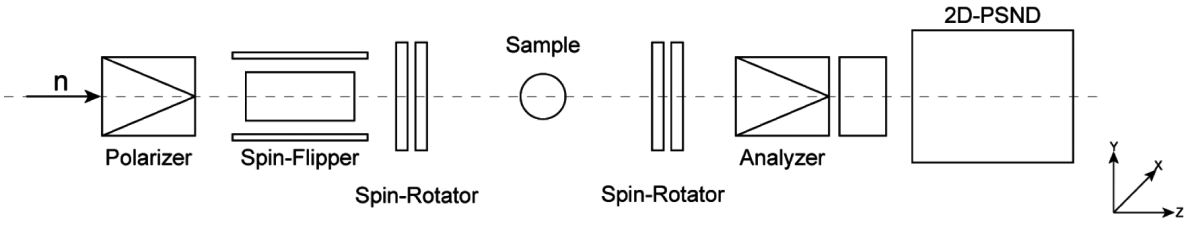

Figure 2. Illustration of the experimental setup. The sample position was 13.80 m, and the neutron detector position was 14.55 m from the neutron source.

At first, a small solenoid coil with a diameter of 5 mm was used as the sample. Then, a soft magnetic metal foil with the thickness of 0.03 mm was tested to visualize the magnetic domain structure inside the foil. A small guide field lower than 1 G along *y* direction was applied at the sample position.

3. Results and Discussions

Polarization images and profiles at several wavelengths obtained for the solenoid coil with the applied current of 2.5 A are shown in Fig. 3 (a) ~ (f). In these figures, the polarization decrease due to the neutron spin precession could be observed at the position of the coil. The wavelength dependence of the normalized polarization at the center of the coil clearly indicates oscillating behavior (Fig. 4). By fitting the data with a function written in Fig. 4, we have evaluated the magnetic field strength to be 5.15 ± 0.20 mT from the oscillation period ω_λ and the tilt angle of the magnetic field relative to the *y* direction to be 40.1 ± 0.9 º from the direction cosine value n_y. These were in good agreement with the designed values.

The images of diagonal elements of the matrix ***D*** obtained for the soft magnetic foil are shown in Fig. 5. The images of D_{xx} and D_{zz} indicate stripe patterns, whose width were 2 ~ 3 mm, while that of D_{yy} was almost homogeneous. These results suggest that the component of the magnetic field vector along *y* axis is homogeneous inside the foil, but those along *x* and *z* axis were different at each position. This feature can be explained by the picture, showing the small guide field applied along *y* axis magnetized the sample but partially there remained some magnetization component which could not align with the applied field. Therefore, the images of D_{xx} and D_{zz} can be regarded as evidences of the magnetic domain structure in the soft magnetic foil.

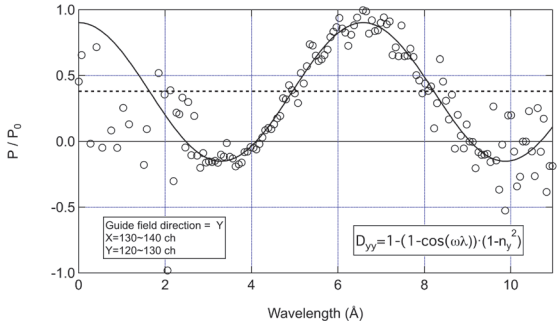

Figure 4. Wavelength dependence of normalized polarization at the center of the coil. The line indicates the result of fitting.

4. Summary

We have performed magnetic field imaging experiments using polarized pulsed neutrons. From the results of the solenoid coil's imaging, we successfully visualized the magnetic field inside the coil and confirmed the possibility of quantification of magnetic field strength and the direction by analyzing the wavelength dependence of polarization. Also, the magnetic domain structure of the soft magnetic foil could be observed using the imaging technique with 3D polarization analysis method.

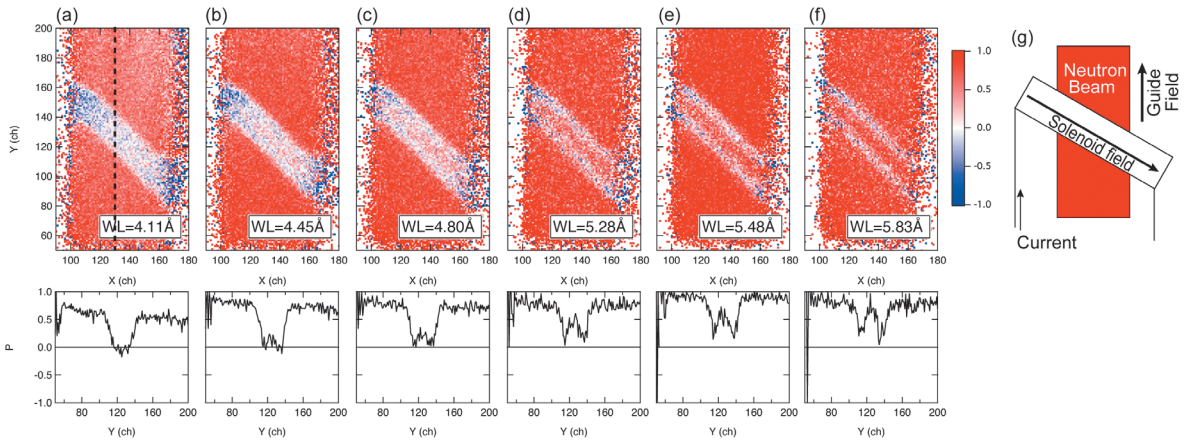

Figure 3. (a) - (f) Polarization images of the coil and polarization profiles along y-axis measured with various wavelengths. (g) represents configuration of the neutron beam and the coil.

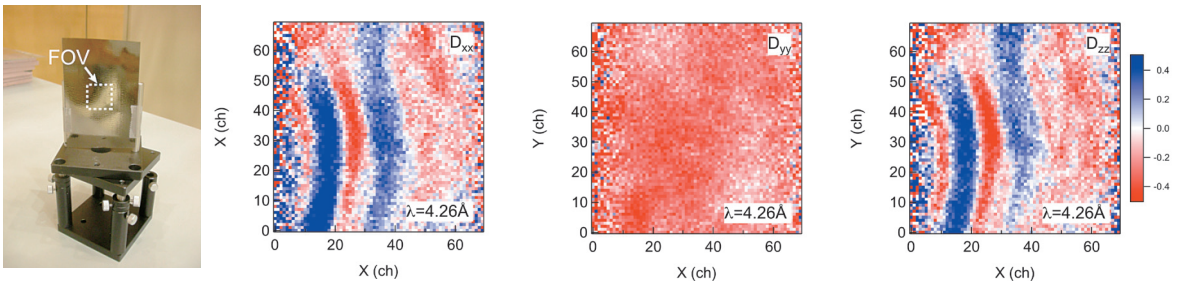

Figure 5. Images of the polarization matrix element D_{ii} (i = x, y, z) obtained for the soft magnetic metal foil sample. The incident neutron wavelength was 4.26 Å. The left figure is the photograph of the soft magnetic metal foil sample.

This work was partially supported by a Grant-in-Aid for Scientific Research (C) from the Japan Society for the Promotion of Science (No. 22604009).

References

[1] N. Kardjilov, *et al.*, Nat. Phys. **4** (2008) 399.
[2] T. Shinohara, *et al.*, Nucl. Instr. and Meth. A (in press).
[3] M. T. Rektveldt, Z. Phys. **259** 391 (1973).

T. Shinohara[1], K. Sakai[1], M. Ooi[1], T. Kai[1], M. Harada[1], K. Oikawa[1], F. Maekawa[1], H. Sato[1], H. Hayashida[1], J. Suzuki[2], K. Aizawa[1], M. Arai[1], and Y. Kiyanagi[3]

[1]Materials and Life Science Division, J-PARC Center; [2]Research Center for Neutron Science and Technology, CROSS; [3]Faculty of Engineering, Hokkaido University

Elemental Analysis of Au-In-Cd Alloy by Using Neutron Resonance Imaging Technique at BL10

1. Introduction

The Ag–In–Cd (AgIC) alloy was adopted as a decoupler material for two decoupled moderators of the J-PARC pulsed spallation neutron source [1]. A high decoupling energy at 1 eV was achieved for the first time in the world in MW-class spallation neutron sources. Although the AgIC decoupler is superior in neutronic performance, its high residual radioactivity originating from Ag imposes a significant difficulty in handling the used moderators. To overcome this difficulty, a new alloy in which Ag in the AgIC alloy is replaced with Au, Au-In-Cd (AuIC) alloy, was proposed by Harada et. al [2]. Radioactivity in the AuIC decoupler can be reduced to about 1/1000 of that in the AgIC decoupler.

Accordingly, we have launched an R&D activity on the AuIC alloy production. As the first step, we made AuIC alloy specimens by melting the three elemental metal pieces in a small furnace and an infra-red heater [3]. Target alloy compositions determined [2] are 74.9, 0.5 and 24.6 atomic % for gold, indium and cadmium, respectively. The elemental distributions of gold and cadmium on a specimen surface were measured by a SEM-EDX (scanning electron microscope - energy dispersive X-ray spectroscopy) and were confirmed to be uniform. However, X-ray peaks of indium were overlapped by X-ray peak tails of cadmium because the indium composition was much smaller than the cadmium composition and the atomic number of indium (49) is next to that of cadmium (48). Therefore, it is difficult to see the indium distribution with the SEM-EDX method. In order to confirm the uniformity of the alloy including indium, we used a neutron time-of-flight imaging technique at BL10.

2. Neutron Resonance Imaging

Most of the elements have resonance cross-sections as shown in Fig. 1. Neutron resonance energies are specific for each nuclide. For example, when we see a transmission image of the AuIC specimen only at t=475 μs, we can see an image contributed by the gold content only (see Fig. 1). Accordingly, we can distinguish certain elements in a sample by the neutron resonance imaging which is one of time-of-flight imaging techniques.

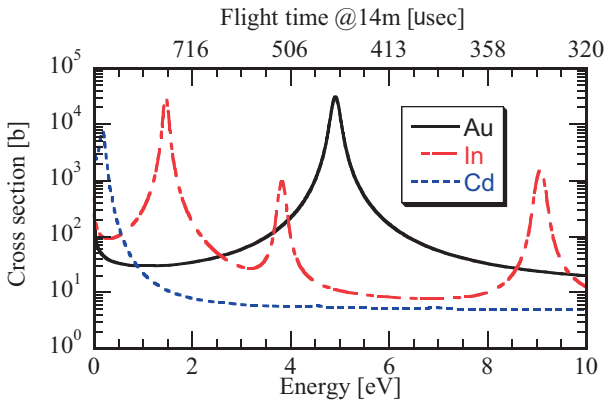

Figure 1. Total cross section of Au, In and Cd.

3. Measurement

One of the specimens was cut to a disk sample with thickness of 0.9 mm and diameter of 6.5 mm. The disk sample was set on a thin aluminum plate with other reference samples, i.e., indium (0.01 mm) and gold (0.5 mm and 1 mm), as shown in Fig. 2. Figure 3 shows the outline of a detector system which was developed by Kureta et.al.

Figure 2. Sample.

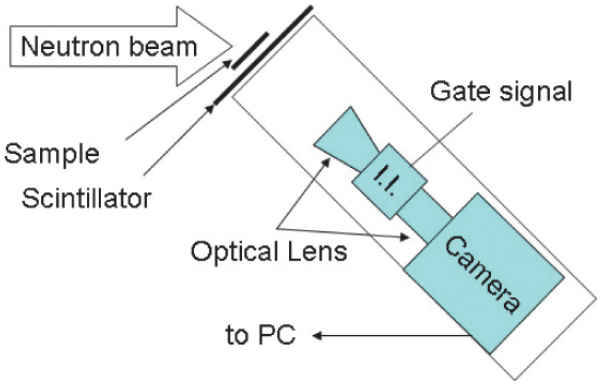

Figure 3. Outline of the imaging system.

A scintillator plate and an optical system were set on 45 degrees with respect to the neutron beam. Visible light from the scintillator was amplified by the image intensifier (I.I.) and recorded by the camera. The I.I was operated in synchronization with external signals to be used as a shutter of the camera. By inputting a gate signal to the I.I. with a certain delay from the T0 timing, we could get an image of a certain energy range of interest. In order to obtain clear images, 4000 or 8000 images were accumulated in one measurement.

4. Results and Discussions

Figure 4 shows the neutron transmission curve of gold and the AuIC sample, and measured images around En=3.88 eV (Au), En=1.44 eV (In), 0.47 eV (Cd) and En=2.23 eV (off-resonance). Due to saturation of the neutron absorption, the measured energy of Au was shifted to its peak energy (4.89 eV) to 3.88 eV. We can see some shadows of the samples in Fig.4. Even in the off-resonance energy, we can see the AuIC disk sample and the gold samples because of the base line of the cross section curves as seen in Fig.1.

In order to remove the base line effect line, we used the following equation.

$$I_r = I_0 \exp(-(\sigma_n + \sigma_r)Nt) \quad (1)$$

$$I_n = I_0 \exp(-\sigma_n Nt) \quad (2)$$

$$-\mathrm{Ln}(I_r / I_n) = \sigma_r Nt \quad (3)$$

Where I_r and I_n are transmitted neutron intensity at the resonance energy and off-resonance energy, respectively, I_0 is neutron intensity without a sample, σ_n off-resonance cross section which is considered almost constant over the measured energy region, σ_r resonance cross section, N atomic density, and t thickness of the material. Eq. (3) can be deduced from Eqs. (1) and (2) to know the material thickness t.

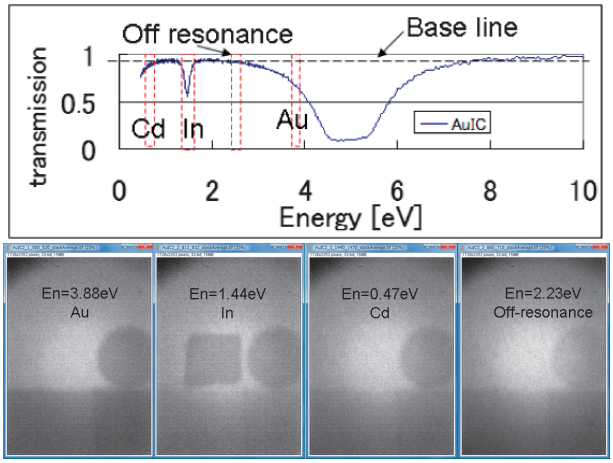

Figure 4. Neutron transmission curve (upper) and raw pictures (lower). En means neutron energy.

Figure 5 shows the function of $\sigma_r Nt$ of gold, indium and cadmium deduced with Eq. (3). In each sub-figure, only the target element is seen. Figure 6 shows intensity profiles along lines A and B in Fig. 5. The $\sigma_r Nt$ values in the gold and indium samples are almost proportional to their real thicknesses.

Although more detailed analysis is needed to obtain the elemental distributions, we could confirm that the distributions of indium in the AuIC alloy disk sample were almost uniform.

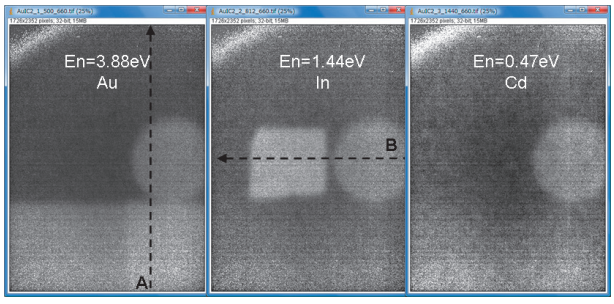

Figure 5. Processed image of Au (left), In (center) and Cd (right).

5. Summary

We adopted the neutron resonance imaging technique to visualize elemental distribution in the AuIC sample, and successfully confirmed the indium distribution in the AuIC alloy to be almost uniform.

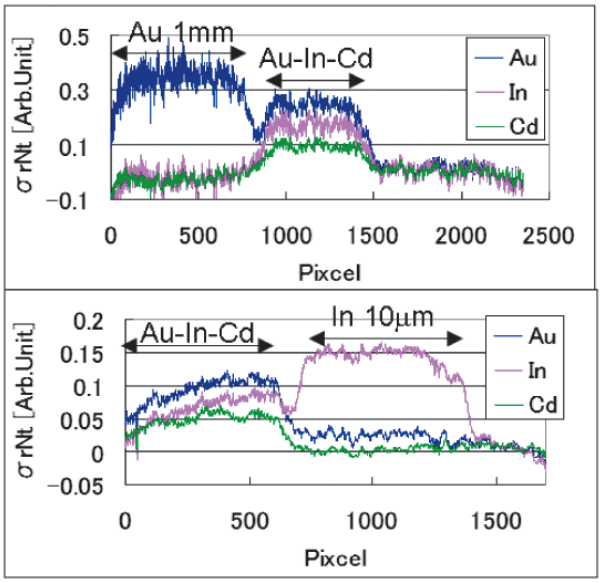

Figure 6. Profile of material thickness. Upper figure is line A. Lower figure is line B.

References

[1] M. Harada, N. Watanabe, M. Teshigawara, T. Kai, Y. Ikeda, Nucl. Instr. and Meth, A **539** 345 (2005).

[2] M. Harada, M. Teshigawara, F. Maekawa, M. Futakawa, J. of Nucl. Mat., **398** 93 (2010).

[3] M. Ooi, M. Teshigawara et.al., J. of Nucl. Mat. To be published

M. Ooi[1], M. Harada[1], M. Teshigawara[1], F. Maekawa[1], E. Hashimoto[2], M. Segawa[2], and M. Kureta[2].

[1]*Materials and Life Science Division, J-PARC Center;* [2]*Nuclear Science and Engineering Directorate, JAEA.*

Pulsed Neutron Imaging on Quenched Iron Rods and Cement Pastes

1. Introduction

Imaging using a pulsed neutron source can give spatial dependence of the crystallographic information of a material with coherent scattering cross section, as well as information concerning molecular and atomic dynamics of the incoherent scatterers, especially hydrogen. The crystallographic image is obtained by analyzing the spatial dependent Bragg edge transmission data, for which we have developed a data analysis code "RITS (Rietveld Imaging of Transmission Spectra)" [1]. With the help of this code we can experimentally study preferred orientation, crystallite size, and lattice spacing. Here, as an example of applications in real engineering components, we study quenched iron rods with different quench thicknesses. Another important application of the pulsed neutron imaging to be developed is hydrogen distribution imaging giving not only the concentration but also the dynamical information. Hydrogen cross section increases with neutron wavelength and the gradient becomes larger with the degree of freedom of the hydrogen motion. Therefore, the gradient of the cross section of hydrogen in water is steeper than that in ice. As the first attempt of the hydrogen motion imaging, we performed transmission measurements on cement pastes of a dry and a wet sample in order to see the difference of the bound state of hydrogen in the cement paste.

2. Bragg Edge Imaging of Quenched Iron Rods

As the Bragg edge imaging application we carried out the proof-of-principle measurement of the quenching depth for typical industrial parts, which are shipped by the manufacturer, with applying a high spatial resolution micro channel plate (MCP) detector developed by Tremsin et al [2]. That detector has a 55 μm pixel resolution and capability for TOF measurement. The experiments were carried out at BL10 "NOBORU". The 26 mm diameter cylindrical samples, which were cut out with thickness of 20 mm from the quenched iron rods, were set in front of the detector window as shown in Fig. 1.

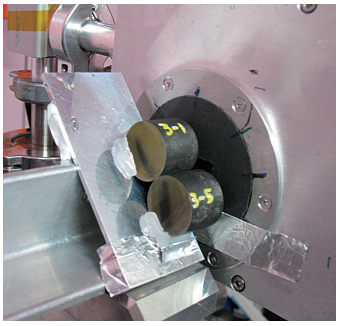

Figure 1. Experimental arrangement of the two sample pieces set in front of the detector.

Figure 2 shows a transmission image of wavelength 1 ~ 5 Å neutrons, and a wavelength-resolved transmission image around the {110} Bragg edge (4.089 ~ 4.100 Å). In the wavelength- resolved image, we can distinguish the quenched zone, although we cannot distinguish it in the wide-wavelength image. We can investigate that the depth of the quenched zone from the surface is 5 mm, which is consistent with the induction hardening designed by the manufacturer.

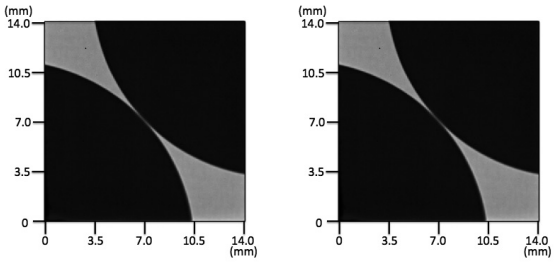

Figure 2. Neutron transmission images of quenching depth 5 mm samples for wavelength 1 ~ 5 Å (left) and 4.089 ~ 4.100 Å (right).

Figure 3 shows images of the real space distribution of the crystal lattice plane spacing of {110} for quenching depth 3, 5 and 7 mm samples. These images were obtained by analyzing the {110} Bragg

edges of position-dependent transmission TOF spectra of the specimens [1]. The quenched zones show the broader lattice spacing, because the martensite transformation is caused by the quenching. It is clear that the quenching depths are increasing as the 3, 5 and 7 mm from the surface of each sample. The quenching zone boundary becomes blurry as the depth of quenching during manufacturing increases.

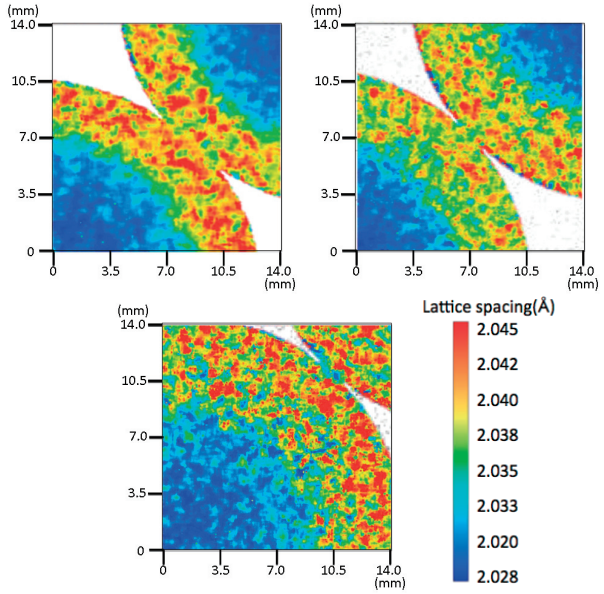

Figure 3. {110} lattice spacing of quenched iron samples; quenching depth 3 mm (upper left), 5 mm (upper right) and 7 mm (lower).

3. Bound State Imaging of Hydrogen in Cement Pastes

Hydrogen exists in many materials and plays an important role. However, the position dependence of hydrogen bound state and its dynamics are not well understood. Pulsed neutron transmission can give information of H_2O molecular dynamics by analyzing the gradient of the total cross section. Therefore, we apply this method for imaging the bound state of hydrogen in cement pastes.

First, we performed total cross section measurements on water and ice at Hokkaido LINAC. The result is shown in Fig. 4. The gradient of the microscopic total cross section of water is steeper than that of ice.

Next, we performed transmission experiments for two kinds of cement pastes at NOBORU. We

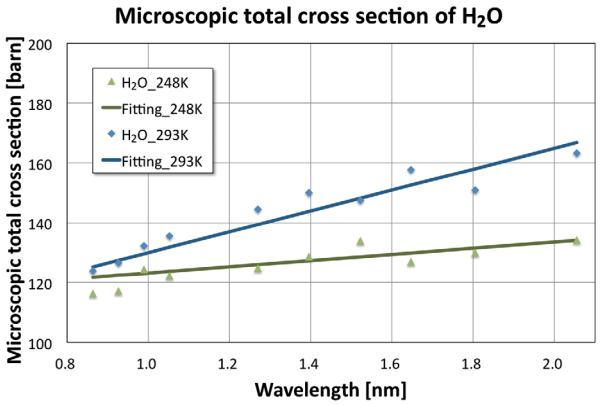

Figure 4. Wavelength dependence of total cross section of water and ice.

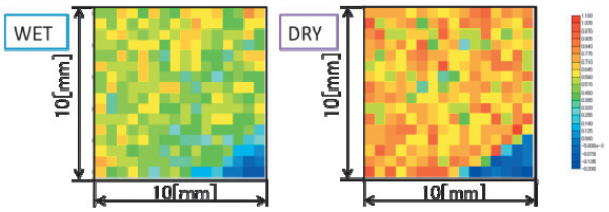

Figure 5. Gradient distributions in a wet sample (left) and a dry sample (right).

think that the water contained in cement pastes is roughly divided into free and bound water. Suppose the wet cement paste contains mainly free water and the dry cement paste ice. Figure 5 shows the imaging of the gradient of the total cross section. The gradient of the wet cement paste is more gradual than that of the dry one.

The result is different from the expected one, in which the gradient of the wet sample would be larger than the dry one.

The reason for the gentle gradient of the wet sample may be due to the effect of up scattering by the H_2O molecule. To investigate it further, the difference of the scattering in water and ice has been studied by simulation using the Particle Heavy Iron Transport cord System code. The transmitted neutron intensities depending on the wavelength and the thickness have been calculated. Figure 6 shows examples of the transmitted neutron intensities of 9 Å incident neutrons through 1 and 5 mm thicknesses. In the ice case the incident neutron peak still exists even at 5 mm, and the shapes are almost the same. So, the neutrons with an incident wavelength play important role for determining the transmit-

ted cross section. On the other hand, in the water case the flux at shorter wavelength increases with increasing the thickness. The calculation conducted with neutrons of different incident wavelength indicates that the transmitted flux has almost the same shape independent of the incident wavelength since the water temperature is much higher than the incident neutron energy. Thus, the total neutron cross section does not depend so much on the incident neutron wavelength.

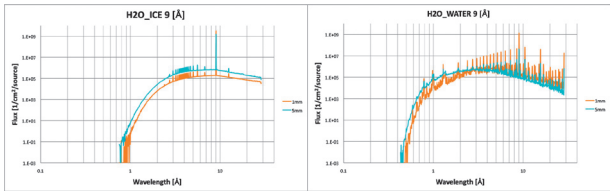

Figure 6. Transmitted neutron intensities through ice (right) and water (left).

4. Summary

The results on the quenched iron rod gave information on the quenched region and the homogeneity, which shows usefulness of the pulsed neutron imaging. Concerning to the hydrogen bound state imaging, the difference of gradient was observed, but more detailed analysis is necessary for quantitative evaluation.

Acknowledgement

This work was supported by KAKENHI (JSPS) 20246136.

References

[1] H. Sato, T. Kamiyama and Y. Kiyanagi, Mater. Trans. JIM, **52** 1294 (2011).

[2] A.S. Tremsin, J.B. McPhate, J.V. Vallerga, O.H.W. Siegmund, J.S. Hull, W.B. Feller, E. Lehmann, Nucl. Instr. Meth. A, **604** 140 (2009).

T. Kamiyama[1], H. Sato[1, 2], R. Takamori[1], N. Ayukawa[1], Y. Iwasaki[1], A. S. Tremsin[3], and Y. Kiyanagi[1]

[1]Graduate School of Engineering, Hokkaido University; [2]Present address, Materials and Life Science Division, J-PARC Center; [3]University of California at Berkeley

High-Pressure Activities Using Engineering Materials Diffractometer, TAKUMI

1. Overview of the Project

In Japan, the high-pressure neutron experiments have been limited typically below 3 GPa, mainly due to the limited flux of domestic neutron sources. The intense pulsed neutron source at J-PARC is about to change this situation. So, we launched the high-pressure project which aims to popularize the high-pressure neutron experiments above 10 GPa. As a guidance, we took two approaches; the one is to use already constructed beamlines (TAKUMI at BL19, NOVA at BL21) and the other is to construct a new beamline specialized for high-pressure purpose (PLANET at BL11). Each one is described as TOPICS in this report (p.15).

The TAKUMI was originally designed for engineering materials use, but the characteristics, such as small gracing volume for sample and wide working area at the sample position, suit the high-pressure experiments. So, we brought several compact high-pressure devices and developed high-pressure neutron diffraction techniques. The final goal of the project is to establish the precise structure determination methods for crystalline and liquid materials above 10 GPa. As compact presses, we selected three types of presses: Palm cubic anvil cell(Palm-cell)[1], Opposed gem anvil cell [2] and Paris-Edinburgh cell (PE-cell). The former two were originally developed by Japanese groups and will allow us to reach the pressure and temperature region inaccessible so far (Fig. 1). The presses and obtained results are being presented in this manuscript. Furthermore, the neutron focusing devices, which are indispensable for approaching much higher pressures, are introduced as well.

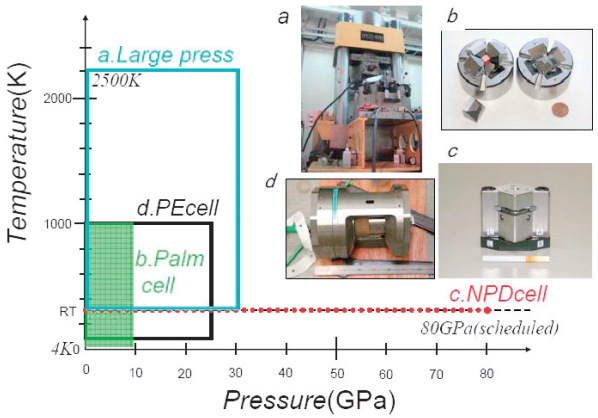

Figure 1. *PT* region each device can access.

2. Explore New States of Ice with Palm Cell

The Palm cubic multi-anvil cell was invented by Uwatoko [1]. It is a miniature of the huge multi-anvil presses which have been developed mainly by Japanese earth's scientists. The size is about 10 cm in diameter and 20 cm in the height (Palm size). This is enough compact to be attached to the cryostat, so it opens the way to investigate the state of the matter under low-temperature and high-pressure condition. At present, the cell can reach the condition of 4 K and about 10 GPa, and therefore becomes a good tool to investigate the hydrogen behavior in the field of the planetary science. This cell was applied to the study of the ferroelectric ices.

The question as to whether or not ferroelectric ices exist in space in a stable form attracts much interest. The ferroelectricity is a very important feature for planetary formation and material (including life origin material) evolution in space because of long-range electrostatic forces. We did in-situ experiment of ice under high pressure and low temperature (about 1 GPa and below 140 K). We observed new ice forms, called ice XV and XVI. Ice XV is theoretically predicted as ferroelectric ice. Ice XVI is considered to be metastable structure of ice XV. We pursued the mysterious properties of ice XV and XVI at low temperatures and high-pressures. The structural study of those ices reveals the existence and properties of high-pressure ferroelectric-ices inside space icy bodies (e.g., Pluto and Kuiper belt objects).

3. Design of a New Opposed Anvil Cell and Its Application to Neutron Diffraction

The compact opposed anvil cells were newly designed for TOF powder neutron diffraction. By using gem-grade anvils, we obtained both accessibility to very high pressure range and wide detection angles ($2\theta = 90^{o} \pm 15^{o}$)(Fig. 2). Depending on the experimental purpose, three kinds of anvil materials are used: single crystal moissanite (SiC) with 5mm flat-top culet, sintered polycrystalline diamond with 4mm concaved culet, and nano-polycrystalline diamond [4] with 3mm flat-top culet. Each anvil was precisely cut and shaped into conical geometric form to endure large force applied by the cell body [2]. With the use of this device, neutron diffraction patterns were taken for a methane hydrate CD_4:5.75D_2O (sample volume: 7mm^3) at pressures of up to 1.2 GPa, and for brucite $Mg(OD)_2$ (sample volume: 5mm^3) at pressures of up to 8 GPa. We also checked the possible detection of signal from very tiny sample for future extension of the maximum pressure range, and confirmed marked signal from Pb sample with the volume of ~1mm^3 at 0.6 GPa [5] within the realistic exposure time.

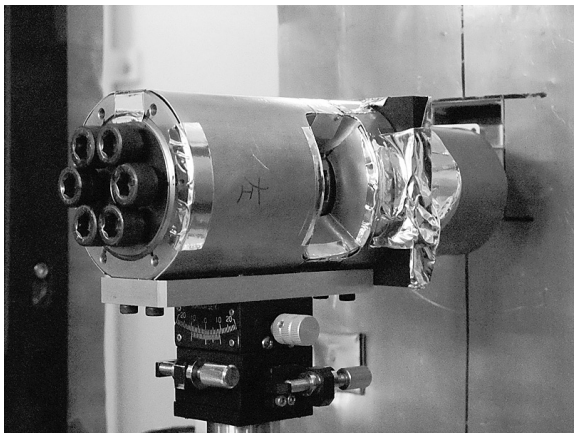

Figure 2. Opposed anvil cell set on TAKUMI.

4. Installation of Paris-Edinburgh Cell and the Development of New Anvil Design

The Paris-Edinburgh cell has been mainly developed in ISIS [3] and is now widely used not only in neutron facilities but also in synchrotron facilities. We first aimed to establish a conventional neutron diffraction technique using PE-cell, and then tried to develop it. A V4-type Paris-Edinburgh cell was installed in the TAKUMI. After many efforts to reduce the background and generate pressure stably, we obtained the neutron diffraction data sufficient for Rietveld analysis up to about 20 GPa (see TOPIC in this report). Simultaneously, we developed a data correction method, which is the key to obtaining reliable structure information. The most important correction in the high-pressure experiments was the absorption correction for the anvils. By employing ray-tracing methods, we calculated the 2θ and λ dependence of absorption. The validity was cross checked by the practical absorption estimated from incoherent scattering intensity of vanadium and by the Rietveld refinement of standard sample (Al_2O_3) (Fig. 3). The obtained structural parameters confirmed the almost identical structural parameters regardless of the use of high-pressure cell. Besides these efforts, we modified the anvil design to gain detection efficiency, and succeeded in increasing the intensities in the order of 3 times compared to the conventional design.

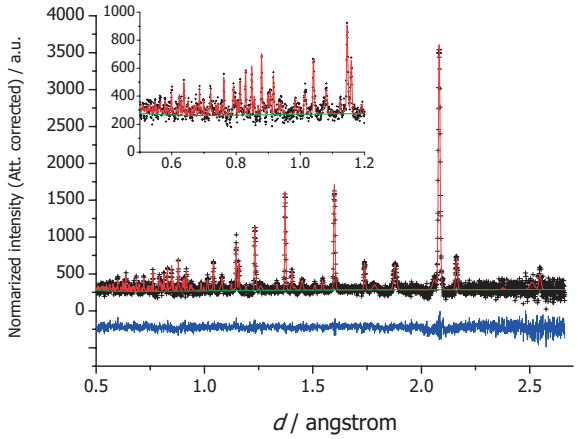

Figure 3. Result of the Rietveld refinement for Al_2O_3 in the Paris-Edinburgh cell at 1.7 GPa. The refined atomic coordinates were well consistent with the reported parameters.

5. Design of Focusing Devices and Their Performance

The higher the pressures we try to reach, the smaller the maximum sample volume becomes. To detect weak signal from the tiny sample, neutron focusing is indispensable. Therefore, we designed super-mirror guides and checked their performance [6]. The key requirements in designing are as follows: (i) to focus neutrons with the wavelength of

0.45-10 Å; (ii) to converge the neutron into the small spot with the size less than a few millimeters. (iii) to realize homogeneous phase space distribution at the sample position. To fulfill such requirements, we designed an elliptical-shaped super-mirror guide with the total length of 1.5 m. The guide consists of four walls and the inside of only the top and bottom walls are coated by multi-layered film with $3Q_c$ to avoid degeneration of Q-resolution in horizontal scattering plane for powder diffraction. Figure 4 shows spatially intensity distribution observed with/without the focusing device. The neutron intensity increases by the factor of 1.4 at the center of the peak. This value is almost identical to the result of ray-tracing simulation.

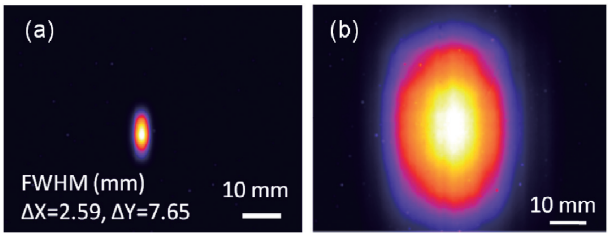

Figure 4. Spatially intensity distributions observed with (a) and without (b) the device.

References

[1] Y. Uwatoko, K. Matubayashi, T. Matsumoto, N. Aso, M. Nishi, T. Fujiwara, M. Hedo, S. Tabata, K. Takagi, M. Tado, and H. Kagi, Rev. High Press. Sci. Tech. **18** 230 (in Japanese) (2008).

[2] T. Okuchi, S. Sasaki, T. Osakabe, Y. Ohno, S. Odake and H. Kagi, J. Phys. Conf. Ser. **215** 012188 (2010).

[3] J. M. Besson, G. Weill, G. Hamel, R. J. Nelmes, J. S. Loveday, and S. Hull, Phys. Rev. B **45** 2613 (1992).

[4] T. Irifune, A. Kurio, S. Sakamoto, T. Inoue and H. Sumiya, Nature **421** 599 (2003).

[5] T. Okuchi, S. Sasaki, S. Ohono, K. Komatsu, H. Kagi, H.Arima, J. Abe, T. Hattori, A. Sano, T. Osakabe, W. Utsumi, S. Harjo, T. Ito, K. Aizawa and T. Irifune, Rev. High Press. Sci. Tech. **20** 175 (2010) (in Japanese).

[6] H. Arima, K. Komatsu, K. Ikeda, K. Hirota, H. Kagi, Nucl. Instrum. Meth. A **600** 71-74 (2009).

T. Hattori[1,2], H. Fukazawa[1], T. Okuchi[3], K. Komatsu[4], and H. Arima[2]

[1]Quantum Beam Science Directorate, JAEA; [2]Materials and Life Science Division, J-PARC Center; [3]Institute for Study of the Earth's Interior, Okayama University;[4]Geochemical Laboratory, The University of Tokyo

Automatic Sample Changer for iMATERIA

1. Introduction

IBARAKI Materials Design Diffractometer (iMATERIA) [1], which is promoted by Ibaraki Prefecture, is a versatile powder diffractometer installed at the 20th beam line (BL20) of MLF. This diffractometer has a high throughput so as to handle a large number of samples; each sample is measured in just 5 minutes at 1MW. iMATERIA has a vacuum chamber in which samples are placed, and this chamber is enclosed in an instrument shield. If a vacuum cannot be maintained in the chamber while exchanging samples, the process of re-establishing the vacuum would become a bottleneck.

Small automatic sample changers have been used in the past, e.g., the 10-sample changer used for Vega [2] and Sirius [3] at the High Energy Accelerator Research Organization (KEK). The largest, which is used for High-Pressure -Preferred Orientation (HIPPO) [4] at Los Alamos Neutron Science Center (LANSCE), can handle 100 samples simultaneously. However, these sample changers cannot add new samples or exchange stocked samples without breaking the vacuum. At minimum, we need an automatic sample changer that is capable of changing 600 samples, but without breaking the vacuum in the main chamber. Moreover we need to be able to exchange the samples during measurement. Accordingly, we developed and manufactured an automatic sample changer that can handle a large number of samples through the vacuum chamber.

2. Automatic Sample Changer

Figure 1 shows an overview of the automatic sample changer, which is organized into five parts: sample storage room, articulated robot system, elevator, pre-vacuum chamber system, and sorting system.

Both the sample storage room and the articulated robot are installed on an instrument shield. The elevator, the pre-vacuum chamber system, and the sorting system are attached to the flange with a port of approximately 800 mm diameter on the main vacuum

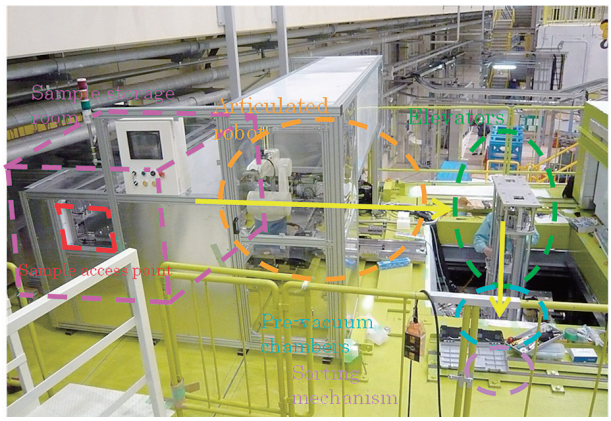

Figure 1. Overview of the automatic sample changer.

chamber, and these parts can be removed easily as a unit. The pre-vacuum chambers connect to the main vacuum chamber through gate valves. The sorting system is set on the bottom side of the flange and handles the samples in the main vacuum chamber.

There are two lines from the sample storage to the sorting mechanism (two elevators and two pre-vacuum chambers). The pressure in each line is independently controlled between atmospheric pressure and vacuum. Thus, samples can be transported to the main chamber while other samples are being measured. Moreover, new samples can be set in place in the sample storage area while one set of measurements is being made. Thus, the sample-exchange time is substantially reduced.

We also developed a new sample holder for this automatic sample changer. This sample holder is made of vanadium (0.1 mm thick) and has a collar. The samples are packed into this sample holder, which has an Al cap and an In seal. A radio frequency identification (RFID) tag is placed on the top of the holder cap (made of poly oxy methylene) with two collars for handling as shown in Fig. 2. Each sample is controlled using RFID.

To allow the addition of new samples, or replacement of stocked samples, during measurement, the sample storage room is located outside the instrument shield. In the sample storage room, there is a

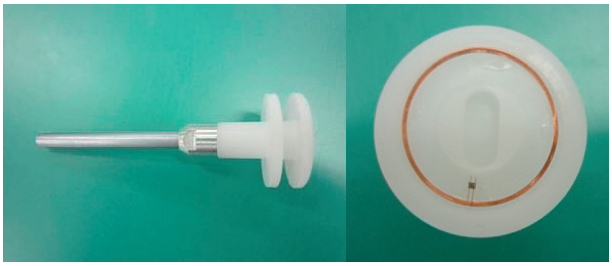

Figure 2. Sample holder with RFID.

shelf for samples. The shelf rotates, and the front side of the shelf presented is automatically changed according to the need. The sample storage system can position 168 trays, each storing 4 samples. Thus, a maximum of 672 samples can be stored in this room.

A sample access point is located to the side of the sample storage room on the instrument shield as shown in Fig. 1. We can position only one tray (4 samples) in this access point at a time. Information on the samples (name, weight, height, ID number, position in the tray, etc.) is held in a sample database, and RFID is used to identify the samples. After checking the RFID information, the tray is put in the sample storage room by the articulated robot. Sample handling uses the tray (4 samples) as a unit. When we want to retrieve a sample after measurement, the articulated robot picks up the tray containing the required sample.

According to a user-defined schedule, the articulated robot picks up a tray from the sample storage room and places it on the sample stage for transport to the elevator. The sample stage moves horizontally to the elevator. The elevator picks up sample holders from the tray, and carries these sample holders vertically to the pre-vacuum chamber. The empty tray then returns to the sample storage room.

The pre-vacuum chamber has a volume of approximately 50 L. A half-round opening provides a pathway for the samples, with a gear-like stock holder at the bottom. This stock holder can store 12 samples. Accordingly, the articulated robot and the elevator transport 3 trays (or a total of 12 samples) to the pre-vacuum chamber.

The vacuum in the main vacuum chamber is maintained. However, the pressure in the pre-vacuum chamber is controlled between atmospheric pressure and vacuum. In addition, the top side of the pre-vacuum chamber is at atmospheric pressure, while the bottom side is at a vacuum. Two gate valves are positioned above and below the pre-vacuum chamber. In addition, there are two pre-vacuum chambers in this system, and there is a stock holder for 12 samples in each pre-vacuum chamber. We can control the pressure for up to 12 samples during the measurement process. Thus, no time needs to be spent reestablishing a vacuum, except when first evacuating the chamber. After evacuating the chamber, the underside gate valve opens, and the gear-like stock holder moves from the pre-vacuum chamber into the main vacuum chamber.

The sorting system is situated within the main vacuum chamber. A sample is picked from the gear-like stock holder (containing 12 samples) and is moved to the neutron beam center. Two collars are needed on the sample holder at this point: one for holding, and the other for handling. The sample height can be changed for each sample. Optionally, the sample can be rotated during measurement.

We manufactured an automatic sample changer with the capacity to handle more samples than any previous design. We have already installed this automatic sample changer, and it has passed an operational check. We developed control software for automatic measurement in order to work with a data acquisition system (DAQ). The control software has been operating since October, 2010.

We would like to thank for awarding us the 1st Michael Meissner Prize (6th International Workshop on Sample Environment at Neutron Scattering Facilities, 2010).

References

[1] T. Ishigaki *et. al.*, Nucl. Instr. Meth. Phys. Res. A, **600** 189-191 (2009).

[2] T. Kamiyama *et. al.*, Physica, B**213**&**214** 875-877 (1995).

[3] T. Kamiyama *et. al.*, Mat. Sci. Forum, **321-324** 302-307 (2000).

[4] H. –R. Wenk, L. Lutterotti, S. Vogel, Nucl. Instr. & Meth. Phys. Res., A**515** 575-588 (2003).

A. Hoshikawa[1], T. Ishigaki[1], M. Yonemura[2], K. Iwase[1], D. Sulistyanintyas[1], T. Kamiyama[2], and M. Hayashi[3]

[1]iFRC, Ibaraki University; [2]Neutron Science Laboratory, KEK; [3]Ibaraki Prefecture

Two-Dimensional Gas-Based Neutron Detector

We are currently developing a gas-based two-dimensional position-sensitive neutron detection system that can read out individual signal lines and ncludes a micro-pixel detector element.

The performances of gas-based two-dimensional neutron the detector, such as spatial resolution and detection efficiency, are improved by increasing the gas pressure. However, it is too much trouble to operate the system properly, because the output signal level decreases under the gas pressure. To measure and process the extreme low level signals, we use a detector system consisting of developed signal processing devices, amplifier-shaper-discriminator (ASD) boards, an optical signal transmission device and a position encoder.

Fig. 1 shows a photograph of the developed detector system. The neutrons generate charge signals, which are collected by the detector element in the pressure vessel. The extreme low level charge signals from the detector element are fed into the developed ASD boards through the pressure vessel. The time response of the analog charge outpour of the boards is less than 180 ns FWHM.

The time response of the signals output from the developed position encoder is shown in Fig. 2. Our system can separate the double pulse at intervals of a microsecond.

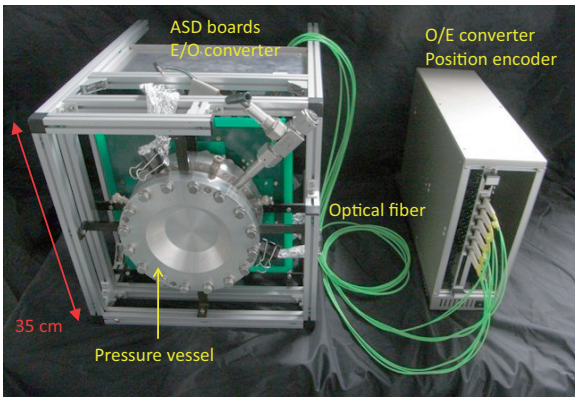

Figure 1. Photograph of the developed two-dimensional neutron detection system.

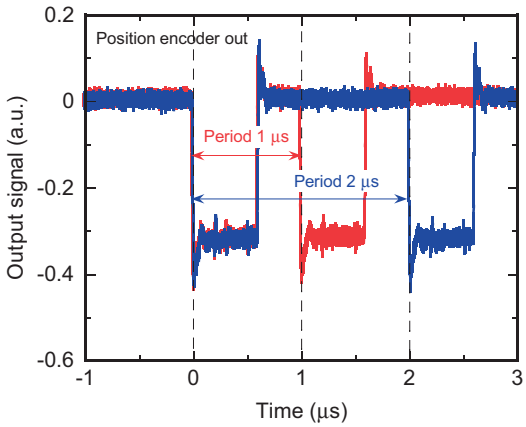

Figure 2. Output signals from the position detection encoder.

These developed signal processing devices such as ASD boards, optical signal transmission device and position encoder will be implemented in a two-dimensional multiwire proportional counter of BL17.

Development of a High Performance Polarizing Supermirror

The neutron polarizing supermirror is one of the most important optical devices for polarizing neutron beams because it allows us to obtain high and uniform polarization over a wide range of wavelengths without loss of intensity. Fe is frequently used to make the magnetic layer of a polarizing supermirror, because it is easily deposited and is a ferromagnetic material with large saturation magnetization. Si or Ge is generally used for the non-magnetic layer because the neutron scattering densities of Si and Ge are close to that of Fe for spin-down neutrons. Good magnetic properties in terms of softness play a critical role in determining the performance of the polarizing supermirrors for practical applications in a variety of polarized neutron scattering researches.

We have developed polarizing supermirrors by using the ion beam sputtering (IBS) technique since it enables the production of layers with high density and small grain size. Hino et al. demonstrated that these characteristics of the IBS lead to higher performance polarizing supermirrors [1]. Test fabrication of Fe/Ge

polarizing supermirror with m=3.3 was performed by using the IBS system installed at the JAEA. Figure 3 shows the result of the polarized neutron reflectivity measurement for the polarizing supermirror under an external field strength of 500 Oe. A flipping ratio higher than 30 is obtained over the wide momentum transfer range of 0.29-0.75 nm^{-1}. We plan to perform further developments on the realization of larger critical angle and higher polarization.

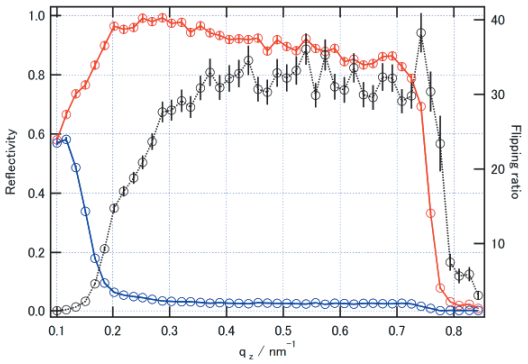

Figure 3. Polarized neutron reflectivity profiles of Fe/Ge polarizing supermirror with m=3.3. The reflectivity profiles of the spin-up and spin-down neutrons are shown in red and blue, respectively. The flipping ratio is shown in black.

Demonstration of Magnetic Domain Imaging with Neutron Spin Interferometer

Understanding the structure of the inner magnetic domain of a bulk body is one of the most important requirements for development of high performance motors and electrical transformers. However, there are no effective methods to obtain information on its inner magnetic domain. A neutron spin phase contrast (NSPC) imaging technique is one of the novel imaging techniques and it uses polarized neutrons. A precession angle of neutron spin caused by magnetic interaction with a magnetic field is given by $\varphi = m\gamma\lambda Bl/h$, where m, γ, λ are the neutron mass, gyromagnetic ratio and wavelength, h is the Plank's constant, l is the length of the flight path in which the neutron spin senses the magnetic field B. In the NSPC method, the φ can be detected as a phase of an interference pattern. Hence the variance of the precession angle due to distributions of magnetic field and flight path can be measured as the shift of the phase. The NSPC imaging technique has been developed and demonstrated [2]. In this study, we tried to visualize a magnetic domain structure of a magnetic thin foil which is applied to electrical transformers.

The experiment was carried out on SUIREN at JRR-3. The picture of the sample and a two-dimensional (2D) map of the phase shift are shown in Fig. 4. An external magnetic field 0.75 mT was applied at the vertical direction of the sample. A positive value of the phase shift means an existing of the parallel element to the external magnetic field in the sample ($B_{//}$). Since an absorption term is not included in the phase and the thickness distribution is within a few micrometers which correspond to the order of the phase shift 0.01, the stripes on the 2D map with the phase shift from 0.40 to 0.60 are expected to show the $B_{//}$ element of magnetic domain structure in the sample.

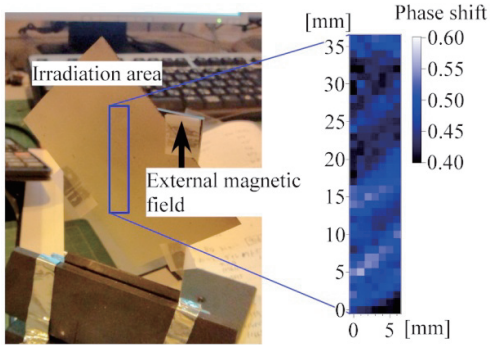

Figure 4. The photograph of the sample setup and the 2D map of the phase shift of the neutron spin.

References

[1] M. Hino, H. Hayashida, M. Kitaguchi, Y. Kawabata, M. Takeda, R. Maruyama, T. Ebisawa, N. Torikai, T. Kume, and S. Tasaki, Physica B **385-386** 1187 (2006).

[2] H. Hayashida, *et al.*, Nucl. Instr. and Meth. A **634** S90 (2011).

K. Soyama[1], K. Sakasai[1], D. Yamazaki[1], T. Nakamura[1], K. Toh[1], R. Maruyama[1], H. Hayashida[1], H. Yamagishi[1], M. Takeda[2], and T. Shinohara[1]

[1]*Materials and Life Science Division, J-PARC Center,* [2]*Quantum Beam Science Directorate, JAEA*

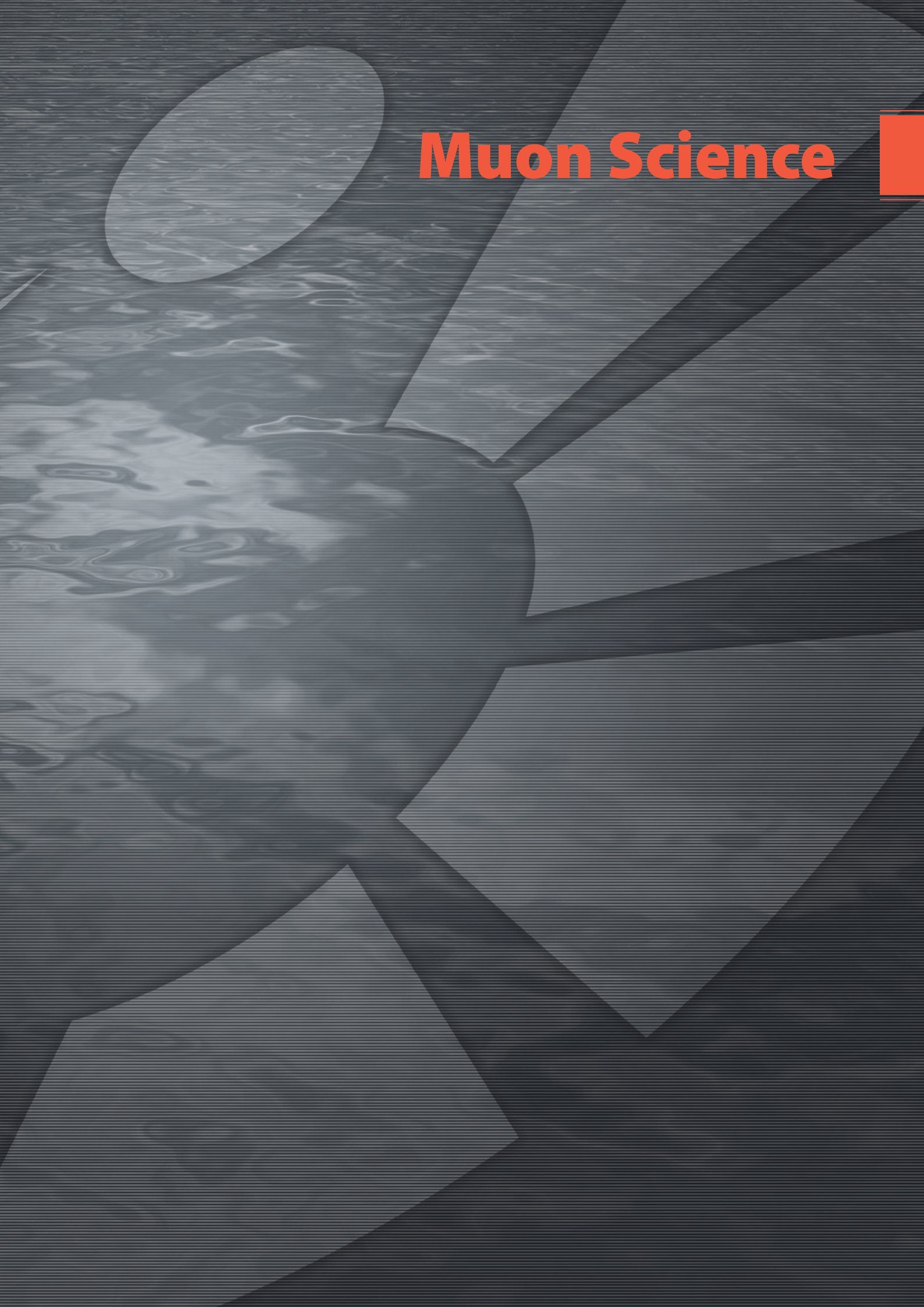

Muon Science

Status of Muon Section

Muon Science Establishment (MUSE) suffered several damages from the earthquake on March 11, 2011, so called "Higashi-Nippon Dai-Shinsai" (East-Japan earth quake). Fortunately the damages found so far were apparently not too serious. They will be fixed within half a year, we expect to restart the user's run in February 2012.

For phase 1, we designed MUSE to provide four secondary beamlines, namely D, U, S and H lines, to extract muon beams from the muon target into the experimental halls [1]. Figure 1 shows the layout of the MUSE muon beamlines that are already completed or under construction.

1. Decay and Surface Muon Beamline, D-Line at MUSE

So far, we succeeded in installing one superconducting decay/surface muon beam line, the so called D-Line, with a modest-acceptance pion injector of about 45 mSr, where either surface muons (μ^+, 30 MeV/c) or decay muons (5–120 MeV/c) are delivered to the area of the experiment [1]. In the fiscal year of 2010 (JFY 2010), we did a modification of the Quadrupole magnets, DQ4 and DQ7, by replacing the smaller aperture (ϕ200 mm) with a larger (ϕ300 mm) one. Since November 26th, 2010, the proton beam power from the RCS has steadily increased up to 220 kW, consequently delivering 3.2 $\times$ 10^6/s of intense surface muon or several 10^6/s of decay muon beam (μ^+ and μ^-). MUSE had been recording the world's strongest pulsed muon source, with increasing the proton beam power, until the earthquake on March 11th, 2011.

One of the scientific topics was an application of μ^- for the non-destructive analysis [2]. At MUSE, a high intensity μ^- beam with an energy as low as 5 MeV/c (corresponding to 2 μm penetrating depth in Au) and up to 120 MeV/c can be used for the experiment, since the μ^- obtained at MUSE originates from a 3 GeV proton having a larger π^- cross section than with 500-800 MeV energy range. The different elements present in a sample of only tiny amount can be quantitatively measured by observing the characteristic X-rays from muonic atoms. Its feasibility has been already studied at the D2 experimented area for the non-destructive analysis studies of the Au and Ag concentration in an old Japanese coin, Tempo-Koban (property of Prof. T. Saito, National Museum of Japanese History) revealing difference in the Au concentration between the surface (~2 μm) and in the bulk.

One of the topics of μ^+SR studies is a research on the layered iridate Ba_2IrO_4 by H. Okabe [3]. They revealed that the magnetic ground state is antiferromagnetic long-range ordered state (T_N~240K) in which the magnetic moment (~0.34μ_B /Ir atom) is significantly reduced by a low-dimensional quantum spin fluctuation with a large intra-plane correlation. It was selected by Editor's suggestion of Physical Review B.

2. U-Line for the Ultra Slow Muon Beam

In addition to Phase 1, as one of the principal muon beamlines at MUSE, we are planning to install the Superomega muon beamline, the so called U-line, which consists of a large acceptance solenoid made of mineral insulation cables (MIC), a superconducting curved transport solenoid and a superconducting axial focusing magnet system. There, we can collect either surface or cloud muons with a large acceptance of 400 mSr. Compared to the conventional beamlines, the large acceptance of the front-end solenoid will allow for the capture of the highest intensity pulsed muon beam in the world. With a muon capture rate of 5 $\times$ 10^8 /s surface muons and an approximate transport efficiency of 80%, we can expect 4 $\times$ 10^8 /s surface muons and 10^7 /s negative cloud muons at the experimental area [4]. The U-line components of the superconducting curved and axial focusing magnets were funded and are now under construction. At the U-line, we are aiming to create a new type of muon

source: the intense ultra-slow muon source.

Ultra-slow pulsed muons are generated by the resonant ionization of thermal Muonium atoms evaporated from the surface of a hot tungsten foil placed at an intense surface muon beamline, which was developed at KEK and RIKEN/RAL. At the RIKEN/RAL muon facility, 20 ultra-slow μ^+/s was extracted at the sample position out of 1.2×10^6/s surface muons [5]. On the other hand, 4×10^8 /s surface muons/s can be extracted at the U-line, gaining a factor of 300 in the surface muon intensity. Taking into account the repetition rate of the pulsed laser system and the muon beam, we can also gain a factor of two, since both the laser and the muon beam can be synchronized to 25 Hz at MUSE, whereas the muon beam (50Hz) is synchronized to every second laser pulse at the RIKEN-RAL facility [5]. Moreover, we have also been developing an intense Lyman-α light of more than 100 μJ/cm^2 needed to saturate the transition of Mu from the 1S state to the 2P state, whereas only about 1 μJ/cm^2 of the Lyman-αlight was produced at RIKEN/RAL. Consequently, we can expect, as a maximum, 1.3×10^6 /s of the ultra-slow μ^+/s at MUSE.

3. S-Line Beam

In addition to the U-line, we are planning to install a dedicated surface muon beamline, so called S-line, with a modest-acceptance of about 50 mSr. A kicker system, matched to the pulse structure of the proton beam, will be installed to feed single pulses to four specific experimental areas in hall No1 with a rate of 10^7/s. At present, the beamline components SQ1-6 and SB1 in the tunnel are already installed or under fabrication.

4. H-Line Beam

A high momentum muon beamline, so called H-line, with an acceptance of about 130 mSr, is also planned to be installed towards the experimental hall No. 1. The H-line is designed to extract either intense surface muons (10^8 /s), or electrons up to 120 MeV/c, for large size particle nuclear physics programs, such as the "g-2" or "μ^-e conversion" experiments, etc. The beamline components in the proton beam tunnel are already funded and under fabrication.

5. Damages by the Earthquake, 'Higashi-Nippon Dai-Shinsai' and Beam Recovery's Schedule

As we mentioned in the beginning, as a result of the earthquake on March 11, 2011, some of the MUSE components became inoperable. After observing the affected areas, we concluded that the problems were not severe. We believe they can be fixed within half a year. The damaged components of MUSE were as follows: 1) All the He ducts, control cables, power cables, and compressed air for the online refrigerator system for the superconducting magnet. This was caused by ground settlements, about 10 cm to 1.5 m downward outside of the MLF building. Also a buffer tank for the He

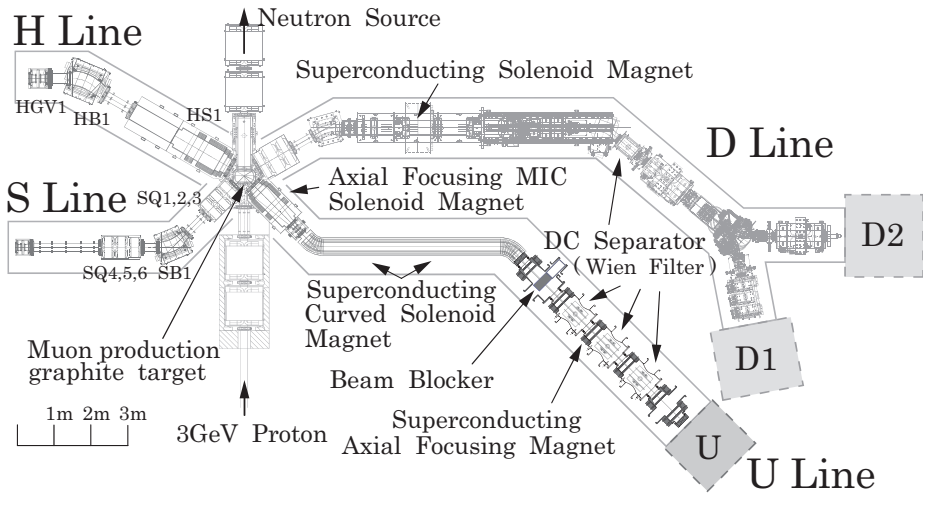

Figure 1. Layout of the MUSE muon beamlines already completed or under construction.

gas was tilted by 2-3 degrees. 2) The air circulation systems for the proton beam tunnels in the vicinity of the muon target were damaged. Particularly, we need to remove and rebuild water pipes and control cables since the wall where they have been fixed was about to fall down. That wall is located at an expansion joint between MLF and the proton beam transport line (3NBT) from 3-GeV RCS. 3) A lot of anchoring bolts of concrete shielding blocks with cracks on them due to strong quakes. 4) An air sealing hatch to prevent flow of activated air between the primary proton beam tunnel (the M2 tunnel) and the MLF experimental hall. 5) A cable rack in the M2 tunnel due to a blow caused by a heavy concrete block.

References

[1] Y. Miyake, K. Nishiyama, N. Kawamura, P. Strasser, S. Makimura, A. Koda, K. Shimomura, H. Fujimori, K. Nakahara, R. Kadono, M. Kato, S. Takeshita, W. Higemoto, K. Ishida, T. Matsuzaki, Y. Matsuda, K. Nagamine, "Muon Beams at the J-PARC Muon Facility and their application", Nucl. Instr. and Meth. in Phys. Res. A 600 (2009) 22-24; P. Strasser, K. Shimomura, A. Koda, N. Kawamura, H. Fujimori, S. Makimura, Y. Kobayashi, K. Nakahara, M. Kato, S. Takeshita, M. Hiraishi, M. Miyazaki, W. Higemoto, T. U. Ito, K. Ninomiya, K. Ishida, M. K. Kubo, R. Kadono, K. Nishiyama and Y. Miyake, "J-PARC decay muon channel construction status", J. Phys.: Conf. Ser. **225** 012050 (2010).

[2] K. Ninomiya, T. Nagatomo, K. M. Kubo, P. Strasser, N. Kawamura, K. Shimomura, Y. Miyake, T. Saito and W. Higemoto, "Development of elemental analysis by muonic X-ray measurement in J-PARC", J. Phys.: Conf. Ser. **225** 012040 (2010).

[3] H. Okabe, M. Isobe, E. Takayama-Muromachi, A. Koda, S. Takeshita, M. Hiraishi, M. Miyazaki, R. Kadono, Y. Miyake, and J. Akimitsu "Ba2IrO4: A spin-orbit Mott insulating quasi-two-dimensional antiferromagnet", Phy.Rev. B **83**, 155118 (2011).

[4] K. Nakahara, T. Adachi, Y. Ikedo, Y. Miyake, K. Shimomura, P. Strasser, K. Nishiyama, N. Kawamura, H. Fujimori, S. Makimura, A. Koda, K. Nagamine, T. Ogitsu, A. Yamamoto, K. Sasaki, K. Tanaka, N. Kimura, Y. Makida, Y. Ajima, K. Ishida, Y. Matsuda, "The Next Generation Muon Source at J-PARC/MLF", AIP Conf. Proc. **1222** 420-424 (2010).

[5] P. Bakule, Y. Matsuda, Y. Miyake, K. Nagamine, M. Iwasaki, Y. Ikedo, K. Shimomura, P. Strasser, S. Makimura, "Pulsed source of ultra low energy positive muons for near-surface μSR studies", Nucl. Instr. and Meth. in Phys. Res. B **266** 335-346 (2008).

Y. Miyake[1,2], K. Shimomura[1,2], N. Kawamura[1,2], P. Strasser[1,2], A. Koda[1,2], H. Fujimori[1,2], S. Makimura[1,2], M. Kato[1,2], K. Nishiyama[1,2], Y. Ikedo[1,2], K.M. Kojima[1,2], R. Kadono[1,2], W. Higemoto[3], T.U. Ito[3], and K. Ninomiya[3]

[1]Muon Science Laboratory, High Energy Accelerator Research Organization (KEK); [2]Muon Science Section, Materials and Life Science Division, J-PARC center; [3]Advanced Science Research Center, Japan Atomic Energy Agency (JAEA)

Fabrication of the To-Be-Installed Rotating Target for Muon Production

At J-PARC/MUSE, the fixed edge-cooling method has been adopted for cooling the muon target. However, it is predicted that the graphite will break down in six months due to radiation damage [1]. To extend the lifetime of the muon target, we are planning to adopt the rotating target method, which can distribute the radiation damage of graphite to a wider area. In the present schedule, a new rotating target will be installed in the beamline in the summer of 2013. The muon target will be so highly irradiated that the maintenance must be performed from the maintenance area located 2.4 m above the beamline level. In addition, a 2-m high plug shield is necessary between the primary proton beam and the maintenance area for radiation shielding. Because of the high radiation, the boundary of the vacuum, the motion drive, the rotation system, and so on, must be positioned at the maintenance area. So far the rotating target itself and a heating and rotating system were fabricated, and endurance tests of the bearings have been performed [2]. In the summer of 2011, the actual rotating target will be fabricated and delivered.

In the actual rotating target, the rotation generated by the servo-motor, which is located at the maintenance area, is transmitted to a bevel gear by a 2.7-m long shaft penetrating a stainless steel rod, called the target rod. The shaft must include an additional shield to prevent radiation from reaching out through the gap between the shaft and the target rod. Since the shaft is supported by bearings, the axial load due to the weight of the additional shield must also be held by the bearings. Considering the high radiation environment, an inorganic solid lubricant is utilized for the bearings. In general, an angular contact ball bearing is used with an axial load. However, since an angular contact ball bearing with lubricant is not commercially available, a deep groove ball bearing with lubricant must be applied to the rotating target. Because the lifetime of the bearing is predicted to be short, the bearing must be easily replaceable from the maintenance area without transporting the whole target assembly to the hot cell [3]. Also, the long shaft is composed of several short shafts because it is too long for manufacturing. The shaft weight is only supported by the upper bearings and the lower bearings supports only the shaft for radial constraints. The rotation of the motor at the maintenance area is transmitted to each shaft by couplings that have keys to avoid slipping in the rotating direction. Simultaneously, only one end of each coupling is rigidly connected to the shaft to absorb the thermal expansion between the shaft and the target rod. Figure 1 shows the actual rotating target under fabrication. It will be delivered in September of 2011.

Figure 1. The actual rotating target under fabrication at the factory.

References

[1] S. Makimura *et al.*, Proceedings of the 2nd Annual Meeting of Particle Accelerator Society of Japan and the 30th Linear Accelerator Meeting in Japan, July 20-22, 2005, Tosu Japan, p173-175.

[2] S. Makimura *et al.*, MLF Annual Report 2009, p103

[3] S. Makimura *et al.*, Proceedings of the 7th Annual Meeting of Particle Accelerator Society of Japan, Aug. 4-6, 2010, Himeji, Japan, p479-483.

S. Makimura, Y. Kobayashi, N. Kawamura, Y. Miyake, P. Strasser, A. Koda, H. Fujimori, K. Shimomura, K. M. Kojima, and R. Kadono

Muon Section, MLF Division, J-PARC Center

Control System for the Rotating Target for Muon Production

At J-PARC/MUSE, the most intense pulsed muon beam has continuously been produced with a proton beam of 120 kW since the run cycle in November of 2009. At present, the fixed edge-cooling method has been adopted for cooling the muon target. However, it is predicted that the graphite will break down in six months due to radiation damage if the proton beam power reaches 1 MW [1]. Because of the high radiation, the boundary of the vacuum, the motion drive, the rotation system, the feedthroughs for the signal cables, the thermo-couples, the water pipes, and so on, must be positioned at the maintenance area. In addition, three positions must be obtained on the muon target location: (1) the muon target position for in-beam operation, (2) the profile monitor position for monitoring the beam profile, and (3) the clear position with no components in the proton beam path. Hence, a target rod consisting of a stainless rod, a muon target and a profile monitor can be precisely moved along an up-down linear motion guide. The signal cables, the thermo-couples, the shaft for a rotation and the water pipes go through the target rod.

To communicate with the entire MLF control system, the rotating target will be controlled through a common PLC (Programmable logic controller) system. Preparing for beam operations under high radiation, newly upgraded servo-motor systems, which are developed by Wako-Giken Co. Ltd. and composed of radiation-resistant materials, are introduced for both the up-down motion and the rotation. In June of 2011, we fabricated the prototype of the PLC control system, which included just a controller for the rotation and the up-down motion. The servo-motor system has a resolver encoder to detect not an absolute position but a relative position, and requires a zero-position determination system. The up-down motion system is located at the maintenance area. If the zero-position is determined through a limit switch at the maintenance area far away from the beam level, a precise positioning of the muon target cannot be guaranteed because of the length variation of the target rod due to temperature fluctuation and distortion from the vacuum load. To achieve a precise position, the zero-position should be physically determined by a mechanical stopping position on the linear motion guide fixed on the plug shield, which is in the vacuum chamber only 1 m away from the beam position. To avoid the servo-motor giving a torque to the target rod directly, the motor stops operating just before the mechanical stopping position decided through a limit switch. In order to determine the zero position, we temporally suppress the servo motor and the brake; the slide mechanism moves slowly due to the pressure difference between the vacuum vessel and the atmospheric pressure so that it hits the limit switch. Figure 1 shows a picture of the control system and the servo-motors.

A logging system to monitor the motor current, thermo-couples, and MPS (Machine Protection System) will be completed before the installation.

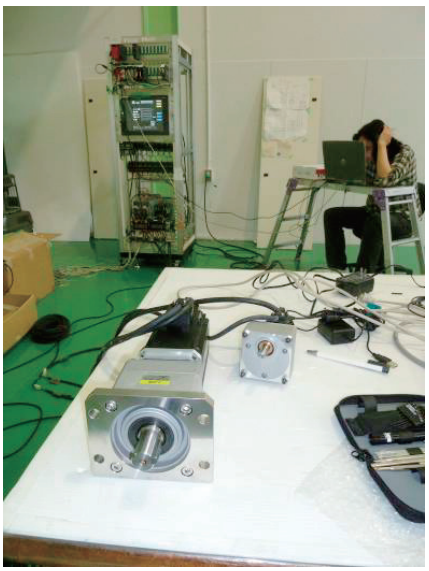

Figure 1. A picture of the control system and the servo-motors.

Reference

[1] 1) S. Makimura *et al.*, Proceeding of the 2nd Annual Meeting of Particle Accelerator Society of Japan and the 30th Linear Accelerator Meeting in Japan, July 20-22, 2005, Tosu Japan, p173-175.

Y. Kobayashi, S. Makimura, and Y. Miyake
Muon Section, High Energy Accelerator Research Organization

Status of Superconducting Solenoid and On-Line Refrigeration System for the Decay/Surface Muon Channel

A conventional superconducting muon channel which can extract surface (positive) muons and decay positive/negative muons up to 120 MeV/c, is success-fully operating at the MLF experimental hall II. The superconducting solenoid magnet of 6 m of length consists of twelve units of 0.5 m coil. The magnet coil is forced-indirectly cooled by a supercritical helium gas (4.8 K at 0.80 MPaG) supplied from the on-line helium refrigeration system. The maximum magnetic field was designed to be up to 5 T (current 730 A) at the operational temperature 6 K. The present magnetic field for normal operation for surface/decay muon extraction is 0.308 T (45 A)/2.33 T (340 A), respectively.

For the long-term stable operation, an on-line helium refrigeration system is employed. The cooling power of the on-line helium refrigeration system is 35 W at 4.5 K and 200 W at 80 K, and it can also produce 8 l/h of liquid helium. The whole system is monitored and controlled by a VME controller combined with a personal computer with dedicated software based on LabVIEW System, and cools down automatically. The typical cooling period from room temperature to operation temperature (~5 K) is about 3 days. The long-term (typically 1 month) operation is now established under quite stable condition.

To prevent any serious damage to the su-perconducting solenoid and the helium refrigeration system, a VME based interlock system is installed. The system can detect any anomaly in the voltage and temperature of the solenoid and the power lead. The trip signals from the helium refrigeration system and the electric power supply are also included. Once any emergency status is detected, the electric power supply immediately stops, then the current supply and the refrigeration system changes to self-operation mode. By adding these interlock systems, this part can also automatically record the temperatures and pressures of the superconducting coils, the helium refrigeration system and the power leads. All rec-orded data are also monitored and stored at the MLF control room by using MELSECNET.

However, these systems were rather old and not fit for remote monitoring via internet. Also, our old control system could not change any parameter during the operation. To improve these points, in JFY 2009, we constructed a new remote monitoring system based on DeMPICS for VME control software and HITS for operating and monitoring DeMPICS, which was basically developed for cryogenic systems of neutrino beamline. All recorded data are also stored at the Neutrino superconducting magnet control room at this time and can be seen by PC in J-LAN. During almost one year of operation, the new system works well.

In JFY 2010, the solenoid and on-line refrigeration system has operated smoothly for more than 5000 hrs, until the gigantic earthquake on March 11th 2011. At that time, the system was just operating, however, it stopped in a safely manner and there was no He gas release. The damage due to the ground sinkage is rather serious, especially the He piping from outside compressor building, which was warped as shown in Fig.1. Therefore we must repair the three He high-pressure pipes, the low pressure from the compressor and the buffer pass. The other components like solenoid, cold box and transfer tubes fortunately were not damaged. Also all the cabling and interlock system seems to be O.K. in a room temperature condition. We will check the leakage and the pressure resistance for all compo-nents. The estimated recovery time is the end of No-vember 2011.

Figure 1. The broken He piping for the refrigerator, which is located just outside of the MLF building.

K. Shimomura, Y. Nemoto, Y. Kobayashi, A. Koda, K. Nishiyama, and Y. Miyake
Muon Science Laboratory , High Energy Accelerator Research Organization (KEK), Tsukuba
[1]*Advanced Science Research Center, Japan Atomic Energy Agency, Tokai*

DC-separator Performance at D-line

In August of JFY 2010 a pair of new high voltage power supplies (Matsusada Precision Inc. +250 kV and -250 kV) were installed for DC separator at D-line which had been operated by ±100 kV power supply. A better suppression of positron background was expected by higher applied electric field and corresponding magnetic field. The same DC- separator was used with minor changes at high voltage electrode terminal and separator stand to enlarge the space to the ground. Also special care was taken for the cable termination at the electrode terminal. At the end of the cable, the isolation was strengthened by corn shape elastomer molded around the cable (Fig1).

Because of the narrowness of D1-tunnel with 1200mm width and 3000mm height, the distance from the electrode terminal to the surrounding object on the earth potential is only 35cm (downward) and 46cm (upward). Even after several days conditioning, discharging with thunder clap was observed frequently at applied voltage over 220 kV, it occurs seldom at 200 kV. For the usual users operation the high voltage was set to 185 kV to achieve very stable performance.

The thunder phenomena were caused mainly by the discharging from positive terminal to the air. Also in the chamber discharge between two electrodes and from electrode to the chamber was observed without large clap noise. During the performance test and even usual beam time, thunder-like discharge caused several incidents of the magnetic power supplies, such as DQ7, DB2, and superconducting solenoid. In some cases the cooling system for the superconducting solenoid was affected and recovering time costed beam time of several hours to a few days. To avoid these mal-functions, noise cutter such as capacitor and ferrite core are added to the control circuit of magnet power supplies.

To hinder the continuous discharge, the high voltage is shut down automatically if the current exceeds the preset limits. Alarm system with red rotating lamp was installed in the cabin to warn experimenters in case of high voltage shut down. Recovery of high voltage can be done manually resetting the power supply on local mode after stopping the correction coil current.

Another problem is the unstable behavior (discharge in the vacuum under magnetic field) at lower voltage (< 45 kV) for lower muon momentum setting less than 10 MeV/c. This phenomenon was found during the muonic X-ray measurement with very low momentum negative muon and will be studied more precisely during the beam shut down period.

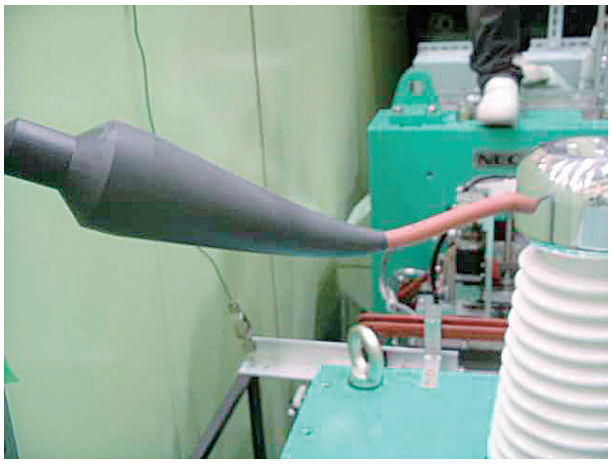

Figure 1. The cable terminal of DC-separator.

K. Nishiyama, Y. Kobayashi, H. Fujimori, P. Strasser, A. Koda, N. Kawamura, K. Shimomura, K. M. Kojima, and Y. Miyake.
High Energy Accelerator Research Organization; [2]University of Tokyo

Muon Kicker System for the Decay Beam Line at J-PARC

1. Introduction

The double pulse proton beam from the J-PARC 3 GeV Rapid Cycling Synchrotron (RCS) hits the muon production target in the Materials and Life Science Facility (MLF), and produces muon pulses. The muon pulses are then transported through the decay muon line to the experimental areas (D1 and D2). A kicker system is used to separate the muon pulses and feed them to each experimental area simultaneously as shown in Figure 1. Fine tuning of the pulse shape to meet the requirements on the rise time and uniformity at the flat top is in progress.

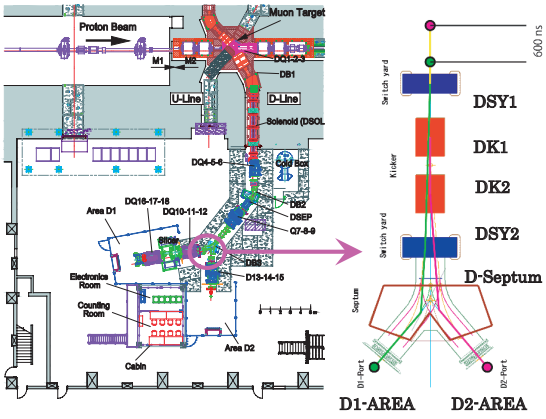

Figure 1. The decay muon line and the muon kicker system.

2. Fine Tuning of the Pulse Shape

The outline of the main circuit is shown in Figure 2. Although both the cable returns (Return) and the housing of the power supply (Housing) are at the same DC potential, they could have a potential difference at high-frequency. In other words, each wiring connecting between them has an inductance at high-frequency region of a few hundred MHz.

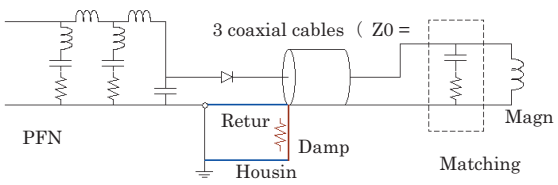

Figure 2. Outline of the kicker main circuit.

In the case the cable return is insulated from or shorted with the housing, the pulse shapes are shown in Figure 3. The former has a structure at the flat top and the latter is slower in rise-time. When a damper (5 Ω) was inserted in between the return and the housing, the pulse shape was improved (see Figure 4). Now the rise time of the peak current from 5% to 95% is about 500 ns and the uniformity at the flat top is less than ±4% for 400ns. Further fine tuning of the pulse shape is needed in order to meet the design requirements of a rise time of less than 300 ns and uniformity at the flat top of ±3% for 300 ns, respectively.

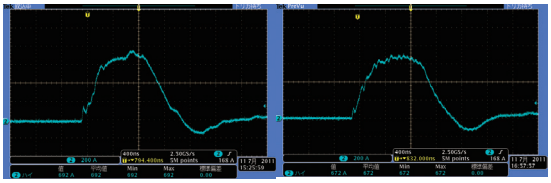

Figure 3. Insulated and shorted pulse shapes.

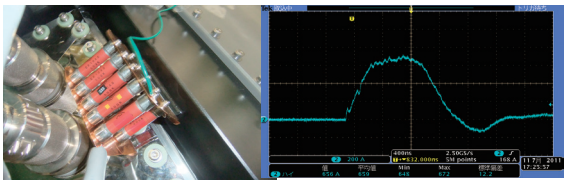

Figure 4. Damper (5 Ω) inserted pulse shape.

The rise time can be effectively shortened by decreasing the inductance load by reducing the pole piece length. In practice one of the two kicker magnets was modified as follows: some ferrite cores from which the pole piece is constructed were replaced with Teflon cores as shown in Figure 5. As a result, the inductance load was reduced from 1.5 μH to 1.1 μH as measured by a LCR detector.

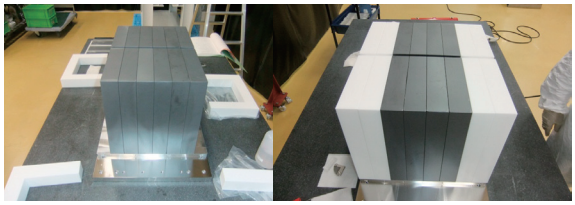

Figure 5. Modified kicker magnet pole piece.

3. Summary

Field measurements with a search-coil are in progress. The installation of the kicker system (see Figure 6) is scheduled for the summer of 2011. After the installation, fine tuning of the pulse shape will continue for the beam operation through the winter of 2011.

Figure 6. Muon Kicker System.

References

[1] H. Fujimori *et al*., KEK-MSL Report 2009, 8

[2] P. Strasser, H. Fujimori *et al*., New Muon Kicker System for the Decay Muon Beamline at J-PARC, Proceedings of the International Conference on Muon Spin Rotation, Relaxation and Resonance (μSR2011), May 16-20, 2011, Cancun, Mexico

H. Fujimori[1], P. Strasser[1], K. Koseki[2], Y. Hori[2], H. Matsumoto[2], Y. Irie[2], J. Nakamura[1], K. Nishiyama[1], and Y. Miyake[1]

[1]*Materials and Life Science Division, J-PARC Center;* [2] *Accelerator Laboratory High Energy Accelerator Research Organization*

Installation of the Dilution Refrigerator at J-PARC MUSE

For studies of material, low temperature electronic and magnetic properties it is often important to clarify an intrinsic ground state of the system. To meet the strong demands from the users for experiments below 1 K, we are installing the dilution refrigerator (DR) at D1 area, MUSE. The DR was previously used at KEK-MSL and it was able to achieve a temperature lower than 20 mK. The main feature of the DR is a "top-loading" system. For a usual dilution refrigerator, the dilution unit must be warmed up to the room temperature to change a sample. Therefore, it takes a few days to change and cool down a sample. Meanwhile, in our top loading DR (Fig. 1), a sample can be changed by unloading or loading just only the sample holder. By using this system, we can change and cool the sample down to lowest temperature within 12 hours. This feature is quite useful for a μSR experiment.

Figure 1. The top loading DR unit.

In February 2010, we transported the DR system from Tsukuba to Tokai, and started installation at J-PARC MUSE. We also constructed the special stage for the DR. Figure 2 shows the DR, mounted on the stage at D1 area.

In the beginning of the installation, we found that there was serious leakage at the plate heat exchanger part of the DR unit. In addition, several problems of the thermometers, the heaters and the vacuum sealing had been found. These problems have been already fixed. Unfortunately, the installation of the DR is partially incomplete, due to the earthquake on March 11th. Therefore, the DR will be available for user experiments in 2012.

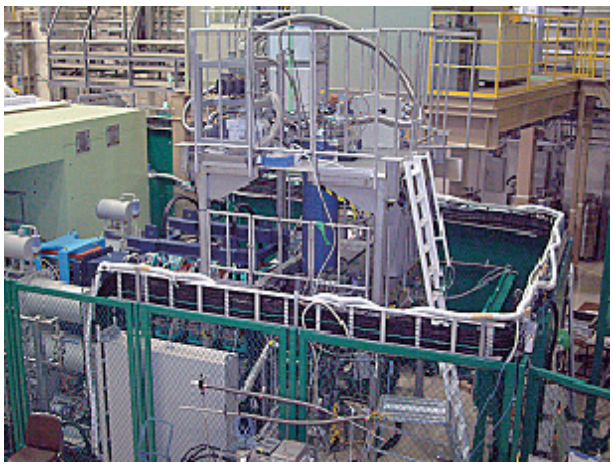

Figure 2. The DR mounted on the stage at the D1 area.

W. Higemoto, and A.Koda[1]
Advanced Science Research Center, Japan Atomic Energy Agency (JAEA)
[1]Muon Science Laboratory, High Energy Accelerator Research Organization (KEK)

Development of a Fly-Past System for the DΩ1 Spectrometer

In J-PARC MUSE, high statistic μSR data is easily obtained utilizing the world's most intense pulsed muon beam. On the other hand, the pulsed μSR has a disadvantage: a signal from the muons which missed a sample cannot be rejected since single event vetoing is not possible. The sample is typically mounted on a large silver plate and the muons stopped in the plate make a nontrivial contribution to μSR asymmetry. The fractional weight for the sample in the full asymmetry is approximately proportional to the ratio of sample cross-section to beam spot size. Thus, a relatively large amount of sample which covers the cross-section > 200 mm^2 is required for conventional pulsed μSR experiments at J-PARC MUSE.

A 'fly-past' system is an answer to overcome this problem. The idea of the fly-past system is drawn in Fig. 1. A long vacuum chamber of a large diameter is attached to the beam exit. A sample is mounted on the same or smaller sized sample holder and these are suspended at the center of the chamber. The sample holder is attached to a cryostat by a metallic plate, which is arranged so that its exposed area to the muon beam is minimized. A moderately collimated muon beam is incident to the vacuum chamber. A part of the muons hit the sample and the decay positrons are detected by coupled positron counters as coincidence events. The muons 'flying-past' the sample are trans-ported downstream in the long vacuum chamber. De-cay positrons emitted from the muons stopped far away from the spectrometer are separable using the coincidence of two counters telescope looking into the sample position. The fly-past technique has been adopted in other pulsed muon facilities (RAL) and contributed to improving the signal to noise ratio (S/N) [1].

We developed a fly-past system for the DΩ1 spec-trometer. The fly-past system was designed so that the vacuum chamber is easily attached to/detached from the beam line for general purpose use. An existing 4 K cryostat can be mounted. We have carried out commissioning experiments in the D1 area using a surface muon beam. We measured transverse field (TF) μSR spectra in a TF of 20 Oe for Ag and Ho samples with the cross sectional areas of 25, 100, and 400 mm^2. The former (Ag) has the μSR asymmetry of A_{Ag+BG}, and the latter (Ho) has the asymmetry of A_{BG} after t > 2 μs. The S/N ratio was extracted from the asymmetries as $(A_{Ag+BG}-A_{BG})/A_{Ag}$ for each sample cross-section. As shown

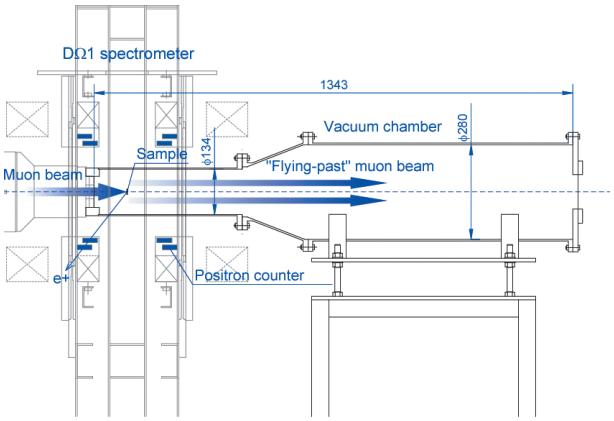

Figure 1. A schematic diagram of the fly-past system for the DΩ1 spectrometer.

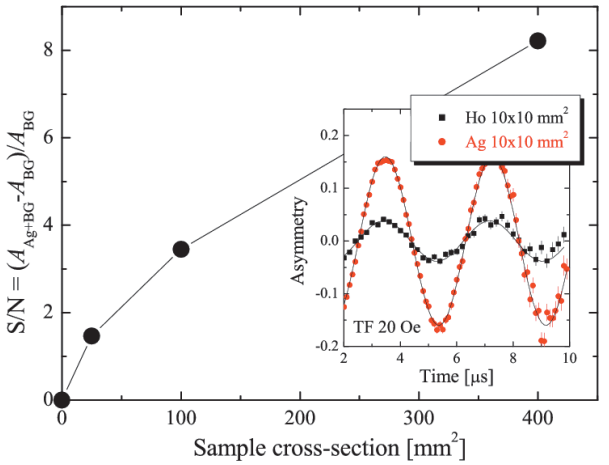

Figure 2. The S/N ratio as a function of sample cross-section. The inset shows typical TF-μSR signals for the Ho and Ag samples after t=2μs.

in the Fig. 2, the installation of the fly-past system has greatly improved the S/N ratio and μSR measurements using a tiny sample as small as 5x5 mm^2 are now possible. On the other hand, beam profile studies using a muon imaging plate indicate that a considerable amount of muons hits the inner wall of the chamber near the positron counters. For further improvement of the S/N ratio, beam pa-rameters must be optimized for the fly-past mode.

Reference

[1] M. C. Lynch *et al*., Physica B **326** 270-274 (2003).

T. U. Ito[1,2], K. Ninomiya[1,2], W. Higemoto[1,2], A. Koda[2,3], K. M. Kojima[2,3], M. Hiraishi[3,4], M. Miyazaki[3,4], and Y. Miyake[2,3]

[1]*Advanced Science Research Center, Japan Atomic Energy Agency*

[2]*Muon Science Section, MLF Division, J-PARC Center*

[3]*Muon Science Laboratory, IMSS, High Energy Accelerator Research Organization(KEK)*

[4]*Department of Materials Structure Science, The Graduate University for Advanced Studies*

Status of Superomega for the U Beamline of MUSE

The Superomega muon beamline, which is designed to deliver as many surface muons as m possible, is currently under construction at the Muon Science Establishment (MUSE) of J-PARC's Materials and Life Science Facility (MLF), . The Superomega beamline consists of normal-conducting capture solenoids, the superconducting curved transport solenoids, and a superconducting axial focusing solenoid. Currently we have a capture solenoid, which was installed in March 2009 [1]. The transport solenoid is now under fabrication by Toshiba Corp.

The conceptual design of the axial focusing solenoid was completed, and the mechanical design is underway.

As an additional functionality of the axial focusing solenoid, three-stage separators of Wien filter type are placed in the spaces between the cryostats of the axial focusing solenoid in order to eliminate the positron background efficiently. The electrodes can be applied with voltages of up to ±400 kV. All positrons are designed to be eliminated by hitting the beamline ducts and the third lower positive electrode.

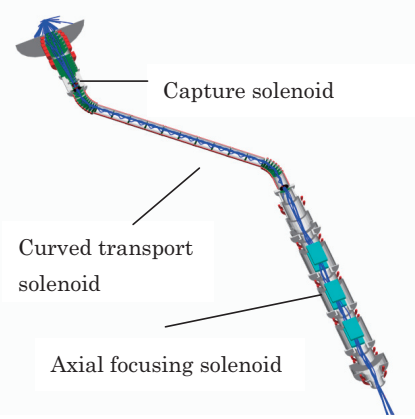

Figure 1. A design sketch and beam transport calculation of the Superomega.

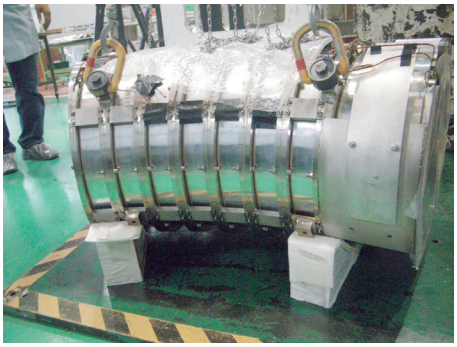

Figure 2. A photo of the first curved section of the Superomega.

References

[1] K. Nakahara *et al.*, Nucl. Inst. and Meth. in Phys. Res., vol. A600, pp.132-134, 2009.

[2] Muons, Inc. 552 Nm Batavia Avenue, Batavia, IL, available at http://www.muonsinc.com.

Y. Ikedo[1], Y. Miyake[1], K. Shimomura[1], P. Strasser[1], K. Nishiyama[1], N. Kawamura[1], H. Fujimori[1], S. Makimura[1], A. Koda[1], T. Ogitsu[1], Y. Makida[1], T. Adachi[2], M. Yoshida[1], T. Nakamoto[1], K. Sasaki[1], T. Okamura[1], W. Higemoto[3], and K. Ishida[4]

[1]High Energy Accelerator Research Organization; [2]University of Tokyo; [3]Japan Atomic Energy Agency; [4]RIKEN

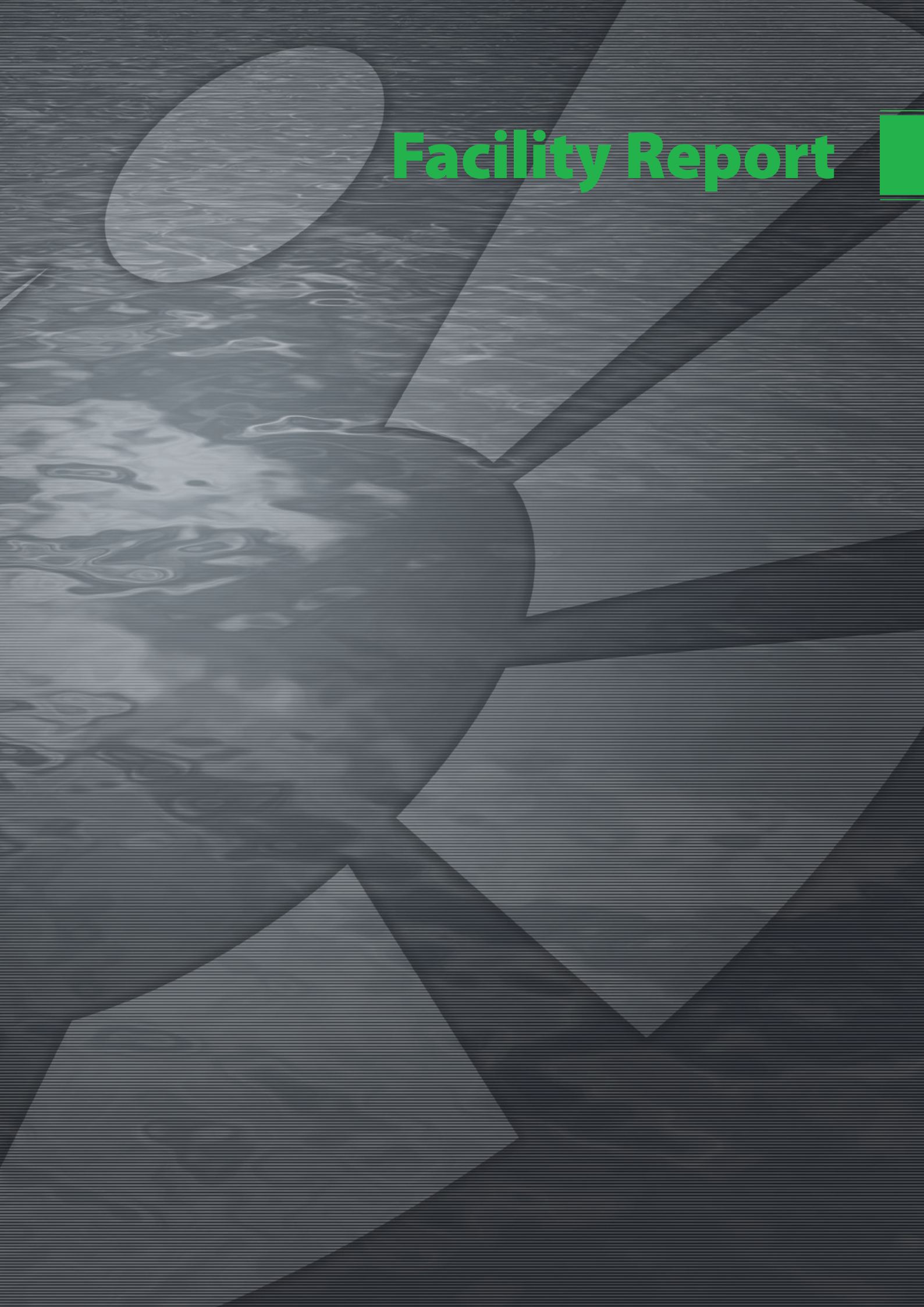

Facility Report

Beam Operation Status at MLF

In February 2009, a leakage was found at the accumulator of the cryogenic hydrogen system in the neutron source and the beam operation was cancelled. In April 2010, the beam operation started for the recovering from the failure of the cryogenic systems. Following Runs #33 and 34, a very stable beam operation was achieved with beam power of 120 kW without significant troubles. Although some troubles due to impurity of helium in the cryogenic system appeared in Run #35, a remarkably good beam availability of about 90 % was achieved.

In JFY 2010, some of the new neutron beam lines were constructed. Because of the budget profile, new beam lines could not be constructed during the summer maintenance period. Eventually, the duration of beam stop for construction of new beam lines was scheduled for the month of December 2011.

Since November 2010 in Run #36, we started a very steady beam operation with power of 200 kW. In order to perform beam operation efficiently, long duration of machine time per one period is required. After Run #36, the duration of the beam operation per one period was extended to two months because of demonstration of a long life ion source. During Run #38, we had the mega earthquake on March 11th. After that, the beam operation was cancelled.

Table 1. Run cycle, scheduled time and availability.

Run#	Scheduled Time (h).	Availability
32	22	93.4
33	487	93.4
34	397	91.7
35	362	42.5
36	925	76.4
37	641	99.5
38	418	19.9

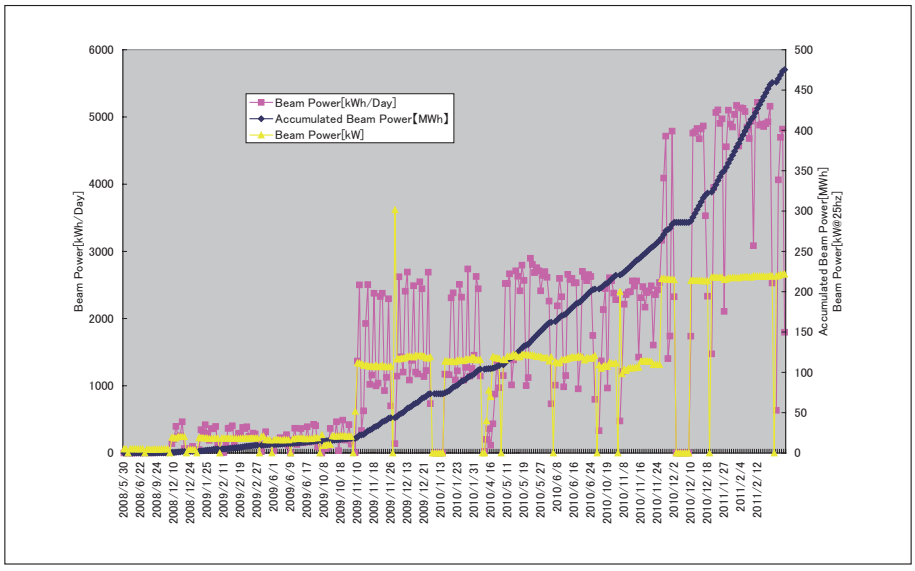

Figure 1. Beam power trend at MLF and cumulative beam power since the first beam.

Users at MLF

In the period of 2010A (June 1st-November 30th) and 2010B (December 1st - March 31st 2011), there are 76 days and 42 days beam operation (scheduled) for user programs, respectively. As of the users in fiscal year 2010, 1,174 visitors came to MLF and 5,558 person-days of beam time were allocated in total. These numbers increased almost 60% from the last year (2009).

Accepted proposals list for MLF experiments in JFY2010A (Noutron)

	Beam Line	Proposal ID	Applicant	Affiliation	Title of experiment
1	BL-01	2010A0003	Naoyuki Katayama	University of Virginia	High energy spin excitation in spin singlet trimer state of $BaV_{10}O_{15}$
2	BL-01	2010A0004	Naoyuki Katayama	University of Virginia	Evolution of magnetic excitations with Se substitution in $Fe_{1.01}Se_xTe_{1-x}$ near the quantum critical point
3	BL-01	2010A0005	Naoyuki Katayama	University of Virginia	Magnetic fluctuations in Sr_2RuO_4
4	BL-01	2010A0014	Hajime Sagayama	Tohoku University	Spin and orbital excitations in spinel vanadate
5	BL-01	2010A0070	Masato Matsuura	Osaka University	Study of Ni-doping effect on the magnetic excitation in high-Tc cuprates $La_{1.85}Sr_{0.15}CuO_4$
6	BL-08	2010A0006	Yasushi Idemoto	Tokyo University of Science	Effects of a synthetic process and a heat-treatment on crystal structures of lithium-rich layered cathode active materials for lithium ion battery
7	BL-08	2010A0019	Je-Geun Park	Sungkyunkwan univ. KOREA	Structural studies of Ir oxides, Sr_2IrO_4 and $Sr_3Ir_2O_7$
8	BL-08	2010A0023	Yuji Noguchi	University of Tokyo	Investigations of ferroelectric crystal structures for Bi-based perovskite ferroelectric oxides
9	BL-08	2010A0030	Masatomo Yashima	Tokyo Institute of Technology	Structural Origin of Large Oxygen Permeability in the Pr_2NiO_4-Based Mixed Conductors
10	BL-08	2010A0037	Masatomo Yashima	Tokyo Institute of Technology	Positional Disorder and Crystal Structure of Ceria-Zirconia Catalysts; Structural origin for high bulk oxygen diffusivity and high catalytic activity?
11	BL-08	2010A0039	Brendan Kennedy	Professor	Phase Separation in $SmVO_3$
12	BL-08	2010A0054	Yingxia Wang	Peking University	HRPD Characterization of two rare earth fluorite-related compounds:$La(Sb_{0.5}Co_{0.5})_3O_x$(1) and $La_{12}CaCr_4O_{30}$(2)
13	BL-08	2010A0060	Ryoji Kanno	Tokyo Institute of Technology	Crystal structure analysis of Thio-LISICONs - Super ionic conductor for lithium batteries
14	BL-08	2010A0068	Shigeomi Takai	Tottori University	Ordering and stabilization of Pb- and Bi- doped $La_2M_{o2}O_9$
15	BL-08	2010A0083	Norihito Kijima	National Institute of Advanced Industrial Science and Technology (AIST)	Neutron Powder Diffraction Studies of Lithium Battery Electrode Materials with Tunnel Structure
16	BL-08	2010A0067	Ayako Yamamoto	RIKEN	Structural study on novel pyrochlore-type oxides showing metal-insulator transition
17	BL-08	2010A0074	Hironori Nakao	High Energy Accelerator Research Organization	Co spin-state ordering in $Sr_{1-x}R_xCo_4O_{10.5}$ (R=Rare Earth)
18	BL-10	2010A0034	Hiroyuki Nojiri	Tohoku University	High Magnetic Field Neutron Diffractions in Frustrated Multi-ferroics
19	BL-10	2010A0021	浅井 弘彰	HIREC Corporation	半導体素子のシングルイベント耐性試験に係る白色中性子場のフィージビリティ評価（その３） Feasibility study on semiconductors under the white neutron field (3)
20	BL-10	2010A0011	Tatsuya Nakamura	Japan Atomic Energy Agency	Development of neutron detectors
21	BL-10	2010A0038	Ishida Takekazu	Osaka Prefecture University	Development of new type MgB_2 neutron detector
22	BL-14	2010A0075	Yukinobu Kawakita	Kyushu University	Relaxation mechanism in molecular liquid with strong intermolecular correlations

	Beam Line	Proposal ID	Applicant	Affiliation	Title of experiment
23	BL-14	2010A0042	Hiroshi Nakagawa	Japan Atomic Energy Agency	Sequence dependent DNA dynamics by TOF-elastic resolution spectroscopy
24	BL-14	2010A0008	Je-Geun Park	Sungkyunkwan univ. KOREA	Spin dynamics of new multiferroic $BiFeO_3$ single crystal
25	BL-14	2010A0044	Maiko Kofu	University of Tokyo	Spin dynamics in novel rare-earth based single-molecule magnets
26	BL-16	2010A0077	Hideki Seto	IMSS KEK	Salt distribution at the interface between water and organic solvent
27	BL-16	2010A0057	Ryoji Kanno	Tokyo Institute of Technology	Interface structure analysis of lithium battery electrodes using neutron reflectometry
28	BL-16	2010A0022	原田 雅史	株式会社豊田中央研究所	ナフィオン / プラチナ界面の構造解析 Structure of the naphion/platinum interface
29	BL-16	2010A0025	簗嶋 裕之	住友化学 (株)	中性子反射率法による高分子薄膜／高分子薄膜界面の構造解析 Structure analysis of polymer interface
30	BL-19	2010A0012	Jun Abe	Japan Atomic Energy Agency	Residual strain measurements of geological material
31	BL-19	2010A0047	Yo Tomota	Ibaraki University	In situ neutron diffraction during bainitic transformation from plastically deformed austenite
32	BL-19	2010A0048	Yo Tomota	Ibaraki University	In situ neutron diffraction during tension-compression cyclic deformation in advanced steels and cast irons
33	BL-19	2010A0050	Masaru Tomita	Railway Technical Research Institute	Flux-pinning-induced stress and magnetostriction in bulk superconductors
34	BL-19	2010A0081	Satoshi Awaji	Tohoku University	Three dimensional strain analysis of the Nb3Sn superconducting composite cables
35	BL-19	2010A0085	Yoshinori Tsuchiya	National Institute for Materials Science	Neutron diffraction study of sintering reaction processes for superconducting materials
36	BL-19	2010A0013	平野 辰巳	（株）日立製作所日立研究所	エンジン用ピストンの残留応力評価 (3) Residual stress in pistons for engines (3)
37	BL-19	2010A0024	濱名 雅之	NISSAN MOTOR CO.,LTD.	自動車アルミ鋳造部品の内部残留応力計測 Internal residual stress measurement in Cast Aluminum for automobile
38	BL-19	2010A0065	鈴木 環輝	新日本製鐵（株）	中性子回折法による超音波打撃処理した十字継手溶接鋼板および溶接まま十字溶接鋼板内部の残留応力測定 Residual stress measurement of welded steels treated by supersonic wave
39	BL-19	2010A0017	Nobuaki Takahashi	Japan Atomic Energy Agency	R&D of a time-spatial-focusing crystal-analyzer for neutron inelastic spectrometers
40	BL-03	2010A0010	Tsunehisa Kimura	Kyoto University	Single crystal neutron diffraction study of microcrystalline powder of biomolecules by pseudo-single crystal method
41	BL-03	2010A0084	Miwako Takahashi	University of Tsukuba	Crystal Structure of a lead-based inorganic-organic perovskite $(C_5H_{10}NH_2)PbBr_3$
42	BL-03	2010A0009	Toshiyuki Chatake	Kyoto University	Neutron Crystallographic analysis of human hemoglobin to reveal its oxygen binding mechanism.
43	BL-03	2010A0027	Andrey Kovalevsky	Los Alamos National Laboratory	Neutron Diffraction study of apo-D-Xylose Isomerase in complex with per-deuterated D-glucose.
44	BL-03	2010A0029	Yoko Sugawara	Kitasato University	Neutron diffraction analysis of disodium uridine 5,-monophosphate heptahydrate in low temperature phase
45	BL-03	2010A0040	Tae-Sung Yoon	Korea Research Institute of Bioscience & Biotechnology (KRIBB)	Neutron diffraction structure analysis of catalytic domains of protein tyrosine phosphatase family

	Beam Line	Proposal ID	Applicant	Affiliation	Title of experiment
46	BL-20	2010A0001	Minoru Soda	Osaka University	Crystal and magnetic structures in (1-*x*)$BiFeO_3$-*x*$BaTiO_3$ with relaxor-like behavior
47	BL-20	2010A0049	Dyah Adipranoto	Ibaraki University	Research on structure-function relationships in the high ion conductor
48	BL-20	2010A0058	Ryoji Kanno	Tokyo Institute of Technology	Crystal structure analysis of Li_2MO_3 (M=Co,Ni,Mn) reduced by metal hydride - New cathode material for lithium batteries
49	BL-20	2010A0064	Takashi Kamiyama	High Energy Accelerator Research Organization	Studies on Jomon Pottery (Cord Impressed Ware from B.C.13000)
50	BL-20	2010A0073	Hidetoshi Oguro	Ibaraki University	Residual strain measurement for Nb_3Sn strand cable by neutron diffraction
51	BL-20	2010A0032	Taku Iiyama	Shinshu University	The investigation of the change of hydrogen-bonding structure of water molecular assemblies with the size of hydrophobic nanospace
52	BL-20	2010A0055	Hiroaki Mamiya	National Institute for Materials Science	Neutron scattering study of the highly diluted spinel ferrite

Accepted proposals list for MLF experiments in JFY2010A (Muon)

	Beamline	Proposal ID	Applicant	Affiliation	Title of experiment
1	D1	2010A0031	Jun Sugiyama	Toyota Central R&D Labs. Inc	The doping effect on the formation of H\muH bond in MgH_2
2	D1	2010A0051	Kenya Kubo	International Christian University	Development of non-destructive multi-elemental analysis system by muonic X-ray
3	D1	2010A0041	Jun Sugiyama	Toyota Central R&D Labs. Inc	Li diffusion in $LiFePO_4$ and related materials
4	D1	2010A0059	Koichiro Shimomura	IMSS KEK	MuSR study on isolated hydrogen charge state in oxgen deficient $SrTiO_3$
5	D1	2010A0028	Masao Doyama	Teikyo University of Science and Technology	Applications of imaging plates to the study of muon science
6	D1	2010A0078	Tadashi Adachi	Tohoku University	Effects of nonmagnetic, magnetic and electrostatic impurities on the Cu-spin correlation and superconductivity in high-Tc cuprates
7	D1	2010A0056	Khashayar Ghandi	Faculty member	Studies of muonium formation in liquids
8	D1	2010A0046	Kazuhiko Ninomiya	Japan Atomic Energy Agency	Study on the relation between molecular structure and muon state of the first step of muon capture phenomena for nitrogen and oxygen compounds (2)
9	D1	2010A0069	Kenji Kojima	IMSS KEK	Magnetism and superconductivity of geometrically frustrated Ir-oxides and sulfides
10	D1	2010A0053	Akihiro Koda	IMSS KEK	Microscopic characterization of the nano-domain ferromagnet FINEMET
11	D1	2010A0062	Xu-Guang Zheng	Saga University	Investigation of exotic magnetic states in geometrically frustrated materials of pyrochlore lattice $Ni_2(OH)_3Cl$ and triangular lattices $Ni_2(OH)_3Br$, $Ni_2(OH)_3I$, $Co_2(OH)_3Br$ and $Co_2(OH)_3I$
12	D1	2010A0026	Roderick Macrae	Marian University	Muon States in Nanostructured Carbon Materials

MLF Division Staff 2010

Director	Masatoshi Arai (JAEA)
Vice Director	Hideki Seto (KEK)
	Takashi Kato (JAEA)

Neutron Source Section

	JAEA	
Leader	Masatoshi Futakawa	Kiichi Ohtsu
Sub-Leader	Hiroshi Takada	Toshiaki Uehara
	Fujio Maekawa	Kiyomi Ikezaki
	Shinichi Sakamoto	Tetsuya Haraguchi
	Katsuhiro Haga	Kohei Hanano
	Shinichiro Meigo	Hideki Tatsumoto
	Sakai Kenji	Motoki Ohi
	Yoshimi Kasugai	Yoshihiko Kawakami
	Makoto Teshigawara	Manabu Ito
	Tomokazu Aso	Hisashi Sakurayama
	Hidetaka Kinoshita	Takeshi Naoe
	Kenichi Oikawa	Atsushi Akutsu
	Masahide Harada	Toru Suzuki
	Shoichi Hasegawa	Masato Ida
	Hiroyuki Kogawa	Kenichi Kanomata
	Takasi Wakui	Hiroshi Tomita
	Tetsuya Kai	Tatsuhiro Tomita
	Masakazu Seki	Kazuki Koishihara
	Akihiko Watanabe	Shizuka Yoshinari
	Akira Ogawa	Chieko Higuchi

Neutron Science Section

	KEK	
Leader	Takashi Kamiyama	Takashi Ino
	Susumu Ikeda	Setsuo Satoh
	Hideki Seto	Hidenori Sagehashi
	Toshiya Otomo	Suguru Muto
	Tetsuya Yokoo	Naokatsu Kaneko
	Norifumi Yamada	Masao Yonemura
	Shuki Torii	
	Tomohiro Seya	JAEA
	Masataka Sakaguchi	Sub-Leader Kazuya Aizawa
	Zhang Junrong	Kentarao Suzuya
	Koichiro Sadakane	Junichi Suzuki
	Hirohiko Shimizu	Kenji Nakajima
	Shinichi Ito	Takayuki Oku

Mitsutaka Nakamura
Ryoichi Kajimoto
Stefanus Harjo
Kaoru Shibata
Takeshi Nakatani
Shinichi Takata
Nobuaki Takahashi
Takenao Shinohara
Yukinobu Kawakita
Seiko Kawamura
Hiroshi Arima
Yasuhiro Inamura
Takayoshi Ito
Hiroshi Kira
Tatsuya Kikuchi
Takuro Kawasaki
Jun Abe
Yoshifumi Sakaguchi
Fumio Mizuno
Hironori Shimakura
Hiroki Ueno
Yuhua Su
Noboru Yoshida

Hiromichi Tanaka
Wataru Kambara
Yukihiro Ito
Takaaki Iwahashi
Atsushi Moriai
Masayasu Takeda
Toyotaka Osakabe
Kazuo Kurihara
Takashi Ohhara
Wataru Utsumi
Shuichi Wakimoto
Takanori Hattori
Itaru Tamura
Koji Kaneko
Asami Sano
Hideo Harada
Atsushi Kimura
Ryoko Aoyama
Chiho Tobe
Yukari Sugikawa
Naoko Shimizu
Junko Akutsu

Neutron Instrumentation Section

JAEA

Leader Kazuhiko Soyama
Kaoru Sakasai
Dai Yamazaki
Kentaro Toh
Tatsuya Nakamura
Ryuji Maruyama

Hirotoshi Hayashida
Hideshi Yamagishi
Satoru Okayasu
Takuro Sakai
Ryo Yasuda
Mana Hirayama

Muon Section

KEK

Leader Yasuhiro Miyake
Ryosuke Kadono
Koichiro Shimomura
Kenji Kojima
Patrick Strasser
Naritoshi Kawamura
Akihiro Koda
Hiroshi Fujimori
Shunsuke Makimura
Mineo Kato

Yasuhisa Nemoto
Yasuo Kobayashi
Kusuo Nishiyama
Yutaka Ikedo
Tetsuya Masuda

JAEA

Wataru Higemoto
Takashi Ito
Kazuhiko Ninomiya

Committee and Meetings

Neutron Instrument Proposal Review Committee

中性子実験装置部会

Koichiro Asahi	Tokyo Institute of Technology, Japan
Muneyuki Imafuku	Tokyo City University, Japan
Kenji Ohyama	Tohoku University, Japan
Toshiji Kanaya	Kyoto University, Japan
Hideaki Kitazawa	National Institute for Material Science, Japan
Mamoru Sato	Yokohama City University, Japan
Mitsuhiro Shibayama	University of Tokyo, Japan
Naoya Torikai	Mie University, Japan
Yasuki Nagai	Osaka University, Japan
Yukio Noda	Tohoku University, Japan
Toshiharu Fukunaga	Kyoto University, Japan
Michihiro Furusaka	Hokkaido University, Japan
Yukio Morimoto	Kyoto University, Japan
Kazuyoshi Yamada	Tohoku University, Japan
Hideki Yoshizawa	University of Tokyo, Japan
Toshio Akai	Mitsubishi Chemical Co., Japan
Yukio Morii	Hitachinaka Techno Center, Japan
Masatoshi Arai	Japan Atomic Energy Agency, Japan
Takashi Kato	Japan Atomic Energy Agency, Japan
Hideki Seto	High Energy Accelerator Research Organization, Japan
Takashi Kamiyama	High Energy Accelerator Research Organization, Japan
Hirohiko Shimizu	High Energy Accelerator Research Organization, Japan
Toshiya Ootomo	High Energy Accelerator Research Organization, Japan
Kazuhiko Soyama	Japan Atomic Energy Agency, Japan
Kenji Nakajima	Japan Atomic Energy Agency, Japan
Kazuhisa Kakurai	Japan Atomic Energy Agency, Japan
Susumu Ikeda	High Energy Accelerator Research Organization, Japan

Materials and Life Science Facility Advisory Board

物質・生命科学実験施設利用委員会

Kazuyoshi Yamada	Tohoku University, Japan
Toshiji Kanaya	Kyoto University, Japan
Toshiharu Fukunaga	Kyoto University, Japan
Mamoru Sato	Yokohama City University, Japan
Mitsuhiro Shibayama	University of Tokyo, Japan
Shinichi Kamei	Mitsubishi Research Institute, Japan
Nobuhiko Shinichi	Tokyo Institute of Technology, Japan
Teiichiro Matsuzaki	RIKEN, Japan
Jun Sugiyama	Toyota Central R&D Lab., Japan
Makoto Hayashi	Ibaraki Prefecture, Japan

Yukio Noda	Tohoku University, Japan
Yoji Koike	Tohoku University, Japan
Yujiro Ikeda	Japan Atomic Energy Agency, Japan
Masatoshi Arai	Japan Atomic Energy Agency, Japan
Kazuhisa Kakurai	Japan Atomic Energy Agency, Japan
Junichiro Mizuki	Japan Atomic Energy Agency, Japan
Wataru Utsumi	Japan Atomic Energy Agency, Japan
Junichi Suzuki	Japan Atomic Energy Agency, Japan
Susumu Ikeda	High Energy Accelerator Research Organization, Japan
Takashi Kamiyama	High Energy Accelerator Research Organization, Japan
Hirohiko Shimizu	High Energy Accelerator Research Organization, Japan
Hideki Seto	High Energy Accelerator Research Organization, Japan
Yasuhiro Miyake	High Energy Accelerator Research Organization, Japan
Ryosuke Kadono	High Energy Accelerator Research Organization, Japan

Materials and Life Science Facility Proposal Review Committee

物質・生命科学研究施設中性子課題審査部会

Masatoshi Arai	Japan Atomic Energy Agency, Japan
Takashi Kamiyama	High Energy Accelerator Research Organization, Japan
Yasuhiro Miyake	High Energy Accelerator Research Organization, Japan
Susumu Ikeda	High Energy Accelerator Research Organization, Japan
Kazuhisa Kakurai	Japan Atomic Energy Agency, Japan
Takashi Kato	Japan Atomic Energy Agency, Japan
Hideki Seto	High Energy Accelerator Research Organization, Japan
Yukio Noda	Tohoku University, Japan
B. Kennedy	University of Sydney, Australia
Yo Tomota	Ibaraki University, Japan
Toshiharu Fukunaga	Kyoto University, Japan
Junichi Suzuki	Japan Atomic Energy Agency, Japan
S. M. Choi	Korea Advanced Institute of Science and Technology, Korea
Mitsuhiro Shibayama	University of Tokyo, Japan
Toshiji Kanaya	Kyoto University, Japan
P. Timmins	Institut Laue-Langevin, France
Mamoru Sato	Yokohama City University, Japan
Yuji Ohashi	Hitachinaka Techno Center, Japan
Kazuyoshi Yamada	Tohoku University, Japan
Hideki Yoshizawa	University of Tokyo, Japan
Takahisa Arima	Tohoku University, Japan
J-G. Park	Seoul National University, Korea
Hideto En'yo	RIKEN, Japan
Makoto Hayashi	Ibaraki Prefecture, Japan
Yoshiaki Akinina	Yokohama City University, Japan
Yukio Morii	Hitachinaka Techno Center, Japan
Yoshiaki Kiyanagi	Hokkaido University, Japan
Xun-Li Wang	Oak Ridge National Laboratory, U.S.A

物質・生命科学研究施設ミュオン課題審査部会

Masatoshi Arai	Japan Atomic Energy Agency, Japan
Yasuhiro Miyake	High Energy Accelerator Research Organization, Japan
Takashi Kamiyama	High Energy Accelerator Research Organization, Japan
Susumu Ikeda	High Energy Accelerator Research Organization, Japan
Yuichiro Nagame	Japan Atomic Energy Agency, Japan
Kenji Ishida	Kyoto University, Japan
Masao Ogata	University of Tokyo, Japan
Shinsaku Kambe	Japan Atomic Energy Agency, Japan
Ryosuke Kadono	High Energy Accelerator Research Organization, Japan
Yuji Koike	Tohoku University, Japan
Kenya Kubo	International Christian University, Japan
Robert De Renzi	University of Parma, Italy
Hiroshi Kobori	Chiba University, Japan
Shinji Tsuneyuki	University of Tokyo, Japan
Yasuo Nozue	Osaka University, Japan
Katsuhiko Ishida	Riken, Japan
Koichiro Asahi	Tokyo Institute of Technology, Japan
Wataru Higemoto	High Energy Accelerator Research Organization, Japan
Kim H. Chow	University of Alberta, Japan

KENS Program Advisory Committee

中性子共同利用実験審査委員会

Koichiro Asahi	Tokyo Institute of Technology, Japan
Kazuaki Iwasa	Tohoku University, Japan
Wataru Utsumi	Japan Atomic Energy Agency, Japan
Hiroyuki Kagi	University of Tokyo, Japan
Mikio Kataoka	Nara Institute of Science and Technology
Toshiji Kanaya	Kyoto University, Japan
Kiyanagi Yoshiaki	Hokkaido University, Japan
Kanno Ryoji	Tokyo Institute of Technology, Japan
Takahara Atsushi	Kyushu University, Japan
Toshiharu Fukunaga	Kyoto University, Japan
Michihiro Furusaka	Hokkaido University, Japan
Kazuyoshi Yamada	Tohoku University, Japan
Hideki Yoshizawa	University of Tokyo, Japan
Susumu Ikeda	High Energy Accelerator Research Organization, Japan
Hideki Seto	High Energy Accelerator Research Organization, Japan
Ryosuke Kadono	High Energy Accelerator Research Organization, Japan
Nomura Masaharu	High Energy Accelerator Research Organization, Japan
Masakazu Yoshioka	High Energy Accelerator Research Organization, Japan
Shinichi Itoh	High Energy Accelerator Research Organization, Japan
Toshiya Otomo	High Energy Accelerator Research Organization, Japan
Takashi Kamiyama	High Energy Accelerator Research Organization, Japan
Hirohiko Shimizu	High Energy Accelerator Research Organization, Japan
Youichi Murakami	High Energy Accelerator Research Organization, Japan

Muon Program Advisory Committee

ミュオン共同利用実験審査委員会

Hiroshi Amitsuka	Hokkaido University, Japan
Yuichiro Nagame	High Energy Accelerator Research Organization, Japan
Masahiko Iwasaki	Riken, Japan
Masao Ogata	University of Tokyo, Japan
Shinsaku Kambe	High Energy Accelerator Research Organization, Japan
Yoshitaka Kuno	Osaka University, Japan
Yoji Koike	Tohoku University, Japan
Atsushi Shinohara	Osaka University, Japan
Kenichiro Suzuya	High Energy Accelerator Research Organization, Japan
Masashi Takigawa	University of Tokyo, Japan
Shinji Tsuneyuki	University of Tokyo, Japan
Hiroyuki Nojiri	Tohoku University, Japan
Katsuyuki Fukutani	University of Tokyo
Isao Watanabe	Riken, Japan
Susumu Ikeda	High Energy Accelerator Research Organization, Japan
Hideki Seto	High Energy Accelerator Research Organization, Japan
Ryosuke Kadono	High Energy Accelerator Research Organization, Japan
Kenji Ito	High Energy Accelerator Research Organization, Japan
Hitoshi Kobayashi	High Energy Accelerator Research Organization, Japan
Takashi Kamiyama	High Energy Accelerator Research Organization, Japan
Kanta Ono	High Energy Accelerator Research Organization, Japan
Keiichiro Nasu	High Energy Accelerator Research Organization, Japan
Yasuhiro Miyake	High Energy Accelerator Research Organization, Japan

The Japan Spallation Neutron Sources International Advisory Committee (NIAC)

NIAC-2 (February 28 - March 2, 2011 at IBARAKI Quantum Beam Research Center)

Member list of NIAC-2

Günter Bauer	Forschungszentrum Jülich GmbH (retired), Germany
Stephen Bennington	Rutherford Appleton Laboratory, UK
Kurt Clausen	Paul Scherre Institute, Switzerland
John Haines	Oak Ridge National Laboratory, USA
Toshiji Kanaya	Kyoto University, Japan
Yoshiaki Kiyanagi	Hokkaido University, Japan
Dan Neumann	National Institute of Standards and Technology, USA (chair)
Robert Robinson	Australian Nuclear Science and Technology Organization, Australia
Kazuyuki Yamada	Tohoku University, Japan

Group photo of NIAC-2

Muon Science Advisory Committee (MuSAC)

MuSAC-9 (February 18-19, 2011 at Tokai Bldg No.1, Tokai Campus, KEK, Japan)

Member list of MuSAC-9

Jun Akimitsu	Aoyama Gakuin University, Japan
Hiroshi Amitsuka	Hokkaido University, Japan
Robert Cywinski	University of Huddersfield, UK
Elvezio Morenzoni	Paul Scherrer Institute, Switzerland
Jean-Michel Poutissou	TRIUMF, Canada
Atsushi Shinohara	Osaka University, Japan
Jeff E. Sonier	Simon Fraser University, Canada
Eiko Torikai	University of Yamanashi, Japan

MuSAC-9 (February 18-19, 2011)

International Advisory Committee on the Single Crystal Diffractometer "SENJU" at J-PARC

August 30-31, 2010, JAEA, Tokai, Ibaraki, Japan

Laurent Chapon (ISIS, UK), Matthias J. Gutmann (ISIS, UK), Leighton Coates (SNS, USA), Eddy Lelievre-Berna (ILL, France), M. Arai (JAEA), F. Maekawa (JAEA), K. Oikawa (JAEA), I. Tamura (JAEA), T. Nakamura (JAEA), K. Kaneko (JAEA), T. Oohara (JAEA), T. Oku (JAEA)

Group photo of International Advisory Committee on the Single Crystal Diffractometer "SENJU" at J-PARC

International Advisory Committee on the vertical neutron reflectometer (BL17) at J-PARC

September 21-22, 2010, JAEA, Tokai, Ibaraki, Japan

K. Anderson (ILL, France), F. Klose (ANSTO, Australia), S. Langridge (ISIS, UK), M. Arai (JAEA), F. Maekawa (JAEA), M. Takeda (JAEA), D. Yamazaki (JAEA), K. Toh (JAEA), T. Nakamura (JAEA), H. Hayashida (JAEA), H. Kira (JAEA), T. Oku (JAEA)

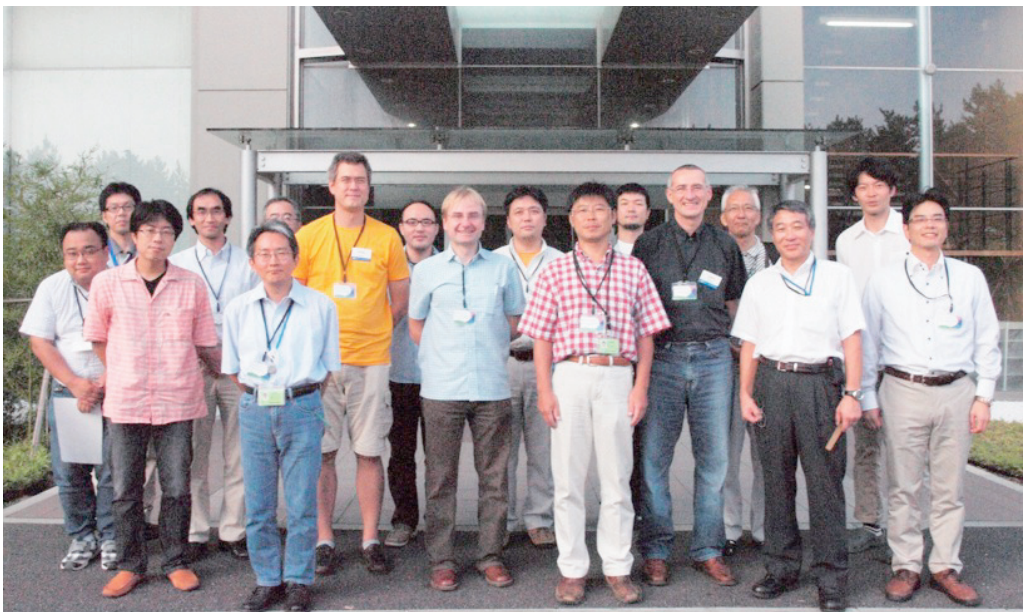

Group photo of International Advisory Committee on the vertical neutron reflectometer (BL17) at J-PARC

Workshop

2011.1.17-18

2nd MLF Symposium (MLF user meeting)

KEK, Tsukuba, with about 200 participants.

Oral presentations (22 for neutron science, 6 for muon science, and a special talk by Prof. Fukuyama at Tokyo University of Science). Poster presentation (54 for neutron science and 16 for muon science)

Masatoshi Arai, Susumu Ikeda

Group photo of 2nd MLF Symposium

Presentation at the hall

Poster Session

Neutron Source

2010.9.29

Review on Separate Type Target

MLF, Tokai, Ibaraki, Japan

N. Watanabe, H. Kyoto (Univ. Tsukuba), A. Kaneko (Univ. Tsukuba), K. Hoshino (Kimura Chemical Plants co., Ltd.), M. Futakawa (JAEA), K. Haga (JAEA), S. Ishihara (Metal Technology Co.Ltd.), T. Wakui (JAEA), K. Kanomata (JAEA), H. Kogawa (JAEA), Y. Kasugai (JAEA), M. Ida (JAEA), Y. Morinishi (Kobelco Research Institute, inc.)

2011.1.25–1.27

SNS – JSNS Collaboration on Source Development

SNS, Oak Ridge, TN, USA

S.Sakamoto (JAEA), T.Kato (JAEA), Y. Kasugai (JAEA), M. Harada (JAEA), H. Kogawa (JAEA), T. McManamy (SNS), B. Riemer (SNS), M. Wendel (SNS), A. Crabtree (SNS), D. McClintc (SNS), P. Rosenblad (SNS), M. Dyton (SNS), J. Janney (SNS), Iverson (SNS), Gallmeier (SNS), W. Lu (SNS), J. Devore (SNS)

Neutron Instruments

2010.8.19

BL09: 電池研究会

Tokai 1Goukan, Tokai, Ibaraki, Japan

Yonemura, Kamiyama, et. al.

2010.10.8

BL12: HRC Workshop

KEK Tokai campus, Tokai, Ibaraki, Japan

H. Seto (KEK), T. Sato (U Tokyo), S. Itoh (KEK), S. Yano (Aoyama Gakuin U), T. Yokoo (KEK), K. Kuwahara (Ibaraki U), D. Kawana (KEK), Y. Tabata (Kyoto U), H. Yoshizawa (U Tokyo), T. Masuda (U Tokyo)

2010.11.15

BL16: BL16 Neutron Reflectivity Workshop

KEK, Tsukuba, Ibaraki, Japan

N. L. Yamada (KEK), T. Kanaya (Kyoto Univ.), K. Tanaka (Kyushu Univ.), D. Kawaguchi (Nagoya Univ.), M. Harada (Toyota Central R&D Lab.), K. Ozeki (Ibaraki Univ.), R. Kanno (Tokyo Inst. Tech.), K. Mitamura (Kyushu Univ./JST), A. Takahara (Kyushu Univ./JST)

2010.11.24

BL21: Workshop on Fundamental Research of Hydrogen Storage Mechanism with High-Intensity Total Diffractometer

KEK Tokai campus, Tokai, Ibaraki, Japan

T. Otomo, N. Kaneko (J-PARC center/KEK), K. Suzuya, Y. Kawakita (J-PARC center/JAEA), H. Ohshita, K. Ikeda, M. Tsubota (KEK), T. Fukunaga (KUR, Kyoto Univ.), K. Itoh (Okayama Univ.), K. Kodama, M. Honda (QuBus, JAEA), Y. Kameda (Yamagata Univ.), K. Yoshida, T. Yamaguchi (Fukuoka Univ.), K. Maruyama (Niigata Univ.)

2010.12.14

BL08 & BL09: Neutron Structure Science Meeting using BL08 & BL09

Tokai 1Goukan, Tokai, Ibaraki, Japan

Y. Noda (Tohoku Univ), S. Torii (KEK), T. Kamiyama (KEK), Zhang (KEK), S. Takeda (Hokaido Univ.), Y. Noguchi Univ. of Tokyo), A. Yamamoto (RIKEN), S. Takai (Tottori Univ.), P. M. Shirage (AIST), K. Miyazawa (AIST), K. Kihou (AIST), C. H. Lee (AIST), H. Kito (AIST), K. Tokiwa (AIST), Y. Tanaka (AIST), H. Eisaki (AIST), A. Iyo (AIST), T. Fukunaga (KURRI), K. Mori (KURRI), K. Kino (KEK), M. Kawai (KEK), J. Suzuki (KEK), H. Nagashima (KEK), S. Terui (KEK), T. Ishigaki (Ibaraki Univ.)

2011.2.22

NASCES11 Satellite Meeting: ESS - J-PARC Technical Meeting on Neutron Instruments & Related Issues

HENDEL Building, J-PARC Center, Tokai, Ibaraki, Japan

M. Arai (JAEA), M. Nakamura (JAEA), N. Takahashi (JAEA), R. Kajimoto (JAEA), Y. Inamura (JAEA), K. Niita (RIST), Kim Lefmann (Univ. Copenhagen, ESS), Peter Kjær Willendrup (Risø-DTU, ESS) , Kaspar Hewitt Klenø (Univ. Copenhagen, ESS), Sonja Lindahl Holm (Univ. Copenhagen, ESS), Morten Sales (Univ. Copenhagen, ESS), Jonas Okkels Birk (Univ. Copenhagen), Linda Udby (Univ. Copenhagen)

2011.2.23－2.25

The International Workshop on Neutron Applications on Strongly Correlated Electron Systems 2011 (NASCES11)

J-PARC Center, Grant-in-Aid for Specially Promoted Research from Ministry of Education, Culture, Sports, Science and Technology (MEXT) “Construction of the 4D Space Access Neutron Spectrometer and Elucidation of Oxide High-Tc Superconductors”

Ibaraki Quantum Beam Research Center, Tokai, Ibaraki, Japan

Invited Speakers: G. Aeppli (University College London), T. Arima (Tohoku Univ.), P. Bourges (LLB-CEA), M. Braden (University Cologne), L. Braicovich (Politecnico di Milano), A. D. Christianson (ORNL), M. Fujita (Tohoku Univ.), B. D. Gaullin (McMaster University), G. E. Granroth (ORNL), K. Iwasa (Tohoku Univ.), R. Kajimoto (J-PARC), H. Kawano-Furukawa (Ochanomizu Univ.), S. Maekawa (JAEA), R. J. Mcqueeney (Ames Laboratory), H. Mutka (ILL), J.-G. Park (Seoul National University), T. G. Perring (ISIS), O. Pieper (Helmholtz-Zentrum Berlin), H. M. Rønnow (EPFL), S. Rosenkranz (ANL), C. Stock (NIST), O. Stockert (Max-Planck-Institut), M. B. Stone (ORNL), Y. Tokura (Tokyo Univ.), K. Tomiyasu (Tohoku Univ.), J. M. Tranquada (BNL)

2011.2.24

BL04: Memorial Symposium on the ANNRI Completion

JAEA, Tokai, Ibaraki, Japan

N. Baba (Hokkaido Univ.), H. Yokomizo (JAEA), Y. Ikeda (JAEA), M. Igashira (Tokyo Institute of Technology), Y. Kiyanagi (Hokkaido Univ.), H. Harada (JAEA), A. Kimura (JAEA), J. Hori (Kyoto Univ.), T. Katabuchi (Tokyo Institute of Technology), K.Nishio (JAEA), S.Meigo (JAEA), H.Utsunomiya (Konan Univ.), T. Hayakawa (JAEA), H. Shimizu (KEK), M. Ebihara (Tokyo Metropolitan Univ.), T. Kamiyama (Hokkaido Univ.)

2011.3.8－3.9

Workshop on the Sample Environments for High-Magnetic Field and High-Pressure Neutron Experiments at MLF, J-PARC

Ibaraki Quantum Beam Research Center, Tokai, Ibaraki, Japan

M. Arai (JAEA), K. Nakajima (JAEA), S. Ohira-Kawamura (JAEA), W. Kambara (JAEA), T. Yokoo (J-PARC, KEK), K.

Kaneko (JAEA, J-PARC), H. Nojiri (Tohoku Univ.), K. Watanabe (Tohoku Univ.), H. Ohta (Kobe Univ.), T. Ono (Tokyo Inst. of Technology), K. Kuwahara (Ibaraki Univ.), M. Soda (Osaka Univ.), H. Nakao (KEK), H. Oguro (Tohoku Univ.), T. Hattori (JAEA, J-PARC), M. Azuma (Tokyo Inst. of Technology), A. Chiba (Keio Univ.), T. Fujiwara (Yamaguchi Univ.), C-H. Lee (AIST), T. Matsumura (Hiroshima Univ.), T. Osakabe (JAEA, J-PARC), M. Uwatoko (Univ. of Tokyo), K. Komatsu (Univ. of Tokyo), K. Kitagawa (Univ. of Tokyo), D. Yamazaki (J-PARC, JAEA)

Muon

2010.6.3－6.4

1st Progress Report Meeting of J-PARC/MUSE

KEK Tokai campus, Tokai, Ibaraki, Japan

R. Kadono (KEK), Y. Miyake (KEK), W. Higemoto (JAEA), M. Azuma (Kyoto U.), K. Tokiwa (Tokyo U. Sci.), M. Kosaka (Saitama U.), H. Chudo (JAEA), M. Hiraishi (Sokendai), M. Aoki (Osaka U.), K. Kubo (Sophia U.), K. Ninomiya (JAEA), K. Ghandi (Mount Allison U., Canada), Y. Ikedo (KEK), H. Sugai (JAEA), K. Shimomura (KEK)

2010.6.4

Report Meeting of Technical Achievements in J-PARC/MUSE

KEK Tokai campus, Tokai, Ibaraki, Japan

K. Nishiyama (KEK), Y. Miyake (KEK), N. Kawamura (KEK), S. Makimura (KEK), H. Fujimori (KEK), A. Koda (KEK), P. Strasser (KEK), K. Shimomura (KEK), W. Higemoto (JAEA)

2010.10.2－10.3

1st Ultra Slow Muon Microscope Workshop

Yamanashi University, Kofu, Yamanashi, Japan

N. Nishida (Tokyo Inst. Tech.), Y. Miyake (KEK), M. Iwasaki (RIKEN), N. Saito (KEK), K. Nagamine (KEK / Univ. Calf. Riverside, USA), W. Higemoto (JAEA), K. Fukutani (U. Tokyo), T. Wada (RIKEN), J. Sugiyama (Toyota Central Research Lab.), and 15 contributing presentations.

Award List

The JSNS Young Researcher Prize
Developments of In-Situ SEOP Polarized ^{3}He Neutron Spin Filter System
The Japanese Society for Neutron Science
Hiroshi Kira, December 2010

The 2011 technical development award of the Atomic Energy Society of Japan (AESJ)
Development of Accurate Neutron- Nucleus Reaction Measurement Instrument
the Atomic Energy Society of Japan (AESJ)
Graduate School of Engineering, Hokkaido University Research Laboratory for Nuclear Reactors, Tokyo Institute of Technology Research Group for Applied Nuclear Physics, Nuclear Science and Engineering Directorate, Japan Atomic Energy Agency, March 2011

The 1st Michael Meissner Prize (Presented for the best Poster at the 6th International SE Workshop)
Automatic sample exchange system for a large number of samples at room temperature
6th International Workshop on Sample Environment at Neutron Scattering Facilities
Akinori Hoshikawa, Toru Ishigaki, Masao Yonemura, Takashi Kamiyama, Kenji Iwase, Dyah Sulistyanintyas, Makoto Hayashi, September 2010

Nishikawa Prize
Developments on high frequency choppers for pulsed neutrons
High Energy Accelerator Science Foundation
S. Itoh, K. Ueno, R. Ohkubo, H. Sagehashi, Y. Funahashi, T. Yokoo, 24 March 2011

平成 21 年度原子力科学研究所長表彰　創意工夫功労賞（日本原子力研究開発機構）
J-PARC 中性子非弾性散乱実験装置『四季』における新たな高効率測定手法の開発
中性子実験装置「四季」測定技術開発グループ
梶本亮一、中村充孝、稲村泰弘、神原理
平成 22 年 3 月 25 日

平成 22 年度理事長表彰　研究開発功績賞（日本原子力研究開発機構）
J-PARC 中性子非弾性散乱実験装置『四季』における新たな高効率測定手法の開発
中性子実験装置「四季」測定技術開発グループ
梶本亮一、中村充孝、稲村泰弘、中谷健、神原理
平成 22 年 10 月 1 日

日本中間子科学会若手奨励賞
(Society of Muon and Meson Science of Japan Young Researcher Prize)
f 電子系 PrPb3 におけるミュオンスピン緩和機構の解明と四重極秩序の研究
日本原子力研究開発機構　先端基礎研究センター
伊藤孝

Publication List

Neutron Section

1 J. Abe, M. Arakawa, T. Hattori, H. Arima, H. Kagi, K. Komatsu, A. Sano-Furukawa, Y. Uwatoko, K. Matsubayashi, S. Harjo, A. Moriai, T. Ito, K. Aizawa, M. Arai, and W. Utsumi
A Cubic-anvil High-pressure Device for Pulsed Neutron Powder Diffraction
Rev. Sci. Inst. **81** 43910 (2010)

2 M. Arai
J-PARC status and Lessons Learnt from Commissioning
Proc. of the 19th Meeting of the Int. Collaboration on Advanced Neutron Sources
PSI-Proceedings 10-01 ISSN-Nr. 1019-6447 FO015 (2010)

3 新井正敏
J-PARC 始動とその道のり
日本中性子科学会誌「波紋」**20** 4 (2010)

4 H. Arima, T. Hattori, K. Komatsu, J. Abe, W. Utsumi, H. Kagi, A. Suzuki, K. Suzuya, T. Kamiyama, M. Arai, and T. Yagi
Designing PLANET: the Neutron Beamline for High-pressure Metarial Science at J-PARC
J. Phys. Conf. Ser. **215** 23025 (2010)

5 阿曽尾一也、友田陽
ＤＰ鋼の引張変形挙動のその場中性子回折による検討
「計算工学による組織と特性予測技術の最前線」日本鉄鋼協会 256 (2010)

6 M. Futakawa, S. Sakamoto, F. Maekawa, and H. Takada
Experience in Early Operation at JSNS of J-PARC
Proc. of the 19th Meeting of the Int. Collaboration on Advanced Neutron Sources PSI-Proceedings 10-01 ISSN-Nr. 1019-6447 TO033 (2010)

7 二川正敏、田中伸厚
高出力パルス核破砕中性子源におけるキャビテーション
混相流 **24** 138 (2010)

8 K. Haga, T. Naoe, H. Kogawa, H. Kinoshita, M. Ida, M. Futakawa, B. Riemer, M. Wendel, D. Felde, and A. Abdou
Distribution of Microbubble Sizes and Behavior of Large Bubbles in Mercury flow in a Mockup Target Model of J-PARC
Journal of Nuclear Science and Technology **47** 849 (2010)

9 H. Harada, M. Oshima, A. Kimura, S. Goko, M. Ohta, K. Furutaka, T. Kin, F. Kitatani, M. Koizumi, S. Nakamura, Y. Toh, M. Igashira, T. Katabuchi, M. Mizumoto, Y. Kiyanagi, K. Kino, M. Furusaka, F. Hiraga, T. Kamiyama, J. Hori, T. Fujii, and K. Takamiya
Status and Future Perspectives of Nuclear Data Measurements at J-PARC MLF BL04
Proc. 2009 Annual Symposium on Nuclear Data (NDS 2009) 9 (2010)

10 M. Harada, K. Oikawa, M. Ooi, T. Kai, K. Sakai, F. Maekawa, N. Watanabe, T. Shinohara, ahd S. Takata
Imaging Experiments on NOBORU at MLF
Proc. of the 19th Meeting of the Int. Collaboration on Advanced Neutron Sources PSI-Proceedings 10-01 ISSN-Nr. 1019 IO077 (2010)

11 M. Harada, K. Oikawa, F. Maekawa, S. Meigo, M. Futakawa, and N. Watanabe
Measurement of Neutronic Characteristics of JSNS
Proc. of the 19th Meeting of the Int. Collaboration on Advanced Neutron Sources PSI-Proceedings 10-01 ISSN-Nr. 1019 TO038 (2010)

12 S. Harjo, K. Aizawa, T. Ito, H. Arima, J. Abe, A. Moriai, K. Sakasai, T. Nakamura, T. Nakatani, T. Iwahashi, and T. Kamiyama
Aspire To Become TAKUMI−TAKUMI Present Status and Research Topics
Materials Science Forum **652** 99 (2010)

13 T. Hattori, Y. Katayama, A. Machida, T. Otomo, and K. Suzuya
For Hgh-pressure Experiments Using total Scattering Spectrometer NOVA at J-PARC
J. Phys. Conf. Ser. **215** 12024 (2010)

14 服部高典、有馬寛、内海渉
「J-PARC 超高圧中性子回折装置 PLANET の設計思想と建設状況」
日本中性子科学会誌「波紋」**20** 39 (2010)

15 A. Horinouchi, Y. Fujii, N. L. Yamada, and K. Tanaka
Surface Reorganization of Thin Poly(Methyl Methacrylate) Films Induced by Water
Chem. Lett. **39** 810 (2010)

16 M. Ida, T. Naoe, and M. Futakawa
The Effect of Gas Bubble Injection for Pressure Wave Mitigation in High-Power Neutron Sources−Differences and Similarities between Mercury and Water
Proc. of the 19th Meeting of the Int. Collaboration on Advanced Neutron Sources PSI-Proceedings 10-01 ISSN-Nr. 1019-6447 TO040 (2010)

17 池田一貴、折茂慎一、齋藤寛之、町田晃彦、片山芳則、青木勝敏
アルミニウム水素化物による水素貯蔵
「水素製造・吸蔵・貯蔵・輸送材料と安全化」サイエンス＆テクノロジー書籍 ISBN978-4-86428-004-4 (2010)

18 Y. Inamura, J-Y. So, K. Nakajima, J. Suzuki, T. Nakatani, R. Kajimoto, T. Otomo, M-K. Moon, C-H. Lee, Y. Yasu, K. Nakayoshi, H. Sendai, U-W. Nam, J-G. Park, and M. Arai
Technical Report on the Korea-Japan Software Collaboration
JAEA-Technology 2010-047 J-PARC 10-03 (2010)

19 Y. Inamura, K. Nakajima, R. Kajimoto, T. Nakatani, M. Arai, T. Otomo, J. Suzuki, J. Y. So, and J. G. Park
Software Development on Chopper Spectrometers for MLF, J-PARC
Proc. of the 19th Meeting of the Int. Collaboration on Advanced Neutron Sources PSI-Proceedings 10-01 ISSN-Nr. 1019-6447 (2010)

20 T. Ito, T. Nakatani, S. Harjo, H. Arima, J. Abe, K. Aizawa, and A. Moriai
Application Software Development for the Engineering Materials Diffractometer, TAKUMI.
Materials Science Forum **652** 238 (2010)

21 S. Itoh, T. Yokoo, T. J. Sato, S. Satoh, S. Yano, J. Suzuki, K. Ueno, K. Kuwahara, T. Kamiyama, K. Iwasa, K. Ohoyama, T. Otomo, Y. Endoh, J. Akimitsu, S. Kuroda, K. Sato, K. Nasu, K. Iwano, H. Yoshizawa, O. Yamamuro, Y. Ohara, Y. Kawamura, T. Asami, and R. Sugiura
Construction Status of High Resolution Chopper Spectrometer (HRC) at J-PARC
Proc. of the 19th Meeting of the Int. Collaboration on Advanced Neutron Sources PSI-Proceedings 10-01 ISSN-Nr. 1019-6447 IO079 (2010)

22 S. Itoh, K. Ueno, T. Yokoo, Y. Funahashi, T. Kamiyama, H. Sato, N. Miyamoto, Y. Kiyanagi, T. J. Sato, T. Otomo, and S. Satoh
Development of Fermi Chopper at KEK
Proc. of the 19th Meeting of the Int. Collaboration on Advanced Neutron Sources PSI-Proceedings 10-01 ISSN-Nr. 1019-6447 IP120 (2010)

23 S. Itoh, K. Ueno, R. Ohkubo, Y. Funahashi, H. Sagaheshi, T. Yokoo, T. J. Sato, T. Otomo, and S. Satoh
Development of T0 Chopper at KEK
Proc. of the 19th Meeting of the Int. Collaboration on Advanced Neutron Sources PSI-Proceedings 10-01 ISSN-Nr. 1019-6447 IP121 (2010)

24 伊藤晋一、上野健治、大久保隆治、下ケ橋秀典、舟橋義聖
T0 チョッパーの開発 (2)
日本中性子科学会誌「波紋」**20** 146 (2010)

25 K. Iwano, T. Yokoo, M. Oguro, and S. Ikeda
Propagating Librations in Ice XI: Model Analysis and Coherent Inelastic Neutron Scattering Experiment
J. Phys. Soc. Jpn. **79** 63601 (2010)

26 H. Iwase, N. Matubayasi, Y. Kameda, K. Itoh, T. Otomo, and M. Nakahara
Newly Designed High-Temperature and High-Pressure Sample Cell for Neutron Diffraction for Liquids
Jpn. J. Appl. Phys. **49** 16602 (2010)

27 Y. Iwashita, M. Ichikawa, M. Yamada, T. Sugimoto, H. Tongu, H. Fujisawa, M. Masuzawa, T. Tauchi, T. Oku, K. Hirota, H. M. Shimizu, C. Shi, and Y. Zhu
Practical Applications of Permanent Magnet Multipoles
IEEE Trans. Appl. Supercond. **20** 842 (2010)

28 T. Kai, M. Ooi, Y. Kasugai, T. Wakui, H. Kogawa, K. Haga, and K. Hanano
Discussions on Spallation Products Behaviour by Measuring Mercury and Substances Adhering Inside the Mercury Circulation System in MLF/J-PARC
Proc. of the 19th Meeting of the Int. Collaboration on Advanced Neutron Sources
PSI-Proceedings 10-01 ISSN-Nr. 1019-6447 TO152 (2010)

29 R. Kajimoto, K. Nakajima, S. Ohira-Kawamura, Y. Inamura, K. Kakurai, M. Arai, T. Hokazono, A. Oozono, and T. Okuda
Temperature and Ag Doping Effect on Magnetic Excitations in the Quasi Two-Dimensional Triangular Lattice Antiferromagnet CuCrO2 Studied by Inelastic Neutron Scattering
J. Phys. Soc. Jpn. **79** 123705 (2010)

30 R. Kajimoto, M. Nakamura, and M. Arai
New Technique for Inelastic Scattering Measurement Is in Practical Use at J-PARC
Neutron News **21** 55 (2010)

31 R. Kajimoto, M. Nakamura, Y. Inamura, F. Mizuno, K. Nakajima, N. Takahashi, S. Ohira-Kawamura, T. Yokoo, R. Maruyama, K. Soyama, K. Shibata, K. Suzuya, T. Nakatani, S. Sato, S. Wakimoto, Y. Ito, T. Iwahashi, W. Kambara, H. Tanaka, N. Yoshida, A. Katabira, K. Aizawa, and M. Arai
Comissioning of the Fermi − Chopper Spectrometer 4SEASONS at J-PARC − Background Study
Proc. of the 19th Meeting of the Int. Collaboration on Advanced Neutron Sources PSI-Proceedings 10-01 ISSN-Nr. 1019-6447 (2010)

32 梶本亮一、中村充孝、稲村泰弘、水野文夫、横尾哲也、中谷健、新井正敏
動き出した J-PARC 中性子非弾性散乱装置「四季」－中性子非弾性散乱実験の新規手法の実証－
固体物理 **45** 79 (2010)

33 梶本亮一、中村充孝
4 次元空間中性子探査装置「四季」
日本中性子科学会誌「波紋」**20** 8 (2010)

34 Y. Kameda, A. Maki, Y. Amo, and T. Usuki
Partial Pair Correlation Functions of Highly Concentrated Aqueous Urea Solutions Determined by Neutron Diffraction with 14N/15N and H/D Isotopic Substitution Methods
Bull. Chem. Soc. Jpn. **20** 131 (2010)

35 Y. Kasugai, K. Otsu, and T. Kai
Monitoring System of Mercury Target Failure Using Radioactivity Measurement
Proc. of the 19th Meeting of the Int. Collaboration on Advanced Neutron Sources PSI-Proceedings 10-01 ISSN-Nr. 1019-6447 TO044 (2010)

36 S. Kato, M. Bielmann, K. Ikeda, S. Orimo, A. Borgschulte, and A. Z'ttel
Surface Changes on AlH_3 During the Hydrogen Desorption
Appl. Phys. Lett. **96** 51912 (2010)

37 K. Kikuchi, M. Teshigawara, M. Harada, S. Saito, F. Maekawa, M. Futakawa, and T. Ishigaki
A Challenge for a High-Resolution Ag-In-Cd Decoupler in Intensified Short-pulsed Neutron Source
Materials Science Forum **652** 92 (2010)

38 Y. Kiyanagi
Neutronic Characteristics of Beam Line BL04 for Nuclear Data Measurements at J-PARC MLF
Proc. 2009 Annual Symposium on Nuclear Data (NDS 2009) 3 (2010)

39 H. Kogawa, K. Haga, T. Naoe, H. Kinoshita, M. Ida, and M. Futakawa
Development of Bubble Injection Technique in JSNS Mercury Target
Proc. of the 19th Meeting of the Int. Collaboration on Advanced Neutron Sources PSI-Proceedings 10-01 ISSN-Nr. 1019-6447 TO047 (2010)

40 F. Maekawa, M. Harada, K. Oikawa, M. Teshigawara, T. Kai, S. Meigo, M. Ooi, S. Sakamoto, H. Takada, M. Futakawa, T. Kato, Y. Ikeda, N. Watanabe, T. Kamiyama, S. Torii, R. Kajimoto, and M. Nakamura
First Neutron Production Utilizing J-PARC Pulsed Spallation Neutron Source JSNS and Neutronic Performance Demonstrated
Nucl. Instrum. Methods Phys. Res. A **620** 159 (2010)

41 F. Maekawa, K. Oikawa, M. Harada, M. Teshigawara, T. Kai, Y. Kasugai, S. Meigo, M. Ooi, M. Futakawa, N. Watanabe, M. Nakamura, S. Torii, and T. Kamiyama
Distinctive Features in Neutronic Performance of JSNS
Proc. of the 19th Meeting of the Int. Collaboration on Advanced Neutron Sources PSI-Proceedings 10-01 ISSN-Nr. 1019-6447 TO049 (2010)

42 S. Meigo, M. Ooi, M. Ito, S. Sakamoto, and M. Futakawa
A Study of Proton Beam Profile on the Target at JSNS
Proc. of the 19th Meeting of the Int. Collaboration on Advanced Neutron Sources PSI-Proceedings 10-01 ISSN-Nr. 1019-6447 AO020 (2010)

43 S. Meigo, M. Ooi, T. Kai, S. Sakamoto, and M. Futakawa
Beam Commissioning at JSNS of J-PARC
Proc. of the 19th Meeting of the Int. Collaboration on Advanced Neutron Sources PSI-Proceedings 10-01 ISSN-Nr. 1019-6447 AO051 (2010)

44 K. Mori, K. Iwase, M. Yonemura, J. Siewenie, T. Proffen, Y. Onodera, K. Itoh, M. Sugiyama, T. Kamiyama, and T. Fukunaga
Ionic Conductivity and Structural Properties of Lithium Lanthanum Titanate Quenched into Liquid Nitrogen Studied by Neutron Powder

Diffraction
J. Phys. Soc. Jpn. Suppl. A **79** 84 (2010)

45 長村光造、ステファヌスハルヨ、伊藤崇芳、相澤一也、淡路智、西島元、高橋弘紀、小黒英俊、辺見努、松井邦浩、土屋佳則、町屋修太郎、鈴木裕士、富田優、鈴木賢次
J-PARC 中性子を用いた超伝導材料・導体の研究
低温工学 **45** 135 (2010)

46 中島健次、柴田薫、梶本亮一
Proceedings of the Workshop on "Possible Scientific View from New Neutron Spectroscopy Opportunities in J-PARC"
JAEA-Review 2010-027 (2010)

47 M. Nakamura, K. Nakajima, Y. Inamura, S. Ohira-Kawamura, T. Kikuchi, T. Otomo, and M. Arai
A New Possibility of Dynamical Study on Solid State Ionic Materials by Inelastic Neutron Scattering
Atom Indonesia **36** 116 (2010)

48 M. Nakamura, M. Arai, Y. Inamura, and Evvy Kartini
Novel Dynamics of Superionic Conducting Glasses Proved by Inelastic Neutron Scattering
J. Phys. Soc. Jpn. Suppl. A **79** 122 (2010)

49 K. Nakayoshi, Y. Yasu, E. Inoue, H. Sendai, M. Tanaka, S. Satoh, S. Muto, J. Suzuki, T. Otomo, T. Nakatani, T. Ito, Y. Inamura, M. Yonemura, T. Hosoya, and T. Uchida
DAQ-Middleware for MLF/J-PARC
Nucl. Instrum. Methods Phys. Res. A **623** 537 (2010)

50 T. Naoe, H. Kogawa, Y. Yamaguchi, and M. Futakawa
Effect of Tensile Stress on Cavitation Damage Formation in Mercury
Journal of Nuclear Materials **398** 199 (2010)

51 野尻浩之
パルス強磁場下中性子回析
RADIOISOTOPES **59** 509 (2010)

52 K. Ohara, Y. Kawakita, L. Pusztai, L. Temleitner, S. Kohara, N. Inoue, and S. Takeda
Structural Disorder in Lithium Lanthanum Titanate: The Basis of Superionic Conduction
J. Phys. Cond. Mat. **22** 404203 (2010)

53 H. Ohshita, S. Uno, T. Otomo, T. Koike, T. Murakami, S. Satoh, M. Sekimoto, and T. Uchida
Development of a Neutron Detector with a GEM
Nucl. Instrum. Methods Phys. Res. A **623** 126 (2010)

54 T. Oku, H. Kira, T. Shinohara, S. Takata, M. Arai, J. Suzuki, and HM. Shimizu,
Development of a Triplet Magnetic Lens System to Focus a Pulsed Neutron Beam
J. Phys. Conf. Ser. **251** 12078 (2010)

55 奥地拓生、佐々木重雄、大野祥希、小松一生、鍵裕之、有馬寛、阿部淳、服部高典、佐野亜沙美、長壁豊隆、内海渉、ステファヌスハルヨ、伊藤崇芳、相澤一也、入舩徹男
大型ナノ多結晶ダイヤモンド対向アンビルを用いた高圧下パルス中性子粉末回折実験
高圧力の科学と技術 **20** 175 (2010)

56 Y. Onodera, K. Mori, T. Otomo, A. C. Hannon, S. Kohara, K. Itoh, M. Sugiyama, and T. Fukunaga
Crystal Structure of $Li_7P_3S_{11}$ Studied by Neutron and Synchrotron X-ray Powder Diffraction
J. Phys. Soc. Jpn. Suppl. A **79** 87 (2010)

57 Junghwan Park, Seongsu Lee, Misun Kang, Kwang-Hyun Jang, Changhee Lee, S. V. Streltsov, V. V. Mazurenko, M. V. Valentyuk, J. E. Medvedeva, T. Kamiyama, and J. -G. Park
Doping Dependence of Spin-lattice Coupling and Two-dimensional Ordering in Multiferroic Hexagonal $Y_{1-x}Lu_xMnO_3$ ($0 \leq x \leq 1$)
Phys. Rev. B **82** 54428 (2010)

58 下ヶ橋秀典
T0 チョッパー制御・計測システムの開発
KEK Internal 2010-2 (2010)

59 K. Sakasai, Y. Imamoto, K. Toh, T. Nakamura, K. Takakura, and C. Konno
Storage Characteristics of KBr:Eu^{2+} Phosphors With Radiators by Irradiation of Fast Neutrons
IEEE Nucl. Sci. Symp. Conf. Record 2010 966 (2010)

60 K. Sakasai, K. Toh, T. Nakamura, S. Harjo, A. Moriai, T. Ito, J. Abe, K. Aizawa, K. Soyama, K. Katagiri, N. J. Rhodes, and E.M. Schooneveld
Development and Installation of Neutron Detectors for Engineering Materials Diffractometer at J-PARC
Proc. of the 19th Meeting of the Int. Collaboration on Advanced Neutron Sources PSI-Proceedings 10-01 ISSN-Nr. 1019-6447 IP131 (2010)

61 坂佐井馨
MLF におけるシンチレーション型検出器
放射線 **36** 131 (2010)

62 坂佐井馨
シンチレーション検出器・イメージングプレート
日本中性子科学会誌「波紋」**20** 171 (2010)

63 S. Shamoto, M. Ishikado, S. Wakimoto, K. Kodama, R. Kajimoto, M. Arai, T. Fukuda, H. Nakamura, M. Machida, and H. Eisaki
Spin Excitations in Iron Oxypnictide Superconductor System
Physica C **470** S284 (2010)

64 柴田薫、高橋伸明、中島健次、中川洋、藤原悟、川北至信、佐藤卓
ダイナミクス解析装置 DNA －装置仕様と建設計画－
日本中性子科学会誌「波紋」**20** 13 (2010)

65 N. Shimura, T. Takeichi, T. Kume, S. Sasaki, H. Shimizu, A. Ohmura, K. Ikeda, Y. Nakamori, and S. Orimo
High Pressure Raman and Visible Absorption Study of AlH_3
J. Phys. Conf. Ser. **215** 12047 (2010)

66 鈴木純市、高田慎一、篠原武尚、奥隆之、吉良弘、鈴谷健太郎、相沢一也、新井正敏、大友季哉、杉山正明
パルス中性子小角散乱装置「大観」の開発
日本中性子科学会誌「波紋」**20** 54 (2010)

67 H. Tatsumoto, Y. Shirai, K. Hata, H. Kobayashi, Y. Naruo, Y. Inatani, T. Kato, M. Futakawa, and K. Kinoshita
Development of a Thermal-Hydraulics Experimental System for High Tc Superconductors Cooled by Liquid Hydrogen
Journal of Physics Conference Series **234** 32056 (2010)

68 達本衡輝、麻生智一、加藤崇、大都起一
J-PARC 中性子源用低温水素システムの動的特性
低温工学 **45** 181 (2010)

69 K. Toh, H. Yamagishi, K, Sakasai, T. Nakamura, and K. Soyama
Operation of Two-dimensional Gas Detector Using Micro-pixel Detector Element Under High Pressure for Neutron Measurement
Proc. of the 19th Meeting of the Int. Collaboration on Advanced Neutron Sources PSI-Proceedings 10-01 ISSN-Nr. 1019-6447 IP138 (2010)

70 友田陽
鉄鋼のミクロ組織と変形応力の定量的関係
「計算工学による組織と特性予測技術の最前線」
日本鉄鋼協会 **113** 122 (2010)

71 S. Wakimoto, K. Kodama, M. Ishikado, M. Matsuda, R. Kajimoto, M. Arai, K. Kakurai, F. Esaka, A. Iyo, H. Kito, H. Eisaki, and S. Shamoto
Degradation of Superconductivity and Spin Fluctuations by Electron Over-doping in $LaFeAsO_{1-x}F_x$
J. Phys. Soc. Jpn. **79** 74715 (2010)

72 山田悟史、鳥飼直也、下ヶ橋秀典、瀬戸秀紀
試料水平型中性子反射率計 ARISA-II
日本中性子科学会誌「波紋」**20** 58 (2010)

73 山岸秀志、藤健太郎
特定用途向け集積回路 (ASIC) 用 MOSFET の雑音評価
JAEA-Technology 2010-030 (2010)

74 D. Yamazaki, R. Maruyama, K. Soyama, H. Takai, M. Nagano, and K. Yamamura
Neutron Beam Focusing Using Large-m Supermirrors Coated on Precisely-figured Aspheric Surfaces
J. Phys. Conf. Ser. **251** 12076 (2010)

75 横尾哲也
HRC 研究会一次元ギャップ系の磁気励起
KEK proceedings 2010 (2010)

76 T. Yokoo, N. Kaneko, S. Itoh, T Otomo, Y. Suetsugu, M. Shirai, and K. Suzuya
Gas Desorption Examination of B4C Resin for Neutron Vacuum Chamber
Proc. of the 19th Meeting of the Int. Collaboration on Advanced Neutron Sources PSI-Proceedings 10-01 ISSN-Nr. 1019-6447 IP144 (2010)

77 横尾哲也、伊藤晋一、佐藤節夫、佐藤卓、矢野真一郎
高分解能チョッパー分光器 (HRC)
日本中性子科学会誌「波紋」**20** 45 (2010)

78 横尾哲也、伊藤晋一
高分解能チョッパー分光器の花
日本中性子科学会誌「波紋」**20** 187 (2010)

79 横尾哲也
6th International Workshop on Sample Environment at Neutron Scattering Facilities
日本中性子科学会誌「波紋」**20** 316 (2010)

Supplement to 2006-2009

1 新井正敏、横尾哲也、梶本亮一、中島健次、社本真一、山田和芳、藤田全基、猪野隆、曽山和彦、中村充孝、相澤一也、大山研司、平賀晴弘、朝岡秀人、樹神克明、稲村泰弘、今井良宗
平成 17 年度～平成 21 年度科学研究費補助金特別推進研究「4 次元空間中性子探査装置の開発と酸化物高温超伝導機構の解明」平成 17 年度研究報告書
JAEA-Review 2006-033 (2006)

2 梶本亮一、新井正敏
科研費特別推進研究・研究会「量子ビームによる高温超伝導機構の解明」講演集
JAEA-Review 2006-006 (2006)

3 T. Kanaya, N. Takahashi, K. Nishida, H. Seto, M. Nagao, and Y. Takeda
Dynamic and Static Fluctuations in Polymer Gels Studied by Neutron spin-echo
Physica B **385-386** 676 (2006)

4 Y. Ogino, H. Fukushima, N. Takahashi, G. Matsuba, K. Nishida, and T. Kanaya
Crystallization of Isotactic Polypropylene Under Shear Flow Observed in a Wide Spatial Scale
Macromolecules **39** 7617 (2006)

5 Y. Ogino, H. Fukushima, G. Matsuba, N. Takahashi, K. Nishida, and T. Kanaya,
Effects of High Molecular Weight Component on Crystallization of Polyethylene Under Shear Flow
Polymer **47** 5669 (2006)

6 鬼柳善明
高強度パルス中性子源を用いた革新的原子炉用核データの研究開発
原子力 eye 66 (2007)

7 N. Takahashi, T. Kanaya, K. Nishida, and K. Kaji
Gelation-Induced Phase Separation of Poly(vinyl alcohol) in Mixed Solvents of Dimethyl Sulfoxide and Water
Macromolecules **40** 8750 (2007)

8 S. Fujiwara, F. Matsumoto, N. Takahashi, H. Nakagawa, and T. Oda
Analysis of F-actin Dynamics
JAEA-Review 2008-067 289 (2008)

9 Stefanus Harjo
Introduction of The Engineering Materials Diffractometer and Application Possibilities
Journal of the Crystallographic Society of Japan **50** 40 (2008)

10 T. Hemmi, K. Matsui, T. Hasebe, Y. Uno, T. Koizumi, Y. Takahashi, K. Okuno, H. Suzuki, S. Harjo, K. Aizawa, Y. Tsuchiya, S. Machiya, and K. Osamura
Plans on Strain Measurements in ITER CS Conductor Using Neutron Diffraction
Abstracts of CSJ Conference **79** 28 (2008)

11 A. Kimura, Y. Toh, M. Koizumi, K. Furutaka, T. Kin, and M. Oshima
Performance of a High Speed and High Density DataAcquisition System for Multiple Gamma-ray Detection
IEEE Nucl. Sci. Symp. Conf. Record 2008 2107 (2008)

12 Y. Kiyanagi
Nuclear Data Measurement Project at J-PARC MLF
JAEA-Conf. 2008-008 26 (2008)

13 社本真一、新井正敏
第 2 回科研費特別推進研究・研究会「量子ビームによる高温超伝導機構の解明」講演集
JAEA-Review 2008-011 (2008)

14 H. Harada, K. Furutaka, S. Goko, A. Kimura, T. Kin, F. Kitatani, M. Koizumi, S. Nakamura, M. Ohta, M. Oshima, Y. Toh, M. Igashira, T. Katabuchi, M. Mizumoto, M. Furusaka, F. Hiraga, T. Kamiyama, K. Kino, Y. Kiyanagi, T. Fujii, J. Hori, and K. Takamiya
Measurements of Neutron Capture Cross Sections Using a 4πGe Spectrometer at the J-PARC/MLF/NNRI
Bulletin of the American Physical Society **54** LC7 (2009)

15 ステファヌス・ハルヨ、相澤一也
「何ができる？どこがすごい？」～各装置の紹介～工学材料回折装置　匠
金属学会会報 **48** 355 (2009)

16 M. Igashira, Y. Kiyanagi, and M. Oshima
Nuclear Data Study at J-PARC BL04
Nucl. Instrum. Methods Phys. Res. A **600** 332 (2009)

17 E. Kartini, M. Nakamura, M. Arai, Y. Inamura, J.W. Taylor, and M. Russina
Universal Dynamics Behavior in Superionic Conducting Glass
Solid State Ionics **180** 506 (2009)

18 T. Katabuchi, M. Igashira, M. Mizumoto, K. Furutaka, S. Goko, H. Harada, A. Kimura, T. Kin, F. Kitatani, M. Koizumi, S. Nakamura, M. Ohta, M. Oshima, Y. Toh, M. Furusaka, F. Hiraga, T. Kamiyama, K. Kino, Y. Kiyanagi, T. Fujii, J. Hori, and K. Takamiya
Measurements of neutron capture cross sections using a NaI(Tl) spectrometer at the J-PARC MLF neutron nucleus reaction instrument
Bulletin of the American Physical Society **54** (2009)

19 A. Kimura, K. Furutaka, S. Goko, H. Harada, M. Igashira, T. Kamiyama, T. Katabuchi, T. Kin, K. Kino, F. Kitatani, Y. Kiyanagi, M. Koizumi, M. Mizumoto, S. Nakamura, M. Ohta, M. Oshima, and Y. Toh
A Dead-Time Correction Method for Multiple Gamma-ray Detection
IEEE Nucl. Sci. Symp. Conf. Record 2009 **138** (2009)

20 T. Kin, K. Furutaka, S. Goko, H. Harada, M. Igashira, T. Kamiyama, T. Katabuchi, A. Kimura, K. Kino, F. Kitatani, Y. Kiyanagi, M. Koizumi, M. Mizumoto, S. Nakamura, M. Ohta, M. Oshima, and Y. Toh
Development of a 4π Germanium Spectrometer for Nuclear Data Measurements at J-PARC
IEEE Nucl. Sci. Symp. Conf. Record 2009 1194 (2009)

21 K. Kino, M. Furusaka, F. Hiraga, T. Kamiyama, Y. Kiyanagi, K. Furutaka, S. Goko, H. Harada, A. Kimura, T. Kin, F. Kitatani, M. Koizumi, S. Nakamura, M. Ohta, M. Oshima, Y. Toh, M. Igashira, T. Katabuchi, and M. Mizumoto
Neutron Beam Provided by the Neutron Nucleus Reactioninstrument at the J-PARC MLF
Bulletin of the American Physical Society **54** LC6 (2009)

22 K. Kino, F. Hiraga, M. Furusaka, Y. Kiyanagi, M. Igashira, M. Mizumoto, and T. Katabuchi
Design of a Collimator System of a Neutron Beam Line for Neutron-nucleus Reaction Measurements
Nuclear Technology **168** 317 (2009)

23 Y. Kiyanagi
Nuclear Data Measurements on the Neutron-nucleus Reaction Instrument (NNRI) at the Materials and Life Science Facility (MLF) at J-PARC
Proc. WONDER2009 9 (2009)

24 J. Kubo, N. Rahman, N. Takahashi, T. Kawai, G. Matsuba, K. Nishida, T. Kanaya, and M. Yamamoto
Improvement of Poly(vinyl alcohol) Properties by the Addition of Magnesium Nitrate
Journal of Applied Polymer Science **112** 1647 (2009)

25 M. Nakamura, R. Kajimoto, Y. Inamura, F. Mizuno, M. Fujita, T. Yokoo, and M. Arai
First Demonstration of Novel Method for Inelastic Neutron Scattering Measurement Utilizing Multiple Incident Energies
J. Phys. Soc. Jpn. **78** 93002 (2009)

26 K. Nishioka, and K. Nasu
Early-stage real-time Dynamics of Interlayer Sp3-bond Formation by Visible-light Irradiation of Graphite
Phys. Rev. B **80** 235420 (2009)

27 高橋伸明
J-PARC における新しい背面反射型分光器 DNA の建設を目指して
日本中性子科学会誌「波紋」**19** 14 (2009)

28 内海渉
「J-PARC における中性子利用高圧研究戦略」
高圧力の科学と技術 **19** 10 (2009)

Muon Section

1 R. Akiyama, Y. Ikedo, M. Månsson, T. Goko, J. Sugiyama, D. Andreica, A. Amato, K. Matan, and T. J.Sato
Short-range Spin Correlations in β-$LiFeO_2$ from Bulk Magnetization, Neutron Diffraction, and μSR Experiments
Phys. Rev. B **81** 24404 (2010)

2 A. Chiba, M. Tomomasa, T. Hayakawa, A. Hinzmann, R. Takahashi, J. Nakamura, T. Tsukatani, T. Kumazawa, and K. Tsuji
Relationship Between Peierls Distortion and Medium-range Order in Liquid Group-V elements and Liquid Group-IV-VI Compounds
J. Phys. Conf. Ser. **215** 12077 (2010)

3 M. Doyama, Y. Kogure, M. Inoue, Y. Miyake, K. Nishiyama, and K. Shimomura
Applications of Imaging Plates to the Study of Positron and Muon Research
J. Phys. Conf. Ser. **225** 12006 (2010)

4 K. Ghandi, and Y. Miyake
Modern Slow Muon Beam Production Techniques
Charged Particle and Photon Interactions with Matter − Recent Advances, Applications, and Interfaces,CRC Press, ISBN978-1439811771 (2010)

5 R.H. Heffner, T. Goko, D. Andreica, K. Ohishi, W. Higemoto, T.U. Ito, A. Amato, J. Spehling, H.-H. Klauss, E.D. Bauer, J.D. Thompson, and Y.J. Uemura
μSR Study of $CeRhIn_5$ Under Applied Pressure
J. Phys. Conf. Ser. **225** 12011 (2010)

6 W. Higemoto, and A. Kawasuso
Advanced Science Research Symposium 2009 Positron, Muon and Other Exotic Particle Beams for Materials and Atomic/molecular Sciences (ASR2009)
J. Phys. Conf. Ser. **225** 11001 (2010)

7 W. Higemoto, T.U. Ito, K. Ninomiya, R.H. Heffner, K. Shimomura, K. Nishiyama, and Y. Miyake
JAEA-ASRC Muon Research at J-PARC MUSE
J. Phys. Conf. Ser. **225** 12012 (2010)

8 M. Hiraishi, R. Kadono, M. Miyazaki, S. Takeshita, Y. Taguchi, Y. Kasahara, T. Takano, T. Kishiume, and Y. Iwasa
Anisotropic Superconducting Order Parameter in Li-intercalated Layered Superconductor Li_xZrNCl
Phys. Rev. B **81** 14525 (2010)

9 H. Hiraka, Y. Hayashi, S. Wakimoto, M. Takeda, K. Kakurai, T. Adachi, Y. Koike, I. Yamada, M. Miyazaki, M. Hiraishi, S. Takeshita, A. Koda, R. Kadono, J.M. Tranquada, and K. Yamada
Incommensurate Spin Correlations Induced by Magnetic Fe Ions Substituted Into Overdoped $Bi_{1.75}Pb_{0.35}Sr_{1.90}CuO_{6+z}$
Phys. Rev. B **81** 144501 (2010)

10 S. Ideta, K. Takashima, M. Hashimoto, T. Yoshida, A. Fujimori, H. Anzai, T. Fujita, Y. Nakashima, A. Ino, M. Arita, H. Namatame, M. Taniguchi, K. Ono, M. Kubota, D. H. Lu, Z.-X. Shen, K. M. Kojima, and S. Uchida
Enhanced Superconducting Gaps in the Trilayer High-Temperature $Bi_2Sr_2Ca_2Cu_3O_{10+\delta}$ Cuprate Superconductor
Phys. Rev. Lett. **104** 227001 (2010)

11 Y. Ikedo, J. Sugiyama, K. Mukai, M. Månsson, T. Goko, D. Andreica, A. Amato, K. Ariyoshi, and T. Ohzuku
μ^+SR Study on Triangular Antiferromagnet $LiCrO_2$
J. Phys. Conf. Ser. **225** 12016 (2010)

12 Y. Ikedo, J. Sugiyama, O. Ofer, M. Månsson, H. Sakurai, E. Takayama-Muromachi, E.J. Ansaldo, J.H. Brewer, and K.H. Chow
Comparative μ^+SR Study of the Zigzag Chain Compounds $NaMn_2O_4$ and $LiMn_2O_4$
J. Phys. Conf. Ser. **225** 12017 (2010)

13 S. Ishida, M. Nakajima, Y. Tomioka, T. Ito, K. Miyazawa, H. Kito, C.H. Lee, M. Ishikado, S. Shamoto, A. Iyo, H. Eisaki, K.M. Kojima, and S. Uchida
Strong Carrier-scattering in Iron-pnictide Superconductors $LnFeAsO_{1-y}$ (Ln=La and Nd) Obtained from ChargeTransport Experiments
Phys. Rev. B **81** 94515 (2010)

14 T.U. Ito, K. Nakahara, M. Kawase, H. Fujimori, Y. Kobayashi, W. Higemoto, and Y. Miyake
The EPICS-based Remote Control System for Muon Beam Line Devices at J-PARC MUSE
J. Phys. Conf. Ser. **225** 12022 (2010)

15 T.U. Ito, W. Higemoto, K. Ohishi, K. Satoh, Y. Aoki, S. Toda, D. Kikuchi, H. Sato, and C. Baines
Microscopic Study of Antiferromagnetic Ground State and Possible High-field Ordered State in $CeOs_4Sb_{12}$ Using Muon Spin Rotation and Relaxation
Phys. Rev. B **82** 14420 (2010)

16 K. Kamazawa, M. Harada, Y. Ikedo, J. Sugiyama, M. Tyagi, and Y. Matsuo
Long Range Proton Diffusive Mode of $CsHSO_4$ and $CsHSeO_4$ − High Energy Resolution Quasielastic Neutron Scattering for Superprotonic Conductors −
J. Phys. Soc. Jpn. Suppl. A **79** 7 (2010)

17 S. Kambe, H. Chudo, Y. Tokunaga, T. Koyama, H. Sakai, T.U. Ito, K. Ninomiya, W. Higemoto, T. Takesaka, T. Nishioka, and Y. Miyake
Evidence for Appearance of an Internal Field in the Ordered State of $CeRu_2Al_{10}$ by μSR
J. Phys. Soc. Jpn. **79** 53708 (2010)

18 N. Kawamura, K. Ishida, T. Matsuzaki, H. Imao, and K. Nagamine
Muonic Molecule Formation in Muon-catalyzed Fusion
J. Phys. Conf. Ser. **225** 12025 (2010)

19 N. Kawamura, T. Masuda, P. Strasser, and Y. Miyake
Generation of Negative Slow Muon Beam in J-PARC Muon Facility
J. Phys. Conf. Ser. **225** 12026 (2010)

20 M. Månsson, Y. Ikedo, H. Nozaki, J. Sugiyama, P.L. Russo, D. Andreica, M. Shizuya, M. Isobe, and E. Muromachi
Muon Spin Relaxation Study of Misfit-layered Cobalt Bioxide $[Ca_{0.85}OH]^{RS}_{1.16}[CoO_2]$
Solid State Communication **150** 307 (2010)

21 Y. Miyake, K. Shimomura, N. Kawamura, P. Strasser, S. Makimura, A. Koda, H. Fujimori, K. Nakahara, S. Takeshita, Y. Kobayashi, K. Nishiyama, W. Higemoto, T.U. Ito, K. Ninomiya, M. Kato, R. Kadono, N. Sato, and K. Nagamine
J-PARC Muon Facility, MUSE
J. Phys. Conf. Ser. **225** 12036 (2010)

22 M. Miyazaki, R. Kadono, K. H. Satoh, M. Hiraishi, S. Takeshita, A. Koda, A. Yamamoto, and H. Takagi
Magnetic Ground State of Pyrochlore Oxides Close to Metal-insulator Boundary Probed by Muon Spin Rotation
Phys. Rev. B **82** 94413 (2010)

23 M. Miyazaki, R. Kadono, M. Hiraishi, K.H. Satoh, S. Takeshita, A. Koda, Y. Fukunaga, Y. Tanabe, T. Adachi, and Y. Koike
Muon Knight shift study of pseudogap state in underdoped

(Bi,Pb)2201
Physica C **470** S55 (2010)

24 K. Mukai, J. Sugiyama, Y. Ikedo, H. Nozaki, K. Kamazawa, D. Andreica, A. Amato, M. Månsson, J.H. Brewer, E.J. Ansaldo, and K.H. Chow
Microscopic Magnetic Study on the Nominal Composition Li[Li1/3Mn5/3]O4 by Muon-Spin Rotation/Relaxation Measurements
J. Phys. Chem. C **114** 11320 (2010)

25 K. Mukai, J. Sugiyama, Y. Ikedo, Y. Aoki, D. Andreica, and A. Amato
Structural and Magnetic Nature for Fully Delithiated Li_xNiO_2: Comparative Study between Chemically and Electrochemically Prepared Samples
J. Phys. Chem. C **114** 8626 (2010)

26 K. Nakahara, T. Adachi, Y. Ikedo, Y. Miyake, K. Shimomura, P. Strasser, K. Nishiyama, N. Kawamura, H. Fujimori, S. Makimura, A. Koda, K. Nagamine, T. Ogitsu, A. Yamamotob, K. Sasaki, K. Tanaka, N. Kimura, Y. Makida, Y. Ajima, K. Ishida, and Y. Matsuda
The Next Generation Muon Source at J-PARC/MLF
AIP Conf. Proc. **1222** 420 (2010)

27 M. Nakajima, S. Ishida, K. Kihou, Y. Tomioka, T. Ito, Y. Yoshida, C. H. Lee, H. Kito, A. Iyo, H. Eisaki, K. M. Kojima, and S. Uchida
Evolution of the Optical Spectrum with Doping in $Ba(Fe_{1-x}Co_x)_2As_2$
Phys. Rev. B **81** 104528 (2010)

28 J. Nakamura, A. Chiba, and K. Tsuji
Pressure-Induced Structural Changes in Liquid $Ge_{33}Te_{67}$ and Liquid $Ge_{15}Te_{85}$
J. Phys. Soc. Jpn. **79** 64604 (2010)

29 K. Ninomiya, T. Nagatomo, K.M. Kubo, P. Strasser, N. Kawamura, K. Shimomura, Y. Miyake, T. Saito, and W. Higemoto
Development of Elemental Analysis by Muonic X-ray Measurement in J-PARC
J. Phys. Conf. Ser. **225** 12040 (2010)

30 O. Ofer, Y. Ikedo, T. Goko, M. Månsson, J. Sugiyama, E.J. Ansaldo, J.H. Brewer, K.H. Chow, and H. Sakurai
Magnetic Structure of the Zigzag Chain Family $Na_xCa_{1-x}V_2O_4$ Determined by Muon-spin Rotation
Phys. Rev. B **82** 94410 (2010)

31 H. Ohta, M. Månsson, Y. Ikedo, J. Sugiyama, C. Michioka, K. Yoshimura, J.H. Brewer, E.J. Ansaldo, S.L. Stubbs, K.H. Chow, and J.S. Lord
Microscopic Magnetic Nature of Water Absorbed $Na_{0.35}CoO_2$ Investigated by NMR, NQR and μ^+SR
Physica C **470** S755 (2010)

32 K. Shimomura, P. Bakule, F. L. Pratt, K. Ohishi, K. Ishida, I. Watanabe, Y. Matsuda, K. Nishiyama, E. Torikai, and K. Nagamine
Pilot Experiment for Muonium Photo Ionization in GaAs
J. Phys. Conf. Ser. **225** 12004 (2010)

33 P. Strasser, K. Shimomura, A. Koda, N. Kawamura, H. Fujimori, K. Nakahara, M. Kato, S. Takeshita, M. Hiraishi, M.Miyazaki, W. Higemoto, T.U. Ito, K. Ninomiya, K. Ishida, M.K. Kubo, R. Kadono, K. Nishiyama, and Y. Miyake
J-PARC Decay Muon Channel Construction Status
J. Phys. Conf. Ser. **225** 12050 (2010)

34 J. Sugiyama, Y. Ikedo, T. Noritake, K. Miwa, S. Towata, T. Goko, O. Ofer, M. Månsson, E.J. Ansaldo, J.H. Brewer, and K.H. Chow
Microscopic Indicator for Thermodynamic Stability of Hydrogen Storage Materials Provided by Muon-spin Spectroscopy
J. Phys. Conf. Ser. **225** 12051 (2010)

35 J. Sugiyama, K. Mukai, Y. Ikedo, H. Nozaki, M. Månsson, and I. Watanabe
A Novel Tool for Detecting Li Diffusion in Solids Containing Magnetic Ions; μ^+SR Study on Li_xCoO_2
J. Phys. Conf. Ser. **225** 12052 (2010)

36 J. Sugiyama, Y. Ikedo, T. Noritake, O. Ofer, T. Goko, M. Månsson, K. Miwa, E.J. Ansaldo, J.H. Brewer, K.H. Chow, and S. Towata
Microscopic Indicator for Thermodynamic Stability of Hydrogen Storage Materials Provided by Positive Muon-spin Rotation
Phys. Rev. B **81** 92103 (2010)

37 J. Sugiyama, Y. Ikedo, M. Månsson, J.H. Brewer, S.L. Stubbs, E.J. Ansaldo, K.H. Chow, J.S. Lord, H. Ohta, C. Michioka, and K. Yoshimura
Magnetic and Superconducting Nature of $Na_{0.35}CoO_2 \cdot yH_2O$ and $Na_{0.35}CoO_2 \cdot yD_2O$ Investigated by Muon-spin Spectroscopy
Phys. Rev. B **82** 214505 (2010)

38 J. Sugiyama, Y. Ikedo, K. Mukai, H. Nozaki, M. Månsson, O. Ofer, M. Harada, K. Kamazawa, Y. Miyake, J.H. Brewer, E.J. Ansaldo, K.H. Chow, I. Watanabe, and T. Ohzuku
Low-temperature Magnetic Properties and High-temperature Diffusive Behavior of $LiNiO_2$ Investigated by Muon-spin Spectroscopy
Phys. Rev. B **82** 224412 (2010)

39 K. Suzuki, T. Adachi, Y. Tanabe, Y. Koike, T. Kawamata, Risdiana, T. Suzuki, and I. Watanabe
Hole Trapping by Ni, Kondo Effect, and Electronic Phase Diagram in Nonsuperconducting Ni-substituted $La_{2-x}Sr_xCu_{1-y}Ni_yO_4$
Phys. Rev. B **82** 54519 (2010)

40 Y. Tanabe, K. Suzuki, T. Adachi, Y. Koike, T. Kawamata, Risdiana, T. Suzuki, and I. Watanabe
Change of the Ground State Upon Hole Doping Unveiled by Ni Impurity in High-T_c Cuprates
J. Phys. Soc. Jpn. **79** 23706 (2010)

Editorial Board of MLF Annual Report 2010

Chief Editor
Tetsuya Yokoo
Neutron Science Section

Yukinobu Kawakita
Neutron Science Section

Shin-ichiro Meigo
Neutron Source Section

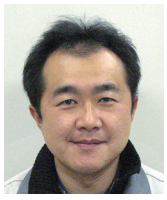

Hiroyuki Kogawa
Neutron Source Section

Kaoru Sakasai
Neutron Instrumentaion Section

Kenji M. Kojima
Muon Science Section

Shinichi Takata
Neutron Science Section